## Article / Book Information

| ( ) | |
|---|---|
| Title(English) | A study of multiple quantum well bistable lasers for application to all-optical signal processing |
| ( ) | |
| Author(English) | Hiroyuki Uenohara |
| ( ) | : , : , : 2779 , :1995 7 31 , : , : |
| Citation(English) | Degree:Doctor of Engineering, Conferring organization: , Report number: 2779 , Conferred date:1995/7/31, Degree Type:Thesis doctor, Examiner: |
| ( ) | |
| Type(English) | Doctoral Thesis |

# A Study of Multiple Quantum Well Bistable Lasers for Application to All-optical Signal Processing

## 全光動作信号処理用
## 多重量子井戸双安定レーザに関する研究

by

Hiroyuki  Uenohara

February  1995

Adviser  : Professor Kenichi Iga

Tokyo Institute of Technology
4259 Nagatsuta, Midoriku, Yokohama 227, Japan

# A Study of Multiple Quantum Well Bistable Lasers for Application to All-optical Signal Processing

## Table of Contents

# Abstract

A segmented-electrode bistable laser is attractive for use in the demultiplexing components of optical transmission systems and in the optical exchange components of optical signal processing systems because of its thresholding or memory operations. The turn-off time of the conventional current-injection-type bistable laser, however, is limited by the recovery time of the saturable absorber, and the introduction of multiple quantum well (MQW) structure was proposed in the GaAs/AlGaAs systems in 1986 in order to reduce the carrier lifetime by applied electric field as well as to control the hysteresis characteristics by using the quantum confined Stark effect. Self-sustained intensity pulsation has been a problem in that material system, but the bistable laser has been attracting one's attention by solving that problem.

The purpose of the study presented in this thesis is to provide the stable and high-speed operation of the MQW bistable laser in long-wavelength systems and to develop an all-optical switching device based on the MQW bistable laser.

First, the static and dynamic characteristics of the InGaAs/InGaAsP and InGaAs/InAlAs systems were studied analytically: the dependence of the switching input light power and the switching time on the bias or operating condition were calculated. Difference in hysteresis characteristics and in switching time were found to attribute to the differential gain coefficient and the carrier escape time for the saturable absorption region. And it was shown that the switching power can be lowered when the input light power is larger or when the bias current approaches the turn-on threshold current and that the reset operation is faster when the applied voltage height is increased.

Then two-segmented MQW bistable lasers were fabricated and their performance was studied experimentally. In this structure, the input light was injected coaxial to the laser cavity. The performance of three kinds of MQW structures, InGaAs/InP, InGaAs/InGaAsP and InGaAs/InAlAs, and of several well numbers were compared. Hysteresis width and the threshold current were controllable for all structures, but the bias conditions in view of the applied voltage to the saturable absorption region were different because of the different absorption spectral characteristics. In input light switching operations, such characteristics as wide wavelength sensitivity, low power switching, and short turn-on time were shown. The dependence of the turn-off time on applied voltage height was investigated and the high-speed switching characteristics due to the reduction of carrier escape time by applied voltage were confirmed.

To develop the MQW bistable laser to all-optical functional devices, the side-light-injection-type MQW bistable laser was proposed. The set operation in this device is accomplished by absorption saturation that is the same as that of two-segmented bistable laser, and the reset operation is realized by gain quenching phenomenon. For the purpose of performing set and reset operations in one device, the input light is injected

perpendicular to the laser cavity and the key regions for absorption saturation and the gain quenching are spatially separated. The static and dynamic characteristics of this type of laser were studied analytically by solving the modified rate equations, demonstrating the possibility of set and reset operations by input light in one device. The dependence of switching turn-off time on differential gain coefficient, i.e., on the MQW material, was calculated and the superiority of a material with large differential gain was shown.

Side-light-injection-type MQW bistable lasers were then fabricated and their static and dynamic characteristics were investigated. The controllability of hysteresis characteristics was similar to that of the two-segmented bistable laser. And as expected from the theoretical analysis, the set and reset operations were achieved by injecting light into the saturable absorption region and into the gain quenching region, respectively. Experimental measurements of turn-on and turn-off time dependence on input light power indicate that high-speed switching operations can be expected.

Finally, the ultimate switching performance has been evaluated by theoretical calculations. In this work, the carrier escape time for the MQW structure under applied electric field was taken into consideration. Pump-probe measurement was performed to investigate the transient response of the absorption saturation. Carrier escape time was derived from the theoretical curve fitting of the differential transmitted signals, and the resultant data were used for calculating the switching time. It is found that high-power injection light (50 kW/cm$^2$) and high reset voltage pulse (2 V peak to peak) result in the sum of the turn-on and turn-off time being less than 40 ps. The repetition rate is limited by the relaxation oscillation, which can be improved by optimizing MQW structure with large differential gain. The high-speed repetition rate over 5 to 10 GHz was predicted from the calculations.

This analytical and experimental investigation of the two-segmented MQW bistable laser has demonstrated the suitability of the bistable laser for use in all-optical functional devices. I believe that this work can contribute not only to high-speed demultiplexing or data storage in transmission systems, but also to the development of all-optical functional devices.

# Chapter 1  Introduction

This chapter introduces the background of my study, reviews the progress of several studies concerned with my study, states the objectives of this study, and closes with a brief outline of this thesis.

## 1.1  Background

Table 1-1 summarizes the background history for this thesis, which is based on the development of laser diodes, especially the development of the quantum well laser diodes operating at long wavelength range, optical devices using the field effect of quantum wells, and bistable lasers.

### 1.1.1  History of Laser Diodes

Optical signal processing systems not only play very important roles in long-haul communication but are also finding new roles in the chip-to-chip, element-to element, and board-to-board interconnection systems. The semiconductor laser has been an indispensable device in these systems, and the first lasing under pulsed operations was reported in 1962 for the homojunction structure in GaAs systems [1]-[4]. The double heterostructure invented in 1970 [5]-[7] improved the laser diode revolutionarily by making possible room temperature CW operation. The low-loss silica-based optical fiber was reported shortly thereafter [8]. The invention and development of these elements impressed the possibility of optical communication systems, but was first necessary to develop high-performance laser diodes operating in the long wavelength range (1.5 μm) where the optical loss of the silica fiber is theoretically minimum. Following the realization of ultra-low loss optical fiber in 1.5 μm range [9], the first long-wavelength laser diodes, InGaAsP/InP system, were reported in 1979 [10]. This stimulated the

## Table 1-1
### Background history for this thesis.

| year | Laser diode | Quantum-effect optical devices | Bistable laser |
|------|-------------|-------------------------------|----------------|
| 1962 | First lasing (GE, MIT, IBM) | | |
| 1964 | | | First proposal (Lasher et al.) |
| 1970 | R.T. CW | Superlattice proposal (Esaki et al.) | |
| 1975 | QW-LD | | |
| 1977 | 1.5-$\mu$m QW-LD | | |
| 1979 | 1.5-$\mu$m InGaAsP LD (Arai et al.) | | |
| 1982 | | Superlattice APD | |
| 1984 | | SEED (AT & T) | Condition calculation (NEC) |
| << optical-fiber transmission system introduced >> | | | |
| 1985 | | QW modulator | System demonstration (NEC) |
| 1986 | 1.5-$\mu$m SLS-QW-LD (Philips) | InGaAsP/InAlAs Superlattice APD | MQW bistable laser proposal (NTT) |
| 1989 | | | 5-GHz operation (Fujitsu) |
| 1991 | | EARS (NTT) | Set & reset operation (Fujitsu)<br>This work (1989. 9~) |

development not only of laser diodes itself but also of the other optical components, and long-haul optical transmission systems were introduced in 1985.

The introduction of quantum well (QW) structure is one of the most important factors improving the performances of laser diodes. The quantum well laser, reported by van der Ziel et al. in 1975 [11], had a quantum well structure consisting of GaAs/AlGaAs grown by molecular beam epitaxy (MBE). Multiple quantum well (MQW) lasers have several characteristics superior to those of bulk structure lasers: (1) low threshold current [12], (2) high-speed modulation [13], (3) single-mode operation under dynamic operation [14] (4) intrinsic TE mode selection [15]. The first 1.55-$\mu$m MQW laser diodes were achieved in 1977 by using liquid phase epitaxy (LPE) [16] and their performance has since been dramatically improved by using metal organic chemical vapor deposition (MOCVD)[17],[18], gas source molecular beam epitaxy[19] or chemical beam epitaxy[20]. Moreover, the strained-layer superlattice has recently been investigated as a better active medium, and several successful results such as low threshold current, high temperature operation, and reduced linewidth have been reported [21]-[24]. This progress has been made possible by the development of several sophisticated growth techniques enabling the fabrication of crystals less than 100 Å thick and with uniformity of monolayer order.

The visible-wavelength laser has been studied as the light source for recording on a densely packed optical storage medium, for a pointer, or for a bar-code reader. Since the first AlGaInP laser was reported [25],[26], special attention has been paid to wavelength shortening and high-temperature operation [27],[28]. Recently, lasing of blue-green lasers was achieved in II-VI compound materials [29],[30] and that is progressing the short wavelength light source.

## 1.1.2   History of Optical Devices using the Field Effect of Quantum Wells

The quantum well has been an attractive structure from the standpoint of design flexibility as well as its superiority to bulk structure in terms of lasing characteristics. Its

development has also affected the application of optical devices. The first proposal of the quantum well was given in 1970 by Esaki and Tsu [31]. They assumed a periodic structure of several-monolayer thickness of materials with wide and narrow energy gap and they predicted the formation of mini-bands within the energy potential.

Many researchers have since studied the electrical and optical properties of quantum well structures and have shown that their distinctive characteristics include (1) high mobility of the two-dimensional gas in a modulation doped structure [32]; (2) a narrow full width at half maximum of the photoluminescence spectrum [33]; (3) a step-like absorption spectrum reflecting the two-dimensional density of state [34],[35]; (4) the existence of a two-dimensional exciton and its field effect, the so called quantum confined Stark effect (QCSE) [36]; and (5) large optical gain [37]. In terms of applying the quantum well to optical devices, the absorption change due to the field effect as well as the large optical gain are among the most important properties. D.A.B. Miller et al. reported the self-electrooptic-effect device (SEED) [38],[39], which shows hysteresis in the input / output characteristics due to the QCSE. The integration of the SEED and electronic devices have been investigated, and free space optical interconnection systems based on them have been demonstrated [40]-[43]. Memory and switching operations have been performed by exciton absorptive reflection switches (EARS) [44], whose operation is based on the QCSE. The red shift and change of the absorption spectrum are also used in the electroabsorption optical modulator [45],[46]. Very-high-frequency modulation, low chirp and low driving voltage have also been reported. In addition to these devices, the quantum well structure is used in optical switches [47] and in avalanche photodiodes [48]-[50].

### 1.1.3 Required Optical Systems and History of Bistable Lasers

The improved performances and reliability of laser diodes, and the development of quantum-effect optical devices have extended the fields in which optical devices can be applied. The representative system is the long-haul transmission system as shown in

Fig.1-1. It mainly consists of a signal source, a signal line, transmitters, and a receiver. Low-loss optical fiber has increased the distance between transmitters. And in this system, the laser diode is used as an electric-optical (E/O) converter and the photodiode is used as an optical-electric (O/E) converter. The electrical components rather than the optical ones, however, play important roles in three aspects of transmission: retiming, reshaping, and regenerating. This is because the conventional laser diodes and photodetectors lack the functionality needed for conversion of signals. They only linearly interconvert the electrical and optical signals. That's why the total time in the transmitter is the sum of the O/E conversion, signal processing in the transmitter, and E/O conversion.

If there were an optical functional device that could reshape or regenerate the input light signal, the total managing time could be reduced to only the operating time of the functional device. To realize these operations, optical devices that convert the input light nonlinearly is required. I have paid attention to optical bistability for meeting this requirement. The optical bistable device has two stable states in the output light power for some range of input light. This type of device is very advantageous because (i) threshold and memory operations can be easily achieved, (ii) one chip operates as threshold or memory device so that the total number of components can be reduced and the simple systems can be configured, and (iii) the optical device can expand its application into the wavelength domain multiplexed (WDM) systems by combining wavelength conversion operation. A system using optical bistable device is shown in Fig.1-2. Now let me consider what kind of performance is required in the optical device. The bit-rate of the optical data stream in the optical transmission system, optical exchange system or the optical data link is thought to be over Gbit/s. At least, the bistable device has to operate at the speed over the repetition rate in the system. The duration of each time-slot is thus less than 1 ns, so roughly speaking, the transition time from nonlasing to lasing state (which is called "turn-on time" in the following) and that from lasing to nonlasing state (which is called "turn-off time" in the following) must be less than 250 ps. To avoid degradation of the bit-error-rate due to the turn-on delay (pattern effect),
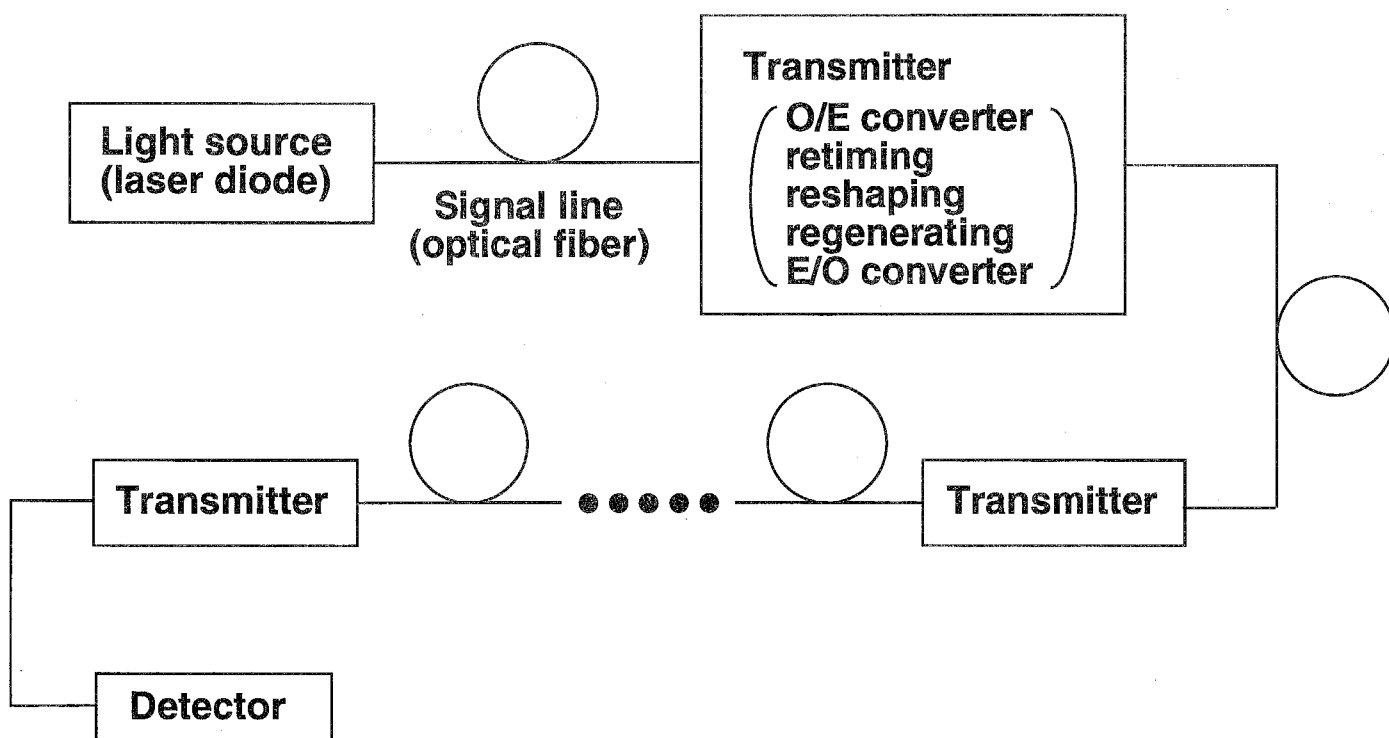
**Fig.1-1**

Optical transmission system.
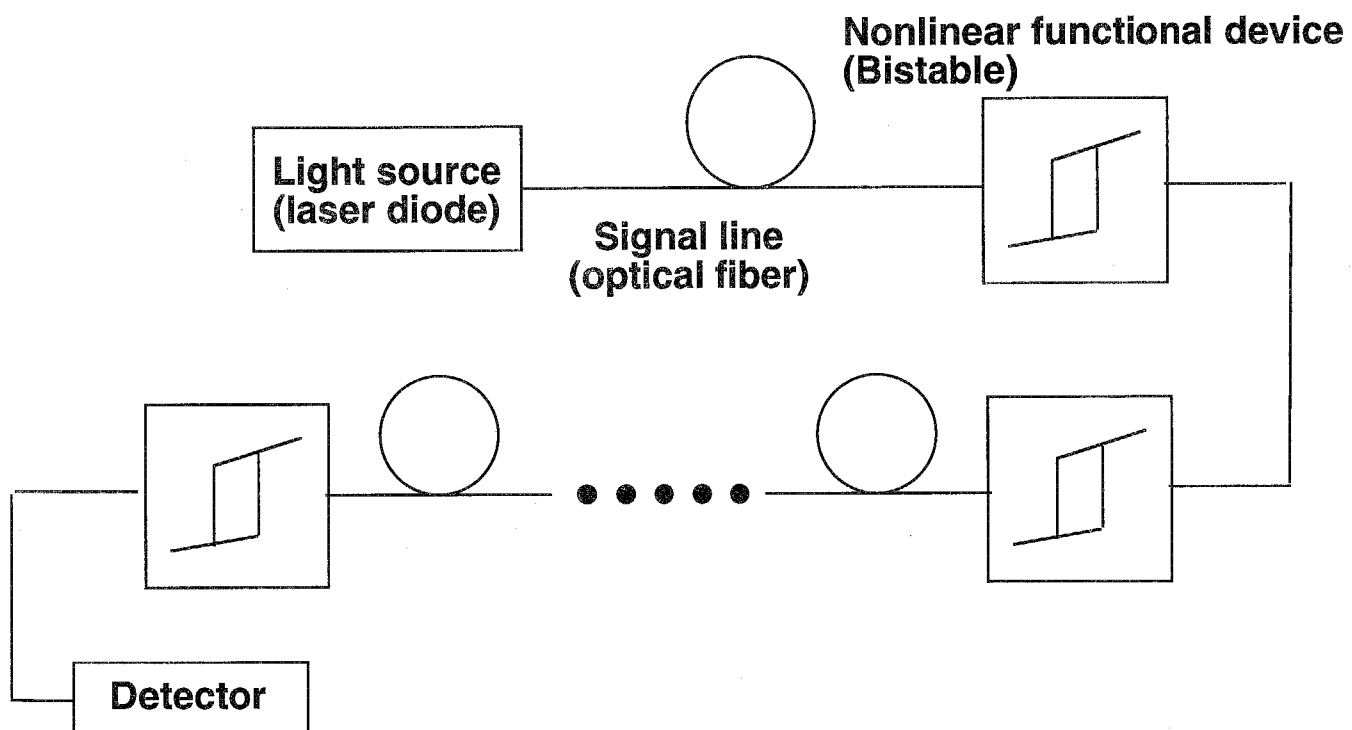
**Fig.1-2**
**All-optical transmission system.**

faster switching time is desired. And also, the bistable device must operate by low input light power to obtain the stable switching operation by the input light signal attenuated through transmission. Moreover, the small dependence of the switching performance on the input light wavelength is required because both input light wavelength and resonance wavelength of the bistable device fluctuate by ambient temperature or the change of carrier density due to modulation. Optical bistable devices must satisfy these requirements for practical use.

Semiconductor bistable devices have superior characteristics such as small size and capability of integration with other semiconductor devices, so their performance has been investigated by many researchers. The bistable devices are mainly divided into two categories: (a) absorptive bistability and (b) dispersive bistability. The operating principle of the absorptive bistability is the absorption saturation when input light power changes. The bistable laser is representative of this type of device [51]-[56]. A device with dispersive bistability, on the other hand, uses the refractive index change that occurs when the input light intensity changes. For example, the nonlinear etalon, semiconductor amplifier, and injection-locking of a semiconductor laser of this type, have been reported [57]-[61]. The switching power, switching time, insertion gain, and wavelength sensitivity of each type are listed in Table 1-2. The bistable laser is considered to be superior to other bistable devices because of its (1) faster switching speed [54], (2) lower switching power [62], (3) larger insertion gain[63], (4) wider wavelength range [64], and (5) larger on/off ratio[62], and its performance meets the system requirements mentioned above.

The bistable laser was first proposed by Lasher et al. in 1964 [65]. Since then, the bistability condition in semiconductor lasers have been studied [66], and segmented-electrode [52]-[56] and partial impurity-diffusion bistable laser [51] have been fabricated. All-optical transmission or exchange systems were demonstrated by using the bistable laser [64],[67],[68]. Odagawa et al. has reported that a repetition frequency of 5 GHz has been reached by using a low-voltage-biased bistable laser [54]. Odagawa's group has also studied the reset operation due to gain quenching effect and has investigated the

## Table 1-2

Comparision of properties of bistable devices.

| property | absorptive | dispersive |
|---|---|---|
| switching power | several microwatts or several femtojoules | several tens of microwatts |
| switching time | < nanoseconds (< carrier lifetime) | several tens of nanoseconds (carrier lifetime limit) |
| insertion gain | > 20 dB | < 0 dB (passive case) |
| wavelength sensitivity | wide > 50 nm (gain bandwidth) | very narrow (several gigahertz) |

dependence of this operation on the input light peak intensity and the pulse width [69]. The MQW structure was introduced into the bistable laser in GaAs/AlGaAs system to control the hysteresis characteristics by adjusting the applied voltage [70]. In addition to intensity bistability, wavelength conversion by the use of bistability [71],[72], the bistability of wavelength in DFB lasers [73],[74] and bistability of input light polarization [75],[76] have been reported.

Conventional bistable lasers show bistability by using nonuniform current injection. In this operating principle, the turn-off time is limited by the carrier lifetime in the saturable absorber. The turn-off time for a MQW bistable laser can be reduced by extracting carriers in the saturable absorber, but the stable switching operation has not yet reported in detail. And also, the reset operation is performed by decreasing injection current down to threshold current, so the switching operation of the conventional bistable laser still depends partly on the electrical signal.

## 1.2 Objectives of this study

The background of this study is summarized as follows:

(1) The reproducibility has been a problem in current-injection-type bistable lasers. And their switching speed is limited by the nanosecond-order carrier lifetime in the saturable absorber.

(2) The multiple quantum well (MQW) structure has been introduced into the bistable laser and the controllability of hysteresis by applied voltage has been reported [70]. But the stable switching operation has not been reported in detail. In addition to this, no precise investigations about the potential of the switching power and the switching speed were given.

(3) There are few reports concerned with devices that show set and reset operations only by input light.

(4) It has become possible to grow high-quality MQW structures in the long wavelength range by using sophisticated crystal growth techniques.

Accordingly, the objectives of this thesis are the following:

(1) Contributing to the construction of all-optical transmission and signal processing systems through investigating the feasibility of the in-line light-injection MQW bistable laser in terms of the controllability and the switching performance.

    (a) Estimating the switching power and switching time by constructing the rate equations taking into account the carrier escape time dependence.

    (b) Evaluating the controllability of the hysteresis characteristics by applied voltage and its dependence on the MQW structures.

    (c) Evaluating the relation between switching power and input light wavelength, and evaluating the turn-on and turn-off time.

(2) Investigating the potentiality of the side-light-injection MQW bistable laser for application to all-optical switching system for the purpose of developing the in-line light-injection MQW bistable laser.

    (a) Estimating the switching power and switching time of the set and reset operations by calculations.

    (b) Verifying the set and reset operations by input light in one device under the same bias conditions.

    (c) Evaluating the switching power and the switching time in both set and reset operations.

## 1.3   Outline of this thesis

The outline of this thesis is as follows.  In Chapter 2, the principle of the bistable laser and the factors limiting its switching speed are reviewed.  It also describes the main

point of introducing the MQW structure. In Chapter 3, the hysteresis characteristics and the switching behavior are estimated by calculations. The rate equations taking into consideration carrier escape time for saturable absorber are constructed. The switching speed limit in the turn-off time is predicted and the dependence of the performance on the MQW structure is discussed. In Chapter 4, the fabrication of two-segmented MQW bistable lasers are described and the their static and dynamic characteristics are examined. This chapter also describes the stable switching behavior and its dependence on MQW structure. In Chapter 5, a new device for all-optical switching, side-light-injection MQW bistable laser, is proposed. Its performance is estimated by solving the rate equations and the lasing and switching characteristics are discussed. In Chapter 6, the predicted performance of the side-light-injection MQW bistable laser is confirmed by evaluating the switching power of the set and reset operations and by evaluating the dependence of switching speed on the input light power. In Chapter 7, the ultimate response of the MQW bistable laser is predicted. The carrier escape time from the MQW structure under applied electric fields is estimated from the measured time response. And the rate equations including the dependence of the carrier escape time on the applied voltage tell us the switching speed limit. The method for realizing the ultimate response is discussed. In Chapter 8, I conclude this thesis.

# References

[1]  R.N. Hall, G.E. Fenner, J.D. Kingsley, T.J. Solty and R.O. Carlson, "Coherent light emission from GaAs junctions", Phys. Rev. Lett., vol.9, pp.366-368, 1962.

[2]  M.I. Nathan, W.P. Dumke, G. Burns, F.H. Dill, Jr. and G. Lasher, "Stimulated emission of radiation from GaAs P-N junctions", Appl. Phys. Lett., vol.1, pp.62-64, 1962.

[3]  N. Holonyak, Jr. and S.F. Bevacqua, "Coherent (visible) light emission from $Ga(As_{1-x}P_x)$ junctions", Appl. Phys. Lett., vol.1, pp.82-83, 1962.

[4]  T.M. Quist, R.H. Rediker, R.J. Keyes, W.E. Krag, B. Lax, A.L. Mcwhorter and H.J. Zeiger, "Semiconductor maser of GaAs", Appl. Phys. Lett., vol.1, pp.91-92, 1962.

[5]  Zh.I. Alferov, V.M. Andreev, D.Z. Garburov, Yu.V. Zhilyaev, E.P. Morozov, E.L. Portnoi and V.G. Trofim, "Investigation of the influence of the AlAs-GaAs heterostructure parameters on the laser threshold current and the realization of continuous emission at room temperature", Sov. Phys. Semicond., vol.4, pp.1573, 1971. (Translated from Fiz. Tekh. Poluprovodn., vol.4, pp.1826, 1970.)

[6]  I. Hayashi, M.B. Panish, P.W. Foy and A. Sumski, "Junction lasers which operate continuously at room temperature", Appl. Phys. Lett., vol.17, pp.109-111, 1970.

[7]  H. Kressel and F.Z. Hawrylo, "Fabry-Perot structure $Al_xGa_{1-x}As$ injection lasers with room temperature threshold current densities of 2530 $A/cm^2$", Appl. Phys. Lett., vol.17, pp.169-171, 1970.

[8]  F.P. Kapron, D.B. Keck and R.D. Maurer, "Radiation losses in glass optical waveguides", Appl. Phys. Lett., vol.17, pp.423-425, 1970.

[9]  M. Horiguchi and H. Osanai, "Spectral losses of low-OH-content optical fibres", Electron. Lett., vol.12, pp.310-312, 1976.

[10] S. Arai, M. Asada, Y. Suematsu and Y. Itaya, "Room temperature CW operation of GaInAsP/InP DH laser emitting at 1.51 μm", Jpn. J. Appl. Phys., vol.18, pp.2333-2334, 1979.

[11] J.P. van der Ziel, R. Dingle, R.C. Miller, W. Wiegmann and W.A. Nordland, Jr., "Laser oscillation from quantum well states in very thin GaAs-Al$_{0.2}$Ga$_{0.8}$As multilayer structures", Appl. Phys. Lett., vol.26, pp.463-465, 1975.

[12] W.T. Tsang, "Extremely low threshold (AlGa)As modified multiquantum well heterostructure lasers grown by molecular-beam epitaxy", Appl. Phys. Lett., vol.39, pp.786-788, 1981.

[13] K. Uomi, T. Mishima and N. Chinone, "Ultrahigh relaxation oscillation frequency (up to 30 GHz) of highly p-doped GaAs/GaAlAs multiple quantum well lasers", Appl. Phys. Lett., vol.51, pp.78-80, 1987.

[14] H. Iwamura, T. Saku, T. Ishibashi, K. Otsuka and Y. Horikoshi, "Dynamic behaviour of a GaAs-AlGaAs MQW laser diode", Electron. Lett., vol.19, pp.180-181, 1983.

[15] H. Iwamura, T. Saku, H. Kobayashi and Y. Horikoshi, "Spectrum studies on a GaAs-AlGaAs multi-quantum-well laser diode grown by molecular beam epitaxy", J. Appl. Phys., vol.54, pp.2692-2695, 1983.

[16] E.A. Rezek, N. Holonyak, Jr., B.A. Vojak, G.E. Stillman, J.A. Rossi, D.L. Kenne and J.D. Fairing, "LPE In$_{1-x}$Ga$_x$P$_z$As$_{1-z}$ (x~0.12, z~0.26) DH laser with multiple thin-layer (< 500 Å) active region", Appl. Phys. Lett., vol.31, pp.288-290, 1977.

[17] S. Takano, T. Sasaki, H. Yamada, M. Kitamura, I. Mito and T. Suzuki, "Improvements in resonance frequency and T$_0$ value by 1.5 μm InGaAs MQW lasers grown by MOVPE", J. Crystal Growth, vol.93, pp.857-862, 1988.

[18] A. Kasukawa, R. Bhat, S.A. Schwarz, D.M. Hwang, M.A. Koza and T.P. Lee, "Low threshold current density 1.5 μm GaInAs/AlGaInAs graded-index separate-confinement-heterostructure quantum well laser diodes grown by metal organic chemical vapor deposition", Electron. Lett., vol.27, pp.1063-1064, 1991.

[19] Y. Kawamura, A. Wakatsuki, Y. Noguchi and H. Iwamura, "InGaAs/InGaAlAs MQW lasers with InGaAsP guiding layers grown by gas source molecular beam epitaxy", IEEE Photon. Technol. Lett., vol.3, pp.960-962, 1991.

[20] W.T. Tsang, "Chemical beam epitaxial growth of very low threshold $Ga_{0.47}In_{0.53}As/InP$ double-heterostructure and multiple quantum well lasers", Appl. Phys. Lett., vol.19, pp.1010-1012, 1986.

[21] P.J.A. Thijs and T. van Dongen, "High quantum efficiency, high power, modulation doped InGaAs strained-layer quantum well laser diodes emitting 1.55 $\mu$m", Electron. Lett., vol.25, pp.1735-1737, 1989.

[22] L.E. Eng, A. Sa'ar, T.R. Chen, I. Grave, N. Kuze and A. Yariv, "Microampere threshold current operation of GaAs and strained InGaAs quantum well lasers at low temperature", Appl. Phys. Lett., vol.58, pp.2752-2754, 1991.

[23] P.J.A. Thijs, L.F. Tiemeijer, P.I. Kuindersma, J.J.M. Binsma and T. van dongen, "High performance 1.5 $\mu$m wavelength InGaAs-InGaAsP strained quantum well lasers and amplifiers", IEEE J. Quantum Electron., vol.27, pp.1426-1439, 1991.

[24] M. Okai, M. Suzuki and T. Taniwatari, "Strained multiquantum-well corrugation-pitch-modulated distributed feedback laser with ultranarrow (3.6 kHz) spectral linewidth", Electron. Lett., vol.29, pp.1696-1697, 1993.

[25] Y. Kawamura, H. Asahi, N. Nagai and T. Ikegami, "0.66 $\mu$m room temperature operation of InGaAlP DH laser diodes grown by MBE", Electron. Lett., vol.18, pp.163-165, 1983.

[26] I. Hino, A. Gomyo, K. Kobayashi, T. Suzuki and K. Nishida, "Room-temperature pulsed operation of AlGaInP/GaInP/AlGaInP double heterostructure visible light laser diodes grown by metalorganic chemical vapor deposition", Appl. Phys. Lett., vol.43, pp.987-989, 1983.

[27] J. Rennie, M. Okajima, M. Watanabe and G. Hatakoshi, "High temperature ($74°C$) CW operation of 634 nm InGaAlP laser diodes utilizing a multiple quantum barrier", IEEE J. Quantum Electron., vol.19, pp.1857-1862, 1993.

[28] H. Hamada, R. Hiroyama, S. Honda, M. Shono, K. Yodoshi and T. Yamaguchi, "AlGaInP strained multiple-quantum-well visible laser diodes ($\lambda_L \leqq 630$ nm band) with a multiquantum barrier grown on misoriented substrates", IEEE J. Quantum Electron., vol.29, pp.1844-1850, 1993.

[29] M.A. Haase, J. Qiu, J.M. DePuydt and H. Cheng, "Blue-green laser diodes", Appl. Phys. Lett., vol.59, pp.1272-1274, 1991.

[30] N. Nakayama, S. Itoh, T. Ohata, K. Nakano, H. Pkuyama, M. Ozawa, A. Ishibashi, M. Ikeda and Y. Mori, "Room temperature continuous operation of blue-green laser diodes", Electron. Lett., vol.29, pp.1488-1489, 1993.

[31] L. Esaki and R. Tsu, "Superlattice and negative differential conductivity in semiconductors", IBM J. Res. Develop., vol.14, pp.61-68, 1970.

[32] R. Dingle, H.L. Störmer, A.C. Gossard and W. Wiegmann, "Electron mobilities in modulation-doped semiconductor heterojunction superlattices", Appl. Phys. Lett., vol.33, pp.665-667, 1978.

[33] T. Ishibashi, Y. Suzuki and H. Okamoto, "Photoluminescence of an AlAs/GaAs superlattice grown by MBE in the 0.7-0.8 $\mu$m wavelength region", Jpn. J. Appl. Phys., vol.20, pp.L623-L626, 1981.

[34] T. Ishibashi, S. Tarucha and H. Okamoto, "Exciton associated optical absorption spectra of AlAs/GaAs superlattice at 300 K", in Proc. Int. Symp. GaAs Related Compounds, Inst. Phys. Conf. Ser. No.63, pp.587-588, 1981.

[35] D.A.B. Miller, D.S. Chemla, P.W. Smith, A.C. Gossard and W.T. Tsang, "Room-temperature saturation characteristics of GaAs-GaAlAs multiple quantum well structures and of bulk GaAs", Appl.Phys., vol.B28, pp.96-97, 1982.

[36] D.S. Chemla, T.C. Damen, D.A.B. Miller, A.C. Gossard and W. Wiegmann, "Electroabsorption by Stark effect on room-temperature excitons in GaAs/GaAlAs multiple quantum well structures", Appl. Phys. Lett., vol. 42, pp.864-866, 1983.

[37] M. Asada, A. Kameyama and Y. Suematsu, "Gain and intervalence band absorption in quantum-well lasers", IEEE J. Quantum Electron., vol.20, pp.745-753, 1984.

[38] D.A.B. Miller, D.S. Chemla, T.C. Damen, A.C. Gossard, W. Wiegmann, T.H. Wood and C.A. Burrus, "Novel hybrid optically bistable switch: The quantum well self-electro-optic effect device", Appl. Phys. Lett., vol.45, pp.13-15, 1984.

[39] D.A.B. Miller, D.S. Chemla, T.C. Damen, T.H. Wood, C.A. Burrus, A.C. Gossard and W. Wiegmann, "The quantum well self-electrooptic effect device:

optoelectronic bistability and oscillation, and self-linearized modulation", IEEE J. Quantum Electron., vol.21, pp.1462-1476, 1985.

[40] A.L. Lentine, H.S. hinton, D.A.B. Miller, J.E. Henry, J.E. Cunningham and L.M.F. Chirovsky, "Symmetric self-electrooptic effect device: Optical set-reset latch, differential logic gate, and differential modulator/detector", IEEE J. Quantum Electron., vol.25, pp.1928-1936, 1989.

[41] A.L. Lentine, D.A.B. Miller, J.E. Henry, J.E. Cunningham and L.M.F. Chirovsky, "Multistate self-electrooptic effect devices", IEEE J. Quantum Electron., vol.25, pp.1921-1927, 1989.

[42] A.L. Lentine, D.A.B. Miller, J.E. Henry, J.E. Cunningham, L.M.F. Chirovsky and L.A. D'Asaro, "Optical logic using electrically connected quantum well PIN diode modulators and detectors", Appl. Opt., vol.29, pp.2153-2163, 1990.

[43] D.A.B. Miller, M.D. Feuer, T.Y. Chang, S.C. Shunk, J.E. Henry, D.J. Burrows and D.S. Chemla, "Field-effect transistor self-electrooptic effect device: integrated photodiode, quantum well modulator and transistor", IEEE Photon. Technol. Lett., vol.1, pp.61-64, 1989.

[44] C. Amano, S. Matsuo and T. Kurokawa, "Novel photonic switch arrays consisting of vertically integrated multiple-quantum-well reflection modulators and phototransistors: exciton absorptive reflection switch", IEEE Photon. Technol. Lett., vol.3, pp.736-738, 1991.

[45] T. H. Wood, "Multiple quantum well (MQW) waveguide modulators", J. Lightwave Technol., vol.6, pp.743-757, 1988.

[46] K. Wakita, Y. Kawamura, Y. Yoshikuni, H. Asahi and S. Uehara, "Anisotropic electroabsorption and optical modulation in InGaAs/InAlAs multiple quantum well structures", IEEE J. Quantum Electron., vol.22, pp.1831-1836, 1986.

[47] H. Yamamoto, M. Asada and Y. Suematsu, "Intersectional waveguide type optical switch with quantum well structure", Trans. IECE Japan, vol.E68, pp.737-739, 1985.

[48] F. Capasso, W.T. Tsang, A.L. Hutchinson and D.F. Williams, "Enhancement of electron impact ionization in a superlattice : A new avalanche photodiode with a large ionization rate ratio", Appl. Phys. Lett., vol.40, pp.38-40, 1982.

[49] T. Kagawa, Y. Kawamura and H. Iwamura, "InGaAsP-InAlAs superlattice avalanche photodiodes", IEEE J. Quantum Electron., vol.28, pp.1419-1423, 1992.

[50] I. Watanabe, S. Sugou, H. Ishikawa, T. Anan, K. Makita, M. Tsuji and K. Taguchi, "High-speed and low-dark-current flip-chip InAlAs/InAlGaAs quaternary well superlattice APD's with 120 GHz gain-bandwidth product", IEEE Photon. Technol. Lett., vol.5, pp.675-677, 1993.

[51] H. Kawaguchi and G. Iwane, "Bistable operation in semiconductor lasers with inhomogeneous excitation", Electron. Lett., vol.17, pp.167-168, 1981.

[52] H. Kawaguchi, "Bistable operation of semiconductor lasers by optical injection", Electron. Lett., vol.17, pp.741-742 , 1981.

[53] Y. Odagiri, "Bistable laser-diode memory for optical time-division switching applications", presented at Conf. Lasers Electrooptics, THJ3, 1984.

[54] T. Odagawa, T. Machida, K. Tanaka, T. Sanadaand and K. Wakao, "Fast optical flip-flop operations of bistable laser diodes", Trans. IEICE, vol. J74-C-I, pp.465-479, 1991.

[55] H. Uenohara, H. Iwamura and M. Naganuma, "Switching characteristics of InGaAs/InP multiquantum well voltage-controlled bistable laser diodes", Jpn. J. Appl. Phys., vol. 29, pp. L2442-L2444, 1990.

[56] H. Uenohara, Y. Kawamura, H. Iwamura, K. Nonaka, H. Tsuda and T. Kurokawa, "Operation characteristics of a side-light-injection multiple-quantum-well bistable laser for all-optical switching", Jpn. J. Appl. Phys., vol. 33, pp. 815-821, 1994.

[57] P.W. Smith, E.H. Turner and P.J. Maloney, "Electrooptic nonlinear Fabry-Perot devices", IEEE J. Quantum Electron., vol.14, pp.207-212, 1978.

[58] H.M. Gibbs, S.S. Tarng, J.L. Jewell, D.A. Weinberger, K. Tai, A.C. Gossard, S.L. McCall, A. Passner and W. Wiegmann, "Room-temperature excitonic optical

bistability in a GaAs-GaAlAs supperlattice etalon", Appl. Phys. Lett., vol.41, pp.221-222, 1982.

[59] K. Otsuka and H. Iwamura, "Analysis of a multistable semiconductor light amplifier", IEEE J. Quantum Electron., vol.19, pp.1184-1186, 1983.

[60] K. Otsuka and S. Kobayashi, "Optical bistability and nonlinear resonance in a resonant-type semiconductor laser amplifier", Electron. Lett., vol.19, pp.262-263, 1983.

[61] H. Kawaguchi, "Bistable output characteristics in semiconductor laser injection locking", IEEE J. Quantum Electron., vol.21, pp.1314-1317, 1985.

[62] P. Blixt and U. Öhlander, "Femtojoule bistable optical switching of inhomogeneously pumped laser diode at 500 MHz using mode-locked tunable diode laser", Electron. Lett., vol.25, pp.699-700, 1989.

[63] H. Kawaguchi, "Optical input and output characteristics for bistable semiconductor lasers", Appl. Phys. Lett., vol.41, pp.702-704, 1982.

[64] S. Suzuki, T. Terakado, K. Komatsu, K. Nagashima, A. Suzuki and M. Kondo, "Experiment on high-speed optical time-division switching", J. Lightwave Technol., vol.4, pp.894-899, 1986.

[65] G.L. Lasher, "Analysis of a proposed bistable injection laser", Solid State Electron., vol.7, pp.707-716, 1964.

[66] M. Ueno and R. Lang, "Conditions for self-sustained pulsation and bistability in semiconductor lasers", J. Appl. Phys., vol.58, pp.1689-1692, 1985.

[67] M. Jinno and T. Matsumoto, "All-optical timing extraction using a 1.5 μm self pulsating multielectrode DFB LD", Electron. Lett., vol.24, pp. 1426-1427, 1988.

[68] T. Shimoe, S. Kuroyanagi, K. Murakami, H. Rokugawa, N. Mekada and T. Odagawa, "An experimental 512 Mbps time-division photonic switching system", in Tech. Dig. Photon. Switching, 1989, FC2, pp.136-138.

[69] T. Odagawa and S. Yamakoshi, "Optical set-reset operations of bistable laser diode with single-wavelength light", Electron. Lett., vol.25, pp.1428-1429, 1989.

[70] S. Tarucha and H. Okamoto, "Voltage-controlled optical bistability associated with two-dimensional exciton in GaAs-AlGaAs multiple quantum well lasers", Appl. Phys. Lett., vol.49, pp.543-545, 1986.

[71] H. Kawaguchi, K. Magari, H. Yasaka, M. Fukuda and K. Oe, "Tunable optical-wavelength conversion using an optically triggerable multielectrode distributed feedback laser diode", IEEE J. Quantum Electron., vol.24, pp.2153-2159, 1988.

[72] S. Yamakoshi, K. Kondo, M. Kuno, Y. Kotaki and H. Imai, "An optical-wavelength conversion laser with tunable range of 30 Å", OFC'88, postdeadline paper PD10, Jan., 1988.

[73] H. Shoji, Y. Arakawa and Y. Fujii, "New bistable wavelength switching device using a two-electrode distributed feedback laser", Electron. Lett., vol.24, pp.888-889, 1988.

[74] M. Kuznetsov, "Picosecond switching dynamics of a bistable-wavelength-latch two-segment distributed feedback laser", IEEE Photon. Technol. Lett., vol.2, pp.623-625, 1990.

[75] Y. Mori, "Dynamic properties of transverse-magnetic wave injected semiconductor lasers", IEEE J. Quantum Electron., vol.27, pp.2415-2421, 1991.

[76] H. Kawaguchi, I.H. White, M.J. Offside and J.E. Carroll, "Ultrafast switching in polarization-bistable laser diodes", Opt. Lett., vol.17, pp.130-132, 1992.

# Chapter 2  Principle and Expected Performances of Bistable Lasers

This chapter introduces the principle of the bistable laser operation. The basic principle of the voltage-controlled-type bistable laser with a multiple quantum well structure is compared with that of the conventional current-injection-type bistable laser. Then the expected performances in terms of its switching speed limit are described.

## 2.1  Principle of Bistable Laser

The basic principle of the bistable laser is that a saturable absorber is introduced into the laser cavity. Bistability is mainly divided into two categories: (1) absorptive bistability [1]-[4], (2) dispersive bistability [5]-[9]. The bistable laser that is being paid attention in this study is the absorptive bistability. It is well known that the uniform injection laser diodes sometimes show kink or self-sustained pulsation in the light output versus current characteristics when some kind of damage exists in the laser cavity. This is because the damage does not work as the gain medium but it absorbs the light in the cavity. The relation between absorption and light intensity is not linear and absorption saturates at large light intensity. That is why this kind of absorber is called a "saturable absorber." The main problem with this device is that the damage is introduced by happening and we cannot obtain lasers whose characteristics are reproducible.

The main purpose of constructing the segmented electrode laser is to introduce the saturable absorber intentionally. Figure 2-1 schematically shows the conventional current-injection-type bistable laser. Its active region typically consists of bulk material. The two electrodes are electrically separated by removing the contact layer or by proton-implanted high-resistance region. The shorter region is usually used as a saturable absorption region and the other works as a gain region. Currents are injected into both regions, but the injection levels are not uniform. The current density of the gain region is set higher than that of the saturable absorption region.
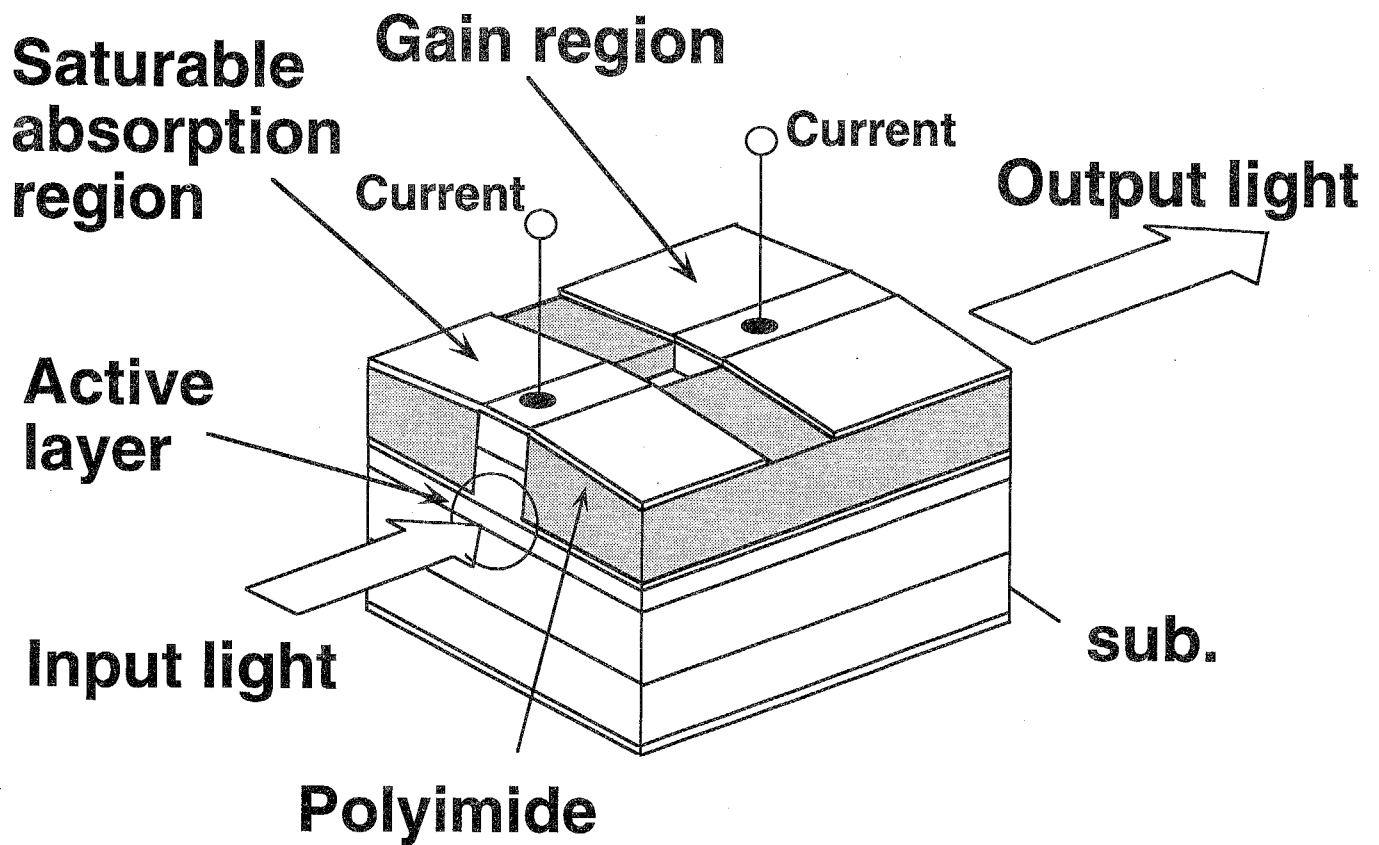
**Fig. 2-1**

Schematic view of a conventional current-injection-type
two-segmented bistable laser.

The carrier distributions in each region is illustrated in Fig.2-2. The energy band in both regions are depicted. C.B. and V.B. means conduction and valence band, respectively. The Fermi level in the saturable absorption region is lower than that in the gain region, so that the emission light from the gain region is absorbed in the saturable absorption region. When the electrons are excited to the conduction band, the Fermi level moves toward the higher energy because of the increase in the total amount of electrons. Too much excitation of electrons prevents more excitation because of the shortage of electron states in the conduction band. This results in the decrease of absorption in the saturable absorption region. And this also briefly explains the reason for the semiconductor showing saturable absorption when the input light intensity is high.

In a semiconductor laser, the high-intensity light corresponds to the amplified spontaneous or stimulated emission under high current injection or light injection. Once the saturable absorption region becomes "transparent" due to absorption saturation, the stimulated emission is strongly amplified by positive feedback effect. Then the lasing occurs suddenly and the output light changes its state from spontaneous emission (OFF) to lasing (ON). On the other hand, the decrease of the light intensity in the laser cavity with lowering the current injection or disappearance of the injection light reduces the amount of electrons in the conduction band because of radiative or nonradiative recombination. In this situation, the lasing state is maintained when the carrier recombination rate is slower than the carrier excitation rate; that is, when the carrier lifetime is rather long. Thus the bistability, which is represented as the hysteresis in the light output versus current characteristics, emerges.

The controllability of hysteresis characteristics was improved by the two-segment structure mentioned above. But the current-injection-type bistable laser is not satisfactory in terms of the switching speed because the saturable absorption region is large, typically larger than one tenth the size of the gain region. The reason for the large absorption region is that the hysteresis is caused by inhomogeneous current injection into two-segmented regions. Although the saturable absorption region causes absorption in the laser cavity, the absorption efficiency is comparatively small because of current injection.
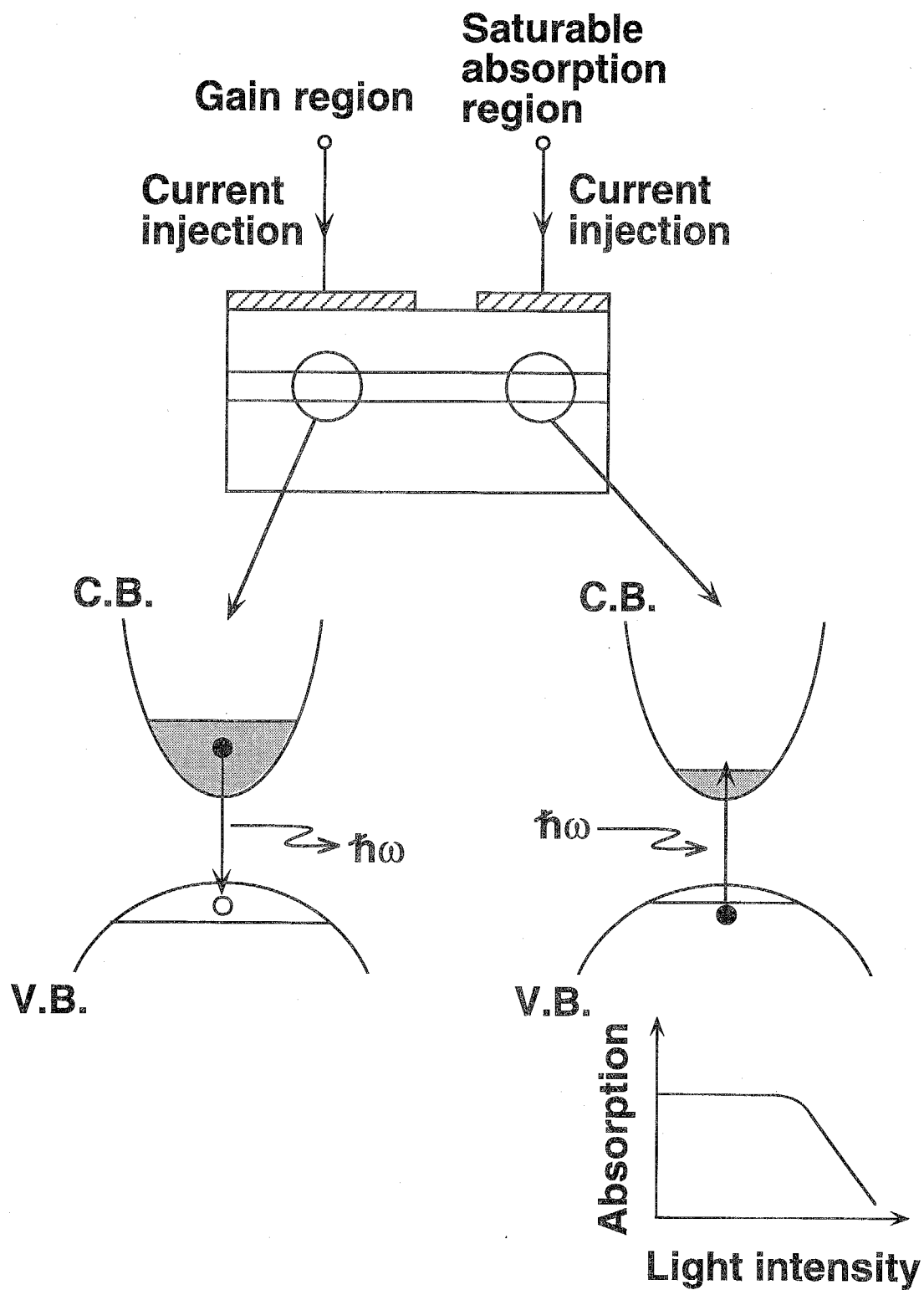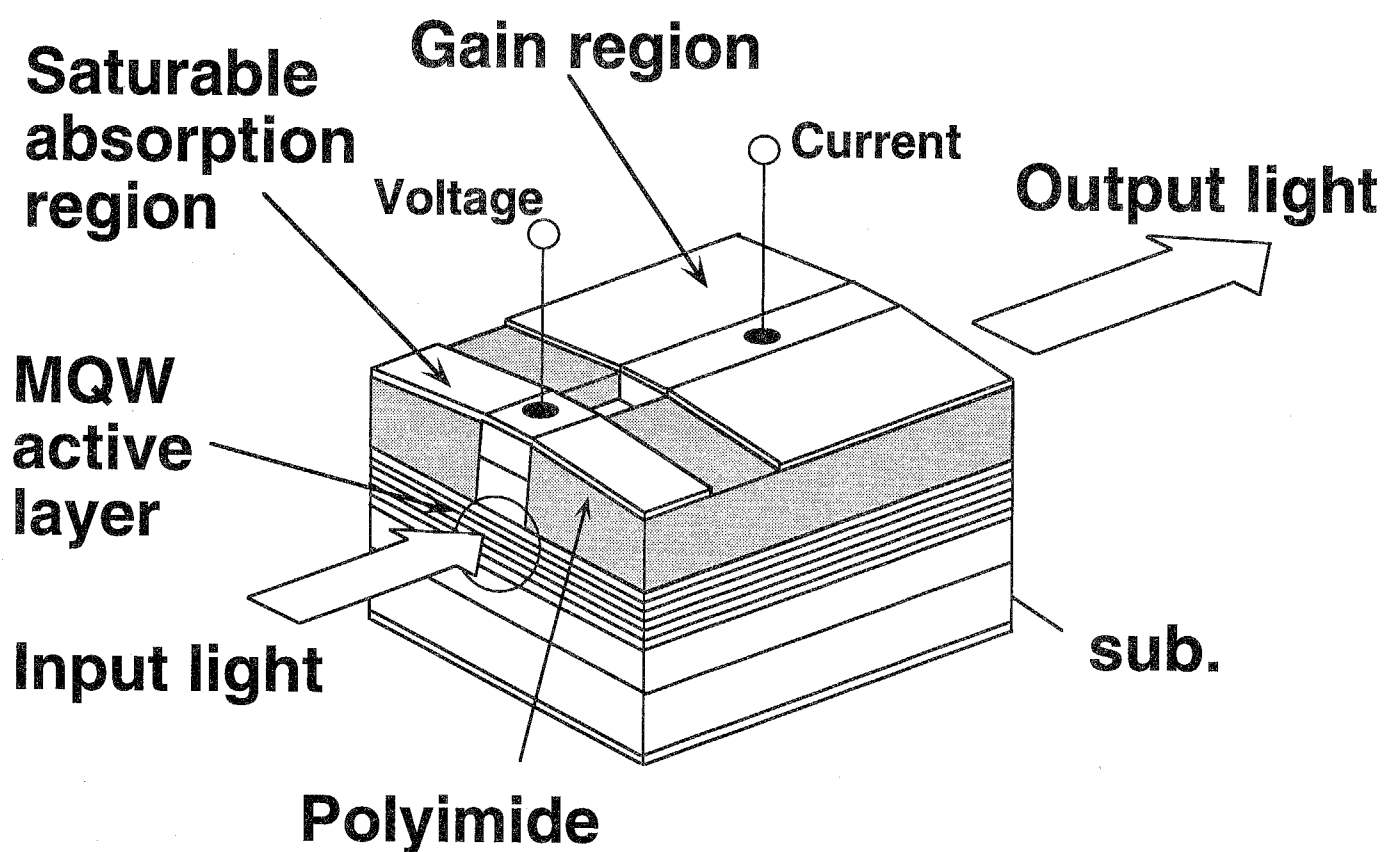
Fig. 2-2

The condition of the bistable operation. The carrier distributions in the
conduction band (C.B.) and in the valence band (V.B.) are shown in the
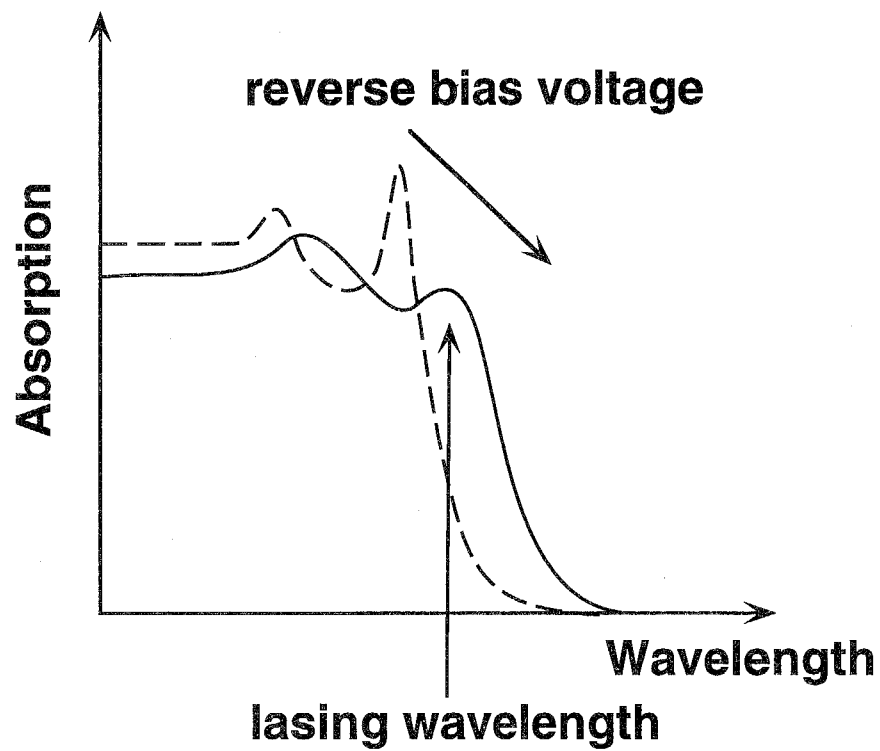gain region, and the saturable absorption region.

That is another reason for the low reproducibility of the device. Moreover, the large electrode results in the large parasitic capacitance and that degrades RF frequency response.

To overcome this problem and to improve the controllability of the hysteresis characteristics, field effect of the MQW structure is introduced to the segmented bistable laser. This method is proposed first by Tarucha et al. [10] in the GaAs/AlGaAs systems, and I have studied the MQW bistable laser in the long wavelength system [11],[12]. The schematic view of the two-segmented MQW bistable laser is shown in Fig.2-3. The structure is almost the same as that of conventional current-injection-type as seen in Fig.2-1. The main differences are that the active region consists of a MQW structure and that the saturable absorption region is much shorter. In this device, the basic control of the saturable absorber is by applied voltage, not injected current. Voltage-controlled-type bistable laser was reported by Odagawa et al, but the active region consisted of bulk structure [4]. The absorption can be easily changed by the externally applied voltage because of the field effect of the MQW. And also, the large differential gain in the MQW structure intrinsically causes high frequency operation. Figure 2-4 illustrates how absorption spectrum of the QW changes with wavelength. The dashed line represents the absorption spectrum with no bias. Because of the band shrinkage effect, the lasing wavelength (shown by the arrow) is usually longer than the absorption peak wavelength (heavy-hole exciton peak) [13]. When the voltage is applied to the absorber and the bias is reduced, the absorption peak shifts toward longer wavelengths. This is the so-called the quantum confined Stark effect (QCSE). This peak shift causes the absorption change larger than that of bulk structure. The absorption can thus be changed by the applied voltage and it is easy to control hysteresis characteristics. Moreover, because the absorption is large in the QW structure, the width of the saturable absorber can be small. From these reasons, the MQW bistable laser is expected to show superior reproducibility.

**Saturable absorption region**

**Gain region**

Voltage

Current

**Output light**

**MQW active layer**

**Input light**

**Polyimide**

**sub.**

**Fig. 2-3**

**Schematic view of a two-segmented MQW bistable laser.**

**Fig. 2-4**

Absorption spectrum of a QW structure and its change by applied voltage.
This field effect is called the quantum confined Stark effect.

## 2.2 Switching Speed Limit of Bistable Lasers

The switching speed of the bistable laser is defined by the turn-on time, the turn-off time, and the interval between the last reset signal and the following set signal. In a conventional bistable laser, the turn-off time is the limiting factor because it is limited by the nanosecond-order carrier lifetime.

The difference between the switching speed limit of the MQW bistable laser and that of the current-injection-type laser is due to their operating principles. As mentioned in section 2.1, absorption in the current-injection-type bistable laser recovers by the carrier recombination. This is shown in Fig.2-5(a). The radiative recombination of carriers occurs on the order of nanoseconds when the injection current density is about $10^{18}$ cm$^{-3}$. The turn-off time can be reduced to be less than carrier lifetime, but the output light from the bistable laser show long tail with nanosecond order. To estimate the turn-off time, I solve the rate equations constructed by Ueno et al. as follows [14], [15]:

$$\frac{dn_g}{dt} = \frac{J_g}{ed} - v_g G_g S - \frac{n_g}{\tau_g} \tag{2.1}$$

$$\frac{dn_a}{dt} = \frac{J_a}{ed} - v_g G_a S - \frac{n_a}{\tau_a} \tag{2.2}$$

$$\frac{dS}{dt} = v_g \xi (1-h) G_g S + v_g \xi h G_a S + \beta \xi (1-h) \frac{n_g}{\tau_g} + \beta \xi h \frac{n_a}{\tau_a} - \frac{S}{\tau_p} + P_{in} \tag{2.3}$$

where $n_i$ (i=g, a) is carrier density, S is photon density, $\tau_i$ (i=g, a) is carrier lifetime, $\tau_{nr}$ is nonradiative recombination time, $\tau_p$ is photon lifetime, $v_g$ is group velocity in the cavity, $G_i$ (i=g, a) is optical gain, h is the ratio of the saturable absorption region to the cavity length, $\beta$ is spontaneous emission factor, $\xi$ is the optical confinement factor, and $P_{in}$ is injected photon rate coupled into the laser cavity. The suffixes g and a in the equations represent the gain region, and saturable absorption region, respectively. Equations (2.1) and (2.2) represent the change of carrier density in the gain and saturable

absorption region, respectively and eqn. (2.3) expresses the change of photon density. In this case, the photon density is assumed to be uniform in the cavity. Optical gain $G_i$ is assumed to be linear with carrier density, and is given by $G_i = g_i (n_i - n_0) \cdot (1 - \varepsilon S)$, where $n_0$ is the transparency carrier density and $\varepsilon$ is the nonlinear gain coefficient. The carrier lifetime in the gain region is attributed to the spontaneous emission, so it is expressed as $\tau_i = 1/(B_{eff} \cdot n_i)$ where $B_{eff}$ is effective recombination coefficient. The calculated time response of reset operation is shown in Fig. 2-5(b). The parameters used in the calculation is listed in Table 2-1. As mentioned above, the output light intensity decreases rapidly just after the reset current pulse but shows following long tail.

For the purpose of reducing the carrier lifetime, proton bombardment in the saturable absorber has been reported [16]. But further study about the reliability of the proton-bombarded device is needed to be evaluated more extensively.

The MQW bistable laser, on the other hand, has the advantage of its driving condition because the voltage is applied to the absorber. And the small absorber allows the device to operate under an applied reverse bias voltage. That situation is illustrated in Fig.2-6. The excited carriers in the saturable absorber are extracted by the external applied electric field, so the turn-off time is limited by the carrier escape time rather than the recombination time. The carrier escape time depends on the electric field, and high-speed reset operation is expected when the high electric field is applied as a reset signal. The theoretical limit to switching speed is investigated in Chapter 7.
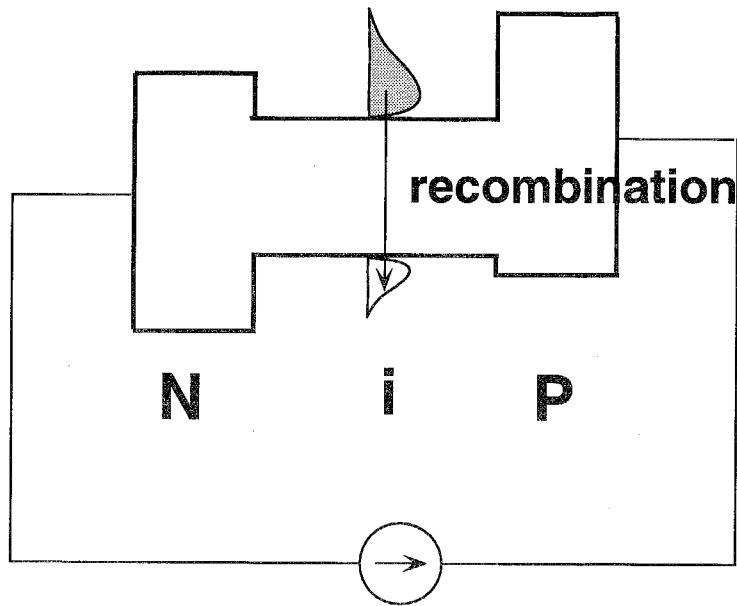
**(a) Schematic of carrier recombination**
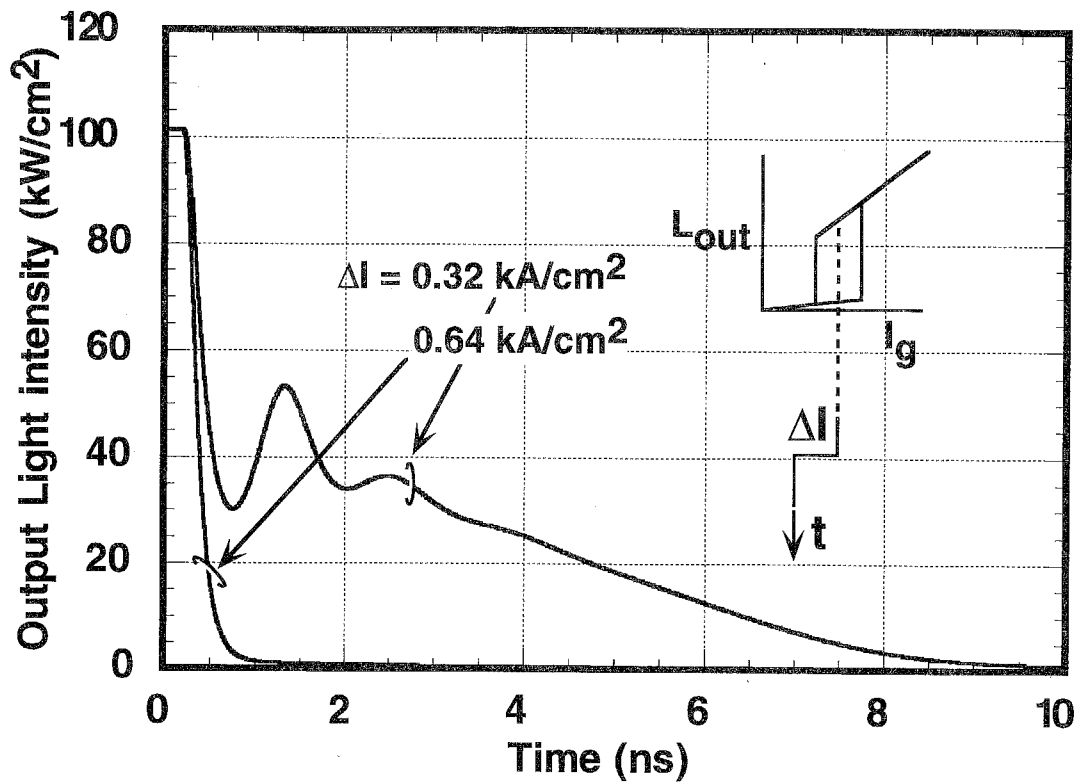


**(b) Turn-off response (Calculation)**

Fig. 2-5

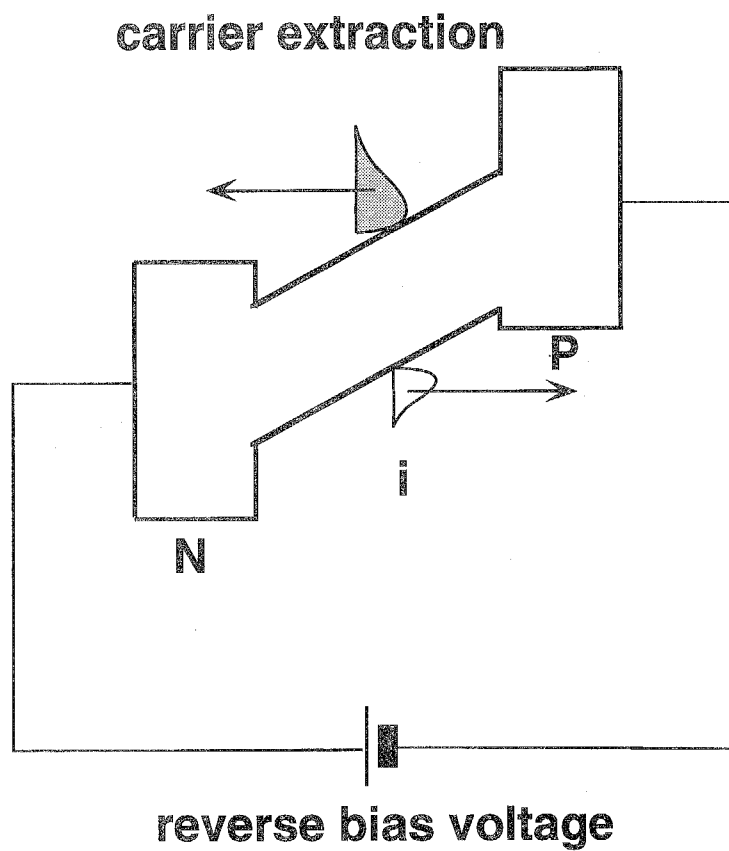Reset operation of current-injection-type bistable laser.
(a) Schematic of carrier recombination in the saturable absorption region
and (b) calculation results of turn-off response.

## Table 2-1

**Numerical values used in the calculations of two-segmented current-injection-type bistable laser.**

| Parameter | Value |
|---|---|
| $g_g$ | $1.35 \times 10^{-16} \, \text{cm}^2$ |
| $g_1$ | $1.35 \times 10^{-16} \, \text{cm}^2$ |
| $\varepsilon$ | $1.0 \times 10^{-17} \, \text{cm}^3$ |
| $\xi$ | $0.14$ |
| $n_0$ | $1.25 \times 10^{18} \, \text{cm}^{-3}$ |
| $B_{eff}$ | $1.0 \times 10^{-10} \, \text{cm}^3/\text{s}$ |
| $\beta$ | $1.0 \times 10^{-5}$ |
| $h$ | $0.5$ |
| $J_a$ | $0 \, \text{kA/cm}^2$ |

carrier extraction

P

i

N

reverse bias voltage

Fig. 2-6

Schematic of reset operation of this work (Carrier extraction by applied voltage).

# References

[1] H. Kawaguchi and G. Iwane, "Bistable operation in semiconductor lasers with inhomogeneous excitation", Electron. Lett., vol.17, pp.167-168, 1981.

[2] H. Kawaguchi, "Bistable operation of semiconductor lasers by optical injection", Electron. Lett., vol.17, pp.741-742, 1981.

[3] Y. Odagiri, "Bistable laser-diode memory for optical time-division switching applications", presented at Conf. Lasers Electroopticas, THJ3, 1984.

[4] T. Odagawa, T. Machida, K. Tanaka, T. Sanada and K. Wakao, "Fast optical flip-flop operations of bistable laser diodes", Trans. IEICE, vol. J74-C-I, pp.465-479, 1991.

[5] P.W. Smith, E.H. Turner and P.J. Maloney, "Electrooptic nonlinear Fabry-Perot devices", IEEE J. Quantum Electron., vol.14, pp.207-212, 1978.

[6] K. Otsuka and H. Iwamura, "Analysis of a multistable semiconductor light amplifier", IEEE J. Quantum Electron., vol.19, pp.1184-1186, 1983.

[7] K. Otsuka and S. Kobayashi, "Optical bistability and nonlinear resonance in a resonant-type semiconductor laser amplifier", Electron. Lett., vol.19, pp.262-263, 1983.

[8] H. Kawaguchi, "Bistable output characteristics in semiconductor laser injection locking", IEEE J. Quantum Electron., vol.21, pp.1314-1317, 1985.

[9] K. Kobayashi, H. Nishino and R. Lang, "Experimental observation of asymmetric detuning characteristics in semiconductor laser injection locking", Electron. Lett., vol.18, pp.54-56, 1982.

[10] S. Tarucha and H. Okamoto, "Voltage-controlled optical bistability associated with two-dimensional exciton in GaAs-AlGaAs multiple quantum well lasers", Appl. Phys. Lett., vol.49, pp.543-545, 1986.

[11] H. Uenohara, H. Iwamura and M. Naganuma, "Switching characteristics of InGaAs/InP multiquantum well voltage-controlled bistable laser diodes", Jpn. J. Appl. Phys., vol. 29, pp. L2442-L2444, 1990.

[12] H. Uenohara, Y. Kawamura, H. Iwamura, K. Nonaka, H. Tsuda and T. Kurokawa, "Operation characteristics of a side-light-injection multiple-quantum-well bistable laser for all-optical switching", Jpn. J. Appl. Phys., vol. 33, pp. 815-821, 1994.

[13] S. Tarucha, H. Kobayashi, Y. Horikoshi and H. Okamoto, "Carrier-induced energy-gap shrinkage in current-injection GaAs/AlGaAs MQW heterostructures", Jpn. J. Appl. Phys., vol.23, no.7, pp.874-878, 1984.

[14] R. Lang and K. Kobayashi, "Suppresion of the relaxation oscillation in the modulated output of semiconductor lasers", IEEE J. Quantum Electron., vol. 12, pp.194-199, 1976.

[15] M. Ueno and R. Lang, "Conditions for self-sustained pulsation and bistabiliy in semiconductor lasers", J. Appl. Phys., vol.58, pp. 1689-1692, 1985.

[16] E. Gaumont-Goarin, J. Jacquet, S. Adevah-Poeuf, C. Labourie, O. Le Gouézigou, F. Gaborit, F. Serre, C. Fortin, G. Ripoche, P. Pagnod, A. Jourdan, P. Ottolenghi, P. Landais and G.H. Duan, "Proton bombardment technique for high speed (>1 Gbit/s) 4 section bistable DBR wavelength converter", 6th international Conf. Indium Phosphide and Related Materials, Santa Barbara, MC4, 1994.

# Chapter 3  Analysis of In-line Light-injection Multiple Quantum Well Bistable Laser Characteristics

The segmented-electrode optical bistable laser is an attractive device to realize optical systems without electronic-optical (E/O) and optical-electronic (O/E) conversions, and several groups have already demonstrated all-optical time-division switching systems using bistable lasers [1]-[3]. The bistable laser has features superior to those of passive devices, such as lower switching power [4], large tolerances in wavelength [2], and large optical gain. The introduction of multiple quantum well (MQW) structure to the active and saturable absorber is promising for further improving the device features, especially the switching speed and the controllability of the hysteresis characteristics. In conventional bistable lasers, the turn-off time is limited by the absorption recovery time [5]. On the other hand, the electric field applied to the saturable absorber can reduce the turn-off time to less than a nanosecond. The applied electric field also results in a large change of the absorption at the lasing wavelength because of the quantum-confined Stark effect (QCSE), and this change makes the control of the hysteresis width easy and reproducible. The change of the threshold current and the hysteresis width in the GaAs/AlGaAs system was demonstrated by Tarucha et al. [6] and the stable optical switching operation in the InGaAs/InP system was reported by our group. [7] The analysis of the dynamic operation, however, is important for realizing the faster switching operation and for optimizing the device design.

In this chapter, I simulate static and dynamic characteristics of a voltage-controlled MQW bistable laser diode, and I design the length of saturable absorption region of the bistable laser by solving the modified rate equation considering the carrier escape time from the saturable absorption region. A short saturable absorption region less than 10 $\mu$m long shows suitability for low-threshold and controllable operation. And a large-gain material, for example, a MQW structure with a large conduction band offset, a large number of quantum wells, or strained-layer-superlattice, shows lower switching power and high-speed switching operations.

## 3.1 Analytical Method

The static and switching characteristics of a two-segmented bistable laser have been calculated by several groups and the conditions of self-sustained pulsation and bistability, polarization bistability with TM mode light injection, have been reported [8]-[13]. These group have constructed the rate equations for the two-segmented structure and taken into consideration the carrier densities in each region and the photon density in the cavity. The carrier lifetime in two regions are usually assumed to be constant or inversely proportional to carrier density [8]-[12], but this assumption is not valid for the MQW bistable laser because carriers in the saturable absorption region escape from MQWs at a rate that depends on the strength of the externally applied electric field. I have therefore modified the rate equation to consider the carrier escape time for the saturable absorption region.

The analytical model used in the following calculations is shown in Fig.3-1. The equations are based on those reported by References 9 and 10, and they are as follows:

$$\frac{dn_g}{dt} = \frac{J_g}{ed} - v_g G_g S - \frac{n_g}{\tau_g} - \frac{n_g}{\tau_{nr}} \tag{3.1}$$

$$\frac{dn_a}{dt} = -v_g G_a S - \frac{n_a}{\tau_a} \tag{3.2}$$

$$\frac{dS}{dt} = v_g \xi(1-h)G_g S + v_g \xi h G_a S + \beta \xi(1-h)\frac{n_g}{\tau_g} - \frac{S}{\tau_p} + P_{in} \tag{3.3}$$

where $n_i$ (i=g, a) is carrier density, S is photon density, $\tau_i$ (i=g, a) is carrier lifetime, $\tau_{nr}$ is nonradiative recombination time, $\tau_p$ is photon lifetime, $v_g$ is group velocity in the cavity, $G_i$ (i=g, a) is optical gain, h is the ratio of the length of the saturable absorption region to the cavity length, $\beta$ is spontaneous emission factor, $\xi$ is the optical confinement factor, and $P_{in}$ is injected photon rate coupled into the laser cavity. The suffixes g and a indicate the gain region and the saturable absorption region. Equations (3.1) and (3.2)
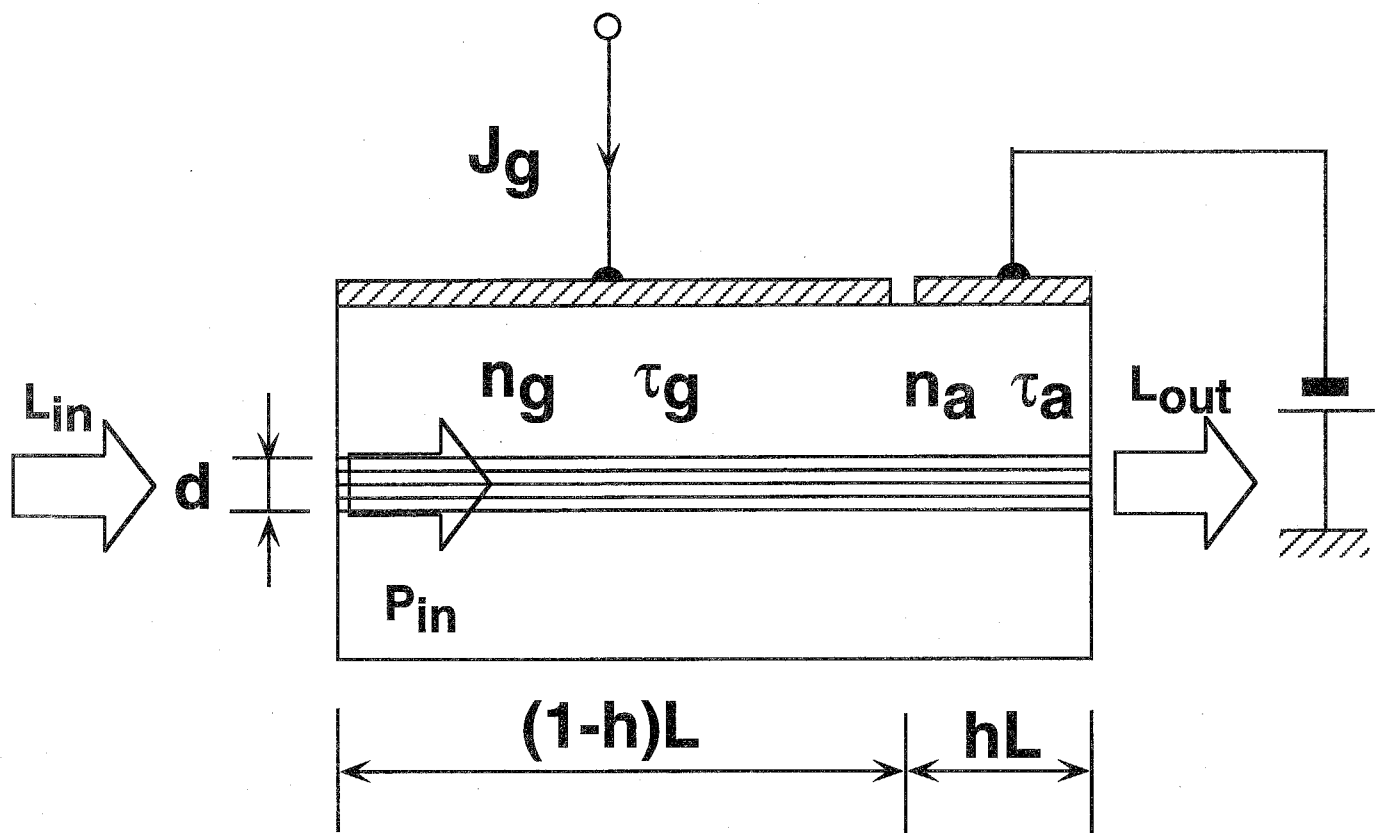
**Fig. 3-1**

Analytical model of the two-segmented MQW bistable laser.

represent the changes of carrier density in the gain and saturable absorption regions and eqn. (3.3) expresses the change of photon density. The photon density is assumed here to be uniform in the cavity. Optical gain $G_i$ is assumed to be linear with carrier density and is given by $G_i = g_i (n_i - n_0) \cdot (1 - \varepsilon S)$, where $g_i$ is the differential gain coefficient, $n_0$ is the transparency carrier density and $\varepsilon$ is the nonlinear gain coefficient. To discriminate between the gain region and the saturable absorption region, the optical gain line in the gain region $G_g = g_g (n_g - n_0) \cdot (1 - \varepsilon S)$ is assumed to cross with that in the saturable absorption region $G_a = g_a (n_a - n_0) \cdot (1 - \varepsilon S)$ at the same carrier density $n_0$ in the horizontal carrier density axis. And the former touches the gain curve in the gain regime, and the latter touches the gain curve in the absorption regime. The carrier lifetime in the gain region is attributed to the spontaneous emission and so it is expressed as $\tau_g = 1/(B_{eff} \cdot n_g)$, where $B_{eff}$ is the effective recombination coefficient. In long wavelength laser diodes, the nonradiative recombination process due to Auger recombination cannot be neglected. To simplify the analysis, it is expressed as nonradiative recombination time $\tau_{nr}$.

The injected photon rate $P_{in}$ is included in the change of photon density (3.3), which expresses the case the input light wavelength is equal to that of lasing wavelength. In this case, the input light itself is amplified in the laser cavity, so the low switching power and the resultant fast switching time are expected. Strictly speaking, this is valid when the laser is a single mode laser, for example, distributed feedback (DFB) laser, distributed Bragg reflector (DBR) laser or vertical cavity surface emitting laser (VCSEL) because eqns.(3.1) to (3.3) are the rate equations for single mode. When the input light wavelength is different from the lasing mode, eqns.(3.1) to (3.3) are modified as follows:

$$\frac{dn_g}{dt} = \frac{J_g}{ed} - \frac{n_g}{\tau_g} - \frac{n_g}{\tau_{nr}} - v_g G_g S - v_g G_g P_{in}' \qquad (3.1')$$

$$\frac{dn_a}{dt} = -\frac{n_a}{\tau_a} - v_g G_a S - v_g G_a P_{in}' \qquad (3.2')$$

$$\frac{dS}{dt} = v_g \xi (1-h) G_g S + v_g \xi h G_a S + \beta \xi (1-h) \frac{n_g}{\tau_g} - \frac{S}{\tau_p} \qquad (3.3')$$

where $P_{in}'$ is the "net" injected photon density which is different from the injected photon rate $P_{in}$ in eqn.(3.3). To include the Fabry-Perot gain for the input light in the laser cavity, the injected photon density coupled into the laser cavity is multiplied by the Fabry-Perot gain $G_{FP}$ for obtaining $P_{in}'$. The Fabry-Perot gain $G_{FP}$ is given by

$$G_{FP} = \frac{(1-R)^2 \exp[G_{net}L]}{1 + R^2 \exp[2G_{net}L] - 2R\exp[G_{net}L]\cos(\delta)} \qquad (3.4)$$

$$\delta = \frac{4\pi}{v_g} L \cdot \Delta f \qquad (3.5)$$

$$G_{net} = \xi G - \alpha_{in} \qquad (3.6)$$

where R is mirror reflectivity, $G_{net}$ is the net gain in the laser cavity, L is the cavity length, $\Delta f$ is the frequency difference between the input light and the lasing mode, G is the gain coefficient, and $\alpha_{in}$ is the cavity loss. When the input light wavelength is different from the lasing wavelength, the Fabry-Perot gain $G_{FP}$ reduces drastically, and the switching power and the resultant switching speed are degraded. To investigate the potential of the device performance, eqn.(3.1) to (3.3) are used in the following calculations.

The difference between the voltage-controlled-type and current-injection-type is revealed in eqn.(3.2). The factors of carrier escape time for the saturable absorber is included in the carrier lifetime in the saturable absorption region $\tau_a$. It is not expressed like the carrier lifetime in the gain region $\tau_g$, and it depends on the applied voltage. In addition to this, the contributions of the field effect of saturable absorber, i.e., the change of the absorption coefficient and of photon lifetime, are introduced in the absorption change in eqn. (3.2) [13]. The cavity loss $\alpha_{in}$ of the bistable laser consists of conventionally treated free carrier loss $\alpha_{fc}$, mirror loss $\alpha_m$, and the linear absorption factor in the saturable absorption region $\alpha(V_c)$:

$$\alpha_{in} = \alpha_{fc} + \alpha_m + \alpha(V_c) \tag{3.7}$$

If we assume the absorption to be linear with applied voltage, then $\alpha(V_c)$ consists of a voltage-independent factor $\alpha_1$ and a voltage-dependent factor $\alpha_2$:

$$\alpha(V_c) = \alpha_1 + \alpha_2 V_c \tag{3.8}$$

Then the photon lifetime $\tau_p$ is given as

$$\tau_p^{-1} = [vg\{\alpha fc + \frac{1}{L}\ln(\frac{1}{R})\} \circledast (1 + r1 + r2 Vc)] \tag{3.9}$$

The parameters $r_1$ and $r_2$ in this equation are the fitting parameters and they depend on the MQW material and the number of quantum wells.

## 3.2   Static Characteristics

### 3.2.1   Current versus Output Light Characteristics

Static characteristics are analyzed by setting the right-hand sides of eqns. (3.1)-(3.3) to zero. To calculate the current versus output light characteristics, first the carrier density in the saturable absorption region $n_a$ is derived from eqn. (3.2) and is substituted into eqn. (3.3). After the carrier density in the gain region $n_g$ is derived from eqn. (3.3), it replaces $n_g$ in eqn. (3.1) and the relation between injection current density $J_g$ and photon density S is plotted. The parameters used in the calculations are listed in Table 3-1. Four kinds of MQW structures, 6 and 12 periods of InGaAs/InGaAsP, 6 and 10 periods of InGaAs/InAlAs, were selected and were compared in view of their performances. They were also later used as the active medium of MQW bistable lasers evaluated experimentally. The difference of MQW structure corresponds to the gain coefficient difference, which affects the static and dynamic characteristics. The values of differential gain coefficient $g_g$ and nonlinear gain coefficient ε were based on References 14 and 15. The parameters concerned with the voltage-dependent absorption factor, i.e.,

## Table 3-1

Numerical values used in the calculations of two-segmented MQW bistable lasers.

| Parameter | Value | | | |
|---|---|---|---|---|
| | InGaAs/InAlAs | | InGaAs/InGaAsP | |
| | 6 wells | 10 wells | 6 wells | 12 wells |
| $g_g$ | $3.5 \times 10^{-16}\ cm^2$ | $5.0 \times 10^{-16}\ cm^2$ | $2.0 \times 10^{-16}\ cm^2$ | $4.0 \times 10^{-16}\ cm^2$ |
| $g_1$ | $50.0 \times 10^{-16}\ cm^2$ | $30.0 \times 10^{-16}\ cm^2$ | $80.0 \times 10^{-16}\ cm^2$ | $50.0 \times 10^{-16}\ cm^2$ |
| $\varepsilon$ | $5.5 \times 10^{-17}\ cm^3$ | $5.5 \times 10^{-17}\ cm^3$ | $2.0 \times 10^{-17}\ cm^3$ | $2.0 \times 10^{-17}\ cm^3$ |
| $r_1$ | 0.6 | 0.6 | 0.4 | 0.4 |
| $r_2$ | -1.2 | -1.2 | -0.6 | -0.6 |
| $\xi$ | 0.14 | 0.25 | 0.15 | 0.29 |
| $n_0$ | $1.25 \times 10^{18}\ cm^{-3}$ | | | |
| $\tau_{nr}$ | 1.0 ns | | | |
| $B_{eff}$ | $1.0 \times 10^{-10}\ cm^3 /s$ | | | |
| $\beta$ | $1.0 \times 10^{-5}$ | | | |
| h | 0.03 | | | |

$r_1$ and $r_2$ in eqn. (3.9), were derived by fitting the experimental results. The experimental results will be described in detail in Chapter 4.

Output light intensity as a function of current density is shown in Fig. 3-2 for various values of applied voltage. The photon density in the laser cavity S in eqns.(3.1) to (3.3) was converted into output light intensity with unit of $kW/cm^2$. These curves were calculated for a MQW structure with 6 periods of InGaAs/InAlAs. The threshold current increases monotonously with decreasing applied voltage. Moreover, the hysteresis width also increases and the "jump-up" intensity, which is defined by the difference of the output light intensity between the two states at the turn-on threshold current, enlarges. These results reflect on the absorption change by applied voltage. In the calculations, the well and barrier thicknesses in InGaAs/InGaAsP of 100 Å and 40 Å, and those in InGaAs/InAlAs of 90 Å and 30 Å, respectively, were used. It was assumed that each structure had a 900-Å optical confinement layer, which were the same as actual devices [16]. The cavity length and the length of the saturable absorption region were fixed to 300 μm and 10 μm.

The effect of the length of the saturable absorption region can be seen in the relation between the applied voltage and the threshold current or hysteresis width. These relations are shown in Figs. 3-3 (a) and (b) for 6 periods of InGaAs/InGaAsP and in Figs. 3-4 (a) and (b) for 6 periods of InGaAs/InAlAs. The lengths of the saturable absorption region used in these calculations were 5, 10, 20, and 40 μm. These figures show that the turn-on, turn-off currents and hysteresis width increase monotonously with increasing absorption region length regardless of the MQW structure, thus indicating that the absorption significantly affects the bistable laser characteristics. An absorption region less than 10 μm long is suitable for obtaining low threshold operation and low power consumption.
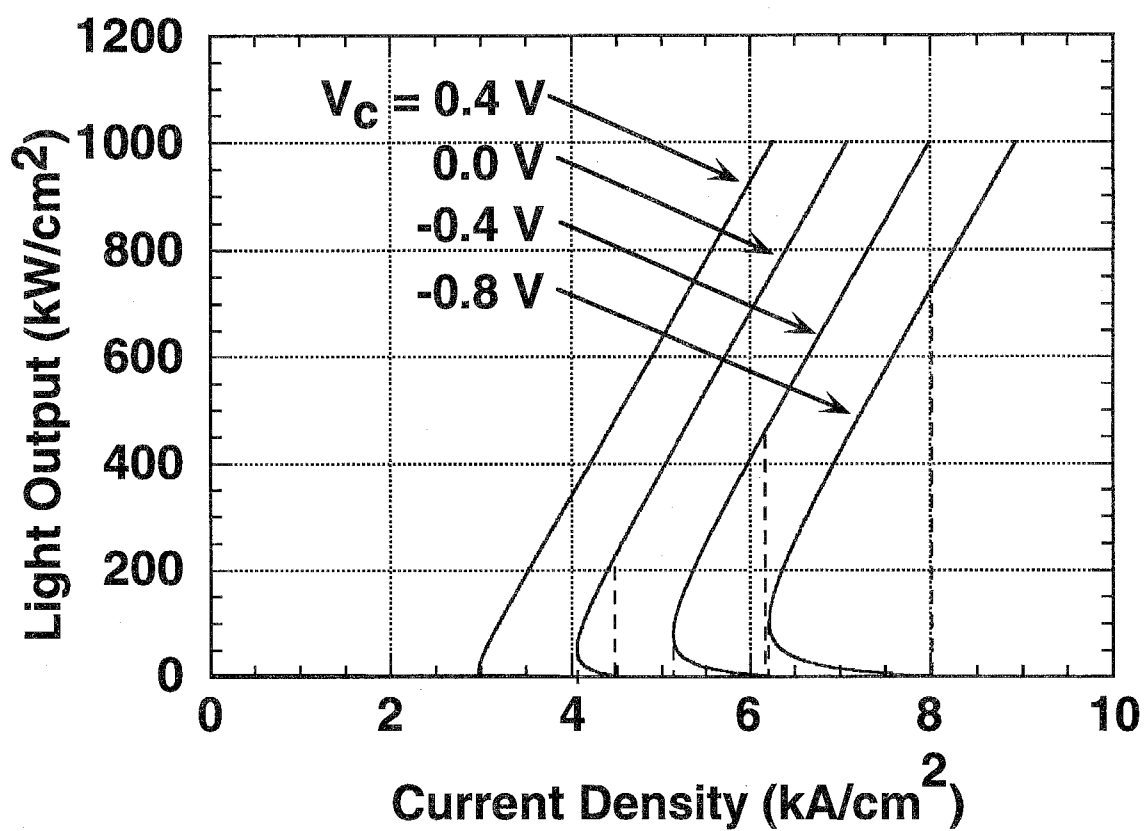
**Fig. 3-2**

Calculated output light intensity versus the current density at various control voltages ( 6 periods of InGaAs/InAlAs MQW structure).
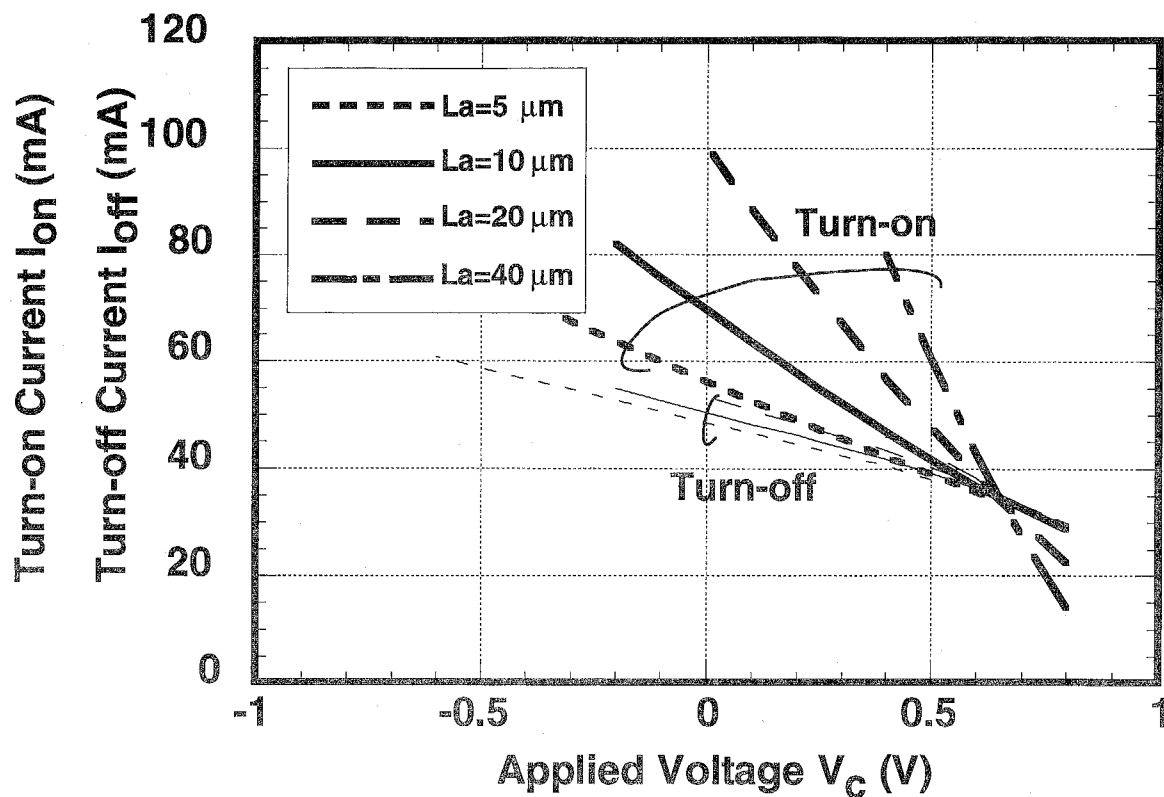
**(a) Turn-on and turn-off threshold current**
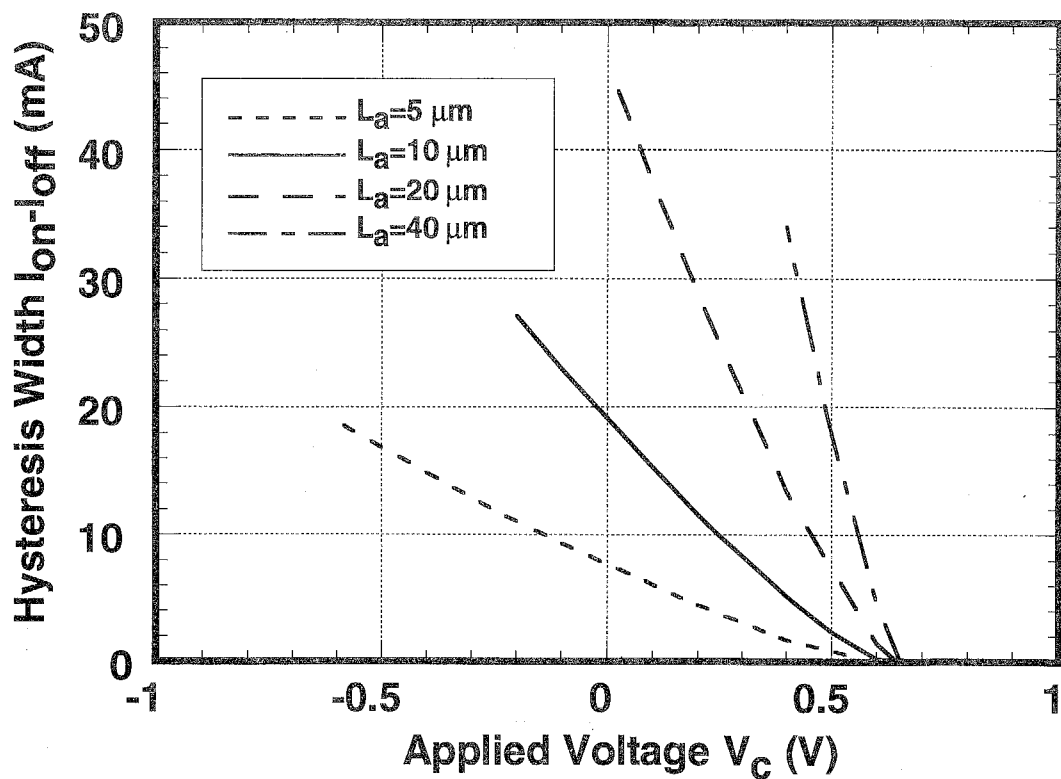


**(b) Hysteresis width**

**Fig. 3-3**

Calculated (a) turn-on and turn-off threshold current versus applied voltage and (b) hysteresis width versus applied voltage for various saturable absorption region lengths $L_a$. 6 periods of InGaAs/InGaAsP MQW structure is assumed.
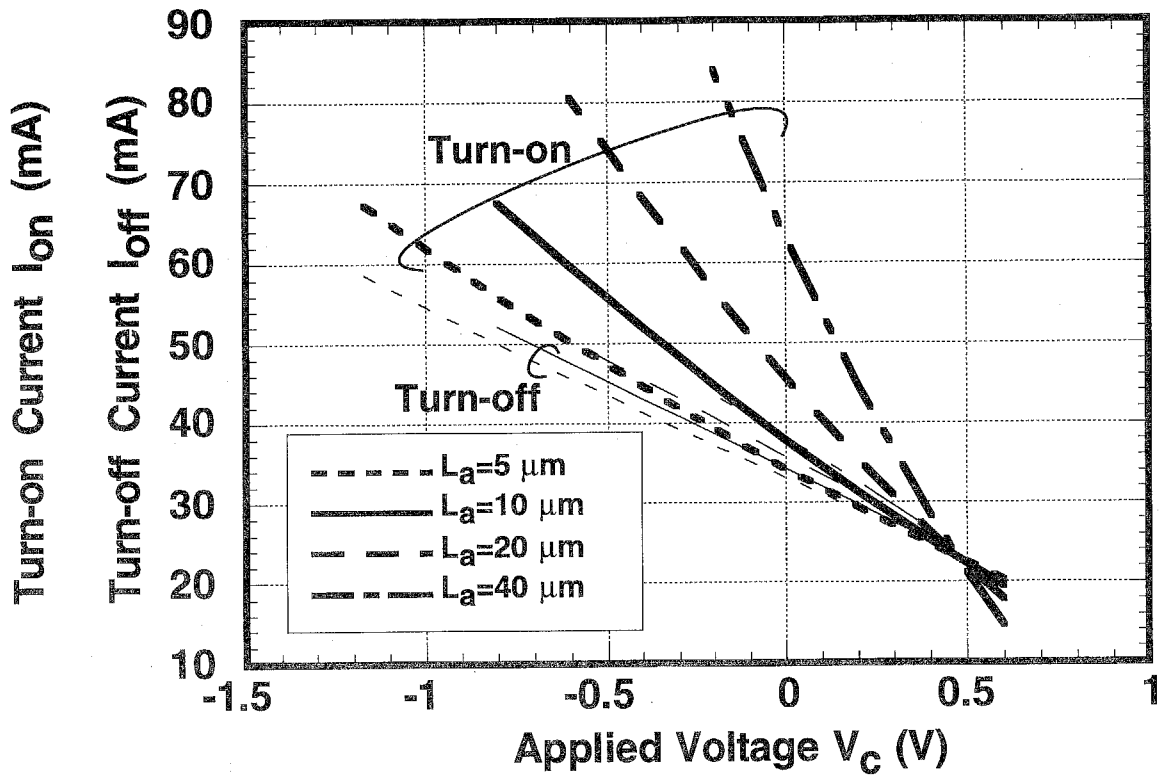
(a) Turn-on and turn-off threshold current
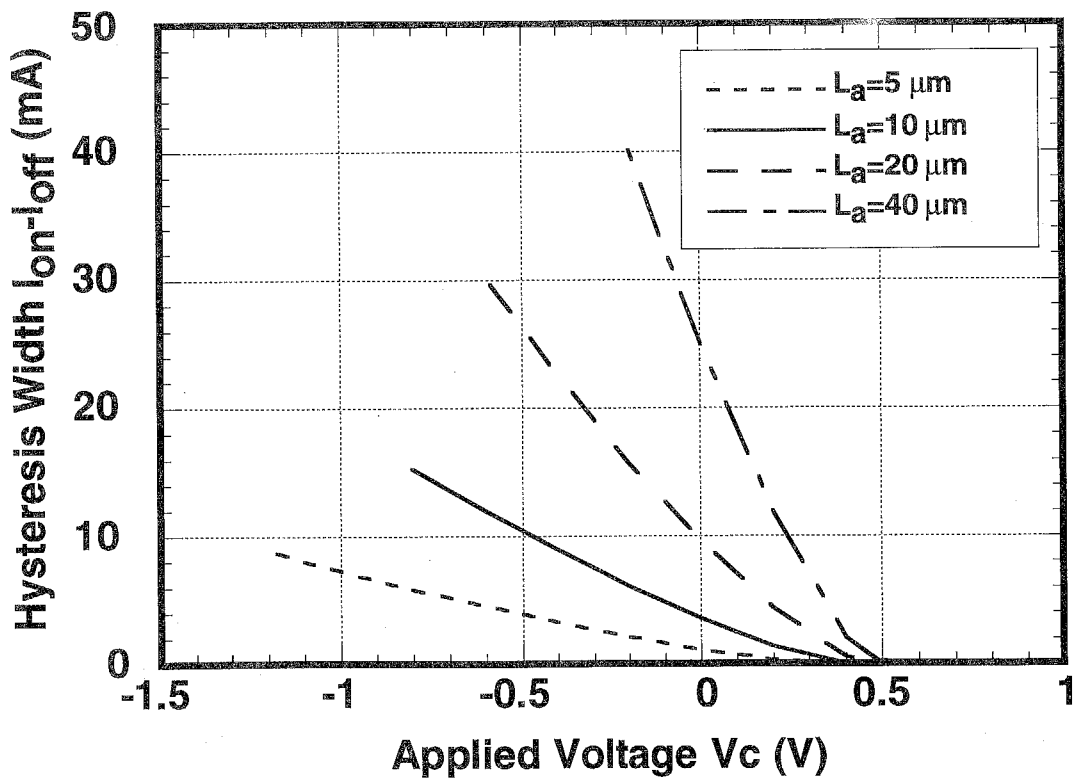


(b) Hysteresis width

**Fig. 3-4**

Calculated (a) turn-on and turn-off threshold current versus applied voltage
and (b) hysteresis width versus applied voltage for various saturable
absorption region lengths $L_a$. 6 periods of InGaAs/InAlAs MQW structure is
assumed.

## 3.2.2 Input Light Switching Power

To calculate the input / output light intensity characteristics, the carrier densities in the gain region $n_g$ and in the saturable absorption region $n_a$ are derived from eqns. (3.1) and (3.2). They are then substituted into eqn. (3.3) and the relation between injection light intensity $P_{in}$ and photon density S are plotted. In these calculations, the laser cavity length and the saturable absorption region length were fixed to 300 and 10 $\mu m$, respectively. The other parameters used in the calculations were the same as those given in Section 3.2.1.

Figure 3-5 shows the input / output light characteristics calculated for 6 periods of InGaAs/InAlAs MQW structures. The injected photon rate $P_{in}$ was converted into input light intensity with unit of $kW/cm^2$. The voltage applied to the saturable absorption region was set so that the hysteresis width was 10 mA, and bias currents were 1, 2, and 4 mA below turn-on current. The initial state is in the "OFF" state, so the bistable laser can be lased by injecting input light of more than threshold power. Once the bistable laser is switched-on and is in the "ON" state, it remains lasing even when the input light diminishes because the bias current is between the turn-on and turn-off currents. As seen in Fig. 3-5, the threshold input light power decreases when the bias current approaches turn-on current.

Calculated threshold input light intensity as a function of bias current is shown in Fig. 3-6(a) for 6 periods of InGaAs/InGaAsP MQW structure and in Fig. 3-6(b) for 6 periods of InGaAs/InAlAs MQW structure. In each calculation, the hysteresis width was varied from 2.5 to 15 mA. For the same difference between the turn-on and bias current, the threshold input light intensity is lower for greater hysteresis width regardless of the MQW structure. This is due to the difference of the absorption efficiency in each bias condition. A greater hysteresis width corresponds to a lower voltage applied to the saturable absorption region, so the absorption coefficient is larger in such a case. It is found that the switching power of less than 10 $\mu W$ (corresponding to 600 $W/cm^2$) can be obtained when the bias current is set within one-fourth of the hysteresis from the turn-on
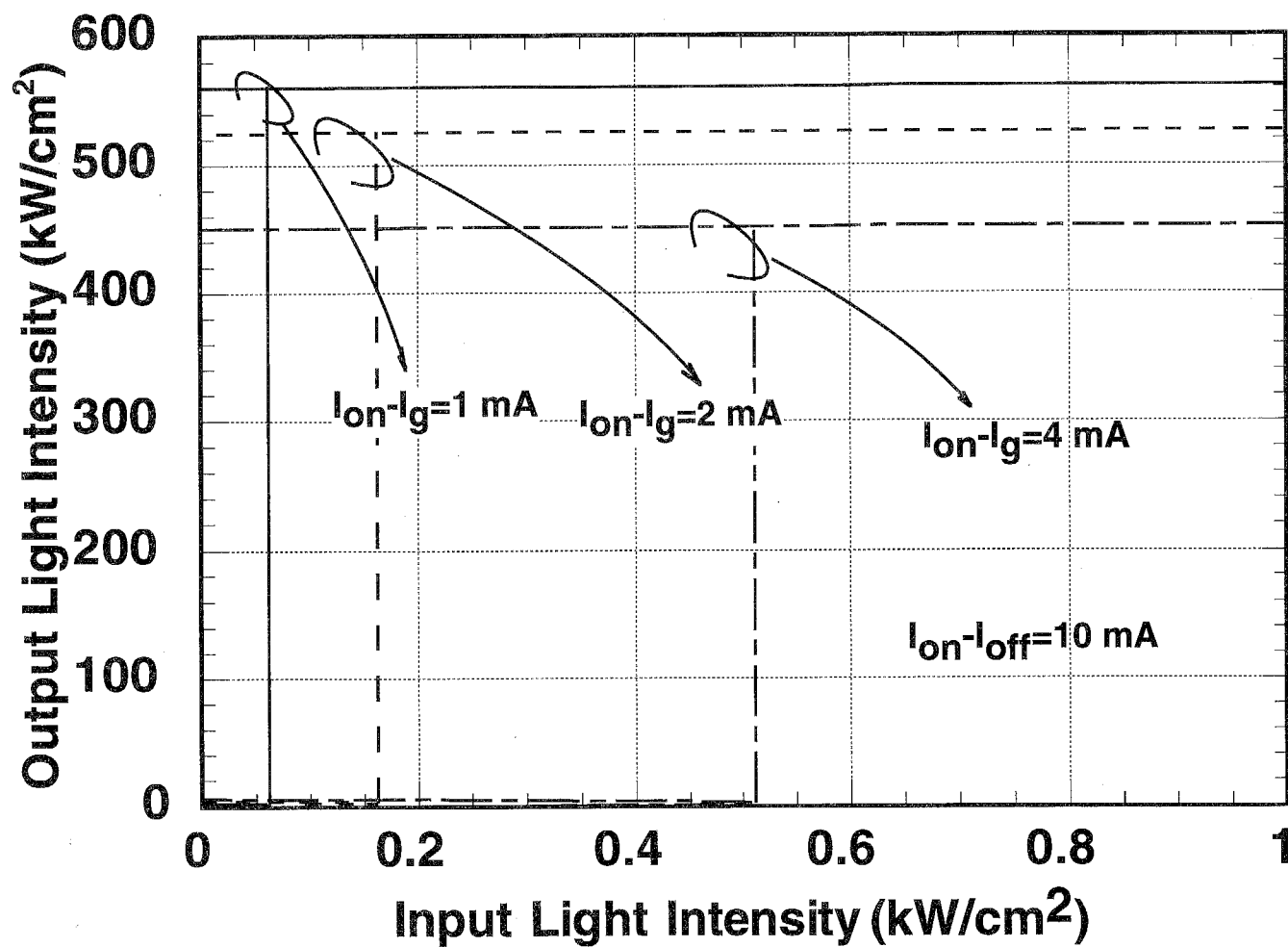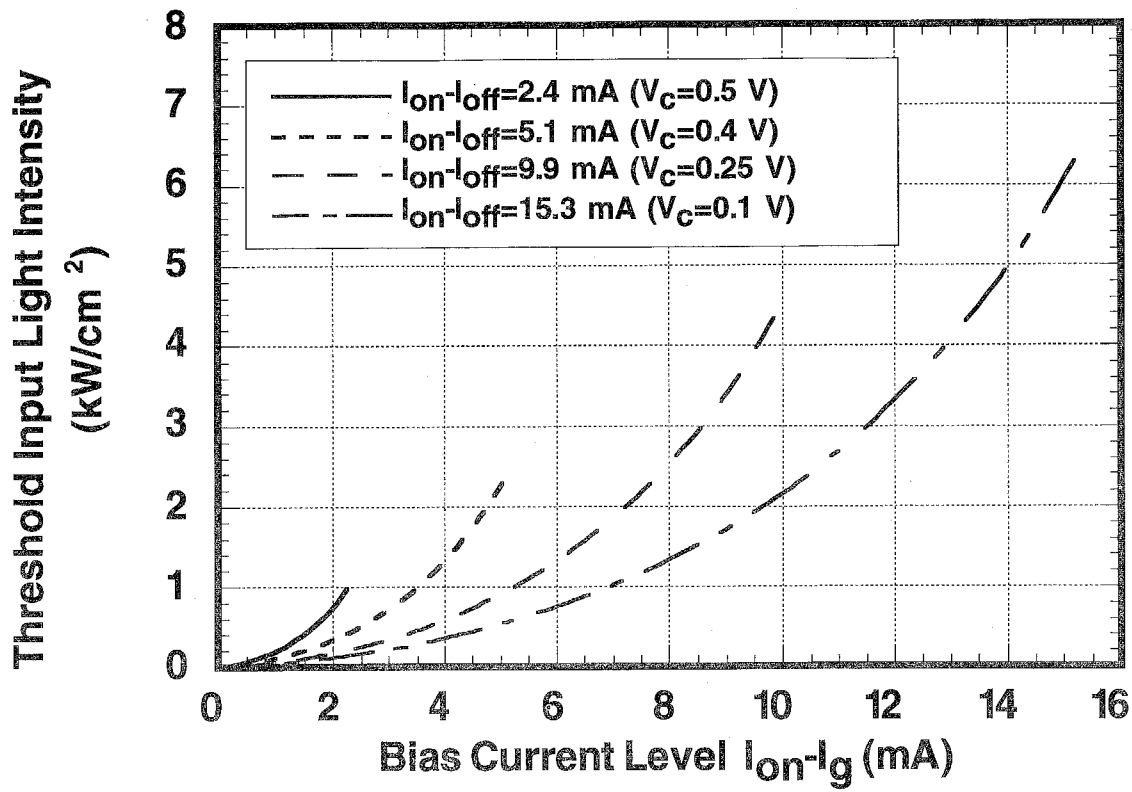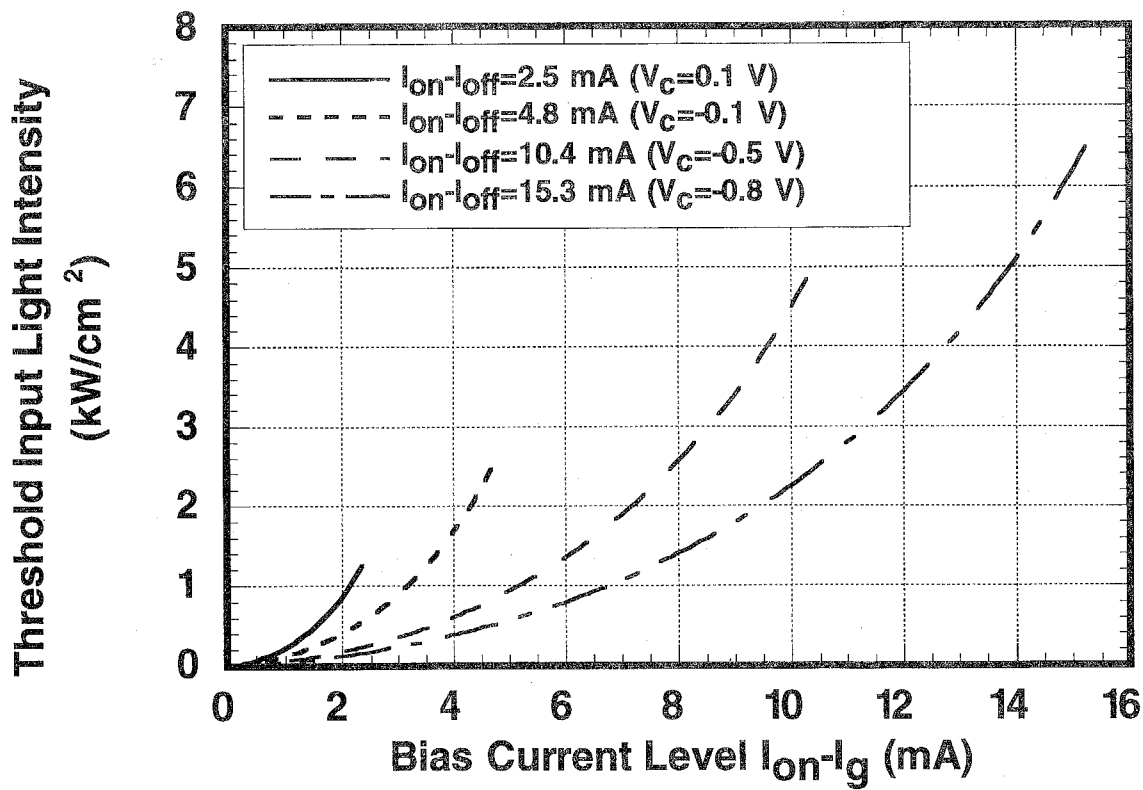
Fig. 3-5

Calculated input/output light intensity characteristics. 6 periods of InGaAs/InAlAs MQW structure is assumed.

(a) 6-well InGaAs/InGaAsP



(b) 6-well InGaAs/InAlAs

Fig.3-6

Threshold input light intensity versus bias current level:
(a) 6 periods of InGaAs/InGaAsP MQW structure, and
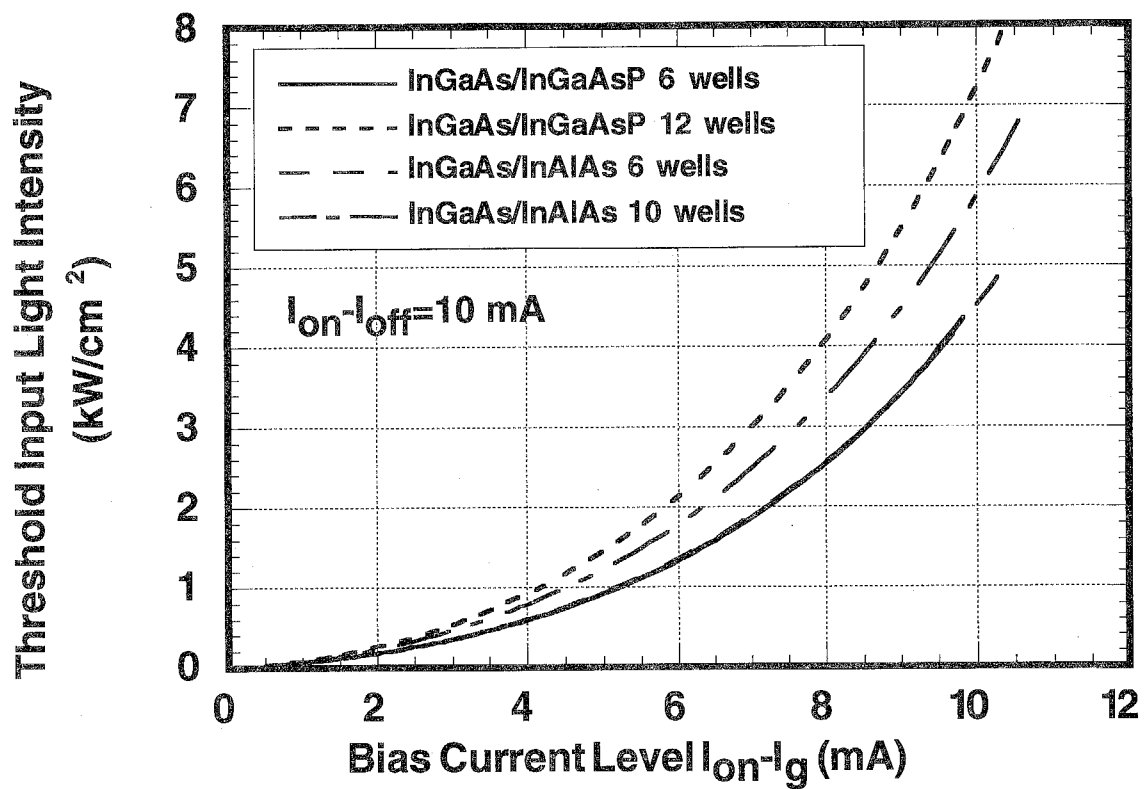(b) 6 periods of InGaAs/InAlAs MQW structure.

**Fig. 3-6(c)**

Threshold input light intensity versus bias current level. The MQW structure is varied as a parameter. The hysteresis width is set at 10 mA.

current. The dependence of the threshold input light intensity on MQW structures is shown in Fig. 3-6(c), where the hysteresis widths are fixed at about 10 mA in each case. The difference of the MQW materials and the number of quantum well is reflected on the difference of the differential gain coefficient. It can be seen that the threshold switching power is larger for larger quantum wells for the same difference between the turn-on and the bias current. This is mainly due to the shorter photon lifetime which compensates the larger differential gain and smaller carrier density fluctuation. The threshold switching power is lower for 10 periods of InGaAs/InAlAs than for 12 periods of InGaAs/InGaAsP because the differential gain coefficient is larger in the 10-period structure.

## 3.3 Dynamic Response

### 3.3.1 Analysis of Dynamic Response

The dynamic responses were calculated by solving eqns. (3.1)-(3.6) by the Runge-Kutta-Gill method. The calculated set operation is shown in Fig. 3-7. In the calculations, the width of the input light pulse was 10 ns to make it clear to show relaxation oscillation response. The parameters for 6 periods of InGaAs/InAlAs were used. The applied voltage is set so that the hysteresis width is 10 mA, and the difference of the bias from the turn-on current was 1 mA. Relaxation oscillation occurs just after the input light is injected. The difference of the input light intensity affects the turn-on time.

The reset operation, on the other hand, can be obtained by applying reverse bias voltage to the saturable absorption region. In the calculations, applying reverse bias voltage is expressed by changing the carrier escape time $\tau_a$ and absorption coefficient (minus gain coefficient) $G_a$ in eqn. (3.2). The calculated reset operation is shown in Fig. 3-8, which shows the output light intensity when the reset voltage pulse is applied at 100 ps. The parameters for a MQW structure with 6 periods of InGaAs/InAlAs were used, the bias voltage was set so that the hysteresis width was 10 mA, and the gain current was
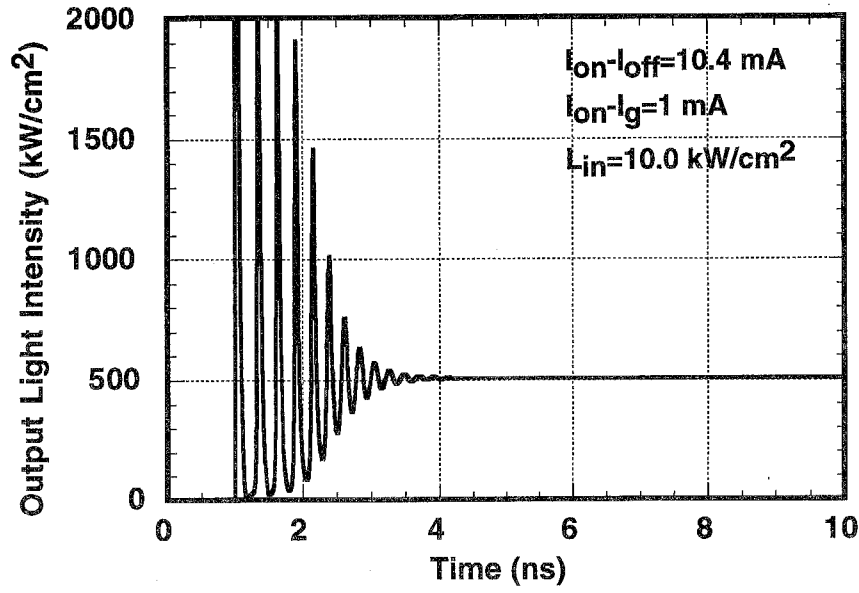
(a) $L_{in}=10.0$ kW/cm$^2$
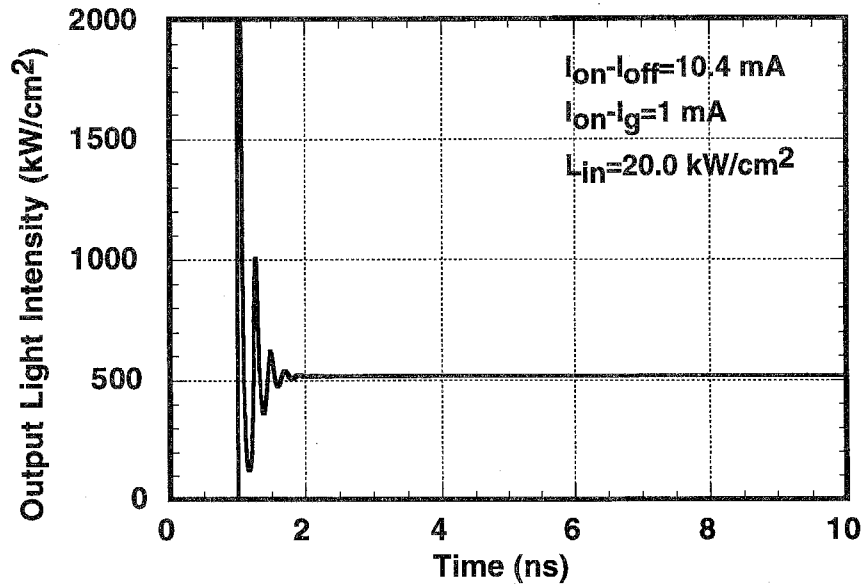


(b) $L_{in}=20.0$ kW/cm$^2$

Fig.3-7

Calculated time response under light injection for a bistable laser with 6 periods of InGaAs/InAlAs MQW structure. Input light intensity is (a) 10.0 kW/cm$^2$ and (b) 20.0 kWcm$^2$.
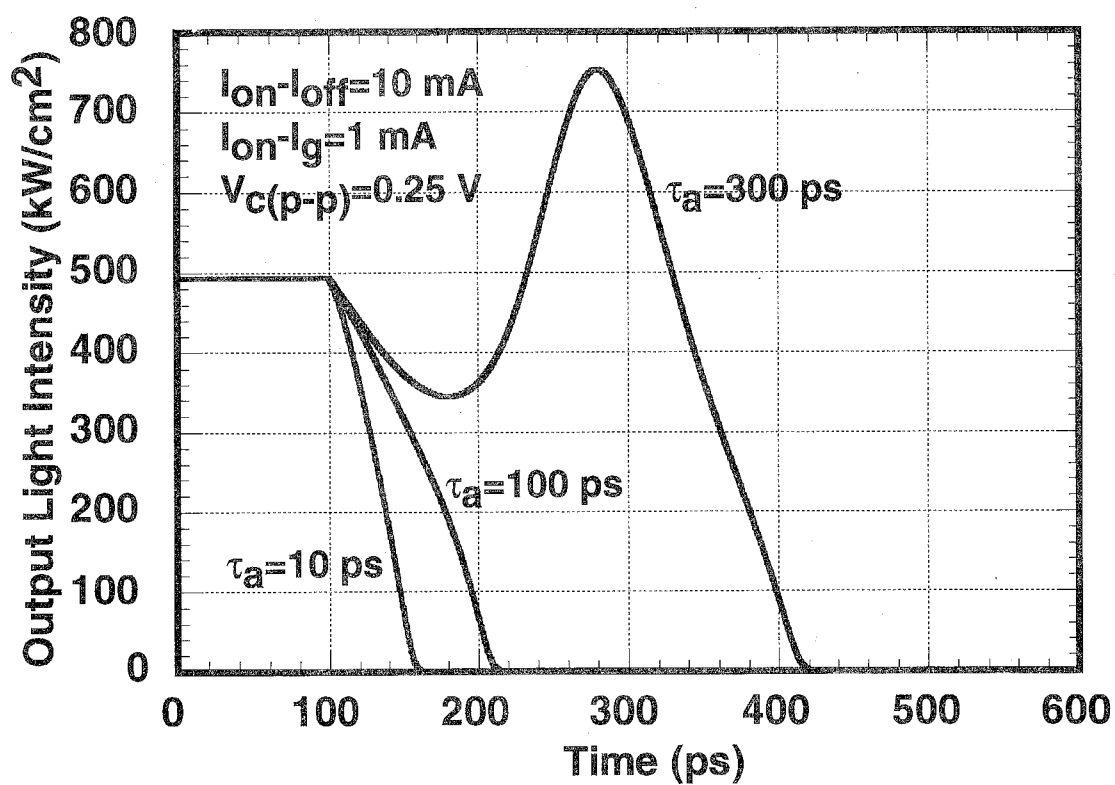
Fig. 3-8

Calculated time response of reset operatation by applied voltage pulse.
6 periods of InGaAs/InAlAs MQW structure is assumed.

1 mA below the turn-on current as in Fig. 3-7. The applied voltage height was 0.25 V in order to clearly show the difference of the time response by changing the carrier escape time. The carrier escape time for the saturable absorption region was varied from 300 to 10 ps. Shorter carrier escape time results in a faster turn-off time because the absorption recovers faster. The light peak after reset voltage pulse with $\tau_a$=300 ps results from relaxation oscillation, which can be seen in low-switching-power operation or slow carrier escape time.

### 3.3.2 Switching Speed Limit

The turn-on and turn-off time dependence on input switching power will be described in the following. First, the turn-on time limit will be discussed. In the following discussions, the turn-on time is defined as the time between the light being injected and the output light intensity reaching the first peak of the relaxation oscillation. The dependence of the turn-on time on the input light intensity is shown in Fig. 3-9, for which the parameters and the bias voltage are the same as for Fig. 3-7. The difference between the bias current and the turn-on current was changed from 0.5 to 4 mA. In each case, the turn-on time decreases with increasing input light intensity and, on the other hand, it increases drastically when the input light intensity approaches the threshold input light power. This is the so-called "critical slowing down". The difference of the threshold switching power with bias current coincides with results shown in Fig. 3-6(c). Faster set operation can be achieved under the same input light intensity for larger bias current because the threshold power is smaller, but the minimum switching time is almost the same in each bias current under much larger input light. The MQW structure dependence of turn-on time is shown in Fig. 3-10, for which the hysteresis widths were 10 mA and the difference of the bias and the turn-on currents was 1 mA in each case. At the same input light intensity, the turn-on time is shorter for InGaAs/InAlAs than for InGaAs/InGaAsP, and it is shorter for a larger number of quantum wells. These results indicate the potential of high-speed switching in a material that has a larger differential
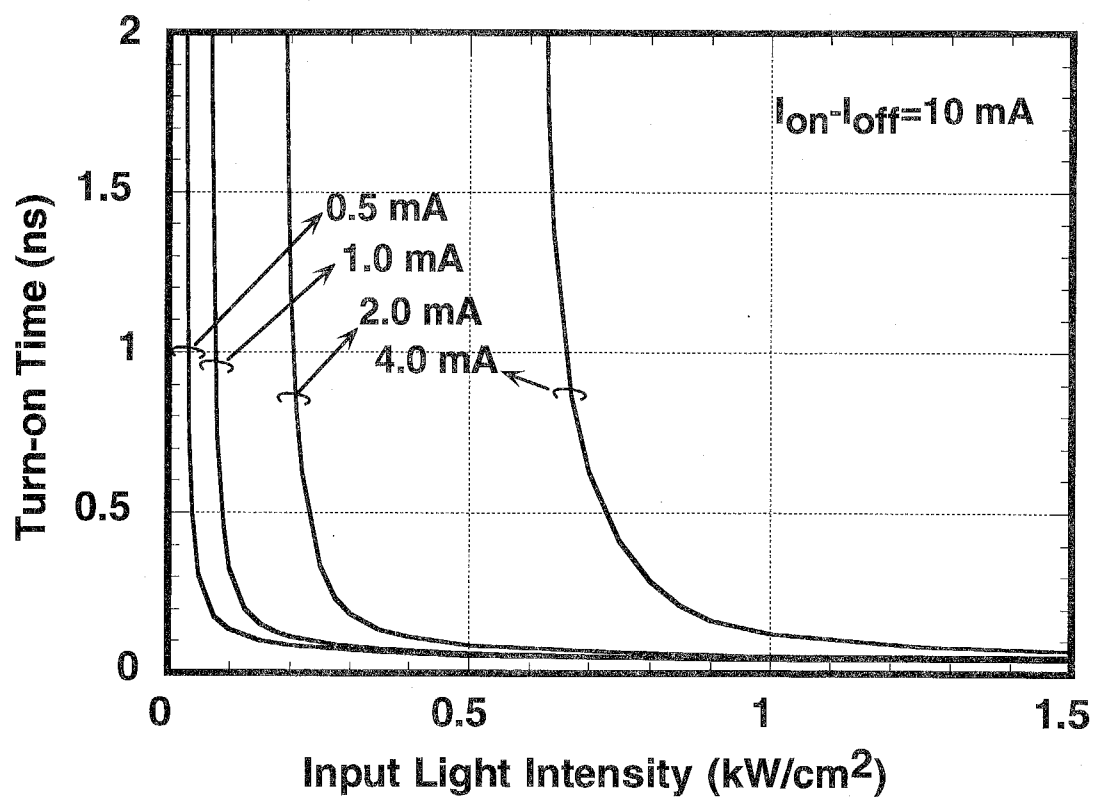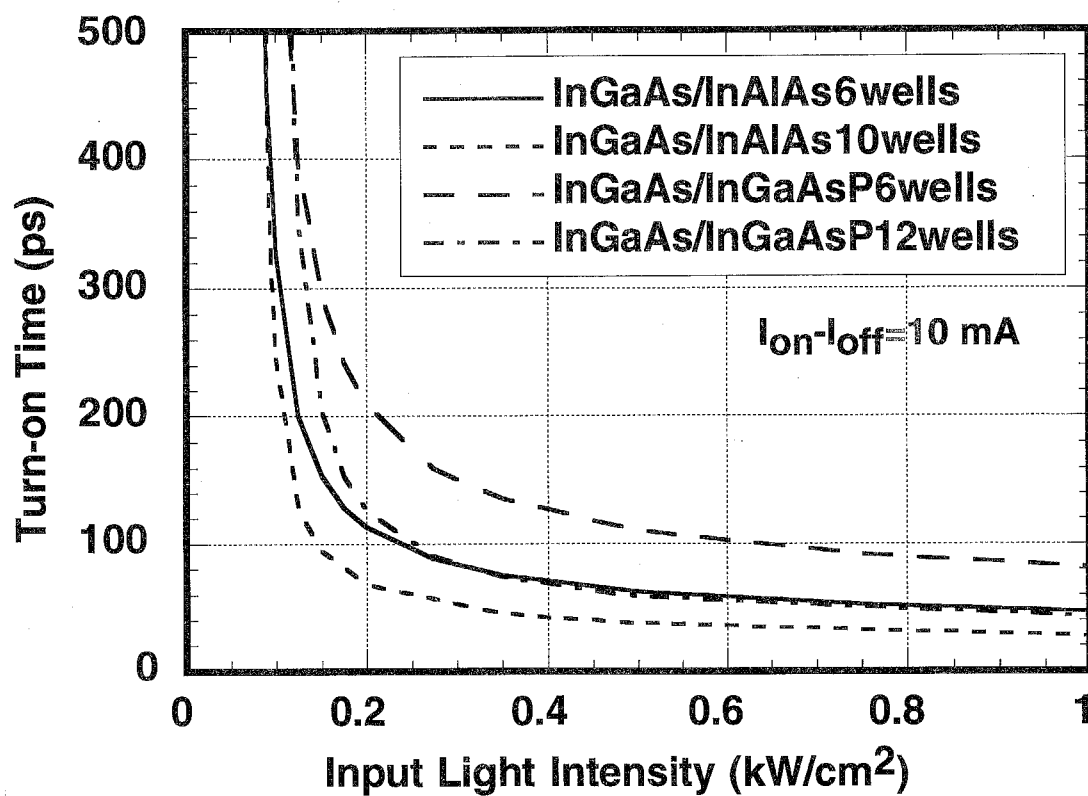
**Fig. 3-9**

Calculated turn-on time as a function of input light intensity for various difference between bias current and turn-on current.

**Fig. 3-10**
Calculated turn-on time as a function of the input light intensity.
Four kinds of MQW structures are calculated.

gain. They also show that switching can be obtained in less than 25 ps when the MQW with large differential gain is used and a powerful input light is injected.

Next, the turn-off time limit is discussed. The turn-off time can be estimated from the calculated time response shown in Fig. 3-8. It is defined as the time from 90% to 10% for the transition from the lasing state to the spontaneous emission state. The dependence of the turn-off time on the bias current is shown in Fig. 3-11. In the following, the bias current level is expressed as the difference between the turn-on threshold current and the bias current. The parameters used in the calculations were the same as those for Fig. 3-8. The turn-off time decreases when the bias current level increases, i.e., when the bias current approaches the turn-off threshold current. This is because less switching power is needed to recover the absorption in the saturable absorption region. And the shorter carrier escape time also reduces the turn-off time because of the faster carrier extraction. Figure 3-12 shows the turn-off time dependence on the applied voltage height $V_{c(p-p)}$. In these calculations, the bias current and the carrier escape time were varied as parameters. The effects of the bias current and the carrier escape time are the same as those shown in Fig. 3-11. And the larger voltage height results in the faster reset operation. The larger voltage height corresponds to a larger change of the absorption in the saturable absorption region in the calculation, so the calculation results indicate that the recovery from the saturation state to the absorption state is faster in the saturable absorption region with larger voltage height. The effect of the differential gain coefficient in the gain region is shown in Fig. 3-13, where carrier escape time of (a) 100 ps and (b) 10 ps are compared. The differential gain coefficient used in the calculation were 2.0, 3.5, and $5.0 \times 10^{-16} cm^2$, each corresponding to 6-well InGaAs/InGaAsP, 6-well InGaAs/InAlAs and 10-well InGaAs/InAlAs MQW structures. For both escape time, the turn-off time is lower when the differential gain is larger. This is caused by the faster recovery rate of the absorption from the saturation state. In Fig. 3-13(a), the calculation curves with $g_g = 2.0 \times 10^{-16} cm^2$ and $3.5 \times 10^{-16} cm^2$ crossed because the slow turn-off occurred because of relaxation oscillation, as shown in Fig. 3-8 in $\tau_a = 300$ ps case. As shown in Fig. 3-13(b), the turn-off time can be reduced to about 15 ps
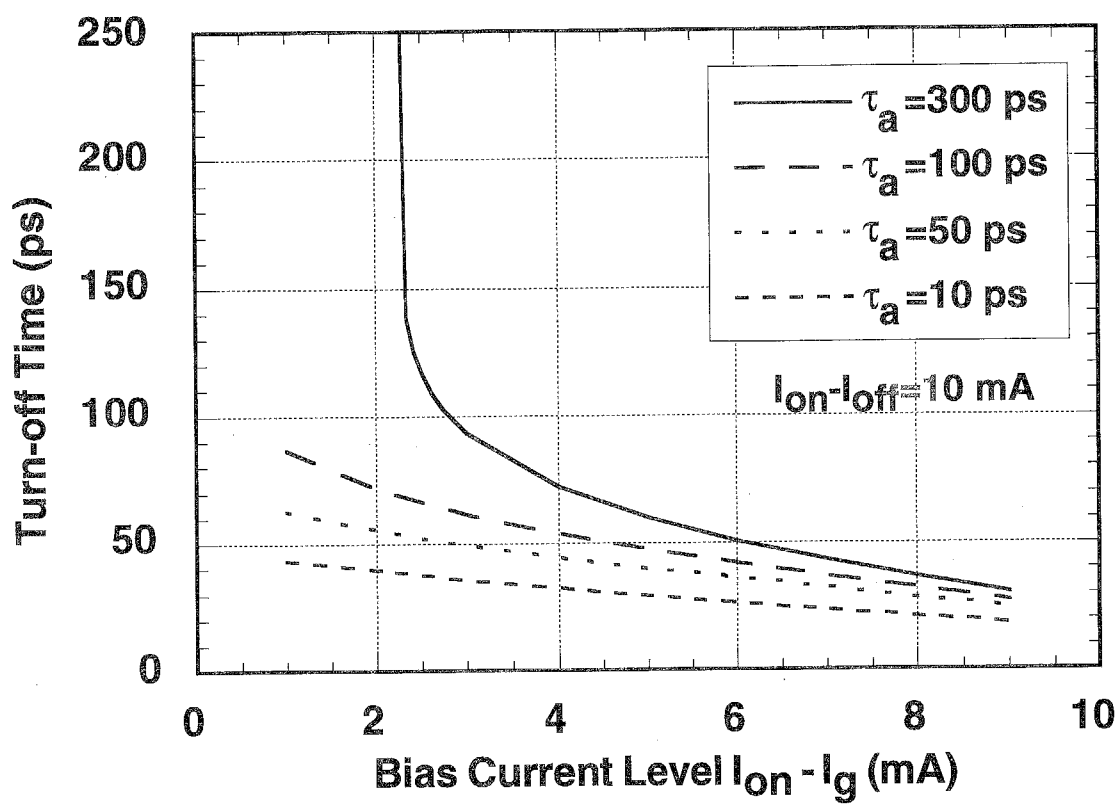
**Fig. 3-11**

Calculated dependence of turn-off time on bias current level.
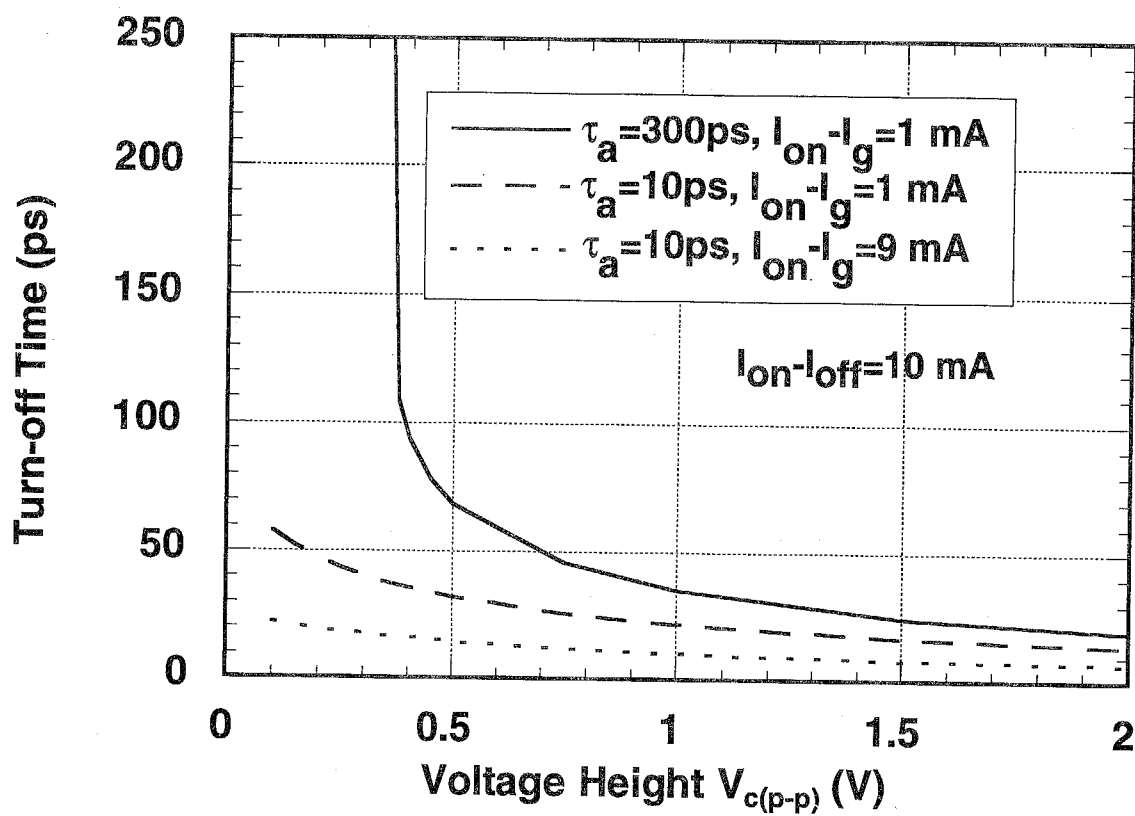6 periods of InGaAs/InAlAs MQW structure is assumed.

**Fig. 3-12**

Calculated turn-off time as a function of applied voltage height.
6 periods of InGaAs/InAlAs MQW structure is assumed.
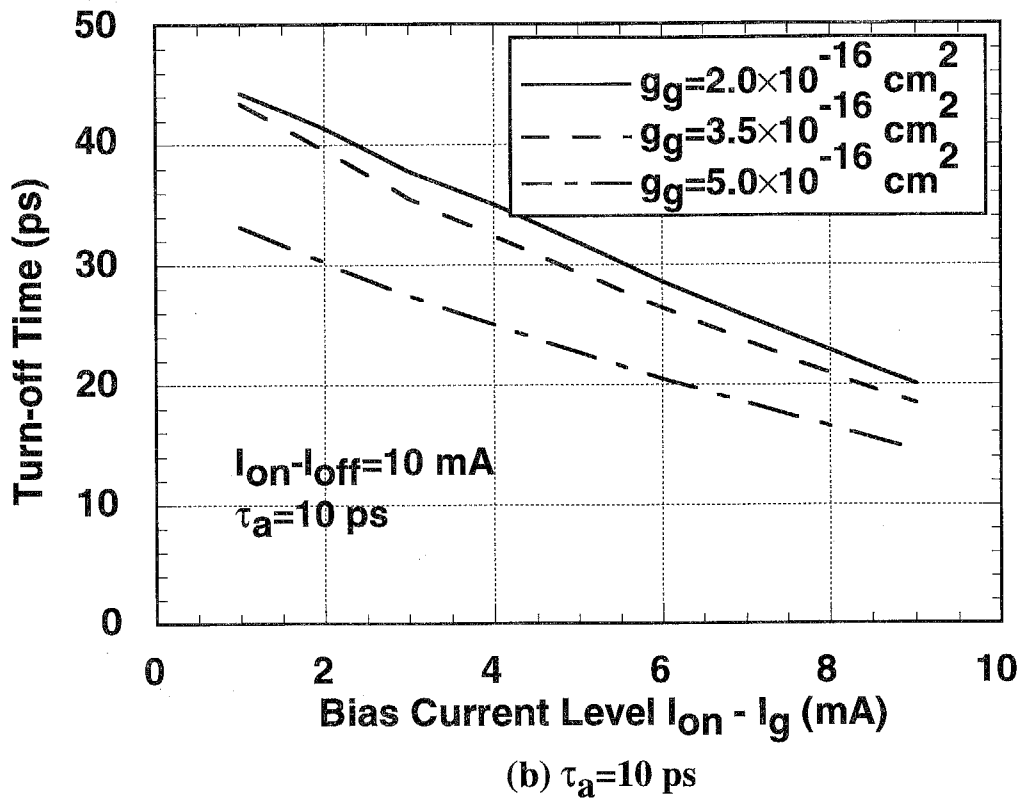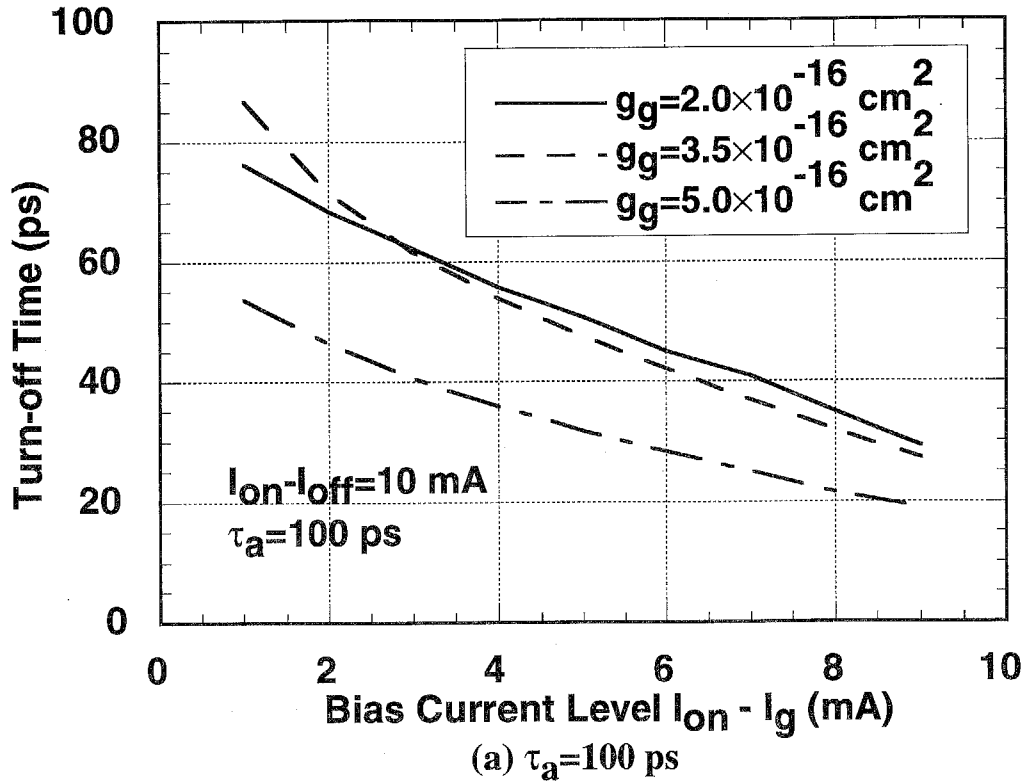
(a) $\tau_a=100$ ps



(b) $\tau_a=10$ ps

**Fig. 3-13**

Turn-off time versus bias current level for various differential gain coefficients in the gain region as a parameter. Carrier escape time for saturable absorption region is assumed to be (a) 100 ps and (b) 10 ps.

when the differential gain is large, the bias current is small, and carrier escape time is fast. When the hysteresis width is set to be small, a turn-off time of less than 10 ps can be expected.

In Figs. 3-11 to 3-13, the carrier escape time was treated as a parameter unrelated to applied voltage height. Actually, however, the carrier escape time is closely related to applied voltage height. The turn-off time theoretically attainable will be discussed in Chapter 7.

## 3.4 Summary

I have constructed the rate equations modified for two-segmented MQW bistable lasers, and have analyzed the static and dynamic operations of the bistable lasers. Light output versus current characteristics show that a short saturable absorption region is suitable for obtaining low threshold current. The static input / output light characteristics indicated that low threshold switching power can be achieved by adjusting the bias conditions so that gain current approaches the turn-on threshold current as well as by using the MQW structure with a large differential gain. Then the switching speed of the MQW bistable laser was calculated and its limit was estimated. Calculations show that very fast turn-on and turn-off time, respectively, less than 25 ps and less than 10 ps, can be expected when the MQW structure has a large differential gain coefficient, that is, when the number of quantum wells is large, the structure has high potential barriers, or strained-layer-superlattice is used.

# References

[1] M. Jinno and T. Matsumoto, "All-optical timing extraction using a 1.5 μm self pulsating multielectrode DFB LD", Electron. Lett., vol.24, pp. 1426-1427, 1988.

[2] S. Suzuki, T. Terakado, K. Komatsu, K. Nagashima, A. Suzuki and M. Kondo, "An experiment on high-speed optical time-division switching", vol.LT-4, pp.894-899, 1986.

[3] T. Shimoe, S. Kuroyanagi, K. Murakami, H. Rokugawa, N. Mekada and T. Odagawa, "An experimental 512 Mbps time-division photonic switching system", in Tech. Dig. Photon. Switching, 1989, FC2, pp.136-138.

[4] P. Blixt and U. Öhlander, "19 ps switching of a bistable laser diode with 30 fJ optical pulses", IEEE Photon. Technol. Lett., vol. 2, pp. 175-177, 1990.

[5] A. Tomita, T. Terakado and A. Suzuki, "Turn-off characteristics of bistable laser diode", J. Appl. Phys., vol.59, pp. 1839-1842, 1986.

[6] S. Tarucha and H. Okamoto, "Voltage-controlled optical bistability associated with two-dimensional exciton in GaAs-AlGaAs multiple quantum well lasers", Appl. Phys. Lett., vol.49, pp. 543-545, 1986.

[7] H. Uenohara, H. Iwamura and M. Naganuma, "Switching characteristics of InGaAs/InP Multiquantum well voltage-controlled bistable laser diodes", Jpn. J. Appl. Phys., vol. 29, pp. L2442-L2444, 1990.

[8] H. Kawaguchi, "Absorptive and dispersive bistability in semiconductor injection lasers", Optical and Quantum Electron., vol.19, pp.S1-S36, 1987.

[9] M. Ueno and R. Lang, "Conditions for self-sustained pulsation and bistability in semiconductor lasers", J. Appl. Phys., vol.58, pp. 1689-1692, 1985.

[10] R. Lang and K. Kobayashi, "Suppresion of the relaxation oscillation in the modulated output of semiconductor lasers", IEEE J. Quantum Electron., vol. 12, pp.194-199, 1976.

[11] Y. Mori, "Dynamic properties of transverse-magnetic wave injected semiconductor lasers", IEEE J. Quantum Electron., vol.27, pp.2415-2421, 1991.

[12] M. Okada, K. Takizawa, H. Kikuchi and H. Fujikake, "Undershooting and set-reset operation in bistable laser diodes with inhomogeneous excitation", IEEE J. Quantum Electron., vol.26, pp.850-857, 1990.

[13] J. O'Gorman, A.F. Levi, R.N. Nottenburg, T. Tanbun-Ek and R.A. Logan, "Dynamic and static response of multielectrode lasers", Appl. Phys. Lett., vol.57, pp.968-970, 1990.

[14] A. Wakatsuki, Y. Kawamura, Y. Noguchi and H. Iwamura, "Effect of conduction-band discontinuity on lasing characteristics of 1.5 mm InGaAs/In(Ga)AlAs MQW-FP lasers", IEEE Photon. Technol. Lett., vol.4, pp.383-386, 1993.

[15] M.C. Tatham, "Resonance frequency, damping, and differential gain in 1.5 mm multiple quantum-well lasers", IEEE J. Quantum Electron., vol.28, pp.408-414, 1992.

[16] H. Uenohara, Y. Kawamura, H. Iwamura, K. Nonaka, H. Tsuda and T. Kurokawa, "Operation characteristics of a side-light-injection multiple-quantum-well bistable laser for all-optical switching", Jpn. J. Appl. Phys., vol. 33, pp. 815-821, 1994.

# Chapter 4  Performance of In-line Light-injection Multiple Quantum Well Bistable Lasers

This chapter investigates the static and dynamic characteristics of a multiple quantum well (MQW) voltage-controlled bistable laser diode emitting in the 1.5 μm range. MQW bistable lasers with InGaAs/InP, InGaAs/InGaAsP, and InGaAs/InAlAs systems and with various well numbers were fabricated and their hysteresis characteristics and switching operation with injection light were compared. Easy controllability of the hysteresis width and of the threshold current, wide wavelength sensitivity in input light switching, and high-speed switching time have been observed. The reset operation performed by applying a voltage to the saturable absorption region also indicated the high-speed performance of this type of laser.

## 4.1  Device Structure and Fabrication

The two-segmented MQW bistable lasers with the structure shown in Fig. 4-1 were fabricated. The laser structure was grown on (100) Sn-doped InP substrates by gas source molecular beam epitaxy. Atomic beams of Ga, In, and Al from effusion cells were used as group III sources, and the sources of arsenic and phosphorus were $AsH_3$ and $PH_3$. Be and Si are used for p-type and n-type dopants, respectively.

The layer structure consisted of a 0.5-μm-thick Si-doped InP cladding layer, a undoped MQW active layer, a 1.2-μm-thick Be-doped InP cladding layer and a 0.2-μm-thick Be-doped InGaAs contact layer. For comparing laser characteristics and switching speed, the following kinds of MQW structures were prepared:

(i)  12 periods of 70 Å thick $In_{0.53}Ga_{0.47}As$ and 30 Å thick InP

(ii)  6 periods of 100 Å thick $In_{0.53}Ga_{0.47}As$ and 40 Å thick InGaAsP ($\lambda g = 1.2$ μm) sandwiched between 900 Å thick undoped InGaAsP ($\lambda g = 1.2$ μm)
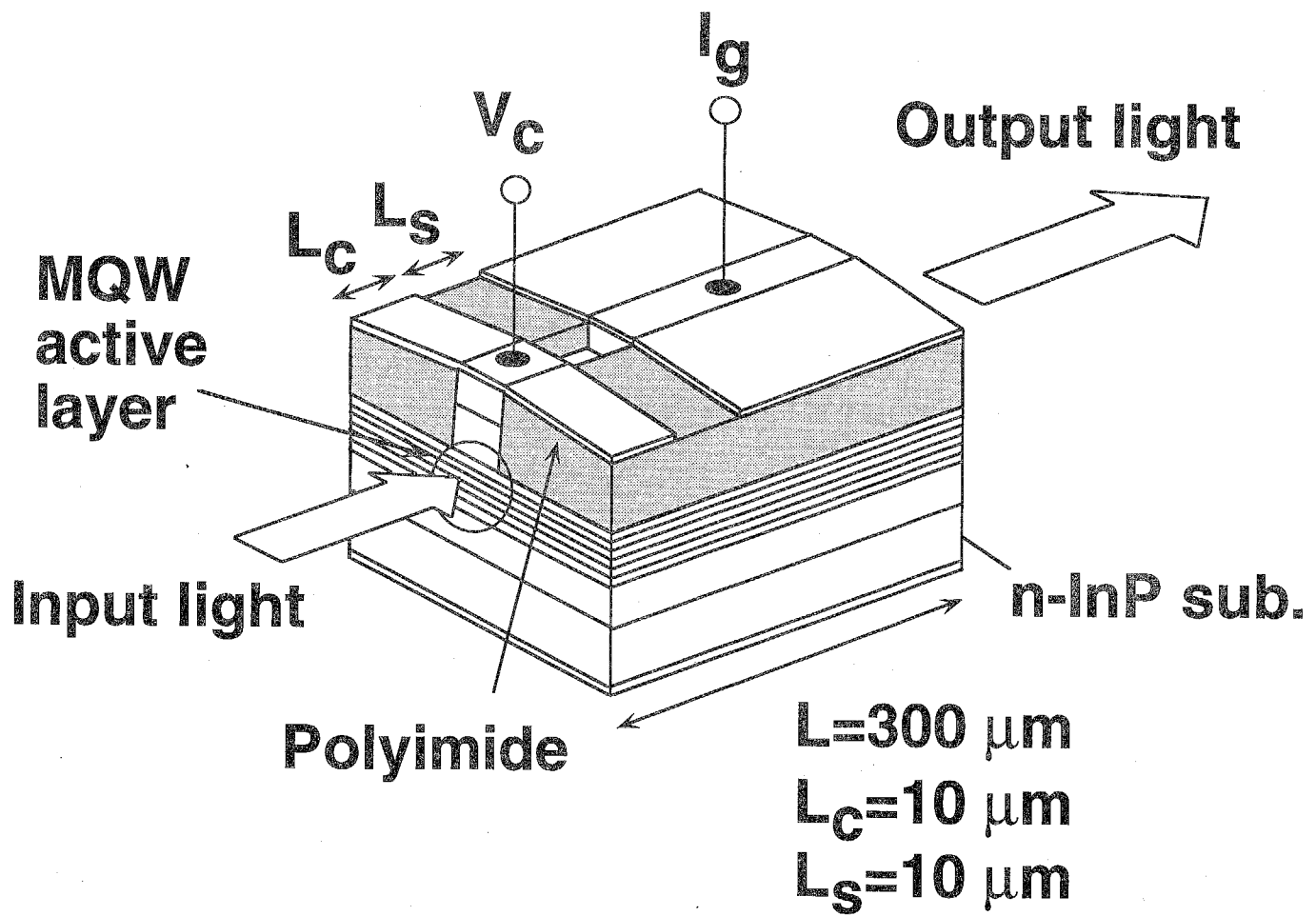
(iii) the same structure as (ii) but with 12 periods

Fig. 4-1

Schematic view of a two-segmented MQW bistable laser.

(iv) 6 periods of 90 Å thick $In_{0.53}Ga_{0.47}As$ and 30 Å thick $In_{0.52}Al_{0.48}As$ sandwiched between 900 Å thick undoped InGaAsP ($\lambda g$ = 1.2 μm)

(v) the same structure as (iv) but with 10 periods

These structures are summarized in Table 4-1, and their potential diagrams of three structures are shown in Fig. 4-2. Structure (i) has a higher electron barrier than do structures (ii) and (iii), but it has no optical confinement layer and no energy band-offset between the cladding and barrier layers. Structures (iv) and (v) have a conduction band discontinuity $\Delta E_c$ of 0.5 eV and a valence band discontinuity $\Delta E_v$ of 0.2 eV [1]. Because the electron barriers with structures (iv) and (v) are the highest in all structures enough to enhance the quantized effects, they are expected to improve the characteristics of the absorption saturation [2]. These structures also have the advantage of suppressing hole pile-up due to their small valence band discontinuity so that the high-speed switching operation is expected. In view of the optical gain, the higher the potential barrier height, the larger both gain and differential gain. The optical gain of InGaAs/InGaAsP and InGaAs/InAlAs QW structures were calculated by using density-matrix method[3] and was given as follows:

$$g(\lambda) = \frac{2\pi c}{\lambda}\sqrt{\frac{\mu}{\varepsilon}}\frac{me^* mh^*}{me^* + mh^*} \circledast \frac{1}{\pi\hbar^2 Lw}$$
$$\times \sum_{n=0}^{M-1} \int_{Een+Ehn+Eg}^{\infty} <Re\,h^2> \frac{(fe - fh)(\frac{\hbar}{\tau in})}{(Eeh - \hbar\omega)^2 + (\frac{\hbar}{\tau in})^2} dEeh \qquad (4.1)$$

where $\lambda$ is the wavelength, c is the velocity of light in the vacuum, μ is susceptibility, $\varepsilon$ is dielectric permeability, $m_e^*$ and $m_h^*$ are electron and hole effective mass, $\hbar$ is Plank's constant divided by $2\pi$, $L_w$ is well thickness, M is the number of quantized states, $E_{en}$ and $E_{hn}$ are the quantized states energy in the conduction and valence band, respectively, $<R_{eh}^2>$ is dipole moment, $f_e$ and $f_h$ are Fermi-Dirac distribution function, and $\tau_{in}$ is intraband relaxation time. The calculated results for gain and differential gain are shown in Figs. 4-3(a) and (b). Both peak gain and differential gain are larger in InGaAs/InAlAs

## Table 4-1.
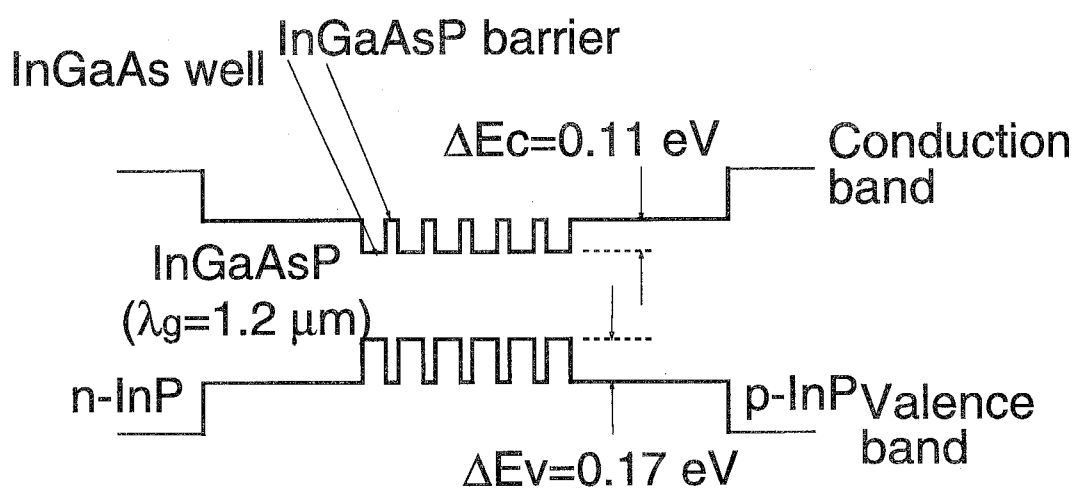## Parameters of MQW structures used for bistable lasers.

| No. | Well thickness $L_W$ (Å) | Barrier thickness $L_B$ (Å) | Well number $N_W$ |
|---|---|---|---|
| i | InGaAs 70 | InP 30 | 12 |
| ii | InGaAs 100 | InGaAsP ($\lambda_g$=1.2 μm) 40 | 6 |
| iii | InGaAs 100 | InGaAsP ($\lambda_g$=1.2 μm) 40 | 12 |
| iv | InGaAs 90 | InAlAs 30 | 6 |
| v | InGaAs 90 | InAlAs 30 | 10 |

# (a) InGaAs/InP

InGaAs well, InP barrier

ΔEc=0.24 eV

Conduction band

n-InP

p-InP

Valence band

ΔEv=0.36 eV

# (b) InGaAs/InGaAsP

InGaAs well, InGaAsP barrier

ΔEc=0.11 eV

Conduction band

InGaAsP ($\lambda$g=1.2 μm)

n-InP

p-InP Valence band

ΔEv=0.17 eV

# (c) InGaAs/InAlAs

InGaAs well, InAlAs barrier

ΔEc=0.5 eV

Conduction band

InGaAsP ($\lambda$g=1.2 μm)

n-InP

p-InP Valence band

ΔEv=0.2 eV
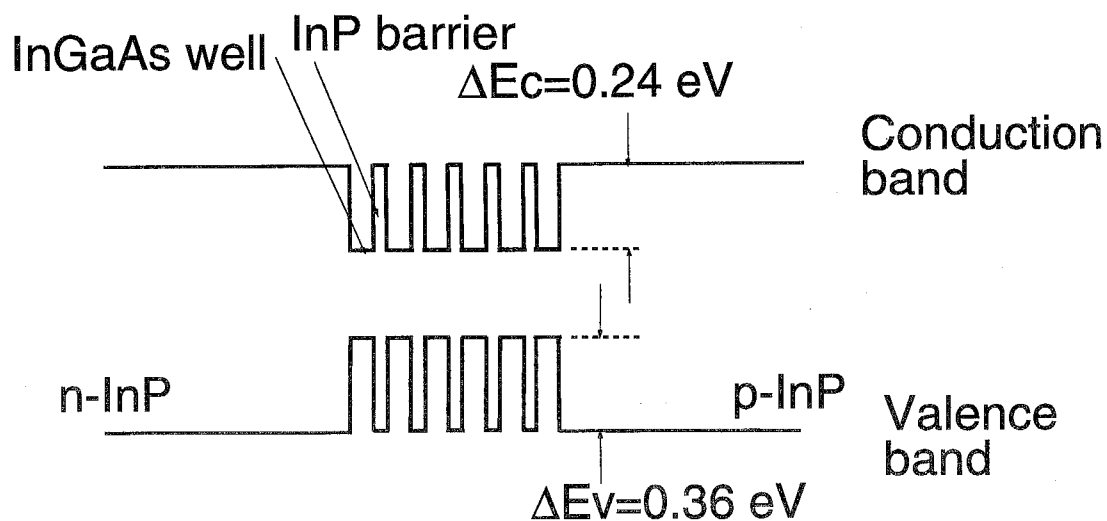
**Fig. 4-2**

**Potential diagrams of (a) InGaAs/InP, (b) InGaAs/InGaAsP, and (c) InGaAs/InAlAs MQW structures.**
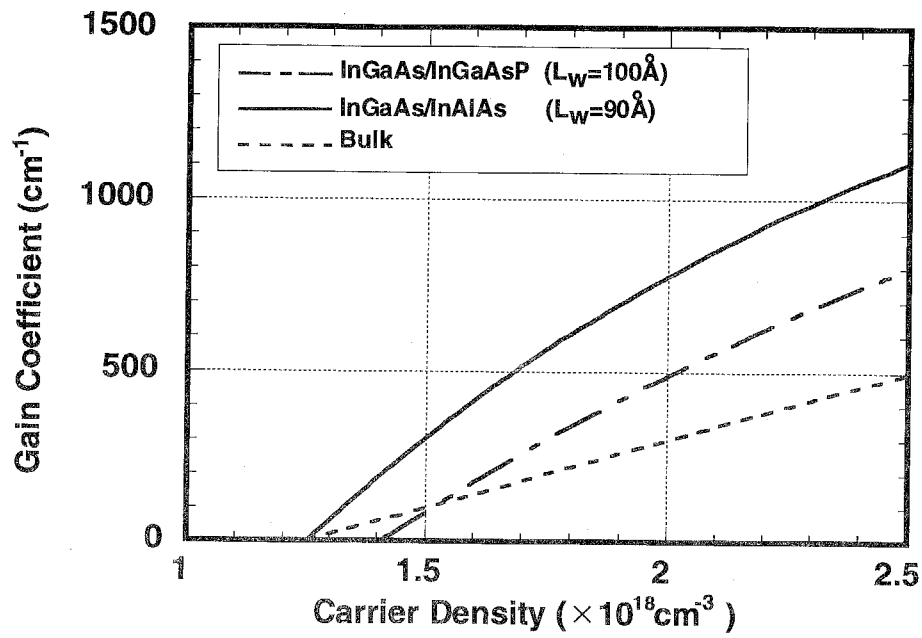
(a) Gain coefficient
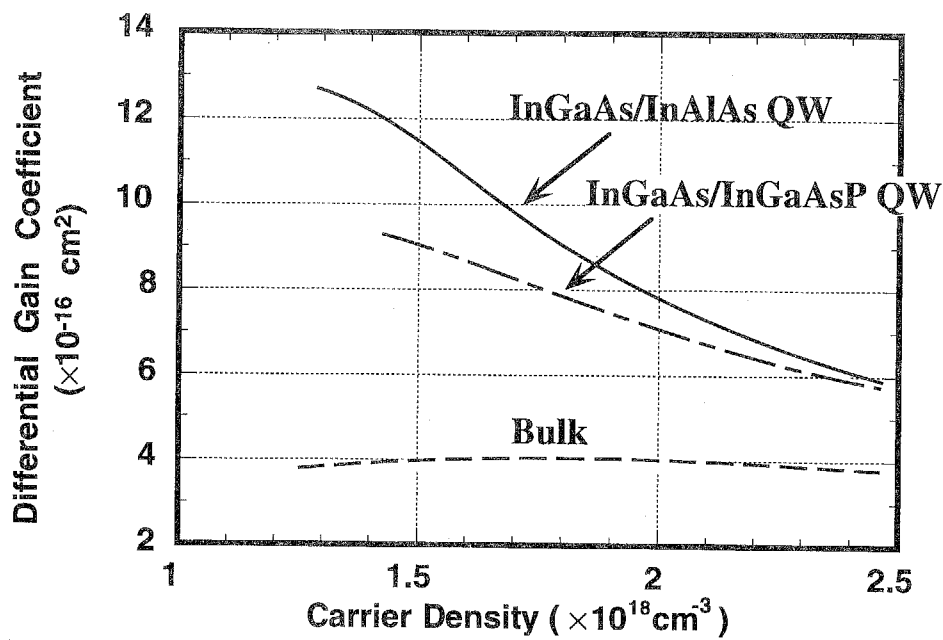


(b) Differential gain coefficient

Fig. 4-3

The calculated results of optical gain for InGaAs/InGaAsP, and
InGaAs/InAlAs QWs and for bulk structures.

than that in InGaAs/InGaAsP because of the difference of the conduction band offset. Superior performances is therefore expected for the InGaAs/InAlAs MQW structures.

Next, the fabrication procedure is briefly explained. The cap and upper cladding layer were first selectively etched down to form ridge structures just above upper optical confinement layer. The ridge structures were formed along the $<0\bar{1}1>$ direction. The polyimide was spin-coated to obtain a flat surface and to reduce parasitic capacitance in the saturable absorption region. After etching back to expose the top of the ridge structure, the two-segmented electrode was formed by using the lift-off technique. The electric separation between two electrodes was achieved by chemically etching the InGaAs contact layer and an isolation resistance of 1 kΩ was obtained. Each device was cleaved, mounted on a heat sink, and bonded with gold wire. The saturable absorption region length $L_c$, the separation region length $L_s$, and the voltage $V_c$ applied to the saturable absorption region affect the lasing characteristics. Typical device size was as follows: the ridge width was 3 μm, the cavity length was 300 μm, the gain region length was 280 μm, the saturable absorption region length was 10 μm, the separation region length was 10 μm.

## 4.2  Static Characteristics

### 4.2.1  Light Output versus Gain Current Characteristics

The lasing characteristics of MQW bistable lasers differed in some points between the InGaAs/InP, InGaAs/InGaAsP, and InGaAs/InAlAs structures. The light output versus gain current characteristics are shown in  Fig.4-4 for the InGaAs/InP structure. The InGaAs/InP MQW devices have shown lasing operation only under pulsed condition (1-μs pump pulses with 10 kpps repetition rate) and the threshold currents were higher than 100 mA regardless of the applied voltage range [4]. The main reason for the high thresholds are thought to be the lack of optical confinement layers and the weak carrier confinement in wells. The kinks seen in the lasing characteristics when the applied
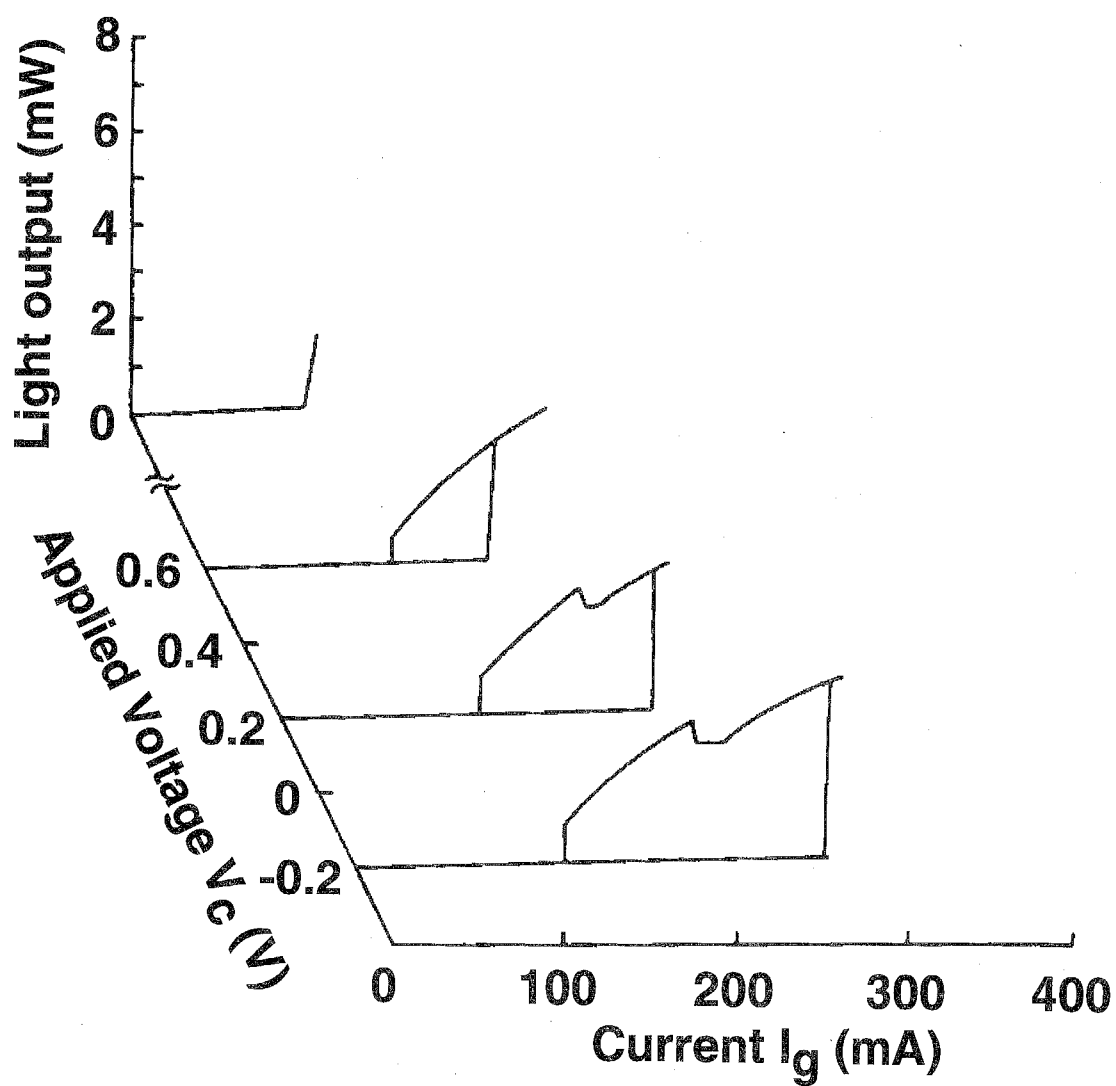
**Fig. 4-4**

Light output versus gain current characteristics of a two-segmented bistable laser with InGaAs/InP MQW structure.

voltage is +0.2 V or -0.2 V are the sign of the change of the transverse mode. The dependence of the turn-on and turn-off threshold current on applied voltage is shown in Fig. 4-5(a), and that of hysteresis width shown in Fig. 4-5(b). The turn-on and turn-off threshold current increases monotonously with decreasing applied voltage (increasing reverse bias voltage), and the measured hysteresis width was 68 mA at +0.6 V and 218 mA at -0.6 V. When the applied voltage became large enough to be in the current-injection regime, hysteresis disappeared. This characteristics differs from that of the conventional inhomogeneous-current-injection-type bistable lasers.

It is important to optimize the lengths of the saturable absorption region and the separation region because the turn-on threshold current and the hysteresis width are extremely sensitive to the total absorption along the laser cavity. Figure 4-6(a) shows the turn-on threshold current as a function of the length of the separation region. In this experiment, the gain and the saturable absorption region were electrically common, and the dependence of the minimum threshold current on the length of the separation region could be obtained. The relation of the turn-on threshold current to the length of the saturable absorption region, on the other hand, is shown in Fig. 4-6(b). The saturable absorption region was electrically open in order to investigate the effect of the saturable absorption region length against threshold current. In both cases, the turn-on current increased monotonously with increasing length of the separation region or saturable absorption region. These results indicate that absorption is large at the lasing wavelength. It is therefore effective to reduce the length of the saturable absorption region as well as that of the separation region to decrease the threshold current and to make it easier to control. The lengths of saturable absorption region and the separation region in the following devices were thus fixed at 10 μm.

With the InGaAs/InP MQW structure, the output light intensity showed several kinds of stability depending on the applied voltage, and the measured stability map is shown in Fig. 4-7. The upper and lower lines show the turn-on and turn-off threshold conditions, respectively. And the lasing region above the upper line can be divided into three parts: a stable region (relaxation oscillation gradually damps with time), pulsation
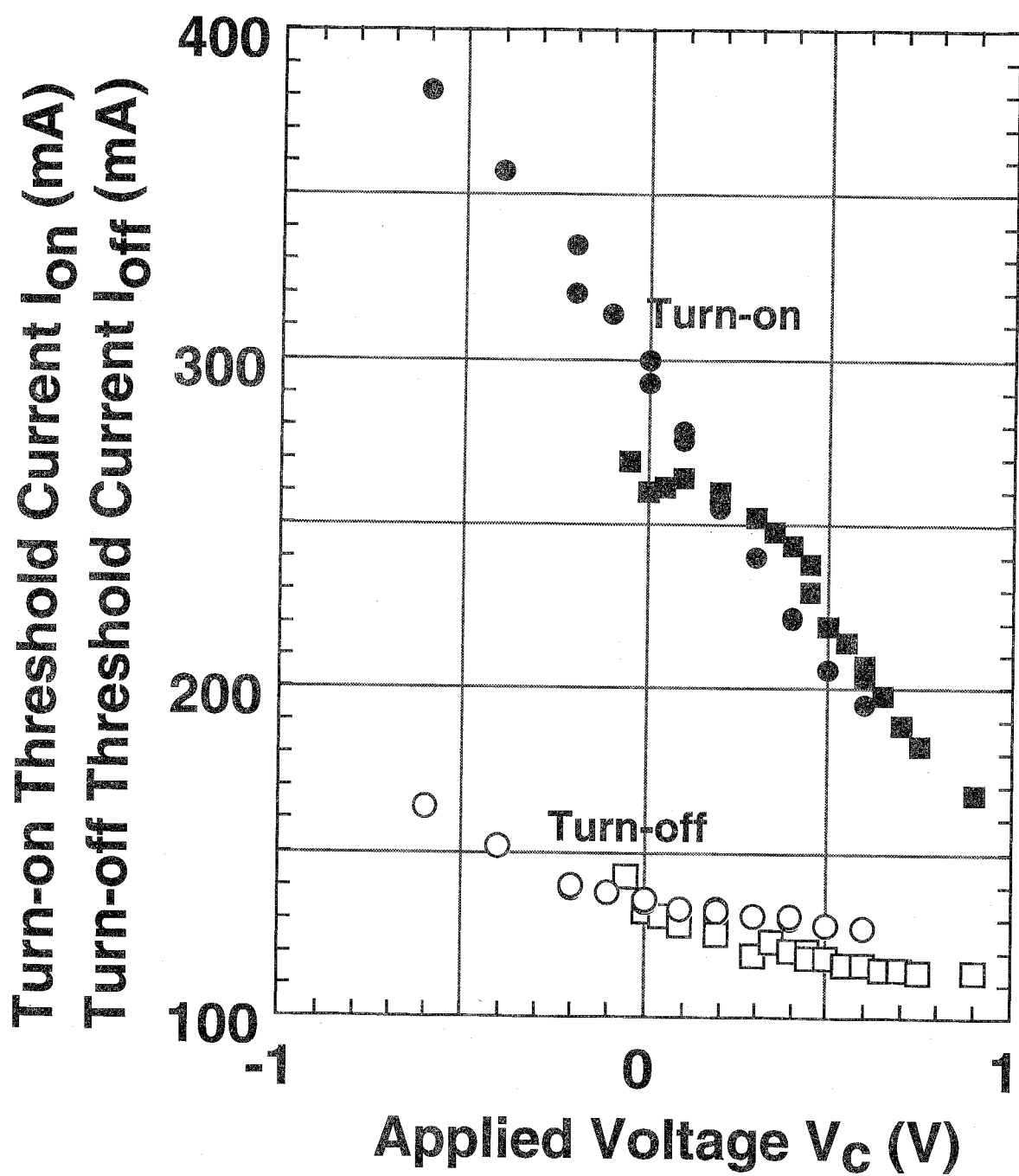
Fig. 4-5(a)
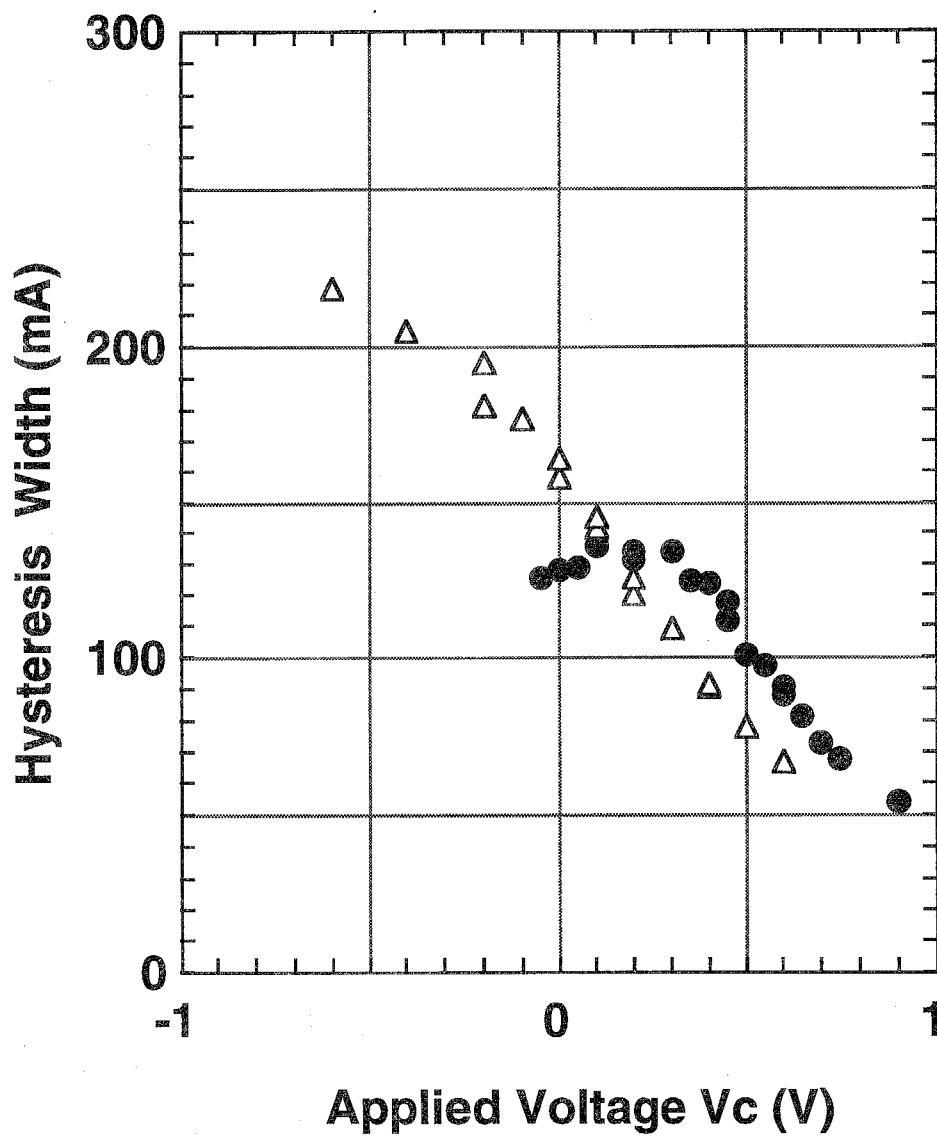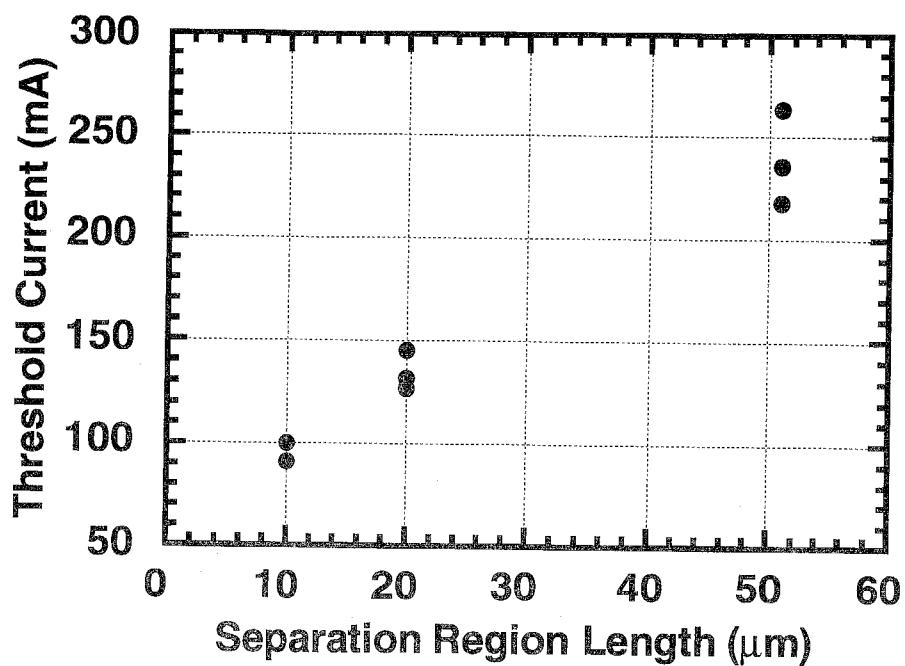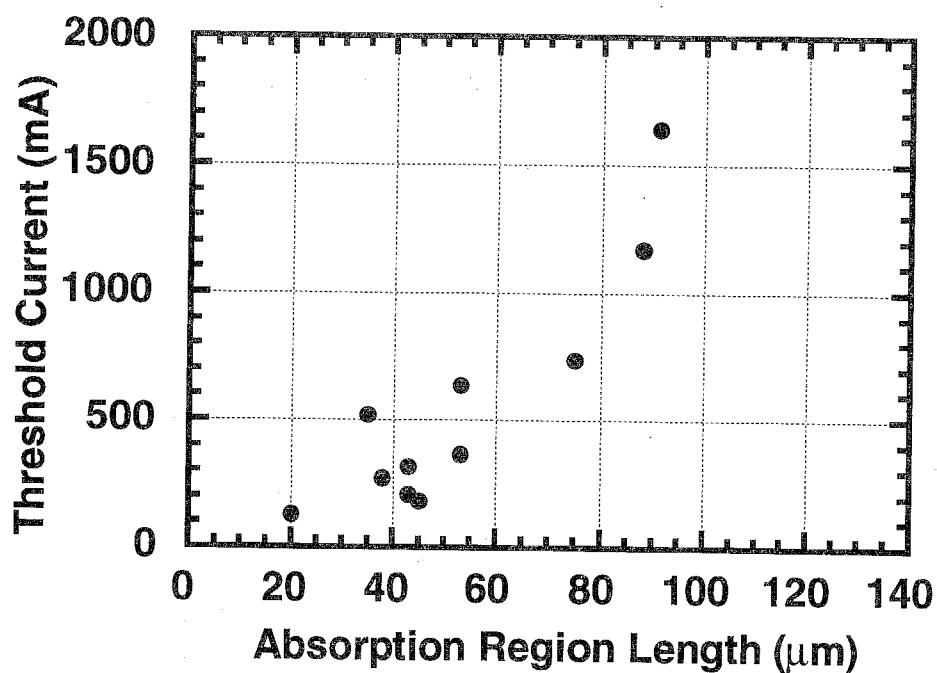Turn-on and turn-off threshold current versus applied voltage.

**Fig. 4-5 (b)**

The dependence of hysteresis width on voltage applied
to the saturable absorption region.

(a) Separation region length dependence



(b) Absorption region length dependence

Fig. 4-6

The threshold current dependence on (a) the separation region length and (b) the saturable absorption region length. In (a), the gain and saturable absorption region are common. In (b), the saturable absorption region is open.
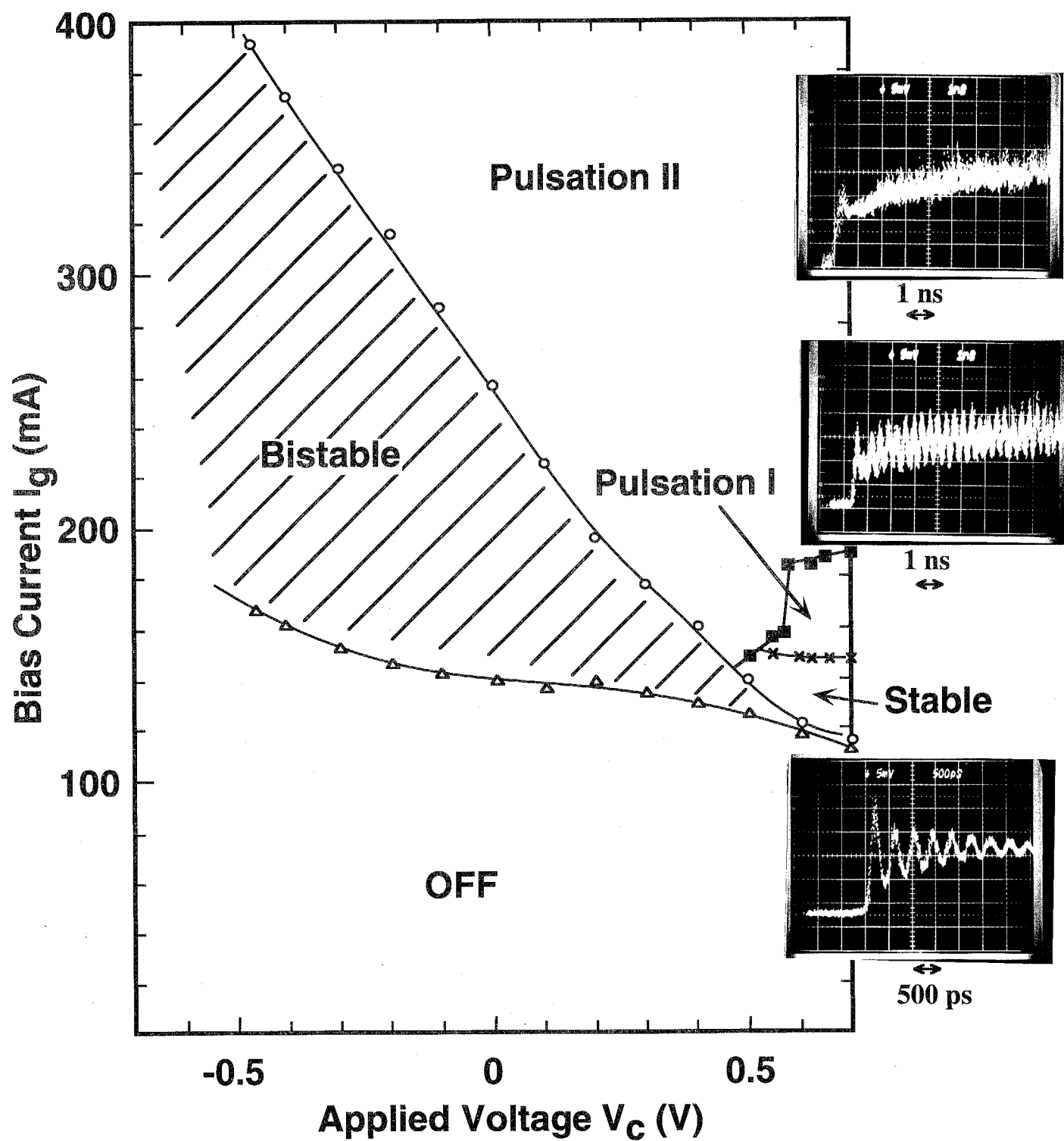
**Fig. 4-7**

**Stability map for InGaAs/InP MQW bistable laser.**

region I (relaxation oscillation continues during each pulse of the bias current), and pulsation region II (self-sustained pulsation occurs). The transient responses of the output light in each condition are shown in the insets. With small applied voltage, self-sustained pulsation occurs because the differential gain coefficient becomes large or the carrier lifetime becomes small. This was predicted theoretically by Ueno et al [5].

The devices with InGaAs/InGaAsP and InGaAs/InAlAs MQW structures, on the other hand, achieved CW operation. Both structures show clear hysteresis characteristics and the easy controllability by the voltage applied to the saturable absorption regions as seen in Figs. 4-8(a) and (b). The heat-sink temperature was stabilized by Peltier control at 20.0 degrees with 0.1-degree resolution. The turn-on threshold current changes from 35 mA to 80 mA, and the hysteresis width from 0 mA to more than 20 mA within the applied voltage change of 1 V. The applied voltages for InGaAs/InAlAs structures, however, are lower than those for InGaAs/InGaAsP MQW structures. Figure 4-9 shows the turn-on and turn-off threshold current for four 6-well InGaAs/InGaAsP MQW bistable lasers as a function of applied voltage. The reproducible controllability of hysteresis was obtained. The fluctuation of turn-on threshold current is seen at low applied voltage (< 0.2 V) due to thermal effect caused by high threshold current. The turn-on and turn-off threshold currents are summarized in Fig. 4-10 as a function of the voltage applied to the saturable absorption region. In InGaAs/InAlAs MQW structure, the hysteresis and comparatively low threshold current can be obtained with applied voltage of minus range. In InGaAs/InGaAsP MQW structure, the hysteresis appears around the built-in voltage and operation with reverse bias voltage is possible only when the threshold current is much higher. This is thought to be due to the sharper absorption edge of the InGaAs/InAlAs MQW. The photocurrent spectra for 10 periods of InGaAs/InAlAs MQWs and 12 periods of InGaAs/InGaAsP MQWs are shown in Fig. 4-11. Clearer heavy-hole exciton in addition to sharper absorption edge are due to the larger quantized effects of InGaAs/InAlAs MQW and these phenomena are consistent with the difference of bias voltage. It is predicted that high-speed reset operation can be
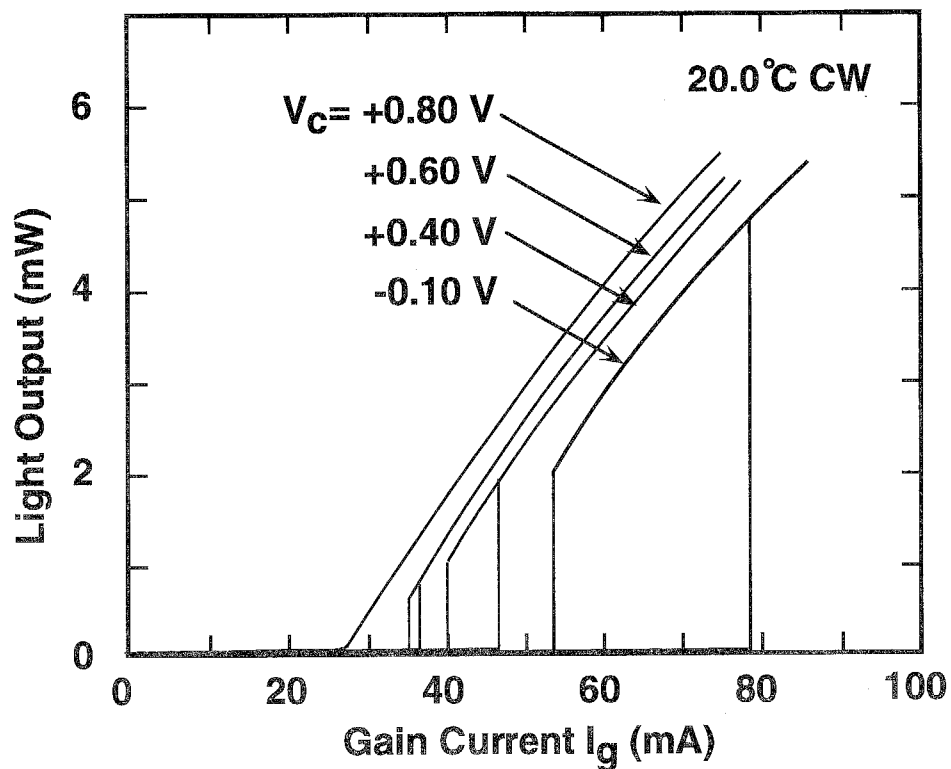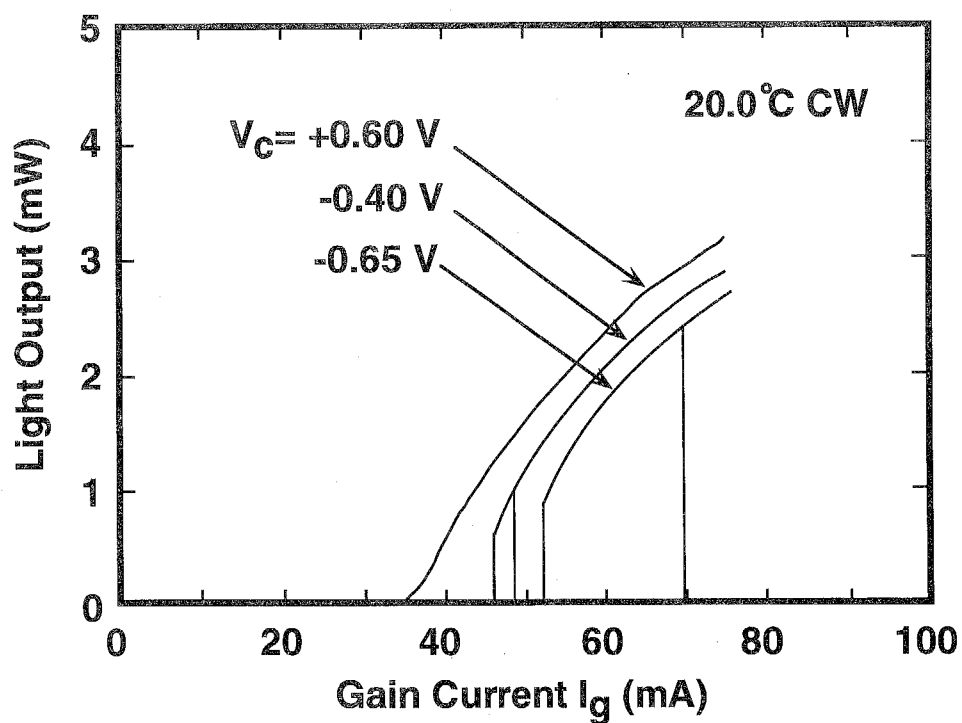
**Fig. 4-8**

Light output versus gain current characteristics for MQW bistable lasers with (a) 6 periods of InGaAs/InGaAsP and (b) 6 periods of InGaAs/InAlAs.
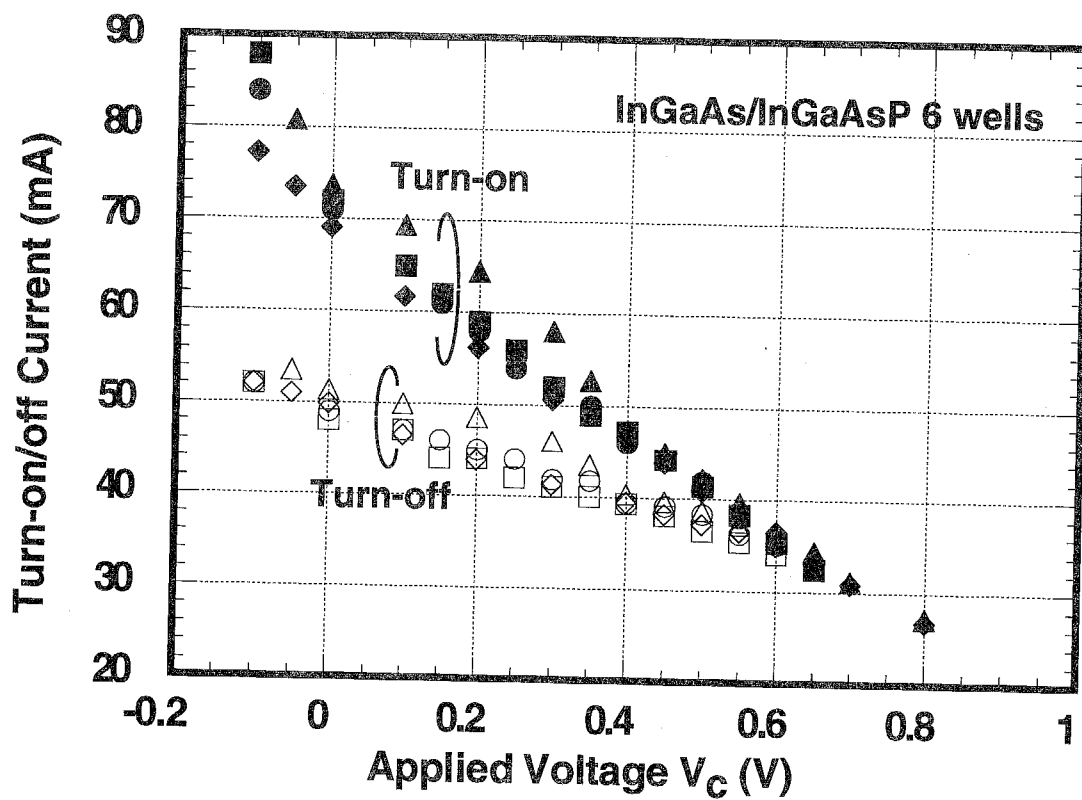
**Fig. 4-9**

Turn-on and turn-off threshold current for four 6-well InGaAs/InGaAsP MQW bistable laser as a function of applied voltage.
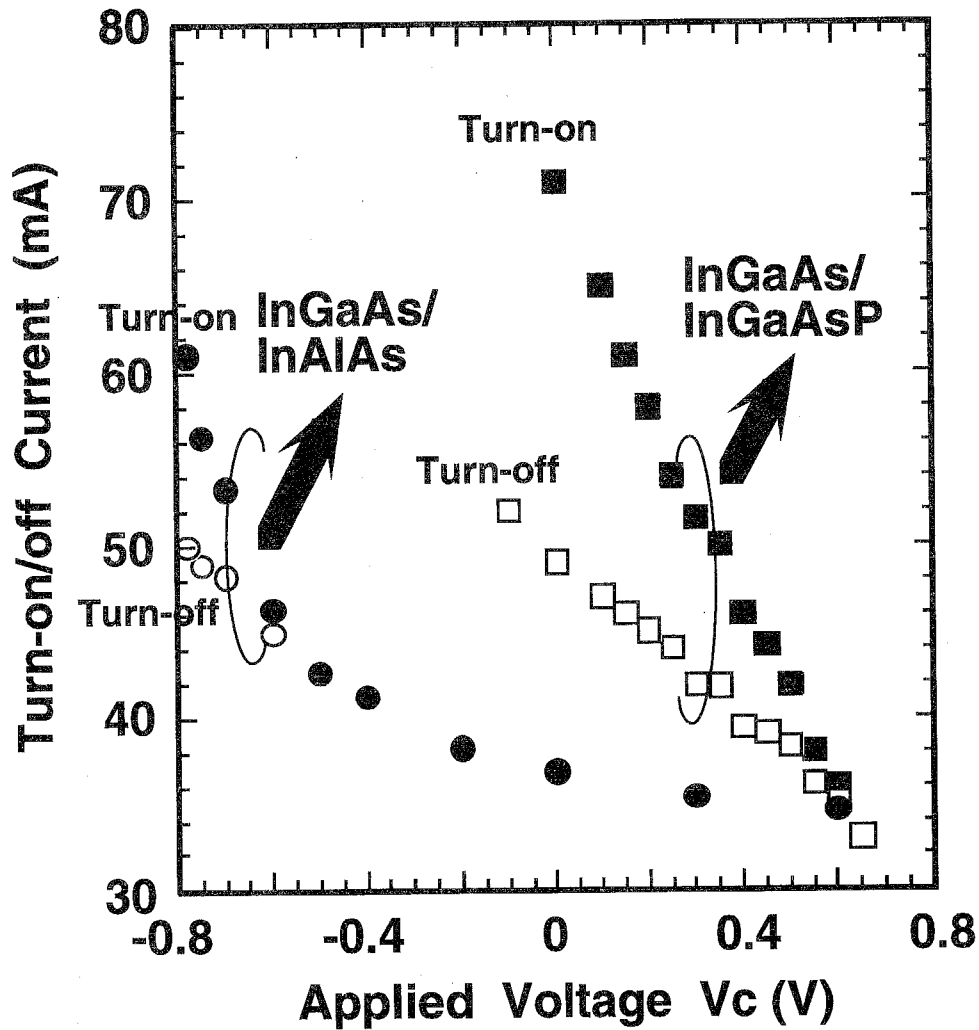
Fig. 4-10

The dependence of the turn-on and turn-off threshold currents on the voltage applied to the saturable absorption region of bistable lasers with InGaAs/InGaAsP and InGaAs/InAlAs MQW structures.
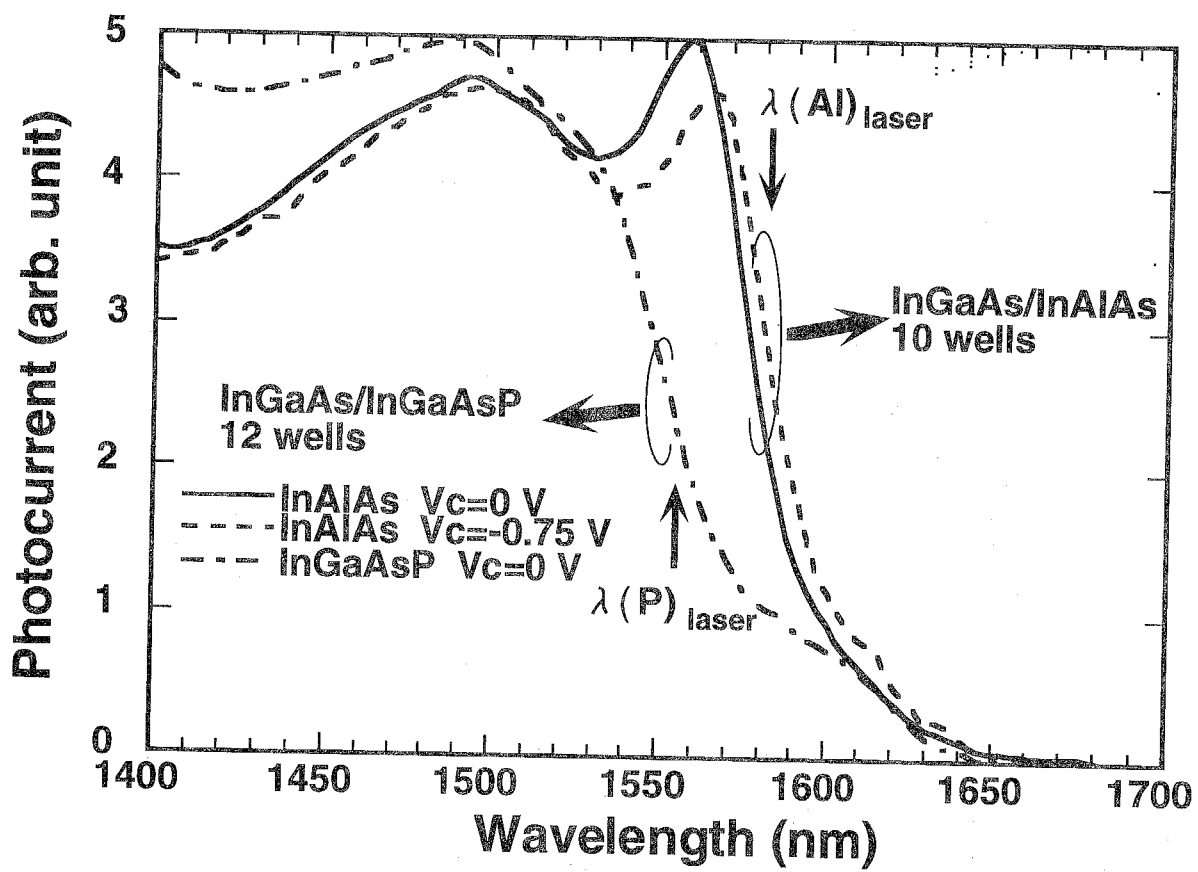
**Fig. 4-11**

Photocurrent spectra of InGaAs/InGaAsP and InGaAs/InAlAs MQW structures.
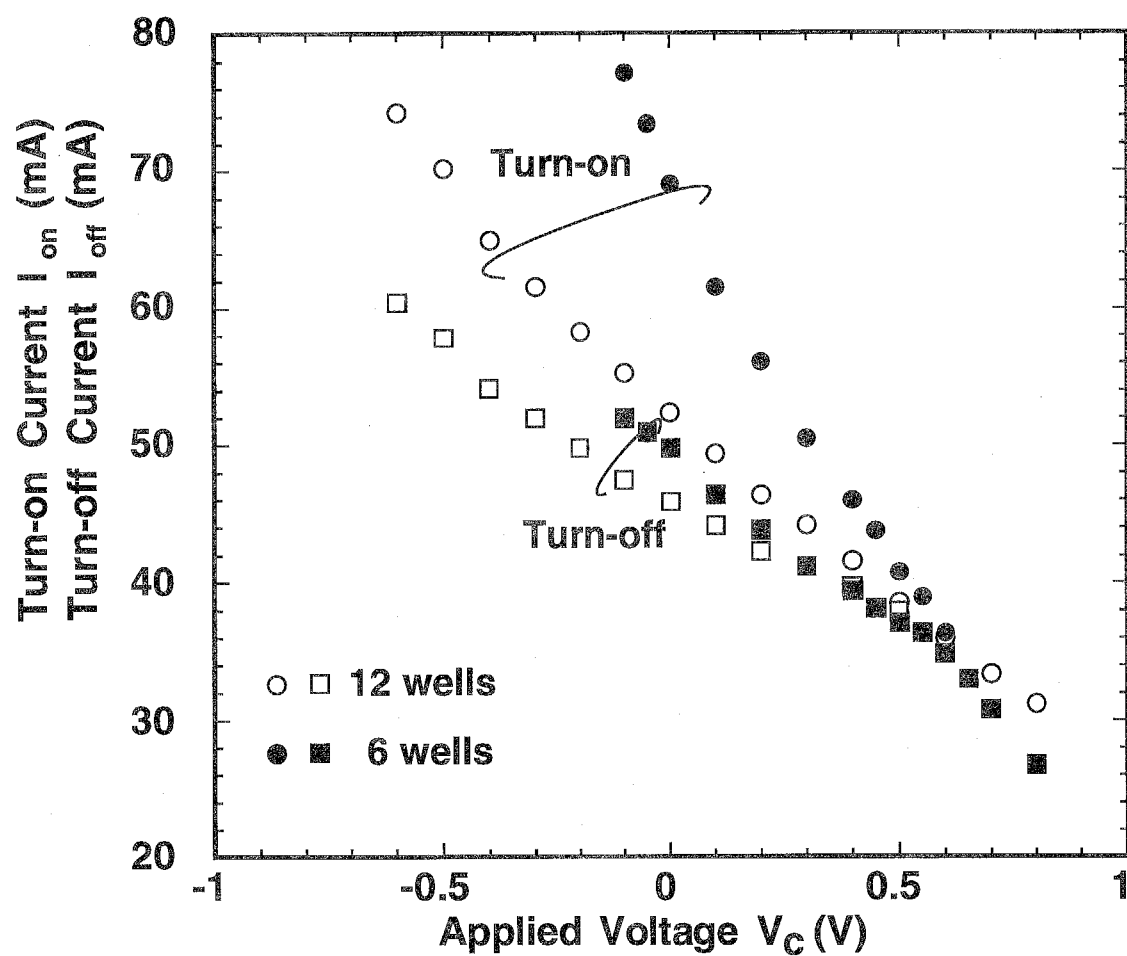
**Fig. 4-12(a)**

Turn-on and turn-off threshold current versus voltage applied to the saturable absorption region of bistable lasers with InGaAs/InGaAsP MQW structures.
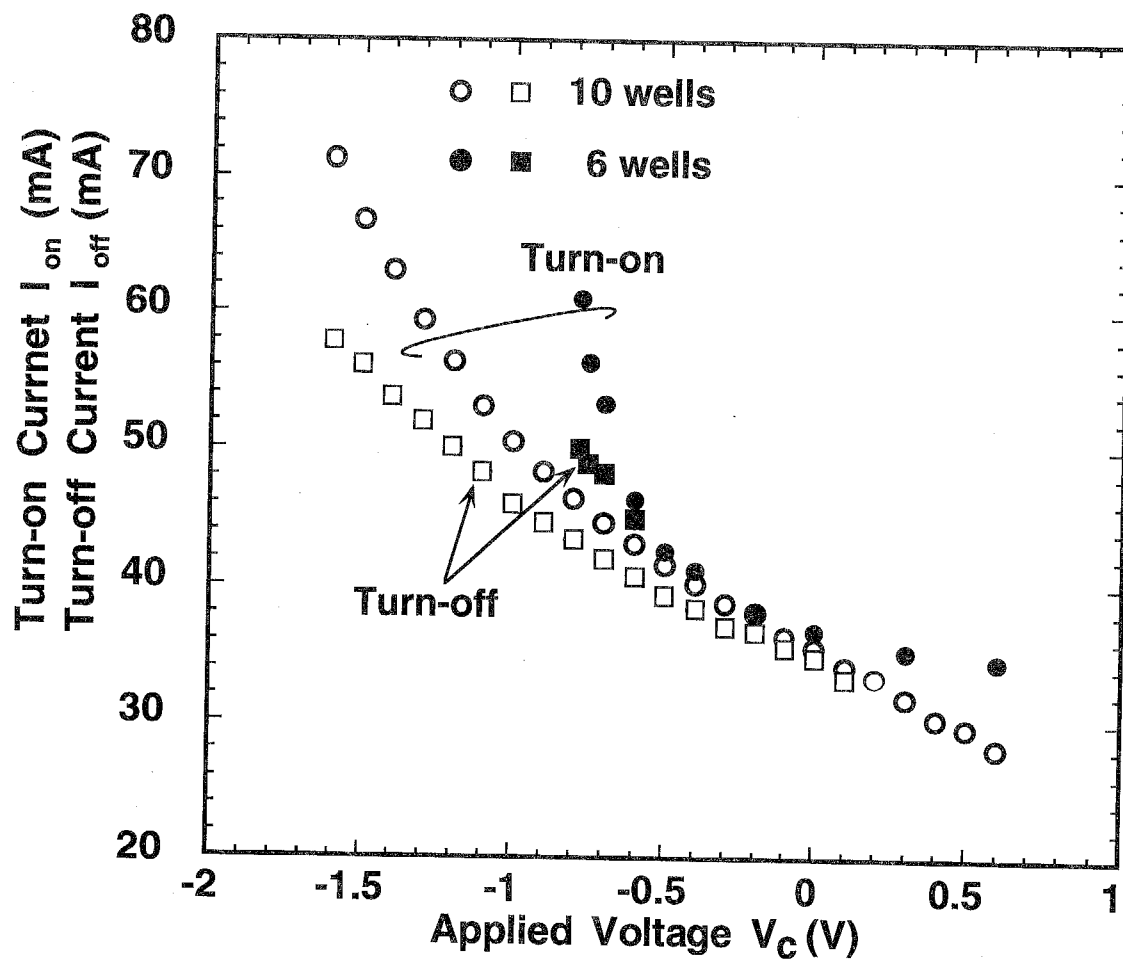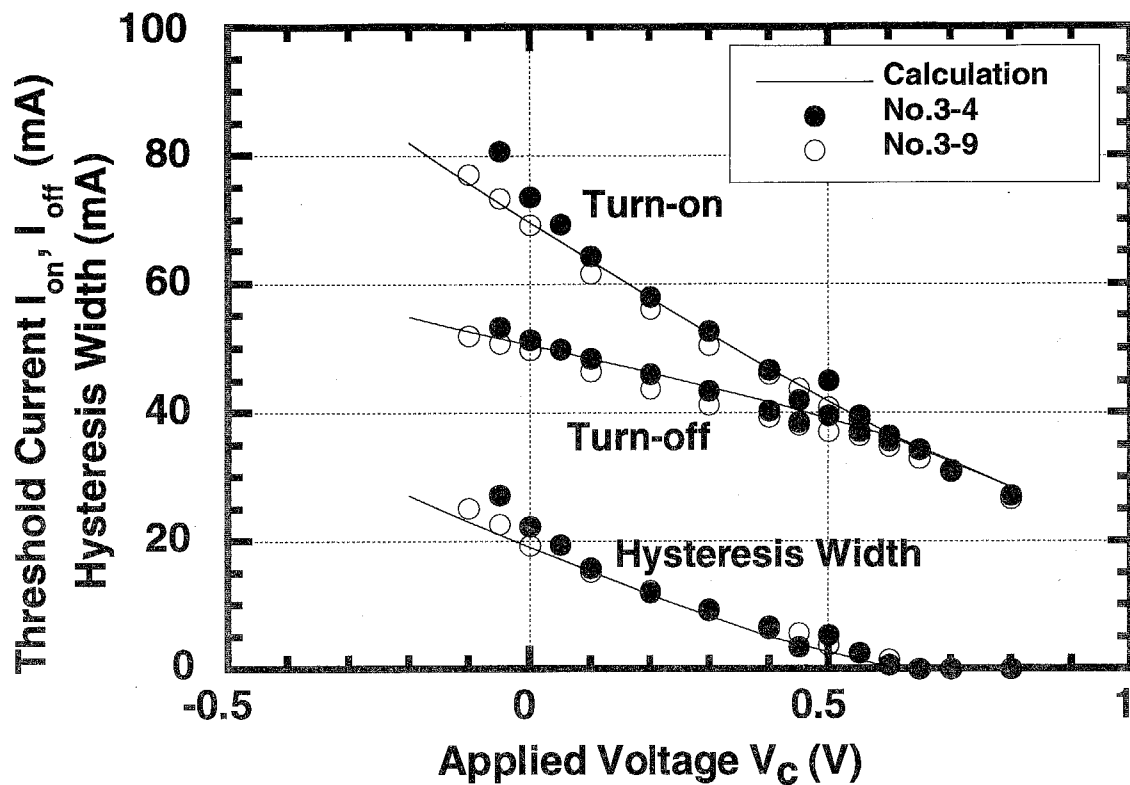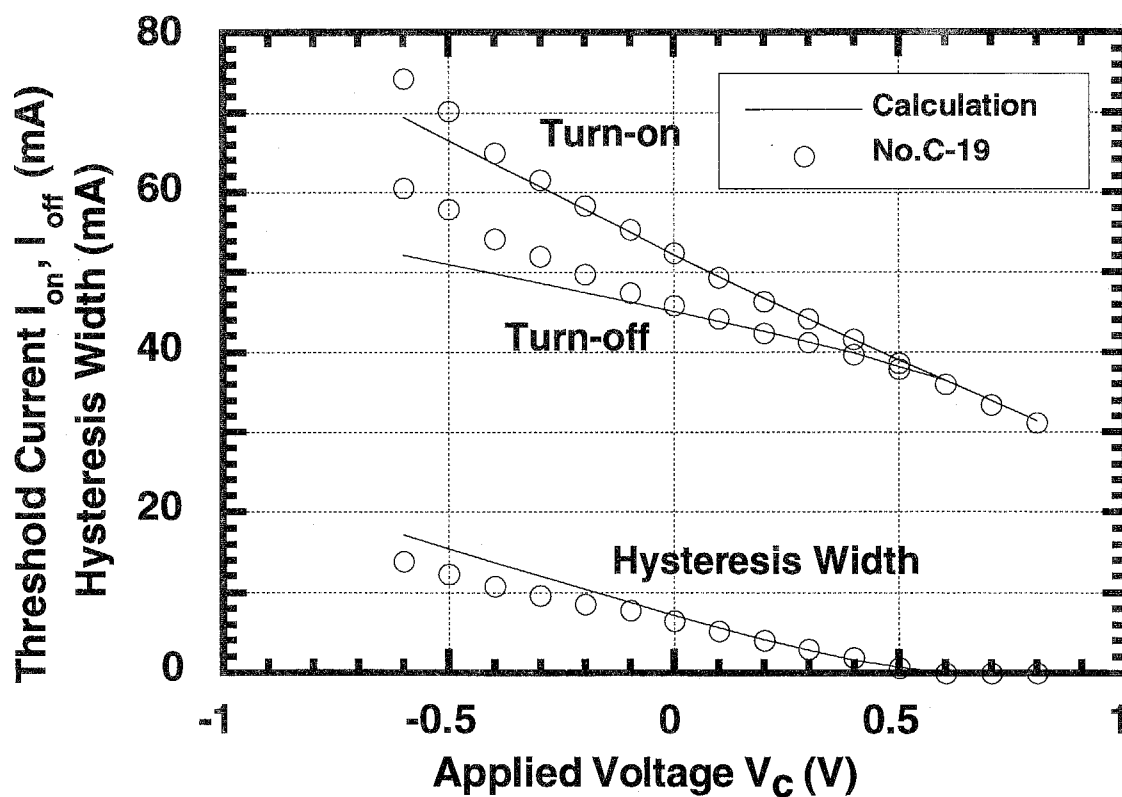
**Fig. 4-12(b)**

Turn-on and turn-off threshold current versus voltage applied to the saturable absorption region with InGaAs/InAlAs MQW structures.

Fig. 4-13

Calculated turn-on, turn-off currents and hysteresis width as a function of applied voltage. ( a) 6 periods of InGaAs/InGaAsP MQW structure and (b) 12 periods of InGaAs/InGaAsP MQW structure.

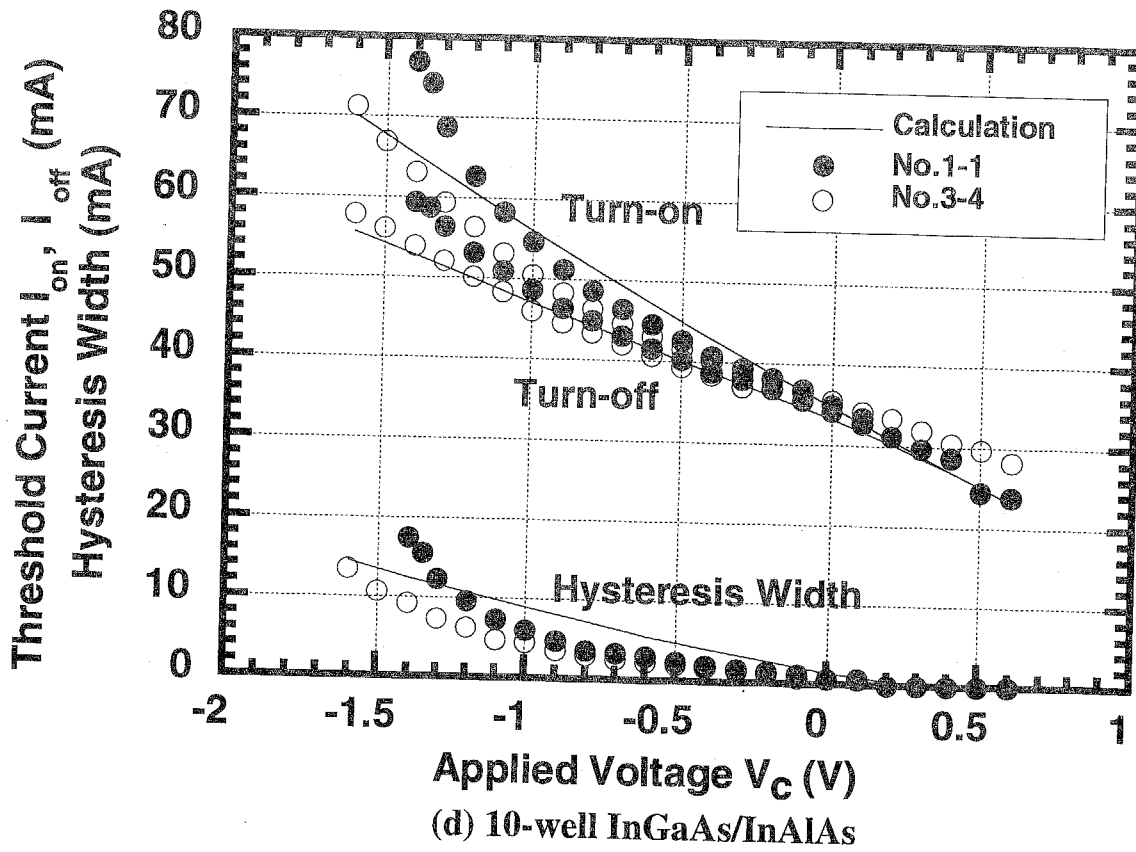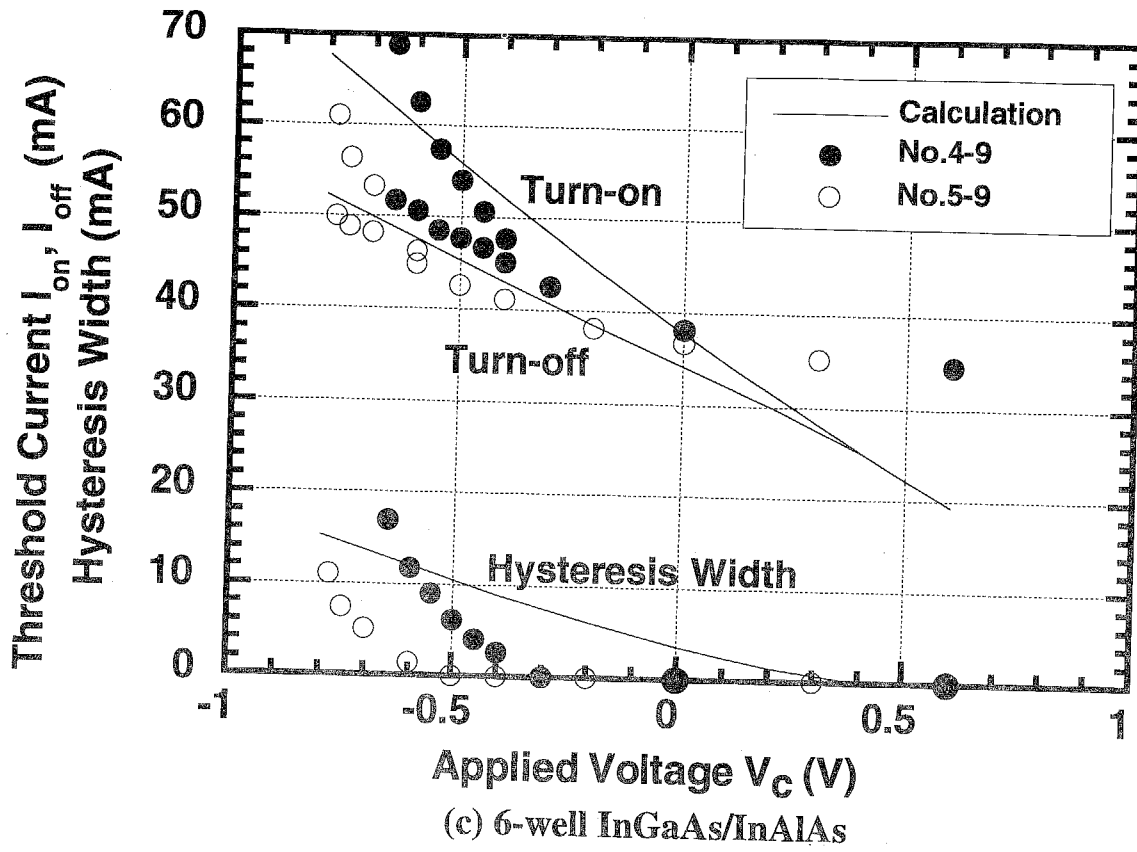(c) 6-well InGaAs/InAlAs



(d) 10-well InGaAs/InAlAs

Fig.4-13

Calculated Turn-on, turn-off currents and hysteresis width as a function of applied voltage. (c) 6 periods of InGaAs/InAlAs MQW structure and (d) 10 periods of InGaAs/InAlAs MQW structure.

achieved with InGaAs/InAlAs MQW structures because the carrier escape time can be reduced by applying a large electric field.

Figures 4-12(a) and (b) show the dependence of turn-on and turn-off threshold currents on well number for InGaAs/InGaAsP and InGaAs/InAlAs MQWs. At the same applied "electric field," the structure with more wells has a lower threshold current and a smaller hysteresis width. The main reason is thought to be due to the lower threshold carrier densities in the structures with the larger well number, that causes deviation between the absorption peak and the lasing wavelength. Moreover, the device with a larger number of wells has the advantage in terms of switching speed because its differential gain coefficient is larger.

Figures 4-13(a)-(d) compare the experimental and calculation results (which are obtained in Chapter 3) of the turn-on and turn-off current versus the applied voltage. The difference between InGaAs/InGaAsP and InGaAs/InAlAs MQW structures are the applied voltage at which the hysteresis emerges. This is considered to be due to the difference in absorption steepness and that is reflected in the differential gain coefficient $g_a$ and in the fitting parameters $r_1$ and $r_2$. The structures with the larger number of quantum wells showed slower increments of the hysteresis width against applied voltage, but that is mainly due to the electric field strength in the MQW being weaker at the same applied voltage. The results calculated for InGaAs/InGaAsP MQW structures agreed fairly well with the experimental results, but those calculated for the InGaAs/InAlAs MQW structures did not. The main reason for this deviation is either that the absorption edge shifts nonlinearly with applied voltage or that the internal applied electric field differs from the external applied voltage because it is affected by the large series resistance in the saturable absorption region.

## 4.2.2 Switching Power by Input Light

We have measured the switching operation of MQW bistable laser with input light. The experimental set-up is shown in Fig. 4-14. A CW color-center laser was used
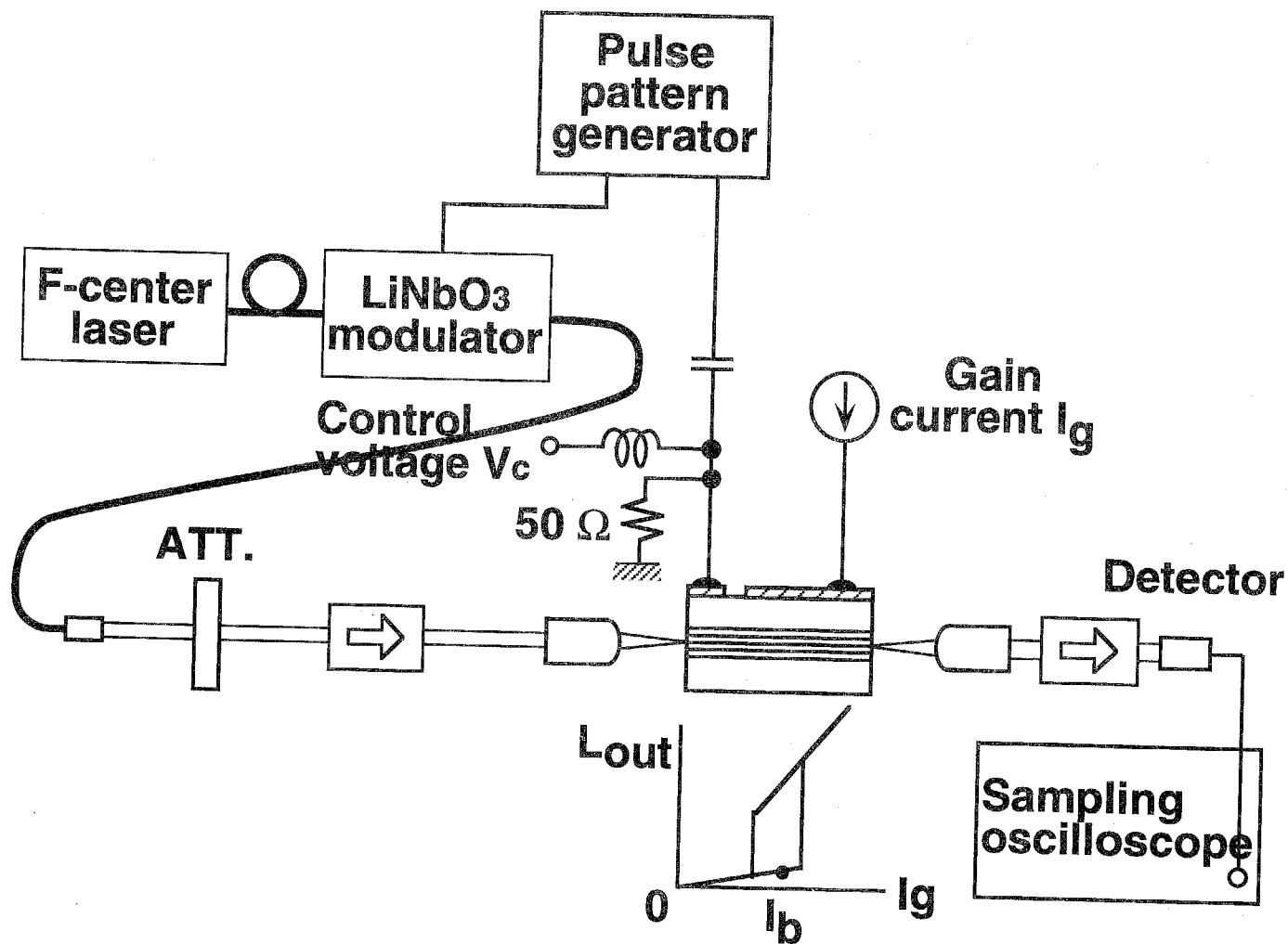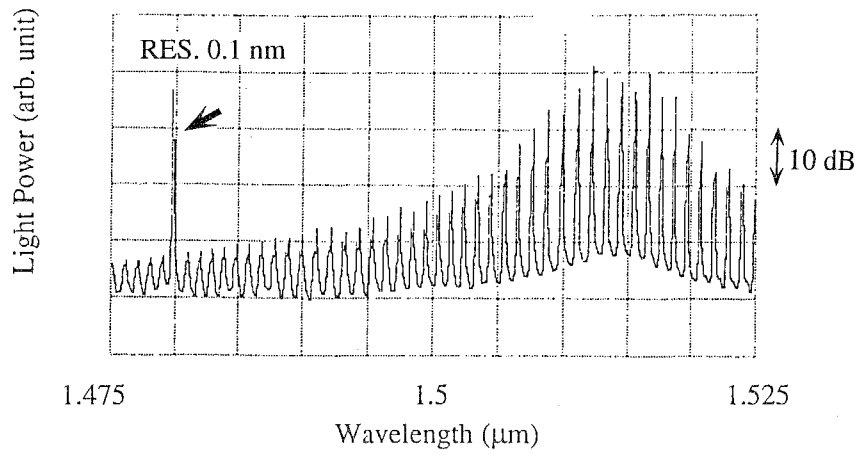
**Fig. 4-14**

Experimental setup for input light switching operation of two-segmented bistable laser.

as a light source, and the wavelength tunable range was from 1.48 to 1.58 μm. The input light pulse with a 1010... pattern was generated by using a LiNbO$_3$ modulator driven by a pulse pattern generator. The input light had a repetition rate of 200 MHz and a pulse width of 600 ps. And also the on/off ratio of input light was greater than 10:1. A quarter-wavelength plate (QWP) and a half-wavelength plate (HWP) aligned the polarization of the input light with TE mode, and this light was injected into the saturable absorption region side of the bistable laser. The input light power was measured in front of the bistable laser by splitting the light by polarization beam splitter (PBS). In the time response experiment, the output signal was detected by an InGaAs photodetector with a 15-GHz bandwidth and the signal waveform was observed by using a digital sampling oscilloscope. The external 50-Ω resistance was terminated because the internal resistance of the saturable absorption region was large under reverse bias voltage. When the input/output light characteristics were investigated, on the other hand, an optical power meter was used instead. The memory operation by the bistable laser was of interest in these experiments, so the gain current was biased between the turn-on and turn-off threshold currents, i.e., inside the hysteresis as depicted in the inset. The laser temperature was stabilized by using Peltier control within the fluctuation less than 0.1 degrees. Set operation was performed by input light and reset operation was achieved by changing the voltage applied to the saturable absorption region.

A bistable laser can be switched-on by input light over a wide range of wavelengths. Figures 4-15(a)-(c) illustrate the optical spectrum of the InGaAs/InAlAs MQW bistable laser when input lights of 1.48 μm, 1.51 μm, or 1.53 μm were injected. In each case, the amplified input light as well as the lasing spectrum of the bistable laser itself can be seen, as pointed out by the arrows. Optical band-pass filter is needed to isolate the output light from the bistable laser from amplified input light. The minimum input light power for set operation versus the input light wavelength is shown in Fig. 4-16. In these experiments, the voltage applied to the saturable absorption region was biased at +0.2 V in the InGaAs/InGaAsP MQW structure and -0.225 V in the InGaAs/InAlAs MQW structure. Both structures had almost the same hysteresis width of

(a) $\lambda_{in} = 1.48 \ \mu m$
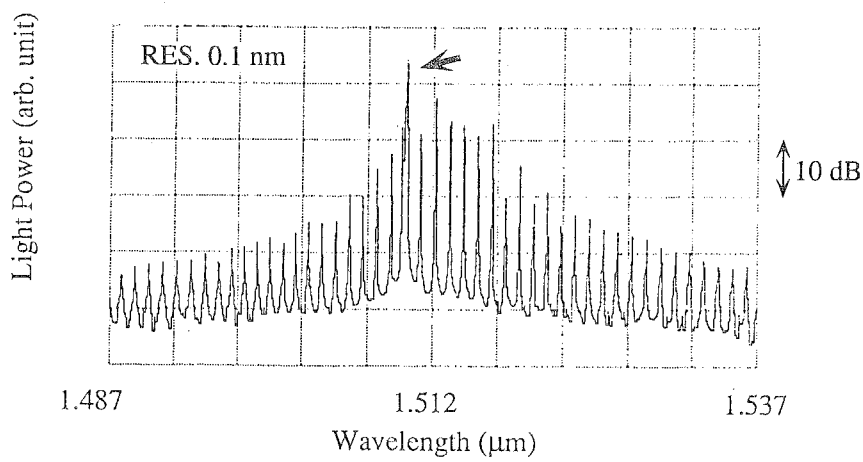
(b) $\lambda_{in} = 1.51 \ \mu m$
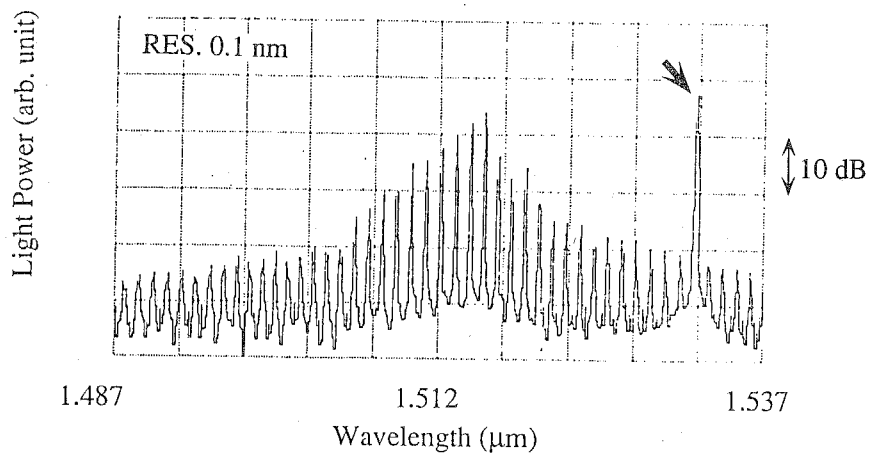
(c) $\lambda_{in} = 1.53 \ \mu m$

**Fig. 4-15**
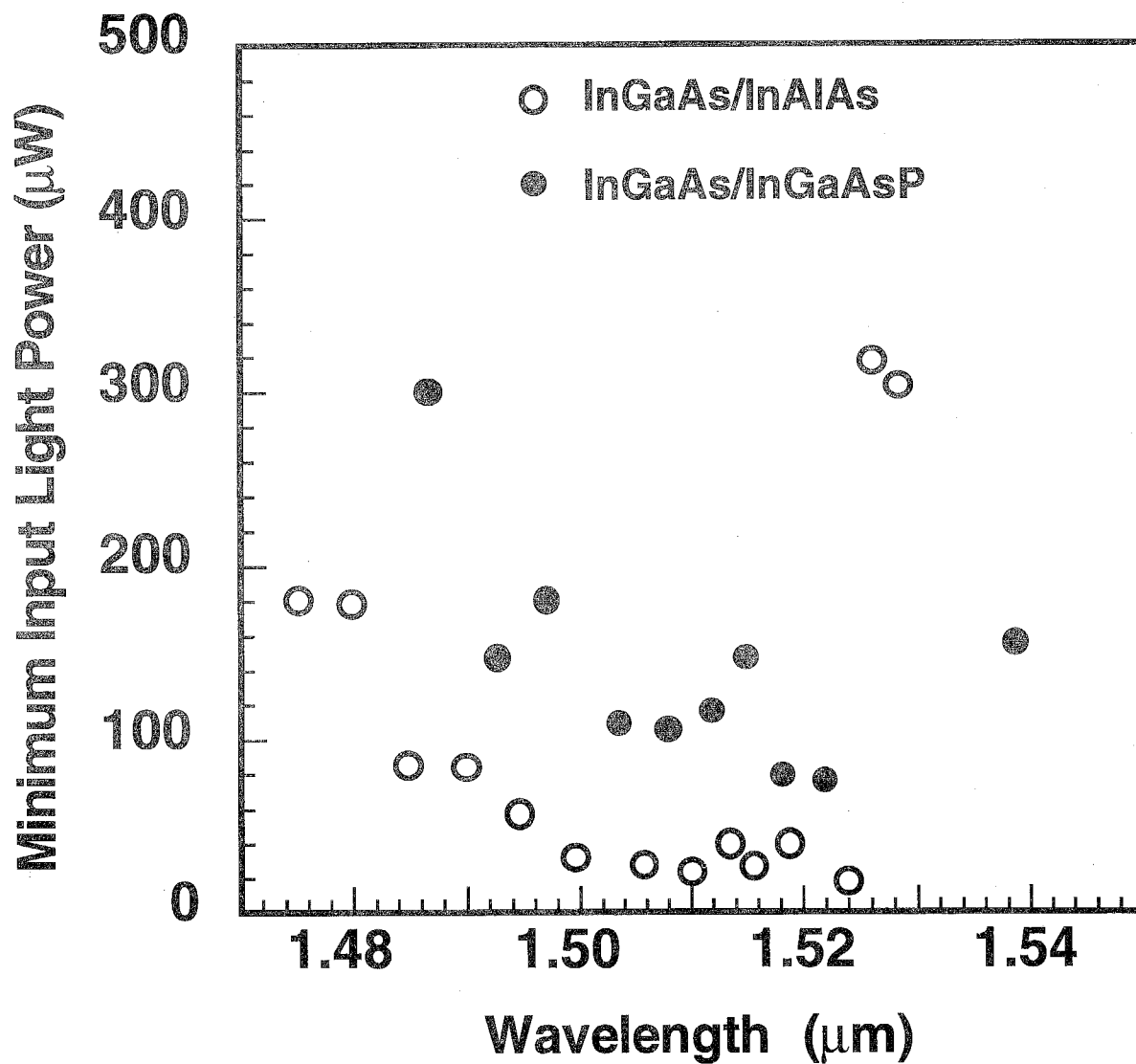**Lasing spectra of the two-segmented MQW bistable laser under light injection**

Fig. 4-16

Minimum input light power for set operation of InGaAs/InGaAsP and InGaAs/InAlAs MQW structures versus input light wavelength. Vertical axis represents the peak power of the input light pulse.

13 mA. The gain currents were biased at 1.0 mA below the electrical turn-on threshold current in both structures, and the input light wavelengths were adjusted to the Fabry-Perot resonance peaks to minimize the switching power. Wavelength tolerances of 50 nm were obtained in both materials. This indicates that the bistable laser can be operated by input light whose wavelength is within the gain bandwidth. The minimum input light peak power in the InGaAs/InAlAs MQW structure was about 20 μW. This is larger than calculation results shown in Fig.3-6(b). The main reason is that the width of the input light pulse was 600 ps and the repetition rate was 5 ns, so the set operation with longer turn-on time could not be measured. In the InGaAs/InGaAsP MQW structure, the minimum input light peak power was around 80 μW and that was higher than that of InGaAs/InAlAs MQW structure. This is different from calculation results as shown in Fig.3-6(a) and (b). From calculations, the threshold input light switching power is almost the same between InGaAs/InGaAsP and InGaAs/InAlAs MQW structures. We consider that the deviation of the experimental results from the calculated ones is caused not by the intrinsic factor but by the extrinsic factors, that is, the coupling loss between the coupling lens and the laser facet and the deviation of the injection light wavelength from the Fabry-Perot resonance peak. The sensitivity of the InGaAs/InAlAs MQW structure was drastically increased at longer wavelengths because the absorption edge of that material was abrupt.

## 4.3   Dynamic Characteristics

### 4.3.1   Switching Operation

In a memory storage device or a device for demultiplexing time-division-multiplexed data, the memory operation shown by bistable lasers is important. Bias current was thus set between the turn-on and turn-off threshold currents (inside hysteresis) in the following experiments. The switching operation was observed when applying a bipolar voltage to the saturable absorption region, and the time response of the output light

is shown in Fig. 4-17. The bistable laser used here was an InGaAs/InP MQW structure. In this experiment, relative to the bias voltage, the set and reset voltages were +0.4 V and -0.7 V, respectively. These were superimposed on +0.2 V bias voltage. Both set and reset pulse widths were 10 ns, and the rise time and fall time were each less than 200 ps. Turn-on time decreases with increasing set-on voltage because the difference of the cavity loss between the bias state and the on state becomes larger for larger set-on voltages and the difference of the inversion population also increases. The turn-on time was less than 200 ps, and the turn-off time decreased with decreasing applied voltage $V_c$ (increasing reverse bias voltage). When the applied voltage $V_c$ was -5 V, the turn-off time was 600 ps.

Figure 4-18 shows the transient curve trace of the switching operation of two-segmented bistable laser with InGaAs/InGaAsP MQW structure when the switching operation was performed by injecting a set-on light pulse. Similar results were obtained in InGaAs/InP and InGaAs/InAlAs MQW structures. When input light was injected into the bistable laser, the output light was switched from the spontaneous emission state (OFF state) to the lasing state (ON state). And just after the reset voltage was applied, the output light switched from ON state to OFF state.

### 4.3.2    Turn-on  Characteristics

Figure 4-19 shows the dependence of the turn-on time on input light peak power in InGaAs/InAlAs and InGaAs/InGaAsP MQWs. The driving conditions, for example, the applied voltage to the saturable absorption region and the gain current, were the same as those given in Section **4.2.2**. The input light wavelength is near lasing wavelength of the main mode, and the turn-on time decreases with increasing input light power. The difference between the two kinds of MQW structures was small and the turn-on time of 86 ps was obtained with 800-$\mu$W input light. The minimum switching energy, which is defined as a product of turn-on time and the input light peak power, was less than 10 fJ. This is about one order of magnitude larger than other group. [6]  However, the bias current was set at 0.1 mA below the electrically turn-on current in reference 6.
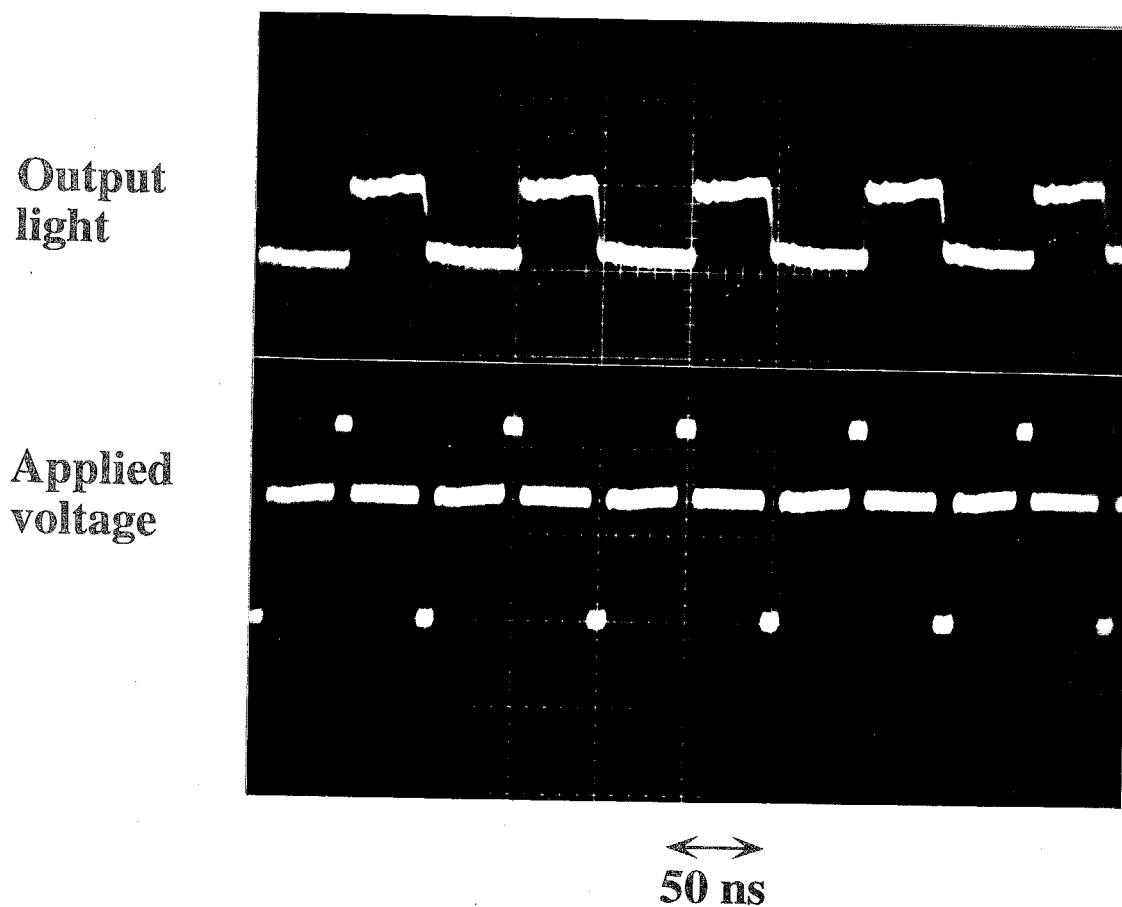
Output
light

Applied
voltage

← 50 ns →
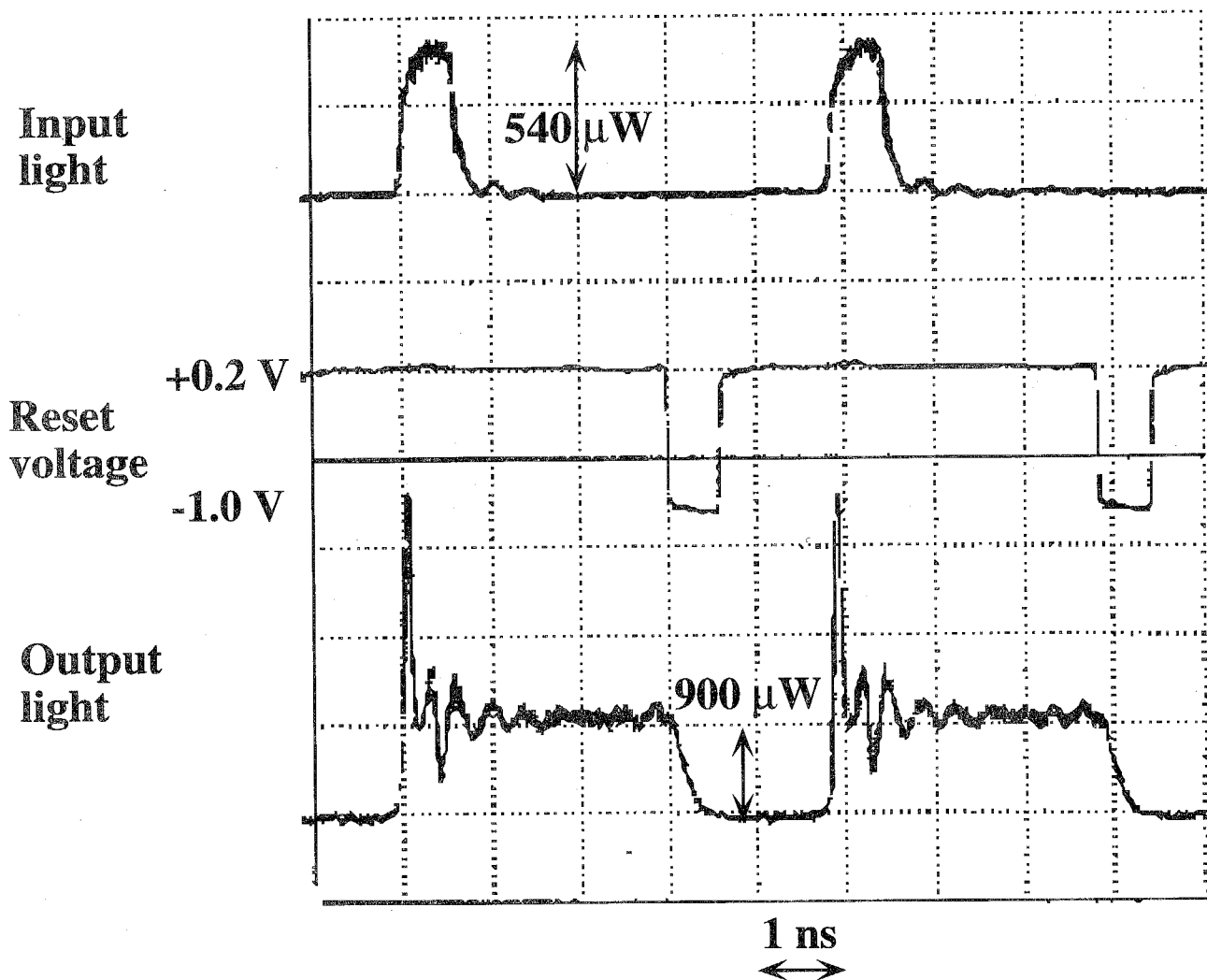
Fig. 4-17

Switching operation by applying bipolar voltage to saturable absorption
region. The active region consists of InGaAs/InP MQWs.

Input
light

540 μW

+0.2 V

Reset
voltage

-1.0 V

Output
light

900 μW

1 ns

Fig. 4-18

Operation characteristics of the two-segmented MQW bistable laser
with an active region consisting of 6 periods of InGaAs/InGaAsP active
region.

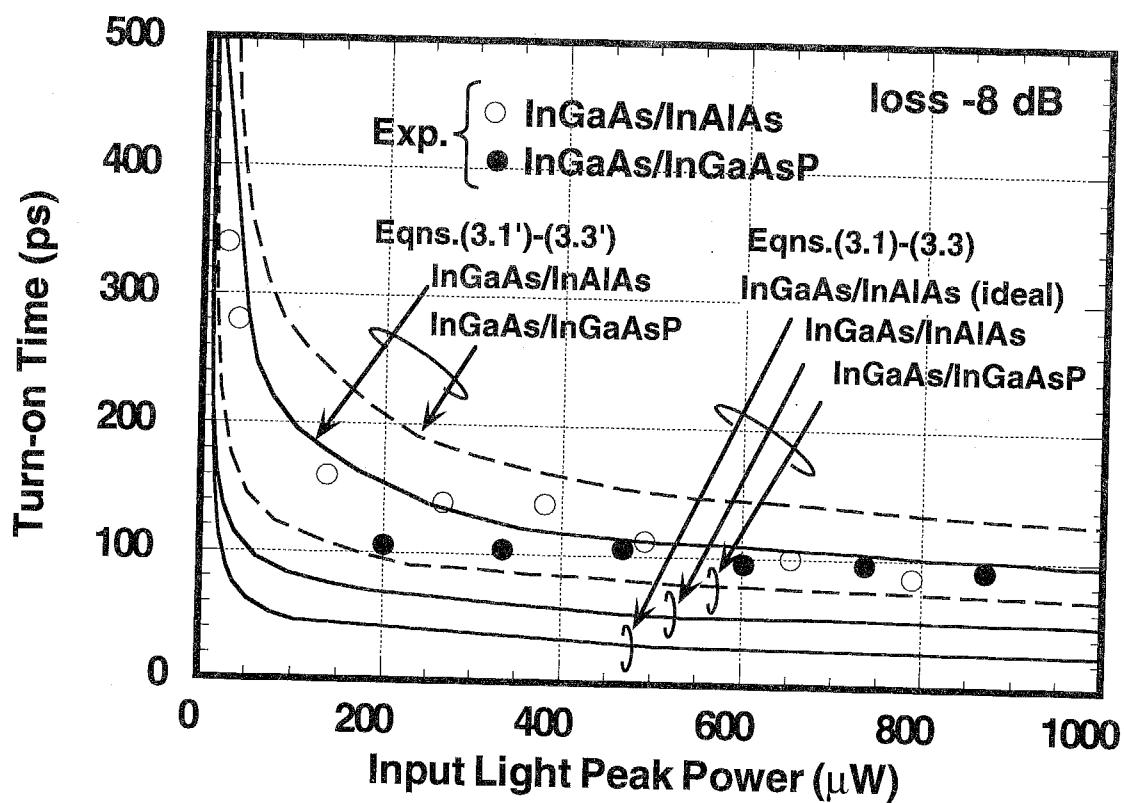**Fig. 4-19**

The dependence of turn-on time on input light peak power for two-segmented bistable lasers with InGaAs/InGaAsP and InGaAs/InAlAs MQW structures. Circles represent the experimental results and lines represent the calculation results.

Comparable switching power can be achieved by reducing the offset of turn-on and the bias current.

Calculation curves in 6 periods of InGaAs/InGaAsP and InGaAs/InAlAs MQW structures as shown in Fig. 3-10 are also plotted in the figure. The solid lines are for 6-well InGaAs/InAlAs MQW structure, and the dotted lines are for 6-wells InGaAs/InGaAsP MQW structures. And also, the calculations using eqns.(3.1) to (3.3), or eqns.(3.1') to (3.3') were compared. As mentioned in Chapter 3, the eqns.(3.1) to (3.3) express the situation that the input light coherently couples into the lasing mode. In case of eqns.(3.1') to (3.3'), the input light contributes to only absorption saturation because of the input light wavelength differing from the lasing wavelength of the main mode. The lowest line represents the calculation results in InGaAs/InAlAs MQW structure without considering the transient time of the input light pulse and the electrical bandwidth of the measurement apparatus. On the other hand, the other lines represent the calculation results with considering the transient time of the input light pulse and the electrical bandwidth. The measured transient time of the input light pulse was 66 ps. The bandwidth of the optical detector was 15 GHz. It is found that both factors affect the switching speed especially in less than 100 ps regime.

To fit the experimental results to the calculation ones, coupling loss of -8 dB is assumed. The -8 dB coupling loss includes the coupling loss for light injection (-3 dB) and for input light wavelength deviation from Fabry-Perot mode (-5 dB). The wavelength deviation can be estimated from eqns.(3.4) to (3.6). By using the peak to valley ratio of the electroluminescense of about 20 dB from measurement, the net gain in the laser cavity of 33.4 cm$^{-1}$ can be obtain by Hakki and Paoli method given as follows [7]:

$$G_{net} = \frac{1}{L} \ln \left( \frac{\sqrt{r_i} - 1}{\sqrt{r_i} + 1} \right) + \frac{1}{L} \ln \left( \frac{1}{R} \right) \qquad (4.1)$$

$$r_i = \frac{P_i + P_{i+1}}{2 v_i} \qquad (4.2)$$

$$G_{net} = \xi G_i - \alpha_{in} \tag{4.3}$$

where $G_{net}$ is the net gain in the laser cavity, L is the cavity length, R is the mirror reflectivity (0.3 for the cleaved facet), $P_i$ and $P_{i+1}$ are the peak light intensity in the ith and (i+1)th mode, $v_i$ is the light intensity in the valley between ith and (i+1)th mode, $G_i$ is the gain in the ith mode, and $\alpha_{in}$ is the internal loss. From eqns.(4.1) to (4.3), the wavelength deviation giving -5 dB Fabry-Perot gain degradation is estimated to be 0.6 Å. The wavelength dependence of the input light switching power caused by Fabry-Perot resonance was reported by Odagawa et al. [8]

The experimental results positioned between the calculation results using eqns.(3.1) to (3.3) and eqns.(3.1') to (3.3'). The switching conditions were near the situations that the input light incoherently coupled into the lasing mode in InGaAs/InAlAs MQW structure, and on the other hand, that the input light coherently coupled into the lasing mode in InGaAs/InGaAsP MQW structure. This difference is considered to be attributed to the difference of the offset of the input light wavelength from the lasing wavelength. The difference of the input light wavelength from the lasing wavelength was 9 nm (almost eight-mode difference) in InGaAs/InAlAs MQW structure, and 2 nm (two-mode difference) in InGaAs/InGaAsP MQW structure, respectively. In addition to this, it is considered that the distortion near the peak intensity of the input light pulse, or the multi-mode of the light emitted from the F-center laser reducing the effective input light power coupled into the laser cavity could degrade the turn-on speed. Therefore, it is very important that the single-mode input light wavelength is adjusted to the lasing wavelength for low switching power and fast switching speed in in-line light-injection MQW bistable lasers.

### 4.3.3   Turn-off Characteristics

The results of investigating reset operations by applied voltage are shown in Fig. 4-20. The gain current was biased at 1 mA below the electrical turn-on threshold current (12 mA above the electrical turn-off current). This condition was the same as that used
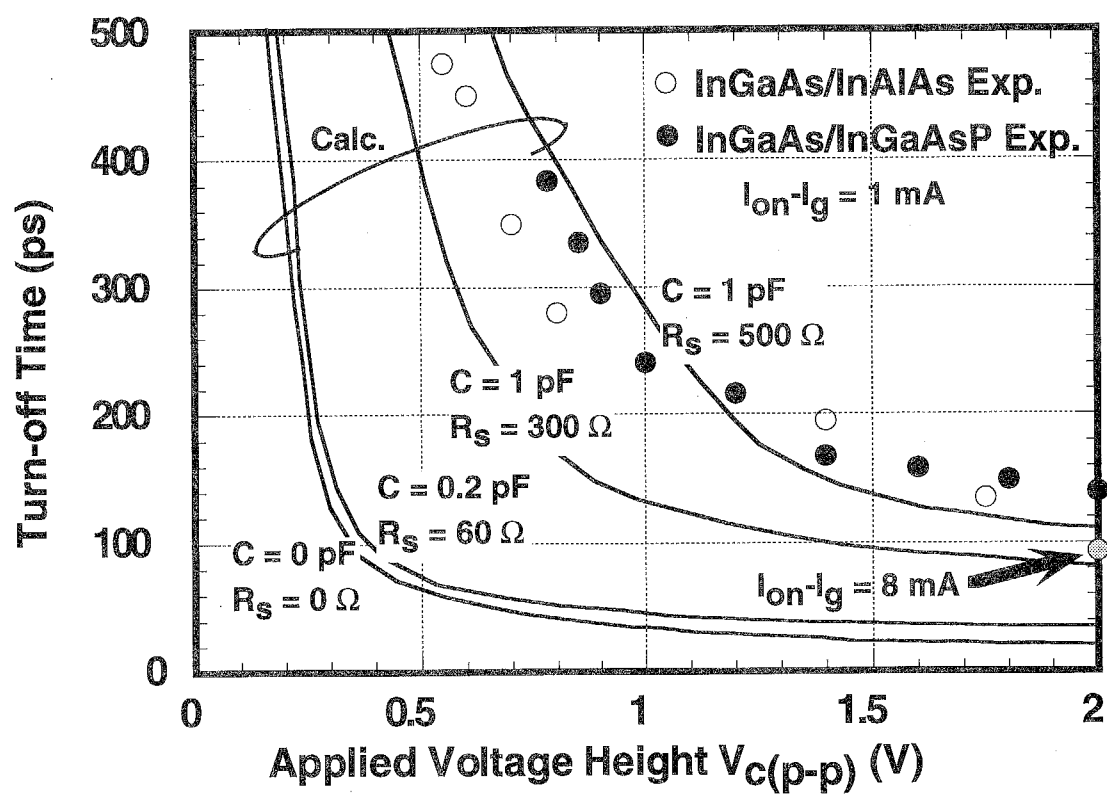
**Fig. 4-20**

The dependence of turn-off time on applied voltage height for two-segmented bistable lasers with InGaAs/InGaAsP and InGaAs/InAlAs MQW structures.

for evaluating set operation. The width of the applied voltage pulse was 600 ps. The turn-off time decreases when the applied voltage height becomes large, and it was slightly shorter in the InGaAs/InAlAs MQW structure than in the InGaAs/InGaAsP MQW structure. This faster turn-off time is thought to be due to the difference of the differential gain and to the fast carrier escape time. A turn-off time of about 100 ps was obtained when the applied voltage height was 2.0 V. The turn-off time decreased when the gain current approached the electrical turn-off current. When the gain current was biased 8 mA below the turn-on current, the turn-off time of 93 ps has been achieved with an applied voltage height of 2 V [9]. The electrical switching energy was estimated to be 7.4 pJ.

The calculated turn-off time (illustrated in Fig. 3-12 or later in Fig.7-9) is also shown in Fig.4-20. In the figure, the parasitic capacitance C and the parasitic (series) resistance $R_s$ were varied as parameters. And electrical bandwidth of measurement apparatus (pulse generator, module, and detector) are also considered. The experimental results are much larger than the calculated results without parasitic components, whereas they agree well with the calculated results considering parasitic capacitance of 1 pF and parasitic resistance of 500 $\Omega$. The parasitic capacitance in the saturable absorption region of 1 pF was obtained by C-V measurement. The resistance in the saturable absorption region (10-$\mu$m length) of 500 $\Omega$ corresponds to 17-$\Omega$ parasitic resistance of 300-$\mu$m cavity laser diodes. The reason for the deviation of experimental and calculation results is considered to be due to the degradation of the electrical bandwidth of the electrical circuit. The electrical bandwidth of the laser module, the leading edge of the pulse pattern generator of about 30 ps, parasitic capacitance and parasitic resistance all degrade the leading edge of the applied voltage pulse. The modulation bandwidth caused in the equivalent circuit is given by $1/(2\pi C R_s)$, so the derived modulation bandwidth is 0.32 GHz (10 %-90 % transition time of 1.1 ns) when the parasitic capacitance is 1 pF and the parasitic resistance is 500 $\Omega$. The reason for the large parasitic resistance is the degradation of the p-contact resistance caused through fabrication process. From this estimation, the parasitic components are considered to be the main cause of the deviation

of the experimental results from the calculation ones as mentioned in Section **3.3.2**. Therefore, reducing the parasitic resistance and the parasitic capacitance by sophisticating the fabrication process and optimizing the structure of the bonding pad is necessary for realizing ultrafast reset operations. When the parasitic capacitance is reduced of 0.2 pF and the parasitic resistance of 60 $\Omega$ is realized, the turn-off time very near ideal values can be achieved as shown in Fig. 4-20. And also, the optimized electrical module is desired.

Figure 4-21 shows the time response of the switching behavior of the InGaAs/InAlAs MQW bistable laser. The upper, middle, and lower traces represent the input light, applied voltage, and output light from the bistable laser, respectively. A repetition rate of 2 GHz was obtained, and the peak intensity of the input light in this experiment was 300 $\mu$W. The voltage applied to the saturable absorption region was biased at -0.225 V and the modulation pulse height was 0.8 V. In this experiment, the repetition rate is mainly limited by the relaxation oscillation frequency because the output light power is around 1 mW and is not large enough for high-speed operation. The switching speed can be increased, however, by optimization of the MQW structure, for example, by introducing larger differential gain material, and by applying lower bias voltage for larger light output.

## 4.4 Comparison between Current-injection and Voltage-controlled Bistable Lasers

The properties of conventional current-injection-type and voltage-controlled bistable lasers are summarized in Table 4-2. The values for current-injection-type lasers and the bulk structure lasers are from References 10 and 11. The points of comparison are the saturable absorption region length, driving condition of hysteresis, and switching speed. The advantage of the voltage-controlled-type of laser are the following:

(1) The length of the saturable absorption region is 5-10 times less than that of current-injection-type. The hysteresis control with short absorption region even under reverse

**Set light**

**Reset voltage**

**Output light**

200 ps
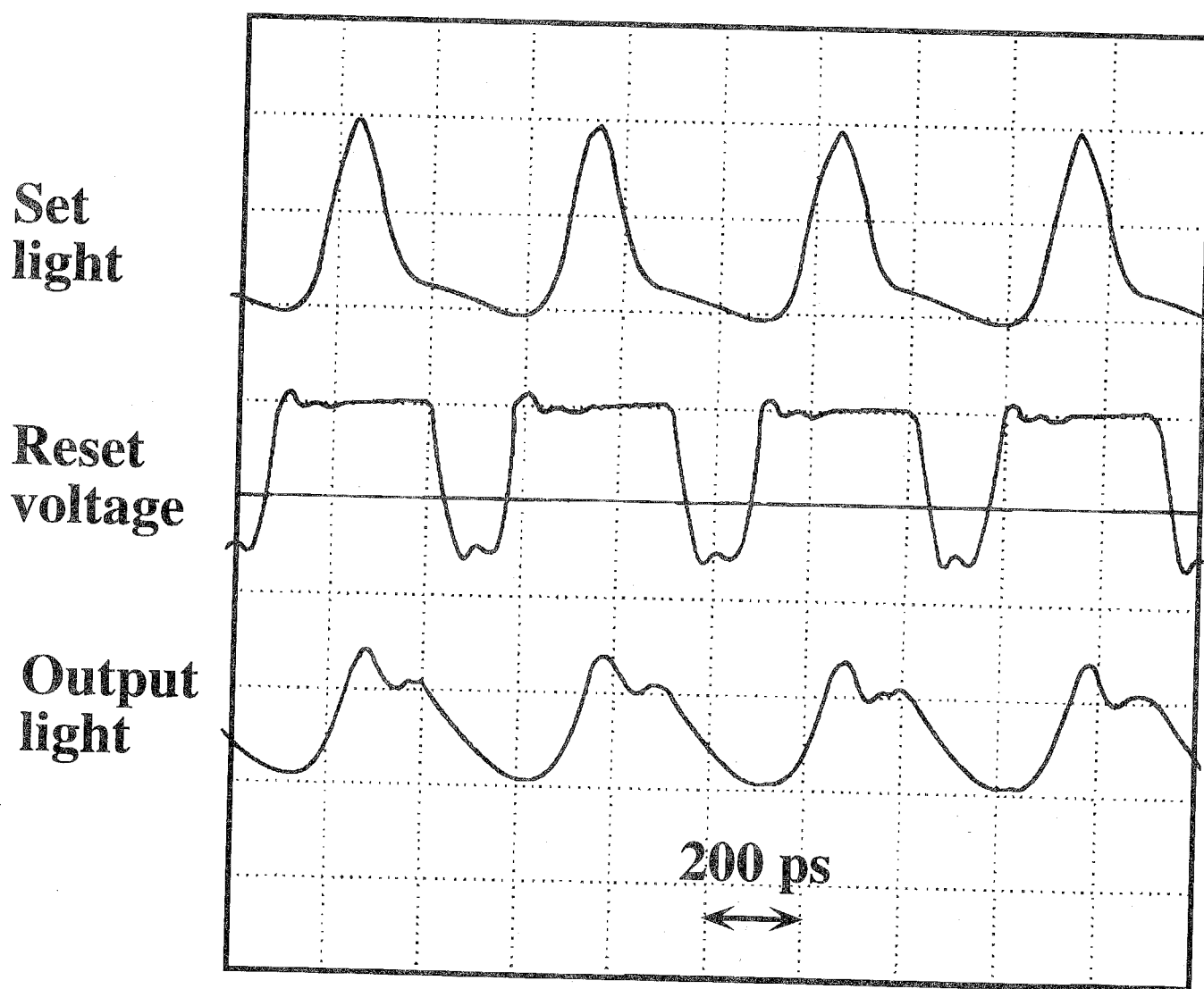
Fig. 4-21

Optical memory operation of a 6-period InGaAs/InAlAs MQW bistable laser with 2-GHz repetition rate.

## Table 4-2

Comparison of current-injection and voltage-controlled bistable lasers.

| | Current injection-type [a] | Voltage-controlled type | |
|---|---|---|---|
| | | Bulk [b] | MQW |
| Saturable absorber size | $50\sim100$ μm | $10\sim30$ μm | 10 μm |
| Hysteresis control | $0\sim30$ mA ($I_a=0\sim35$ mA) | $0\sim10$ mA ($V_c=0\sim0.8$ V) | $0\sim30$ mA ($V_c=-0.6\sim0.6$ V) |
| Switching power | $<10$ μW | $<10$ μW | $<10$ μW |
| Switching speed | turn-off 170 ps | rep. rate 5 GHz turn-on:$<50$ ps turn-off:$<50$ ps | turn-on:$<100$ ps turn-off: $<100$ ps |

[a]  A. Tomita, T. Terakado and A. Suzuki, "Turn-off characteristics of bistable laser diode", J. Appl. Phys., vol.59, pp. 1839-1842, 1986.
[b] T. Odagawa, T. Machida, K. Tanaka, T. Sanada, K. Wakao, "Fast optical flip-flop operations of bistable laser diodes", Trans. IEICE, vol. J74-C-I, pp.465-479, 1991.

bias voltage can be achieved by larger absorption coefficient of MQW structure than that of the bulk structure.

(2) Hysteresis appears when the applied voltage is less than the built-in voltage, below current injection level.

(3) Turn-off time of the voltage-controlled-type is about half of that of current-injection-type.

The fastest switching operation so far reported is for a voltage-controlled-type bistable laser with a bulk active layer [11], but I believe that the MQW bistable laser has the potential for superior performances because of its large differential gain resulting from quantum size effect.

In addition to switching speed, wide wavelength sensitivity over 50 nm was achieved when the input light wavelength was adjusted to the lasing wavelength and this is the same between all type of bistable lasers [12]. But the increase of turn-on time was also observed, which is caused by the increase of switching power due to large wavelength dependence of the switching power around Fabry-Perot resonance mode. This is the intrinsic problem of in-line light-injection-type devices. The method to overcome this problem will be briefly described in the following chapters.

The polarization sensitivity is also important characteristics for system use. Öhlander et al. have reported that the switching power is the lowest at TE mode injection and monotonously increases toward TM mode injection [13]. Larger polarization sensitivity is predicted in the voltage-controlled MQW bistable laser because of the intrinsic TE mode selectivity [14]. One way to avoid the polarization sensitivity is to introduce tensile strained quantum well [15][16]. This is also better for high-speed switching due to the increment of differential gain. But there exists a trade-off between the polarization insensitivity for input light and the polarization selectivity for lasing mode because the polarization of the lasing mode of the tensile strained quantum well laser tends to be TM mode [17].

From these discussions, I consider that in-line light-injection MQW bistable laser is suitable for thresholding or memory device in the optical systems with the bit-rate over

Gbit/s and the single wavelength use. For example, demultiplexing component for the time-division multiplexed data stream is a candidate.

## 4.5. Summary

Fabrication and experimental evaluation of MQW bistable lasers with InGaAs/InP, InGaAs/InGaAsP, and InGaAs/InAlAs MQW systems has shown that, with regard to threshold current and the reverse bias voltage, InGaAs/InAlAs MQW is especially advantageous for high-speed operation. Easy control of hysteresis width and the threshold current can also be obtained reproducibly. Switching within less than 100 ps has been achieved in both set and reset operations, the device can be switched-on by input light in the 50-nm wavelength range, and 2-GHz repetition memory operation was obtained in InGaAs/InAlAs MQW systems. The superior characteristics of the MQW bistable laser include such features as the potential for high-speed operation, easy control of hysteresis characteristics, and high reproducibility. Optimization of the MQW structure and the saturable absorber design will make it possible to create high-bit-rate optical transmission and digital exchange systems.

# References

[1] R. Poeple, K.W.Wecht, K. Alavi and A.Y.Cho, "Measurement of the conduction-band discontinuity of molecular beam epitaxial grown $In_{0.52}Al_{0.48}As/In_{0.53}Ga_{0.47}As$, $N$-$n$ heterojunction by $C$-$V$ profiling", Appl. Phys. Lett., vol.43, pp.118-120,1983.

[2] Y. Kawamura, A. Wakatsuki, Y. Noguchi and H. Iwamura, "InGaAs/InGaAlAs MQW lasers with InGaAsP guiding layers grown by gas source molecular beam epitaxy", IEEE Photon. Technol. Lett., vol. 3, pp.960-962, 1991.

[3] M. Asada, A. Kameyama and Y. Suematsu, "Gain and intervalence band absorption in quantum-well lasers", IEEE J. Quantum Electron., vol.QE-20, No.7, pp.745-753, 1984.

[4] H. Uenohara, H. Iwamura and M. Naganuma, "Switching characteristics of InGaAs/InP multiquantum well voltage-controlled bistable laser diodes", Jpn. J. Appl. Phys., vol. 29, pp. L2442-L2444, 1990.

[5] M. Ueno and R. Lang, "Conditions for self-sustained pulsation and bistability in semiconductor lasers", J. Appl. Phys., vol.58, pp. 1689-1692, 1985.

[6] P. Blixt and U. Öhlander, "Femtojoule bistable optical switching of inhomogeneously pumped laser diode at 500 MHz using mode-locked tunable diode laser", Electron. Lett., vol.25, pp.699-700, 1989.

[7] B.W. Hakki and T.L. Paoli, "Gain spectra in GaAs double-heterostructure injection lasers", J. Appl. Phys., vol. 46, pp.1299-1306, 1975.

[8] T. Odagawa and S. Yamakoshi, "Optical set-reset operations of bistable laser diode with single-wavelength light", Electron. Lett., vol. 25, pp.1428-1429, 1989.

[9] H. Uenohara, Y. Kawamura, H. Iwamura, K. Nonaka, H. Tsuda and T. Kurokawa, "Operation characteristics of a side-light-injection multiple-quantum-well bistable laser for all-optical switching", Jpn. J. Appl. Phys., vol. 33, pp. 815-821, 1994.

[10] A. Tomita, T. Terakado and A. Suzuki, "Turn-off characteristics of bistable laser diode", J. Appl. Phys., vol.59, pp. 1839-1842, 1986.

[11] T. Odagawa, T. Machida, K. Tanaka, T. Sanada and K. Wakao, "Fast optical flip-flop operations of bistable laser diodes", Trans. IEICE, vol. J74-C-I, pp.465-479, 1991.

[12] S. Suzuki, T. Terakado, K. Komatsu, K. Nagashima, A. Suzuki and M. Kondo, "An experiment on high-speed optical time-division switching", vol.LT-4, pp.894-899, 1986.

[13] U. Öhlander, P. Blixt and O. Sahlén, "Operation tolerances od a bistable laser optically switched at 500 MHz with picosecond, ultra-low energy", in Tech. Dig. ECOC, Gothenburg, Sweden, 1989, pp.288-291.

[14] H. Iwamura, T. Saku, H. Kobayashi and Y. Horikoshi, "Spectrum studies on a GaAs-AlGaAs multi-quantum-well laser diode grown by molecular beam epitaxy", J. Appl. Phys., vol.54, pp.2692-2695, 1983.

[15] P.J.A. Thijs, L.F. Tiemeijer, P.I. Kuindersma, J.J.M. Binsma and T. van dongen, "High performance 1.5 µm wavelength InGaAs-InGaAsP strained quantum well lasers and amplifiers", IEEE J. Quantum Electron., vol.27, pp.1426-1439, 1991.

[16] K. Magari, M. Okamoto, H. Yasaka, K. Sato, Y. Noguchi and O. Mikami, "Polarization insensitive traveling wave type amplifier using strained multiple quantum well structure", IEEE Photon. Tech. Lett., vol.2, pp.556-558, 1990.

[17] P.J.A. Thijs, J.J.M. Binsma, L.F. Tiemeijer and T. van Dongen, "Improved performance 1.5 mm wavelength tensile and compressively strained InGaAs-InGaAsP quantum well lasers", in Tech. Dig. ECOC/IOOC, Paris, France, 1991, vol.2, pp.31-38.

# Chapter 5 Analysis of Side-light-injection Multiple Quantum Well Bistable Lasers

This chapter proposes one of the candidates of all-optical functional devices, the side-light-injection multiple quantum well (MQW) bistable laser. This device operates as a memory storage device that can be set and reset by input light. The input light is injected perpendicular to the laser cavity to realize those functions, and the set operation is achieved by absorption saturation; the reset operation, by gain quenching. The lasing and switching characteristics of this device are evaluated here by solving the modified rate equations, and the potential performance of the device is investigated. The switching input light power required for set and reset operations is estimated, as is the minimum switching time.

## 5.1 Principle of Side-light-injection MQW Bistable Lasers

Chapters 3 and 4 described memory operation using input light in a voltage-controlled multiple-quantum-well (MQW) bistable laser [1]. In this device, the set operation is performed by the input light and the reset operation is performed by changing the voltage applied to the saturable absorption region. Further development of optical data transmission and data exchange systems requires not only AND and OR functions but also NAND and NOR functions in the optical regime. The functional operations needed to meet these requirements and to construct photonic integrated circuits will require the set and reset operations to be performed only by input light.

Odagawa and Yamakoshi have reported all-optical set and reset operations that use a Fabry-Perot-type [2], and Nobuhara et al. reported a distributed Bragg reflector (DBR) type multi-segment bistable laser [3]. This device operates by using optical bleaching in the saturable absorption region and gain quenching in both the saturable absorption and gain regions. In this device, the input light is injected into the laser cavity coaxially and the cavity modes drastically affect the switching sensitivity. And the wavelength sensitivity is slightly different between the set and reset operation

because of the refractive index change among electroluminescence and lasing state. That's why the bias condition of the saturable absorption region is limited to a narrow range especially when the same input light wavelength is used for set and reset operations. In addition to this, whether saturable absorption or gain quenching dominates depends on the input light power.

The side-light-injection-type laser [4], [5] is one candidate for improving driving tolerance and wavelength sensitivity. A main laser is located perpendicular to a side laser and both elements are monolithically integrated. However, this device showed only inverter operation. And the reported on/off ratios are small because they do not show threshold characteristics in the input/output characteristics, and the switching time have not been reported in detail.

To overcome the problems of the devices mentioned above, I propose a side-light-injection MQW bistable laser [6],[7] consisting of one main bistable laser and two waveguides perpendicular to the main laser for propagating the input signals into the intersections as shown in Fig. 5-1. There are two intersections in the bistable laser cavity. The one used for set operation is called the "saturable absorption region" and the other used for the reset operation is called the "gain quenching region" because one works by using absorption saturation and the other works by gain quenching phenomena. The features of this device are (1) large controllability of the driving condition because the saturable absorption region and the gain quenching region are formed separately, and the set and reset lights can therefore be injected into different input ports, (2) a large on/off ratio due to bistability, and (3) flat wavelength sensitivity possible compared to conventional bistable lasers because the input light is not affected by the cavity modes of the main laser [8], [9]. This side-light-injection structure can also be used for achieving high isolation between the input and output signals [8], [9].

The principle of the set operation of the side-light-injection MQW bistable laser is the same as that of the two-segmented MQW bistable laser described in Section **2.1**. The principle of the reset operation by input light will be discussed here. The carrier distribution in the gain quenching region is illustrated in Fig. 5-2. If we assume that
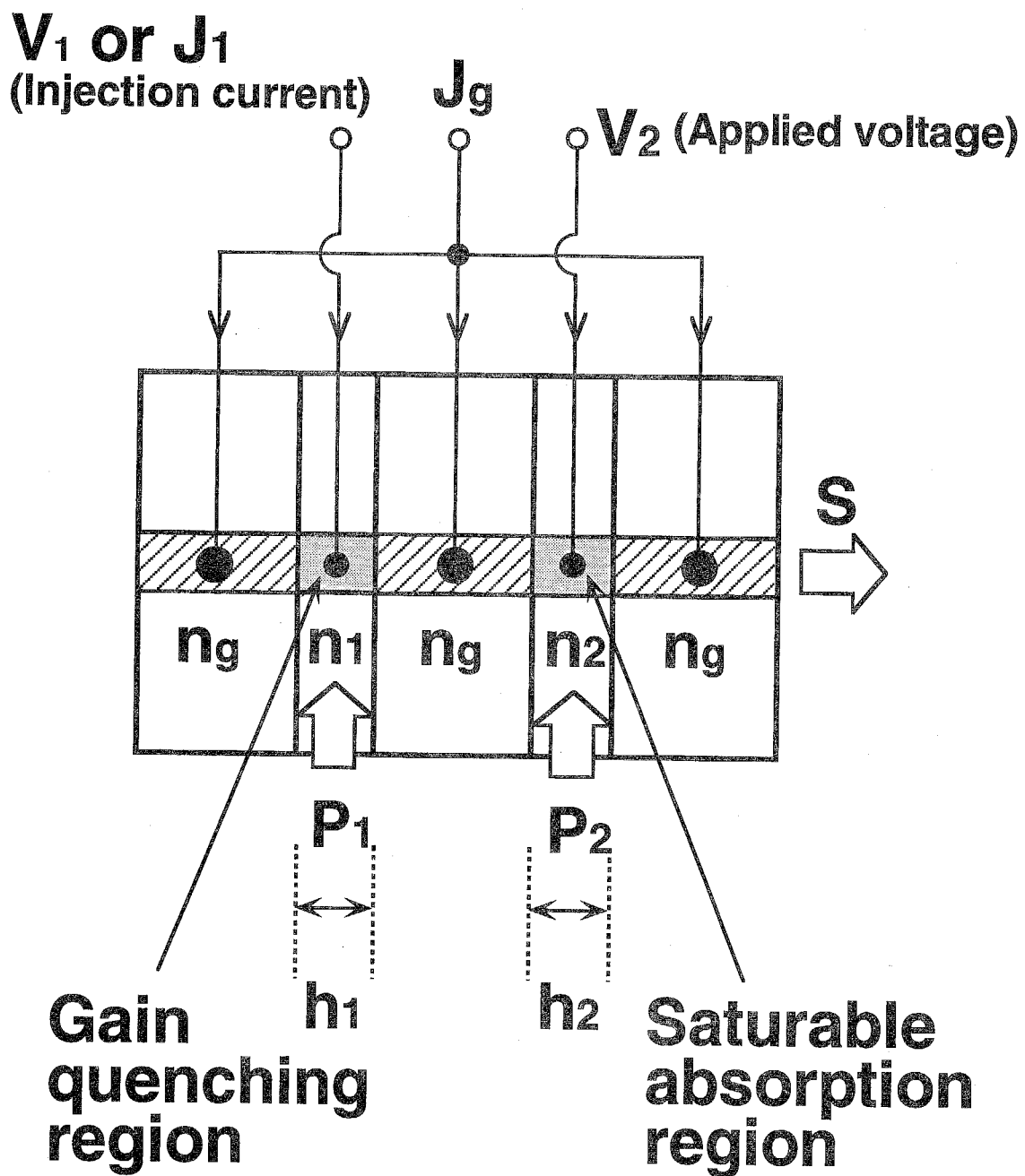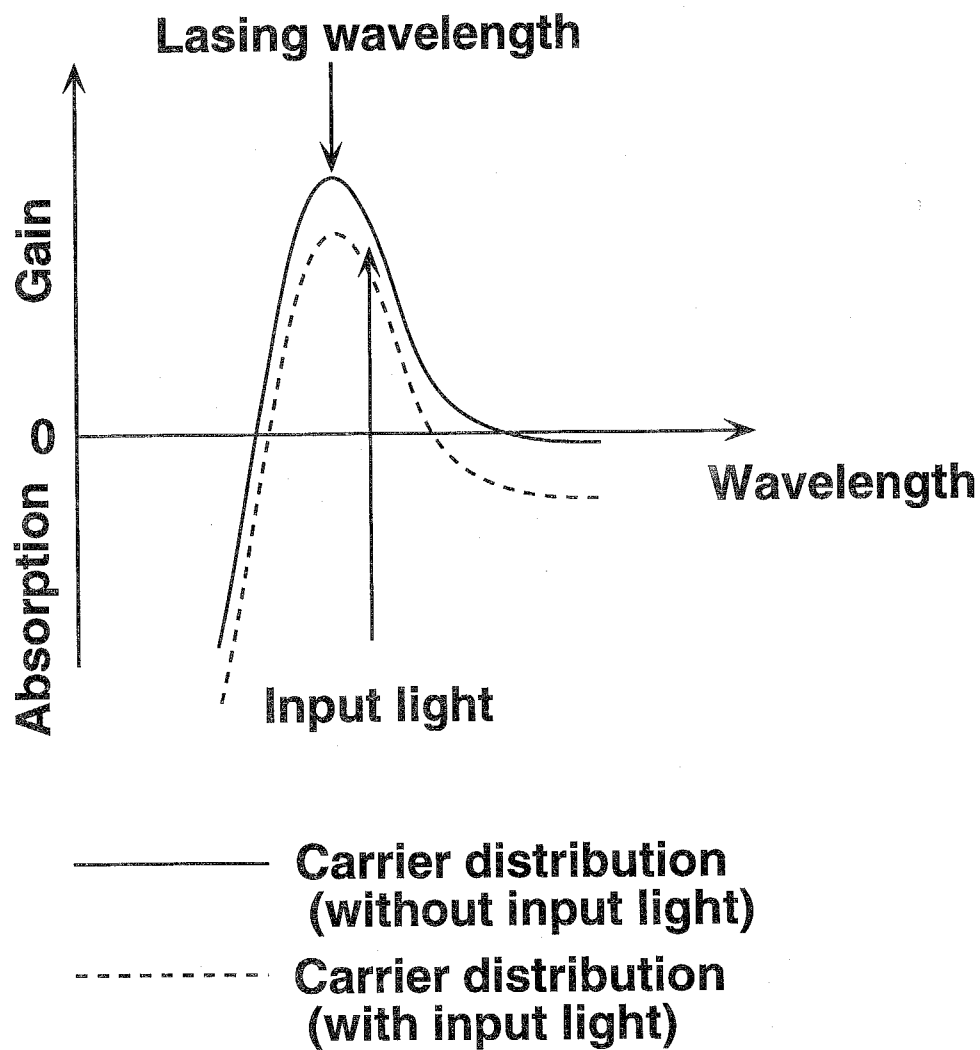
**Fig. 5-1**

Structure and analytical model of a side-light-injection MQW bistable laser.

Fig. 5-2

The explanation of the principle of the gain quenching. The change of
the carrier distribution with and without input light.

some carriers are injected into the gain quenching region as shown by the solid line, optical gain occurs in the range of the gain bandwidth, so the input light with wavelength within the gain bandwidth can be amplified in the gain quenching region. This amplification consumes carriers in the gain quenching region because of the stimulated emission, thus the carrier distribution changes as shown by the dashed line in Fig. 5-2. Before injection of light, carriers in that region contribute part of the gain media for the lasing light of the bistable laser. Therefore the consumption of carriers by amplifying input light reduces the optical gain at the lasing wavelength of the bistable laser. The efficiency of the gain quenching is higher at wavelengths longer than the lasing wavelength, because the absorption coefficient in longer wavelength is smaller than in shorter wavelength. When the gain current is biased just above the threshold current, input light stops the lasing operation. Especially when the bias current is just above the turn-off threshold current of the bistable laser, a large on/off ratio can be obtained because of the sharp change of the output light.

## 5.2 Design of Side-light-injection MQW Bistable Lasers

To find out whether the side-light-injection laser can work and, if so, how much input light power it can operate, it was necessary to simulate the operating characteristics by solving the rate equations [10]. These equations were modified from the conventional ones [11] for inclusion of the saturable absorption and the gain quenching regions. The model structure used in this calculation is shown in Fig. 5-1. Although the actual device has waveguide structures for propagating the input light to the intersection of the laser cavity, these are neglected for simplicity. The rate equations are as follows:

$$\frac{dn_g}{dt} = \frac{J_g}{ed} - \frac{n_g}{\tau_g} - \frac{n_g}{\tau_{nr}} - v_g G_g S \qquad (5.1)$$

$$\frac{dn1}{dt} = \frac{J1}{ed} - \frac{n1}{\tau1} - \frac{n1}{\tau_{nr}} - vgG1S - vgG1P1 \qquad (5.2)$$

$$\frac{dn2}{dt} = -\frac{n2}{\tau2} - vgG2S - vgG2P2 \qquad (5.3)$$

$$\frac{dS}{dt} = vg\xi(1 - h1 - h2)GgS + vg\xi h1G1S + vg\xi h2G2S$$
$$+ \beta\xi[(1 - h1 - h2)\frac{ng}{\tau g} + h1\frac{n1}{\tau1} + h2\frac{n2}{\tau2}] - \frac{S}{\tau p} \qquad (5.4)$$

where $n_i$ (i = g, 1, 2) is carrier density, S is photon density in the main laser cavity, $\tau_i$ (i = g, 1, 2) is carrier lifetime which is expressed by $1/(B_{eff} \cdot n_i)$, $B_{eff}$ is the effective recombination coefficient, $\tau_{nr}$ is nonradiative recombination time, $\tau_p$ is photon lifetime, $v_g$ is group velocity in the cavity, $G_i$ (i = g, 1, 2) is optical gain, which is assumed to be linear with carrier density and is given by $G_i = g_i (n_i - n_0) \cdot (1 - \varepsilon S)$, $g_i$ is differential gain coefficient, $n_0$ is the transparency carrier density, $\varepsilon$ is the nonlinear gain coefficient, $J_i$ (i = g, 1) is injected current density, $h_i$ (i = 1, 2) is the ratio of the length of the gain quenching or saturable absorption region to the length of the main laser cavity, $\beta$ is the spontaneous emission factor, $\xi$ is the optical confinement factor, $P_1$ and $P_2$ are injected photon densities into the gain quenching and the saturable absorption region. The way to discriminate between the gain region and the saturable absorption region is the same as that used for in-line light-injection type bistable laser as shown in Chapter 3. Suffixes g, 1, and 2 represent the gain region, gain quenching region, and saturable absorption region. Equations (5.1) to (5.3) represent the change in carrier densities in the gain region, gain quenching region, and absorption region, respectively. And eqn. (5.4) expresses the change in the photon density in the main laser cavity. Terms for the input lights ($P_1$, $P_2$) are included in the carrier density in the gain quenching region and the saturable absorption region, i.e., in the last terms on the right-hand side of eqns. (5.2) and (5.3). This point is the main difference between in-line light-injection and side-light-injection-type. $P_1$ and $P_2$ are assumed to be the input light intensity just

coupled into the intersections. In the saturable absorption region, the sign of gain coefficient $G_2$ in eqn. (5.3) is negative because the bias voltage is set lower than built-in voltage, so the input light $P_2$ causes the increase of carrier density. That results in the absorption saturation and switches on the device. On the other hand, the bias voltage is higher than built-in voltage in the gain quenching region to cause optical gain, which is represented by a positive gain coefficient $G_1$ in eqn.(5.2). So the input light $P_1$ reduces the carrier density in the gain quenching region and the device is switched off.

## 5.3 Static Characteristics

For calculating the static characteristics, the right hand sides of eqns. (5.1)-(5.4) are set to zero. To calculate the light output versus gain current characteristics, carrier densities $n_1$ and $n_2$ as functions of photon density S are derived from eqns. (5.2) and (5.3). They were substituted into eqn. (5.4) so that carrier density $n_g$ could be expressed as a function of photon density S. Then $n_g$ was substituted into eqn. (5.1) and the relation between current density $J_g$ and photon density S was plotted.

The parameters used for the calculation are listed in Table 5-1. The differential gain coefficient of the gain region was varied as a parameter. The differential gain coefficient of $6.5 \times 10^{-16}$, $4.0 \times 10^{-16}$, and $2.0 \times 10^{-16}$ cm$^2$ correspond to those of InGaAs/InAlAs [12], InGaAs/InGaAsP [13], and bulk structures [13]. The ratio of the differential gain coefficient in the gain quenching region to that of the gain region ($g_1/g_g$) was set equal, and the differential gain coefficient in the saturable absorption region $g_2$ was selected so that the hysteresis width revealed in the light output versus current characteristics is almost the same for each of the three structures. The injected current density $J_1$ is higher in the bulk structure than others because 4.0 kA/cm$^2$ current density is far from reset operation. The calculated current versus output light characteristics are shown in Figs. 5-3(a) and (b). The photon density in the laser cavity S in eqns. (5.1)-(5.4) were converted into output light intensity with unit of kW/cm$^2$. In

Table 5-1

Numerical values used in the calculations.

| Parameter | Value | | |
|---|---|---|---|
| | InGaAs/InAlAs | InGaAs/InGaAsP | Bulk |
| $g_g$ | $6.5 \times 10^{-16} cm^2$ | $4.0 \times 10^{-16} cm^2$ | $2.0 \times 10^{-16} cm^2$ |
| $g_1$ | $6.0 \times 10^{-16} cm^2$ | $3.7 \times 10^{-16} cm^2$ | $1.8 \times 10^{-16} cm^2$ |
| $g_2$ | $70.0 \times 10^{-16} cm^2$ | $40.0 \times 10^{-16} cm^2$ | $30.0 \times 10^{-16} cm^2$ |
| $\varepsilon$ | $5.5 \times 10^{-17} cm^3$ | $2.0 \times 10^{-17} cm^3$ | $1.0 \times 10^{-17} cm^3$ |
| $J_1$ | $4.0 \ kA/cm^2$ | $4.0 \ kA/cm^2$ | $6.0 \ kA/cm^2$ |
| $n_0$ | $1.25 \times 10^{18} cm^{-3}$ | | |
| $\tau_{nr}$ | $1.0 \ ns$ | | |
| $B_{eff}$ | $1.0 \times 10^{-10} cm^3 /s$ | | |
| $\xi$ | $0.14$ | | |
| $\beta$ | $1.0 \times 10^{-5}$ | | |
| $h_1, h_2$ | $0.01$ | | |
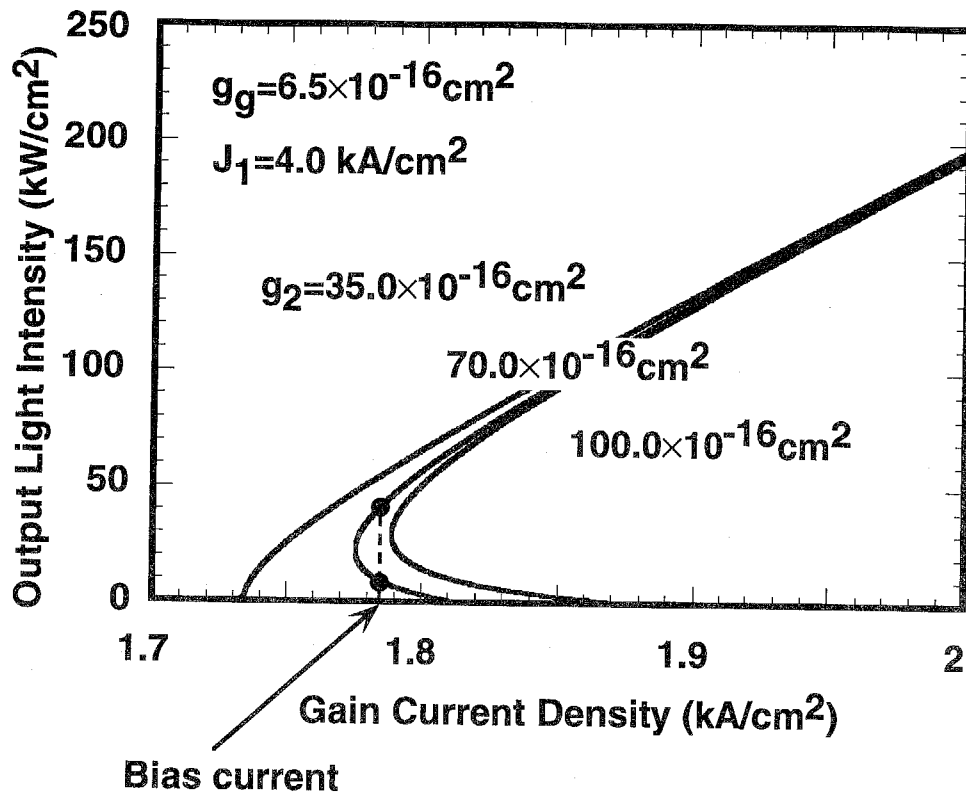
(a) Absorption dependence
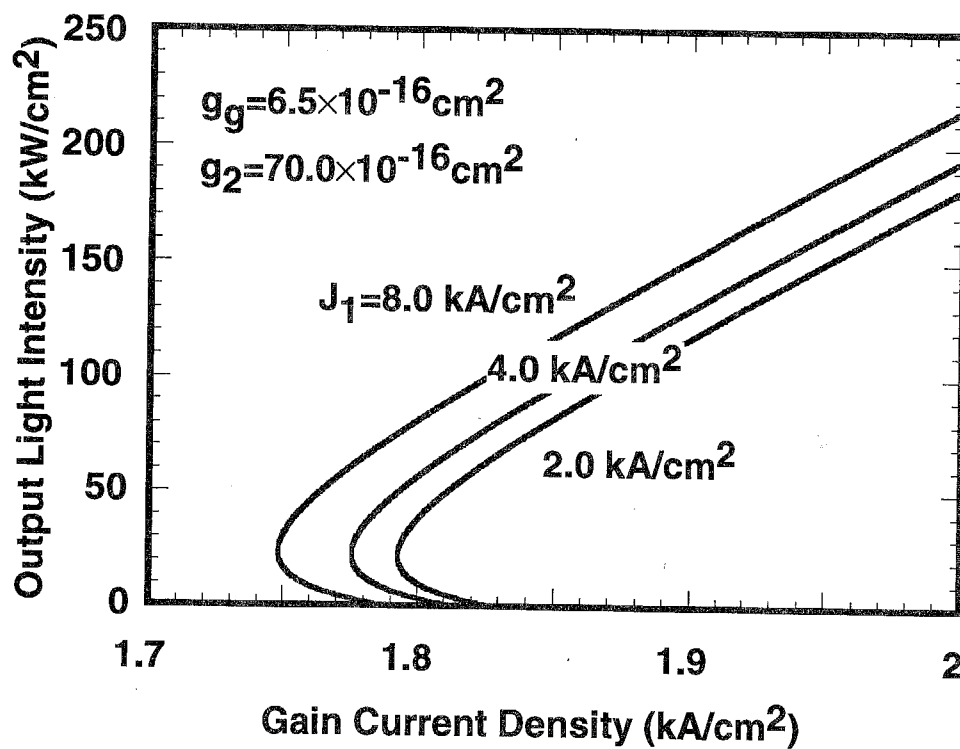


(b) Current dependence

Fig. 5-3

Calculated light output versus current characteristics. (a) The differential gain coefficient in the saturable absorption region is varied, and (b) the injection current into the gain quenching region is varied.

these calculations, the differential gain coefficient in the gain region was fixed at $6.5 \times 10^{-16}$, and the curves plotted in Fig. 5-3(a) were derived by varying the differential gain coefficient in the saturable absorption region. Curves plotted in Fig. 5-3(b) were derived by varying the current density injected into the gain quenching region. The two sets of curves thus correspond to the applied voltage change in the saturable absorption region and in the gain quenching region. As shown in these figures, the decrease of the applied voltage (decrease of differential gain coefficient in the saturable absorption region) or the decrease of the injection current into the gain quenching region resulted in an increased threshold current. The hysteresis widens when the differential gain coefficient in the saturable absorption region increases. But that doesn't change so much with the change of the injection current into the gain quenching region. The main factor of the control of the hysteresis is thus the absorption in the saturable absorption region. The injection current level in the gain quenching region controls the total gain in the main laser cavity, resulting in the control of threshold current. The tendency of the change of the hysteresis is the same as that of the two-segmented MQW bistable laser.

To calculate the input light intensity versus the output light intensity characteristics, the carrier densities in the gain region $n_g$, gain quenching region $n_1$, and saturable absorption region $n_2$ were derived from eqns. (5.1)-(5.3) and they were substituted into eqn. (5.4). The relation between photon density S and injection light intensity into the gain quenching region $P_1$ represents the turn-off characteristics by input light, and the relation between photon density S and injection light intensity into the saturable absorption region $P_2$ represents the turn-on characteristics by input light. The gain coefficients selected for the three parts (gain region, gain quenching region, saturable absorption region) were the same as that of the curve in which the bias current was shown by the dot in Fig. 5-3(a), whose hysteresis width corresponds to 0.6 mA assuming the active region width of 3 $\mu$m and the laser cavity length of 600 $\mu$m. The calculated turn-on and turn-off characteristics are shown in Figs. 5-4(a) and (b). The injected photon density $P_1$ and $P_2$ were converted into input light intensities from the
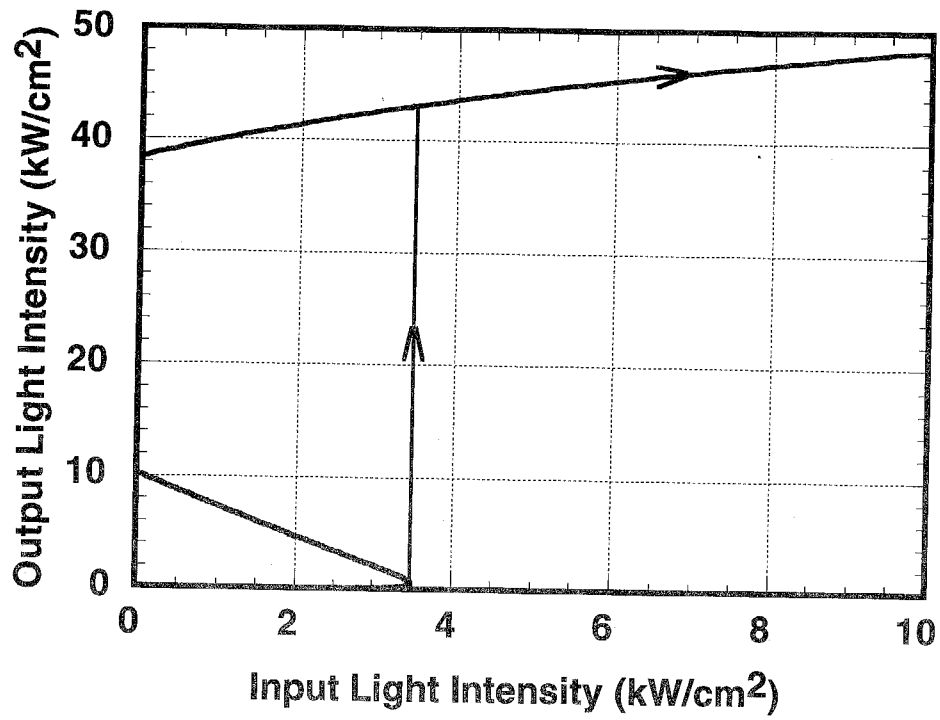
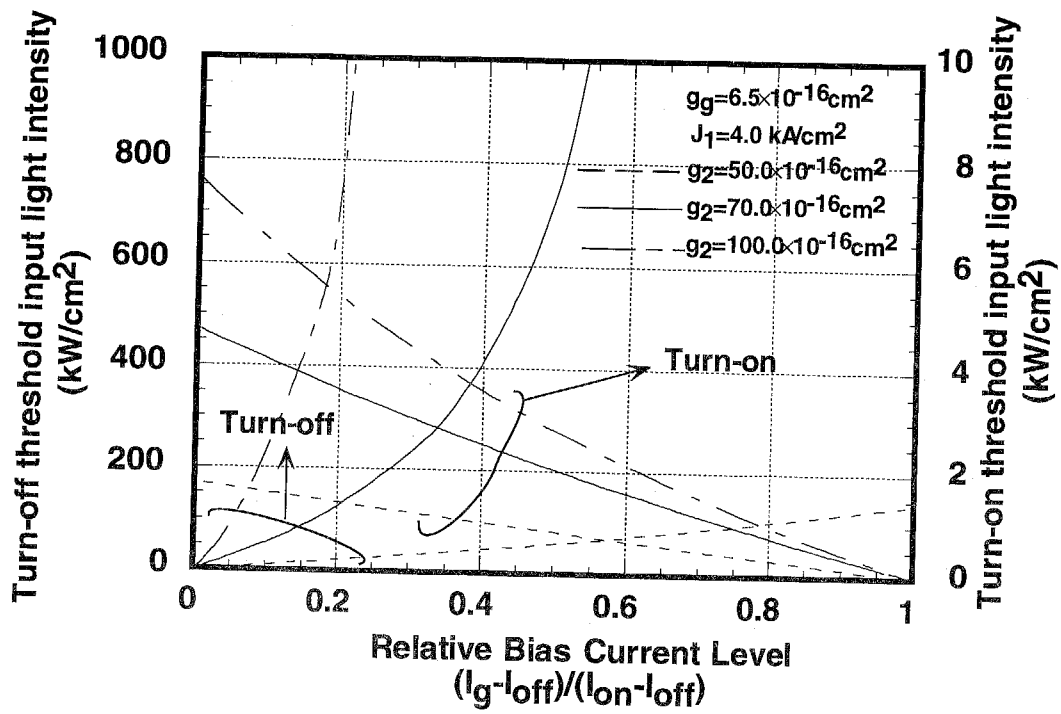(a) Set operation
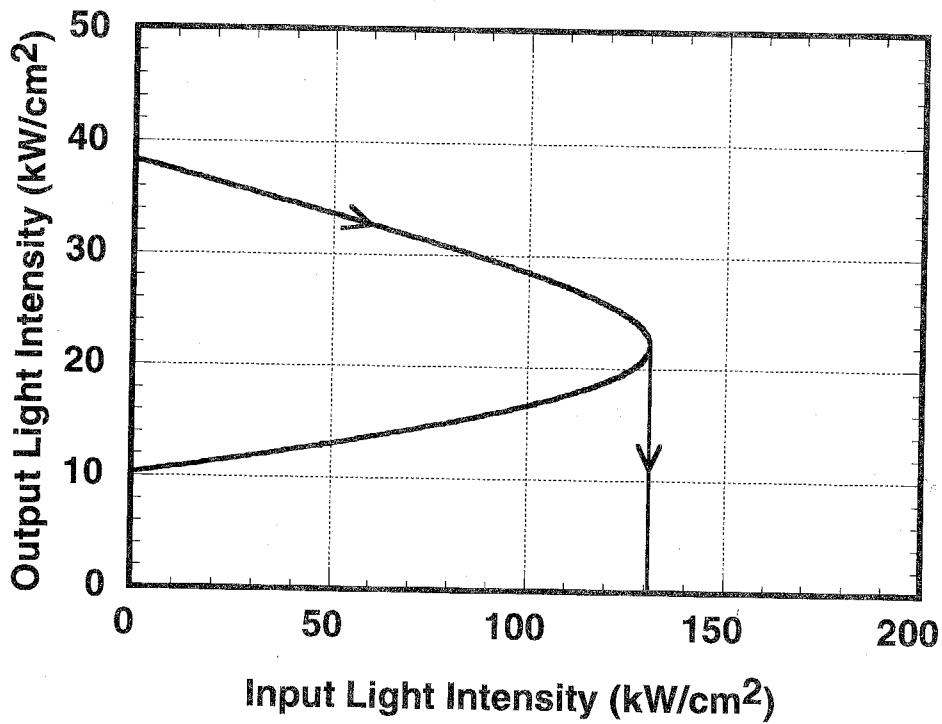


(b) Reset operation

Fig. 5-4

Calculated input / output light characteristics of the side-light-injection
MQW bistable laser.
(a) Set operation and (b) reset operation.

waveguide input port with unit of kW/cm$^2$. The gain in the waveguide region was assumed to be unity in the following calculations. The threshold switching power for both set and reset operation can be linearly reduced by setting the injection current into the waveguide region so as to cause optical gain. The bias current was set between the hysteresis and it was 0.1 mA above the electrical turn-off current, which corresponds to the 0.5-mA offset from turn-on current. Both figures demonstrate that the set and reset operation by input light are possible in one device and under the same bias conditions. Figures 5-5(a)-(c) show the dependence of the threshold input light intensity for set and reset operations on the bias current level. The horizontal axes in these figures is the ratio of the difference between the turn-off current and the bias current to the hysteresis width (difference between the turn-on and turn-off current). In each figure, the turn-on threshold input light intensity decreases nearly linearly as the bias current approaches the turn-on current, whereas the turn-off threshold input light intensity increases drastically. It is also seen that the threshold power for the reset operation is at least one or two orders of magnitude larger than that for the set operation. These tendencies are thought to be due to the difference of the efficiency between the saturable absorption region and the gain quenching region, i.e., due to the difference of the differential gain coefficient.

The effect of the change of absorption coefficient in the saturable absorption region for switching power reduction, on the other hand, is seen in Fig. 5-5(a). Comparing the same relative bias current level, the turn-on threshold input light intensity is lower for a smaller differential gain coefficient in the saturable absorption region because the hysteresis width is less than that for a larger differential gain. At the same difference between the turn-on current and the bias current, the turn-on threshold input light intensity is larger when the differential gain is smaller. This is because the absorption efficiency is lower for a narrow hysteresis condition. For the same difference of the bias current from the turn-off current, the turn-off threshold input light intensity is almost the same, indicating that the absorption change in the saturable absorption region does not affect the turn-off threshold input light intensity. Although

(a) Absorption dependence
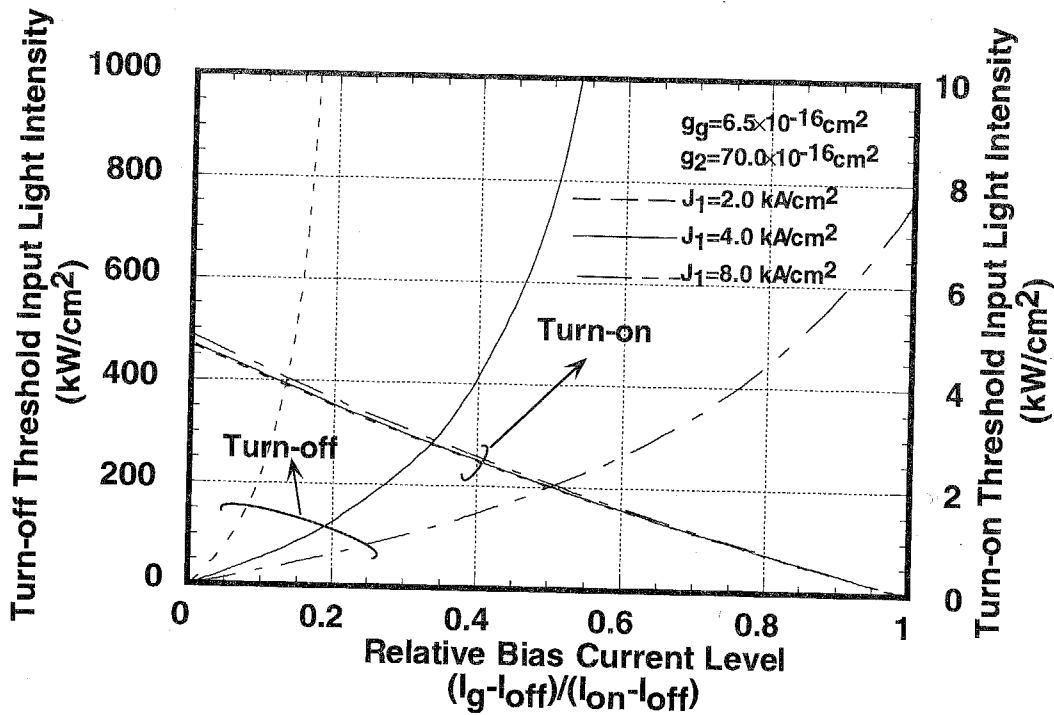


(b) Current dependence

Fig. 5-5

Calculated threshold input light intensity in set and reset operations. (a) The differential gain coefficient in the saturable absorption region is a parameter. And (b) injection current density into the gain quenching region is a parameter.
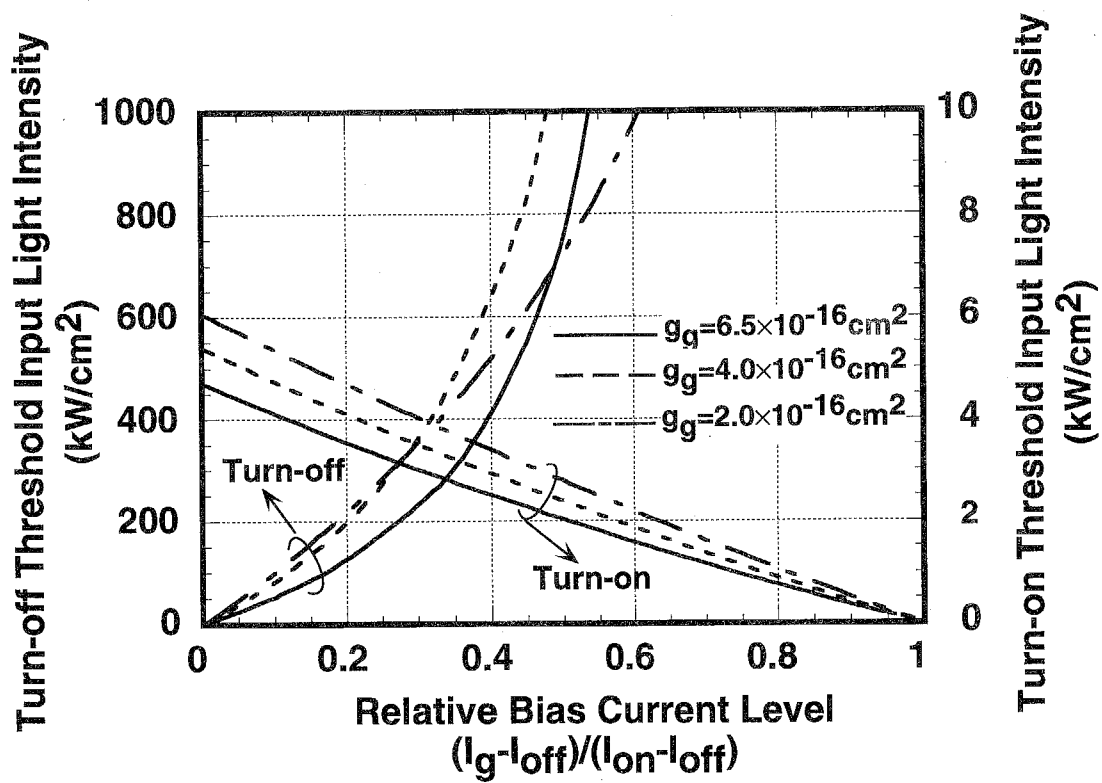
**Fig. 5-5(c) MQW structure dependence**

Calculated threshold input light intensity in set and reset operations. The differential gain coefficient in the gain region is a parameter.

the turn-on threshold input light intensity increases, the small differential gain in the saturable absorption region is suitable because reset operation can be performed under all bias current within hysteresis. The turn-off threshold input light intensity can be reduced by increasing injection current level in the gain quenching region, as seen in Fig. 5-5(b), but increasing the injection current level does not reduce the turn-on threshold input light intensity. The dependence of the threshold input light power on the differential gain coefficient in the gain region (material dependence) is shown in Fig. 5-5(c). The parameters listed in Table 5-1 were used in these calculations and the hysteresis widths were set to be almost equal between each pair of the three sets of parameters. As shown in the figure, both turn-on and turn-off threshold power can be reduced by selecting a large-gain material.

The optimized bias conditions for set and reset operations, and for low switching power are summarized as follows:

(1) An active region material with a large differential gain.

(2) High current injection into the gain quenching region.

(3) Small absorption in the saturable absorption region so as to cause a small hysteresis width.

(4) Biasing gain current near the turn-off threshold current so that the difference between the turn-on and turn-off threshold input light power can be small.


## 5.4 Dynamic Response

The dynamic responses were calculated by using the Runge-Kutta-Gill method to solve eqns. (5.1)-(5.4). Figures 5-6(a) and (b) show the results of simulation of the set and reset operations. The width of the input light pulse was 10 ns so that the pattern effect can be neglected. The bias current was set between the hysteresis, as shown by the dot in Fig. 5-3(a). In the set operation, the turn-on time decreases with increasing input light power ($L_{in}/L_{th(on)}$ in the figure).
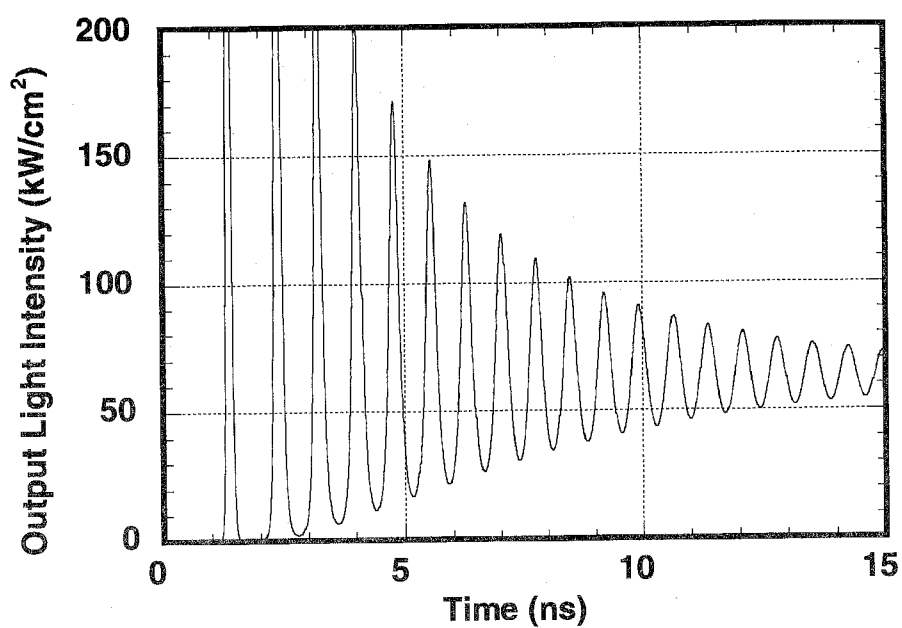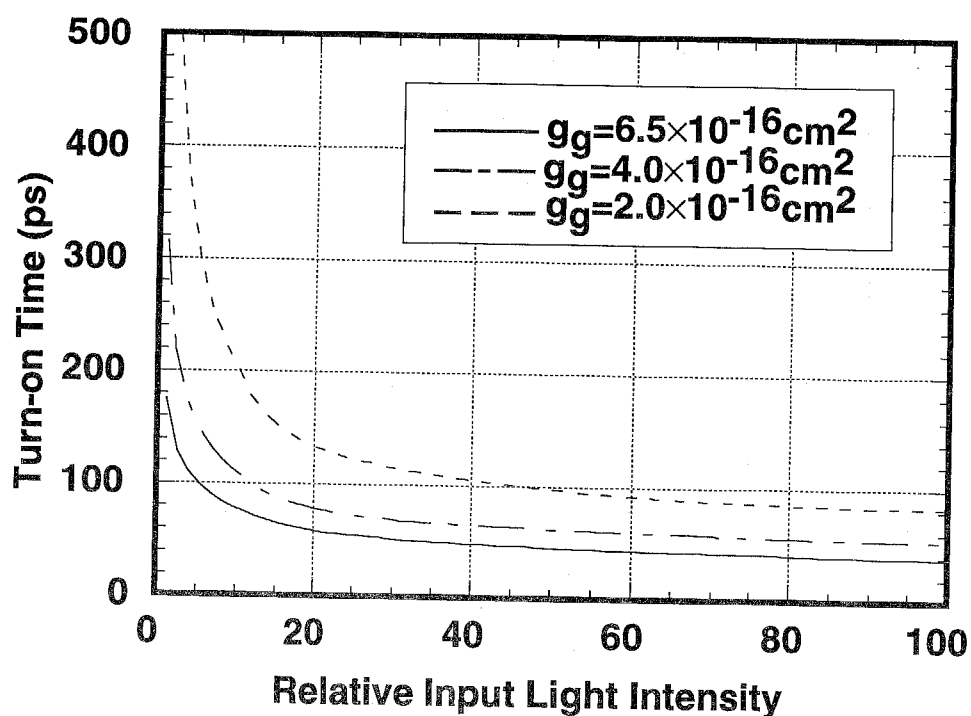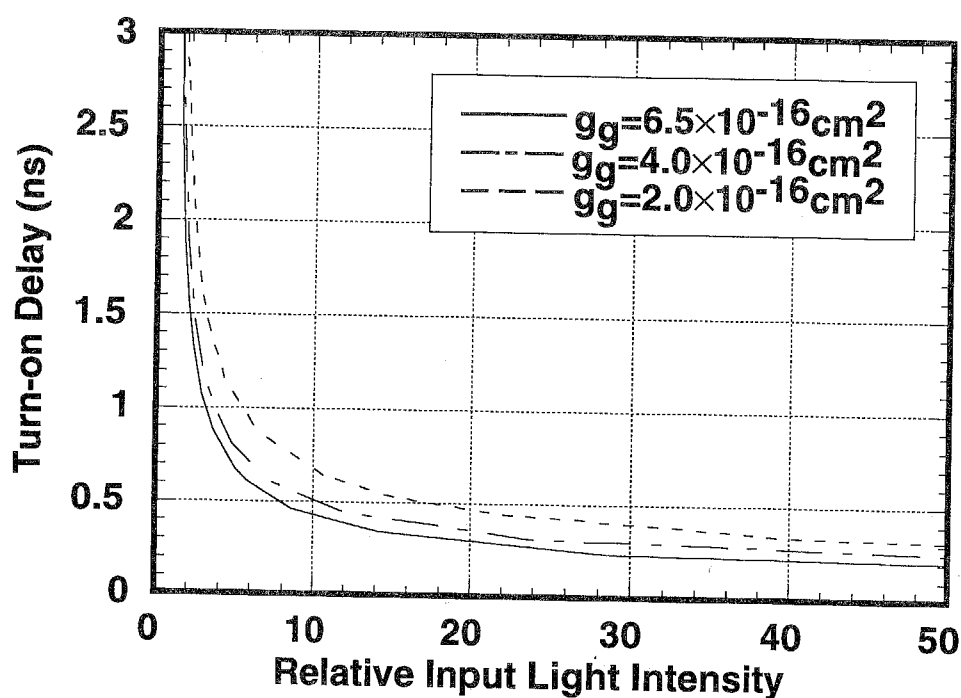
(a) $L_{in}/L_{th(on)} = 20.0$
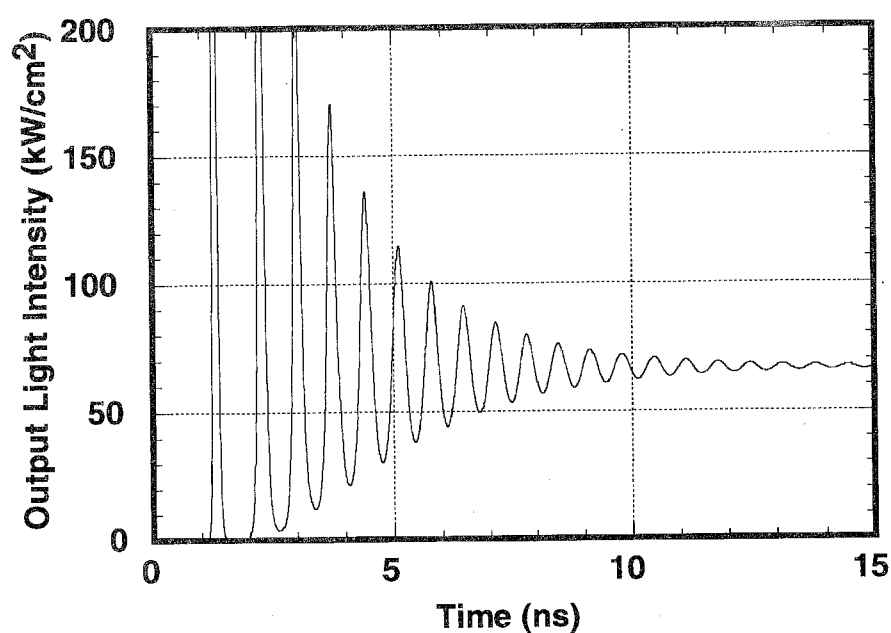


(b) $L_{in}/L_{th(on)} = 30.0$

Fig. 5-6

Calculated time response of set operation. The ratios of input light intensity to threshold power are (a) 20.0 and (b) 30.0.

Fig. 5-7

Calculated (a) turn-on time and (b) turn-on delay as a function of the relative input light intensity. The differential gain coefficient in the gain region is varied as a parameter.

Figures 5-7(a) and (b) show the calculated results of the input light power dependence of the turn-on time and turn-on delay. The turn-on time is defined by the transition time between 10% and 90% of the peak intensity of the first relaxation oscillation, and the turn-on delay is defined by the time between light injection and 10% of the peak intensity. This definition of turn-on time differs from that used in chapter 3 for the in-line light-injection type laser. This is because the turn-on time is slower in the side-light-injection type because the cross-section between injection light and the main laser cavity is small. Input light intensity is normalized by the threshold switching power in the static state. Both turn-on time and turn-on delay decrease with increasing input light intensity and the differential gain coefficient in the gain region. When $g_g = 6.5 \times 10^{-16} cm^2$, the minimum turn-on time is less than 50 ps and the minimum turn-on delay is around 200 ps. To shorten the turn-on time and turn-on delay, it is efficient for the bias current to approach the turn-on current, but there is then a trade-off with the turn-off threshold power as shown in Fig. 5-5(c).

The time response and power dependence of the reset operation are shown in Figs. 5-8 and 5-9, respectively. The turn-off time is defined by the transition time between 90% of the lasing state to 10% over the spontaneous emission state. Figure 5-8 shows that the turn-off time decreases when the input light power increases. The parameters and the bias conditions used in these calculations were the same as those used for the set operation. As the differential gain coefficient increases, the turn-off time decreases, and it is seen that the turn-off time can be less than 250 ps. These results demonstrate the advantage of a large gain material, i.e., the InGaAs/InAlAs MQW structure, a structure with a large number of quantum wells [14], or strained-layer superlattice for improving the high-speed switching performance of side-light-injection MQW bistable lasers and offering the possibility of subnanosecond turn-off time. The other method for fast turn-off time as well as turn-on time is to reduce threshold switching power effectively by enhancing the optical gain in the waveguide region. It is also found that high-speed all-optical switching behavior, i.e., a repetition frequency of higher than 1 GHz is possible.
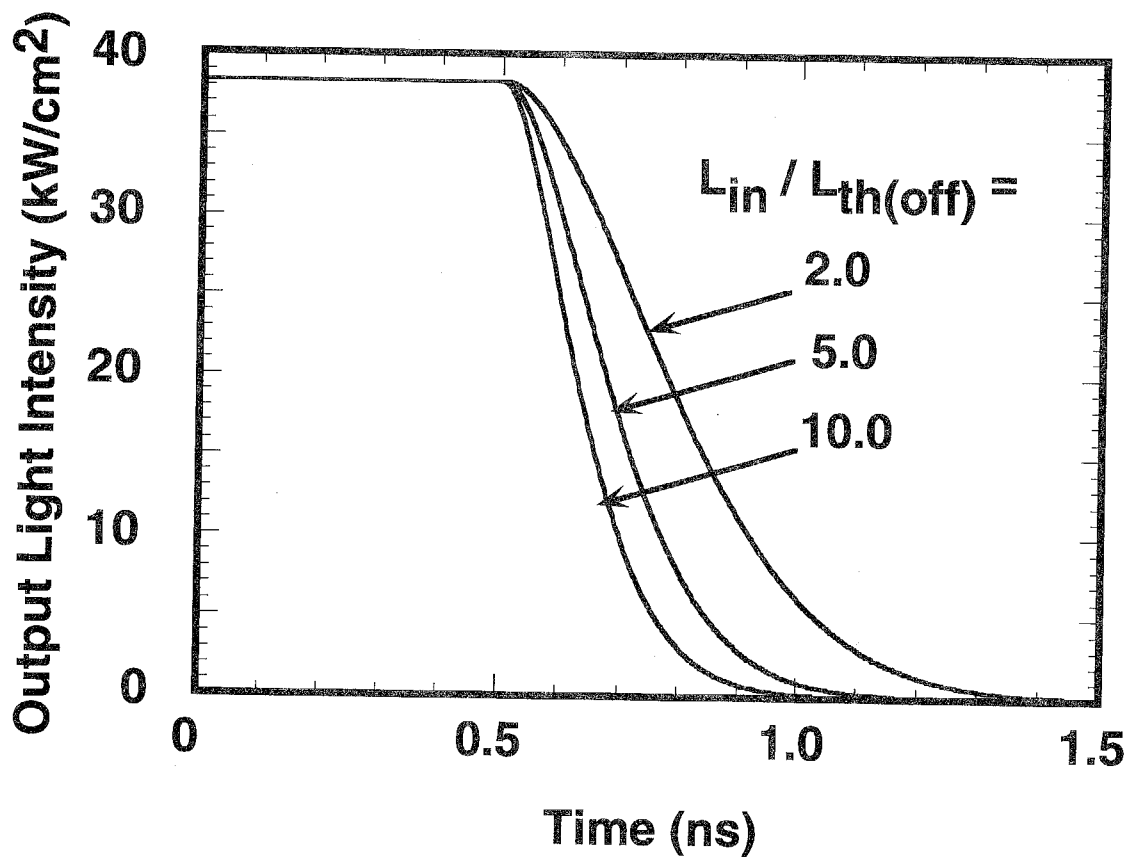
Fig. 5-8

Calculated transient reset operation of a side-light-injection MQW bistable laser.
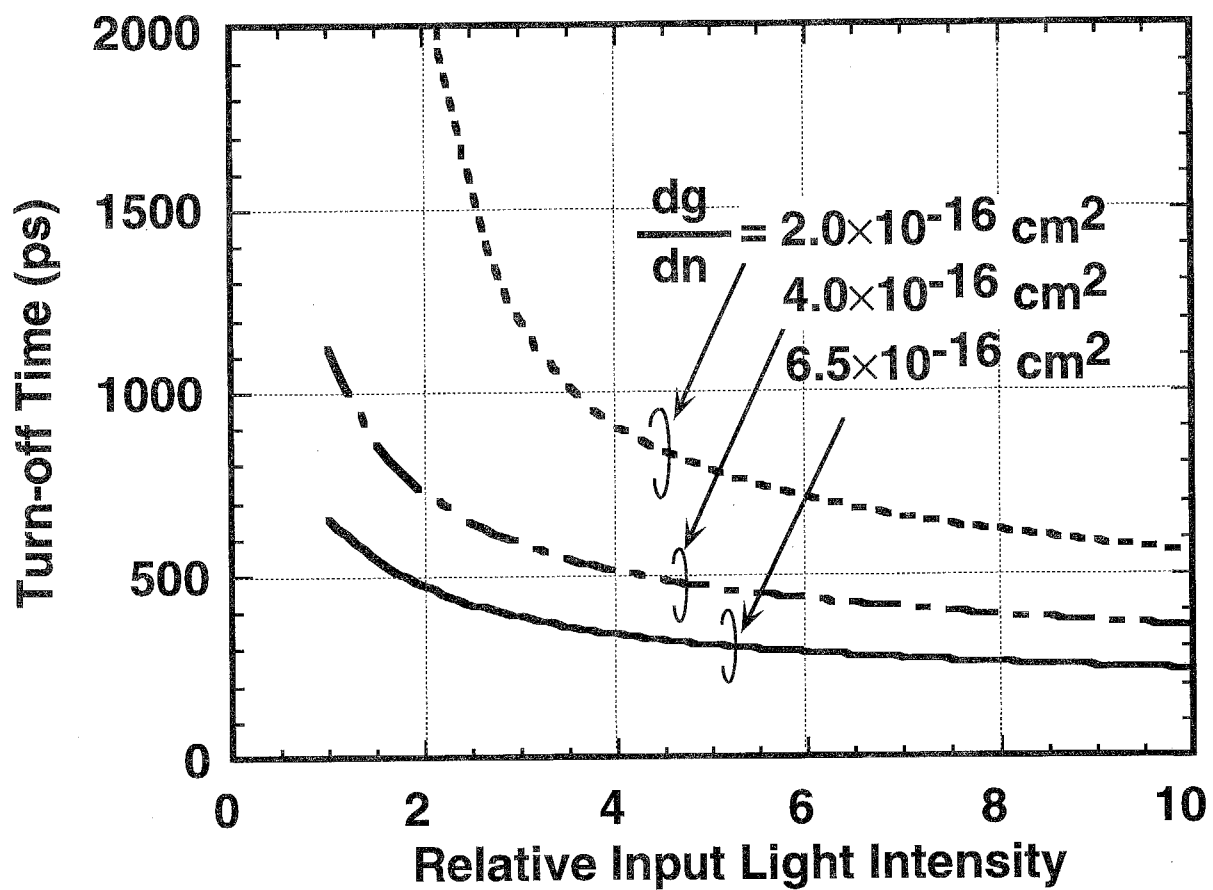
Fig. 5-9

Turn-off time as a function of the input light intensity normalized by the
threshold intensity in the static state.

## 5-5. Summary

I have proposed the side-light-injection MQW bistable laser and analytically evaluated its static and dynamic characteristics. In this device, saturable absorption enables set operation and gain quenching enables reset operation, respectively. Calculations show the possibility of the set and reset operations by input light under the same bias conditions. The dynamic operation calculation demonstrated the advantage of using a high-gain material for high-speed switching and predicts that a repetition rate higher than 1 GHz is feasible.

5-5. Summary

# References

[1] H. Uenohara, H. Iwamura and M. Naganuma, "Switching characteristics of InGaAs/InP multiquantum well voltage-controlled bistable laser diodes", Jpn. J. Appl. Phys., vol.29, pp.L2442-L2444, 1990.

[2] T. Odagawa and S. Yamakoshi, "Optical set-reset operations of bistable laser diodes with single-wavelength light", Electron. Lett., vol.25, pp.1428-1429, 1989.

[3] H. Nobuhara, K. Kondo, S. Yamakoshi and K. Wakao, "Optical logic functions using a tunable wavelength conversion laser diode", IEEE J. Quantum Electron., vol.28, pp.1722-1726, 1992.

[4] W. J. Grande and C. L. Tang, "Semiconductor laser logic gate suitable for monolithic integration", Appl. Phys. Lett., vol.51, pp.1780-1782, 1987.

[5] S. Wakabayashi, T. Tsuruta, K. Idota, Y. Takeuchi, M. Ohshima and Y. Toyoda, "Side-diode-injection laser for optical logic", Proc. Int. Topical Meeting on Photonic Switching, Kobe, 1990, p. 122-124.

[6] H. Uenohara, Y. Kawamura, H. Iwamura, K. Nonaka, H. Tsuda and T. Kurokawa, "Side-light-injection MQW bistable laser using saturable absorption and gain quenching", Electron. Lett., vol.28, pp.1973-1974, 1992.

[7] H. Uenohara, Y. Kawamura, H. Iwamura, K. Nonaka, H. Tsuda and T. Kurokawa, "Set and reset operation dependence on input light intensity of a side-light-injection MQW bistable laser", Electron. Lett., vol.29, pp.1609-1610, 1993.

[8] K. Nonaka, H. Tsuda, H. Uenohara, H. Iwamura and T. Kurokawa, "Optical nonlinear characteristics of a side-injection-light-controlled laser diode with a multiple quantum well saturable absorption region", IEEE Photon. Technol. Lett., vol.5, pp.139-141, 1993.

[9] H. Tsuda, K. Nonaka, H. Hirabayashi, H. Uenohara, H. Iwamura and T. Kurokawa, "Wide range wavelength conversion experiments using a side-injection-light-controlled bistable laser diode", Appl. Phys. Lett., vol. 63, pp.3116-3118, 1993.

[10] H. Uenohara, Y. Kawamura, H. Iwamura, K. Nonaka, H. Tsuda and T. Kurokawa, "Operation characteristics of a side-light-injection multiple-quantum-well bistable laser for all-optical switching", Jpn. J. Appl. Phys., vol.33, Part I, pp.815-821, 1994.

[11] M. Ueno and R. Lang, "Conditions for self-sustained pulsation and bistability in semiconductor lasers", J. Appl. Phys., vol.58, pp.1689-1692, 1985.

[12] A. Wakatsuki, Y. Kawamura, Y. Noguchi and H. Iwamura, "Effect of conduction-band discontinuity on lasing characteristics of 1.5 mm InGaAs/In(Ga)AlAs MQW-FP lasers", IEEE Photon. Technol. Lett., vol.4, pp.383-386, 1993.

[13] M.C. Tatham, "Resonance frequency, damping, and differential gain in 1.5 mm multiple quantum-well lasers", IEEE J. Quantum Electron., vol.28, pp.408-414, 1992.

[14] Y. Arakawa and A. Yariv, "Theory of gain, modulation response, and spectral linewidth in AlGaAs quantum well lasers", IEEE J. Quantum Electron, vol. QE-21, pp.1666-1674, 1985.

# Chapter 6 Performance of Side-light-injection Multiple Quantum Well Bistable Lasers

This chapter describes the structure of a side-light-injection MQW bistable laser and how it works in the static and dynamic state. The characteristics of the output light when input light is injected into the saturable absorption or the gain quenching region have been examined experimentally and are described here. The turn-on and turn-off characteristics by input light were observed in one device and under the same bias conditions for the first time. These characteristics were obtained when the voltages applied to the gain quenching and saturable absorption regions, which are located at the intersections of the main laser and the waveguide regions, were +1.00 and +0.29 V, respectively. The dynamic set and reset operations have also been performed and the input light power dependence of the switching time were investigated. Both turn-on and turn-off time decrease as the input light power increases. The turn-on time is 200 ps when the input light peak power is 1 mW and the turn-off time is 2 ns when the input light peak power is 200 mW. These experimental results agree qualitatively with the numerical predictions in earlier chapters.

## 6.1 Device Structure and Fabrication

Figure 6-1 shows a schematic view of the side-light-injection MQW bistable laser. The MQW wafers were grown by gas-source molecular beam epitaxy [1]. The laser structure consists of a 0.5-μm-thick Si-doped InP cladding layer, a 900-Å-thick undoped lower InGaAsP guiding layer ($\lambda g$ = 1.2 μm), six periods of InGaAs ($L_w$ = 90 Å)/InAlAs ($L_B$ = 30 Å) as a MQW active layer, a 900-Å-thick undoped upper InGaAsP guiding layer ($\lambda g$ = 1.2 μm), a 1.2-μm-thick Be-doped InP cladding layer, and a 0.2-μm-thick Be-doped InGaAs cap layer. An MQW structure is expected to achieve high-speed performance and to improve controllability of the hysteresis characteristics by using the quantum-confined Stark effect as mentioned in Chapter 4
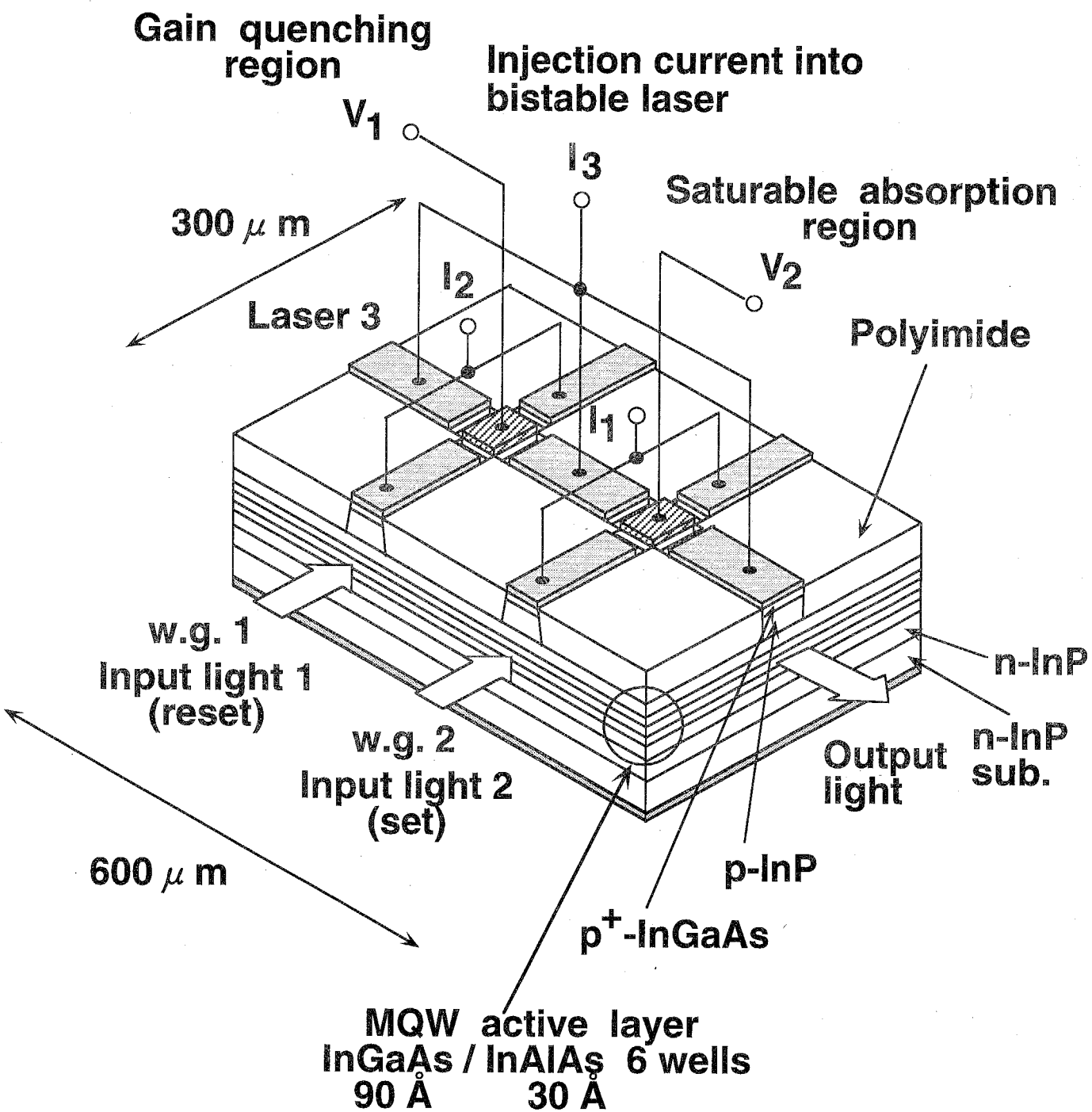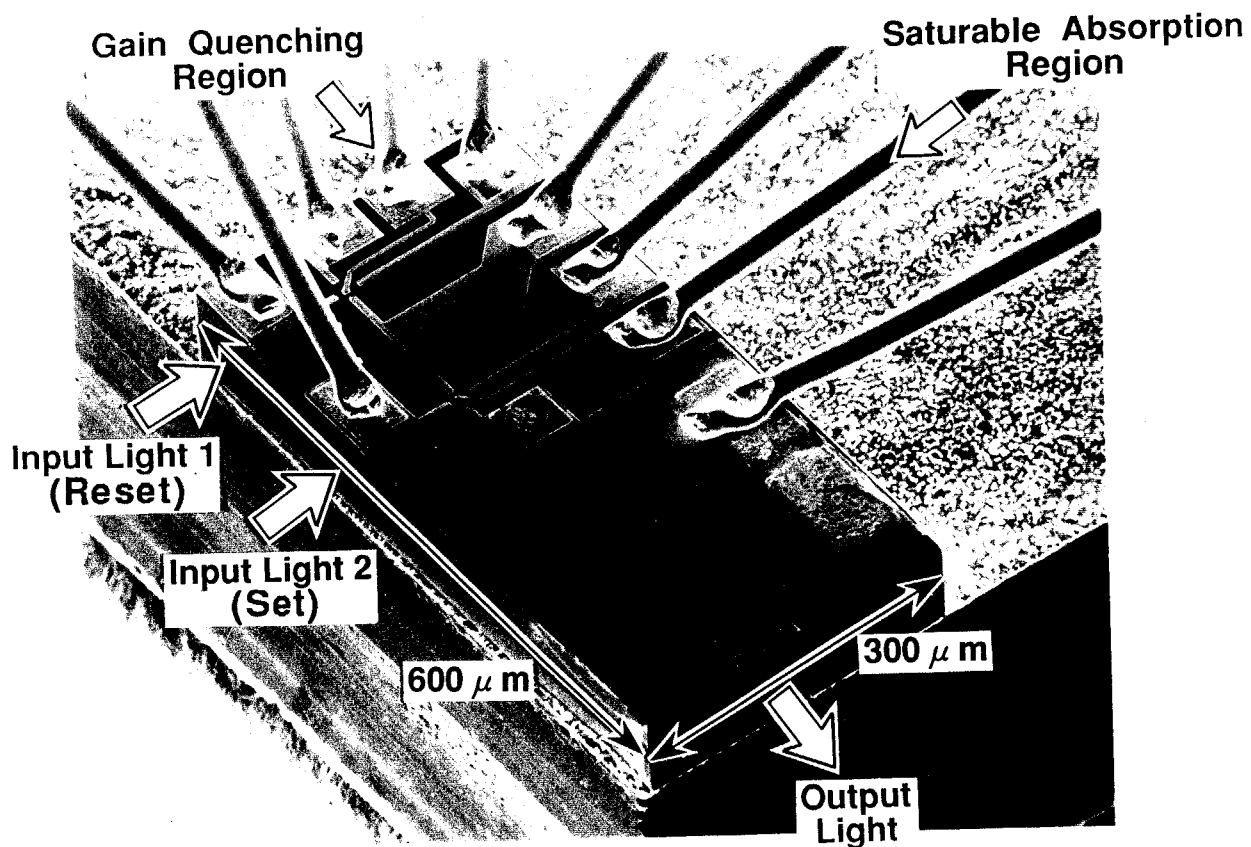
**Fig. 6-1**

Schematic view of a side-light-injection MQW bistable laser.

**Fig. 6-2**

SEM image of a side-light-injection MQW bistable laser.

[2]. The InAlAs barrier layers were used because they improved the characteristics of the absorption saturation due to the large conduction band discontinuity enough to enhance the effects of the two-dimensional exciton [1]. These structures also have the advantage of suppressing hole pile-up because of their small valence band discontinuity as shown by the electroabsorption modulator [3].

The ridge structures of this device were formed by chemical etching. The polyimide was spin-coated to obtain a planar surface and to reduce parasitic capacitance. The nine electrodes were then formed by using the conventional lift-off technique and were electrically separated by removing the cap layer. The isolation resistance between each electrode was more than 1 k$\Omega$. The cavity of the main laser was 600 $\mu$m long and the ridge was 3 $\mu$m wide. The cavity of the main laser was formed in the <0$\bar{1}$1> direction so as to form a reverse mesa structure. There were two 6 $\times$ 6 $\mu$m$^2$ intersections in the middle of the cavity, and the two gain waveguides had a cavity length of 300 $\mu$m and a ridge width of 6 $\mu$m. They were formed in the <011> direction, so their shape was that of an ordinary mesa. After all four facets were cleaved, the device was mounted on a heat sink and bonded with Au wires. All facets had no antireflection coating.

Figure 6-2 shows a scanning electron microscope (SEM) image of the fabricated device. The stripe parallel to the longer side is for the main bistable laser, and the two stripes perpendicular to the longer side are for the waveguide regions. Since the configurations of the two intersections are the same, the difference between the gain quenching region and the saturable absorption region is determined by the applied voltage. If the applied voltage is below the built-in voltage, carriers are depleted in the intersection, absorption dominates, and the intersection thus works as a saturable absorber. Therefore, input light causes absorption saturation and this switches the device from the OFF state to the ON state. When a voltage higher than the built-in voltage is applied, on the other hand, carriers are injected into the intersection, causing optical gain. The input light then consumes carriers and gain quenching occurs, so the intersection works as a gain quenching region. This switches the device

from the ON state to the OFF state. Currents are injected into the waveguide regions to amplify the input light.
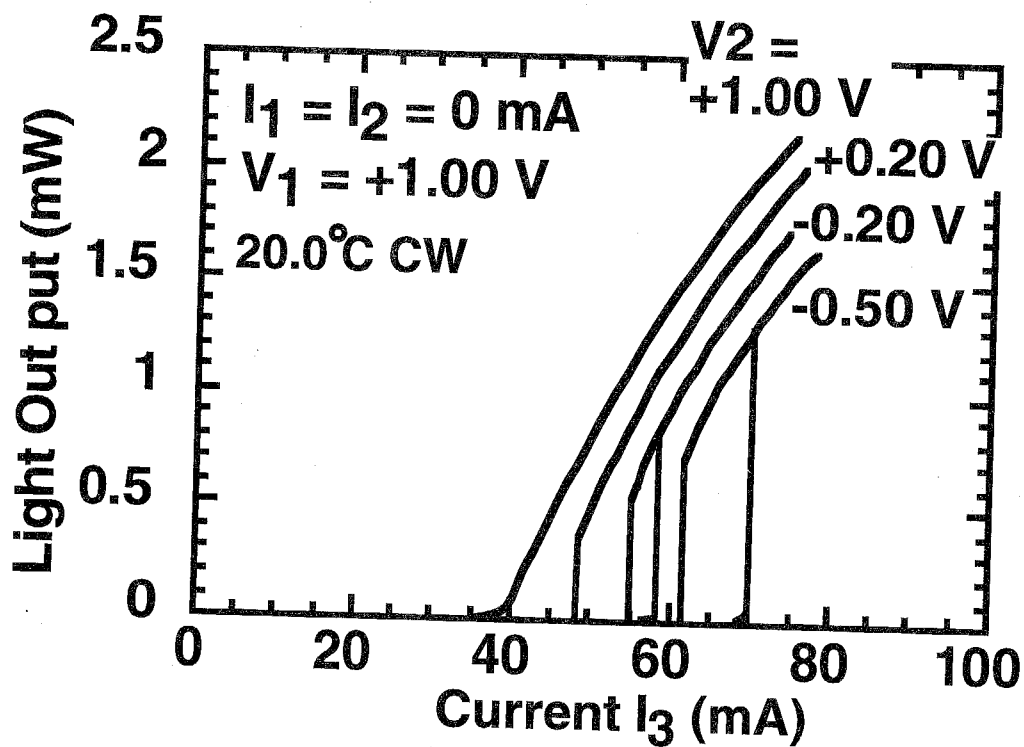
## 6.2 Static Characteristics

### 6.2.1 Light Output versus Current Characteristics

The main laser and the waveguide regions operate as bistable lasers when each part is driven independently. The light output characteristics of the waveguide region and of the main laser are shown in Figs. 6-3(a) and (b) as a function of injection current, respectively. $I_1$, $I_2$, and $I_3$ represent the current injected into the waveguide region except the gain quenching region, the current injected into the waveguide region except the saturable absorption region, and the current injected into the gain region of the main laser, respectively. And $V_1$ and $V_2$ are the voltages applied to the gain quenching region and the saturable absorption region, respectively. For each curve, the operating electrodes, except for the intersections, were common and the voltages applied to the intersection were varied as parameters. No current or voltage was supplied to the other electrodes. Both the threshold currents and the hysteresis widths increase with decreasing applied voltage because the absorption in the intersection increases. The threshold current and the bias voltage are higher in the waveguide region than in the main laser, probably because of the shorter cavity length and higher injection carrier density.

To perform switching operations, not only the main laser but also the two waveguides must work as lasers or optical amplifiers. Figure 6-4 shows the light output of the main laser plotted against the current injected into the gain region. Voltages applied to the gain quenching and the saturable absorption regions were +1.00 and +0.29 V, respectively. Currents of 60.0 mA were injected into both waveguide regions. The threshold current of about 56.5 mA and a hysteresis width of about 1 mA were obtained. The threshold current is several mA higher than that in Fig. 6-3(b)
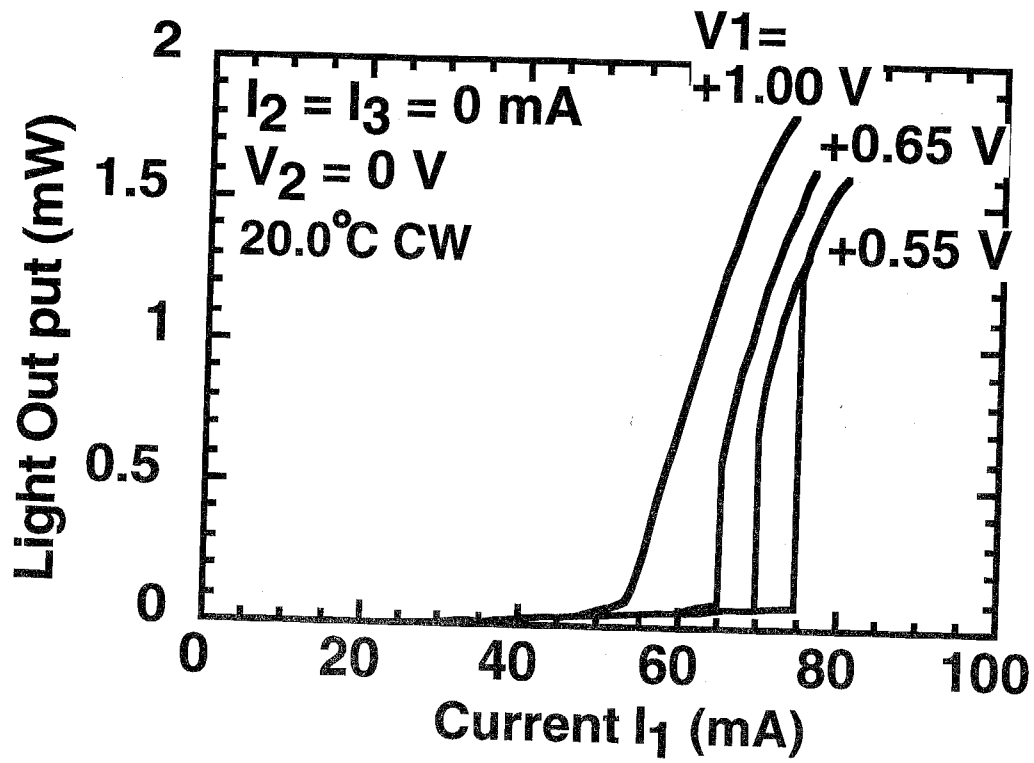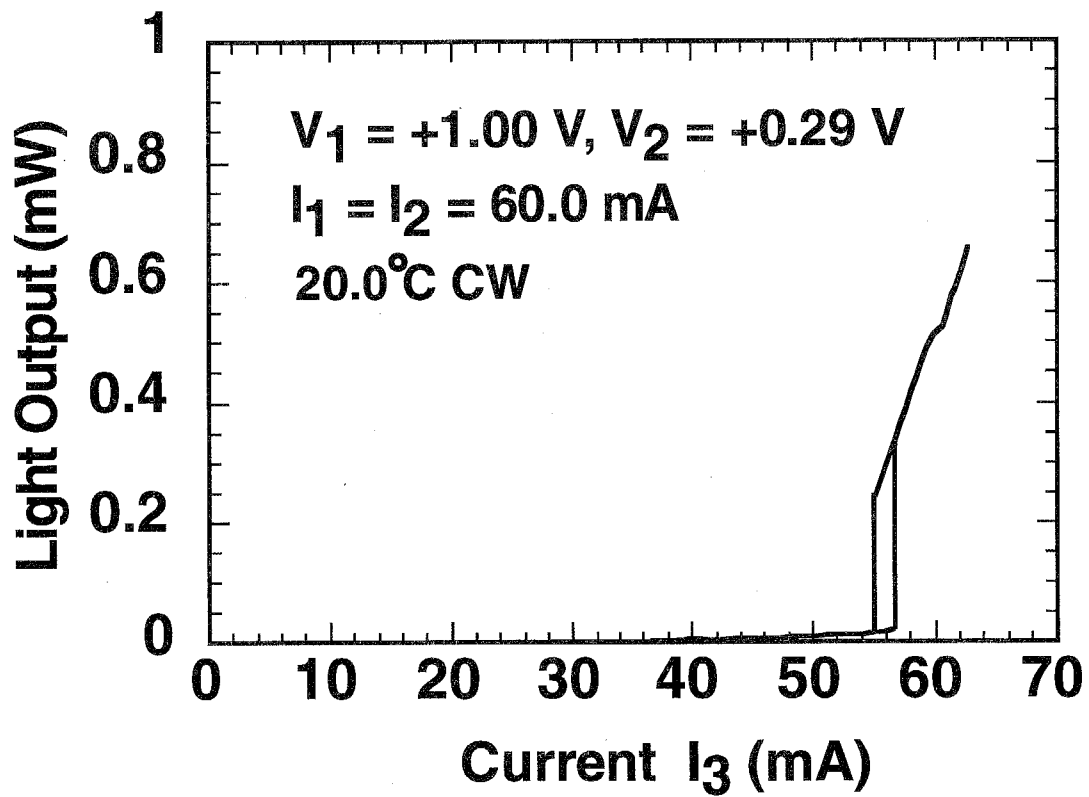
**(a) Waveguide region**

**(b) Bistable laser region**

Fig. 6-3

Light output versus current characteristics of (a) waveguide region and (b) main bistable laser.

**Fig. 6-4**

Light output versus current characteristics of the main laser under current injection into the waveguide regions

because of the thermal effect. The temperature rise has a marked effect on the laser threshold and the three lasers therefore could not lase at the same time.

## 6.2.2 Switching Power by Input Light

Set and reset operations were performed by injecting light into the saturable absorption or the gain quenching regions under the driving conditions specified in Section 6.2.1. The experimental set up is shown in Fig. 6-5. Two DFB lasers with different wavelengths were used for set and reset operations because the wavelength sensitivities differ between saturable absorption and gain quenching. The temperature of all lasers were stabilized by Peltier control within the change of 0.1 degrees. The light emitted from one laser ($\lambda_{in}$ = 1.5357 $\mu$m) was injected directly into the saturable absorption region. Light emitted from the other laser ($\lambda_{in}$ = 1.5533 $\mu$m) was amplified by an Er-doped fiber amplifier and injected into the gain quenching region. The ratio of the input light signal to amplified spontaneous emission was greater than 10:1. The wavelength of the amplified light was intentionally selected so as to be longer than that of the main bistable laser ($\lambda_{out}$ = 1.5456 $\mu$m) because this longer-wavelength input light produces efficient gain quenching. Actually, the light emitted from the DFB laser with a shorter wavelength did not cause gain quenching. Both wavelengths were adjusted to one of the Fabry-Perot resonance peaks of the electroluminescence spectra from each waveguide in order to lower the threshold switching power. Currents of 60.0 mA, slightly below the threshold current of the waveguide region for the reset input port and considerably below that for the set input port, were injected into both of the waveguide regions. Input light power was measured in front of the waveguide input port and the coupling loss between the fiber and the waveguide region for light injection was taken into consideration. Figures 6-6 (a) and (b) show the optical spectra of light emitted from waveguide regions and from the DFB laser for set and reset operations, respectively. The wavelength of the injected light is shown by the arrows in the figures. Because the facets of the waveguide regions were not antireflection
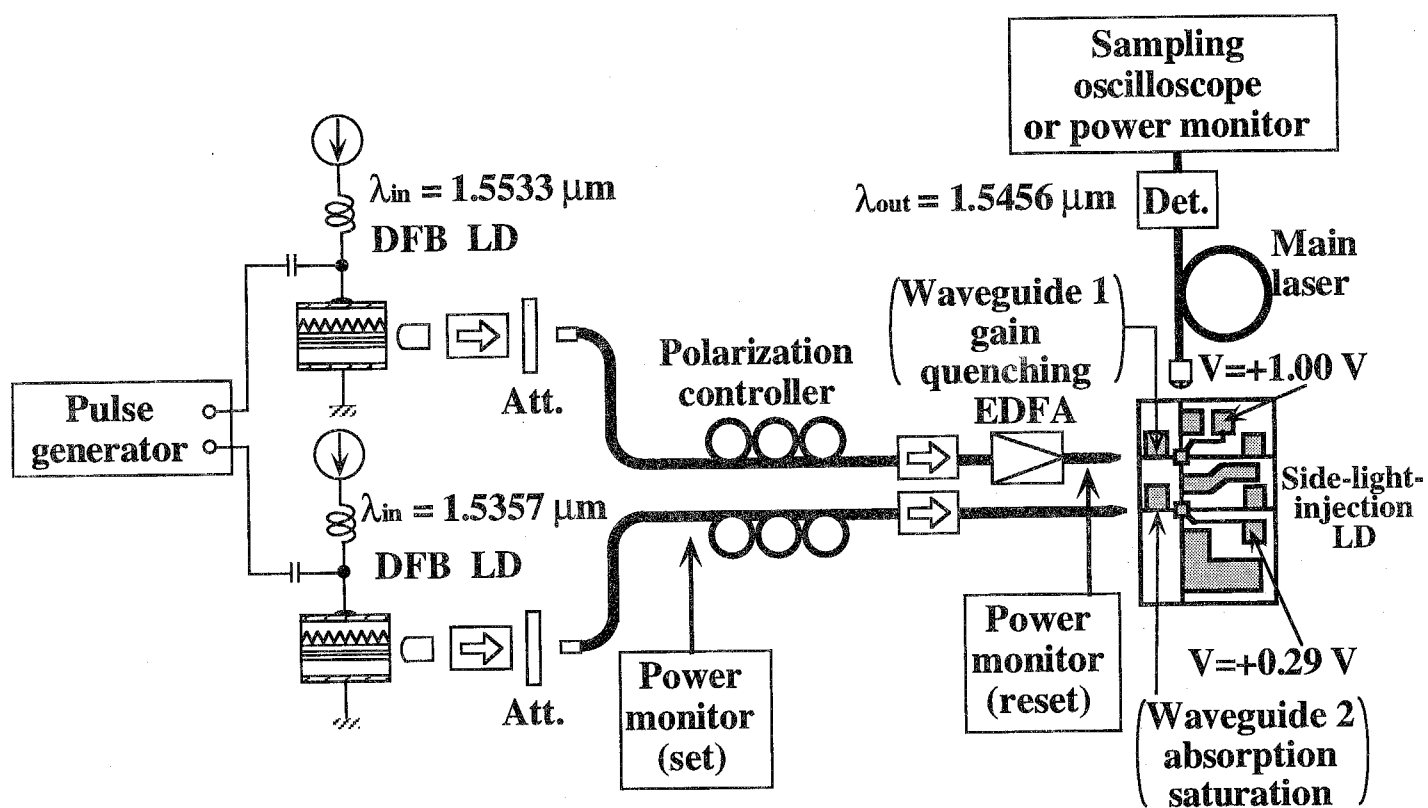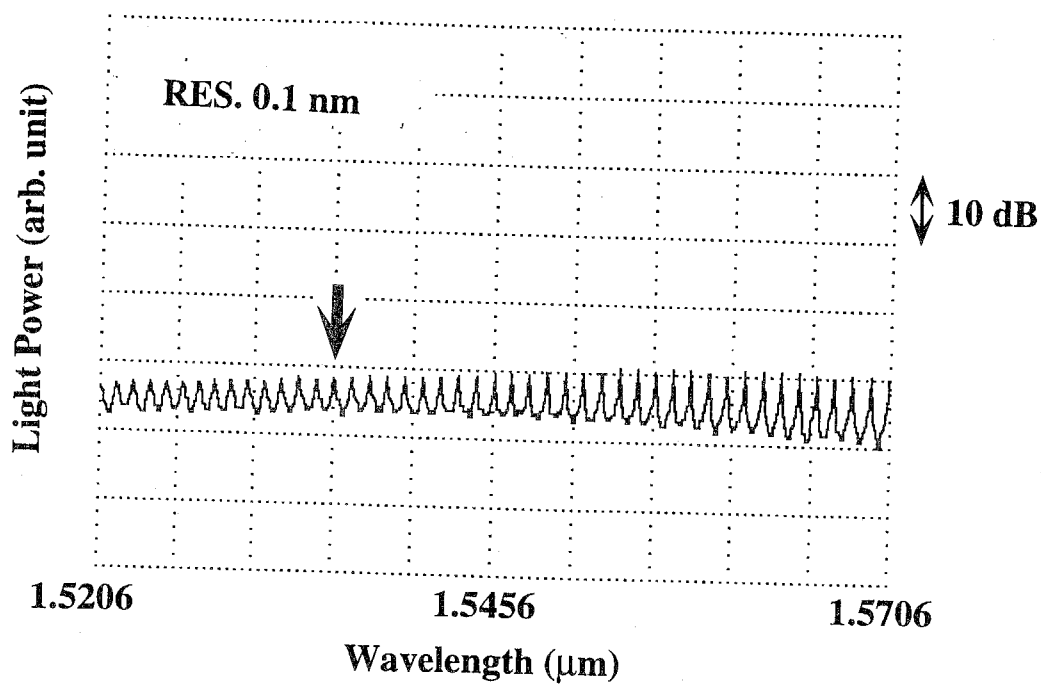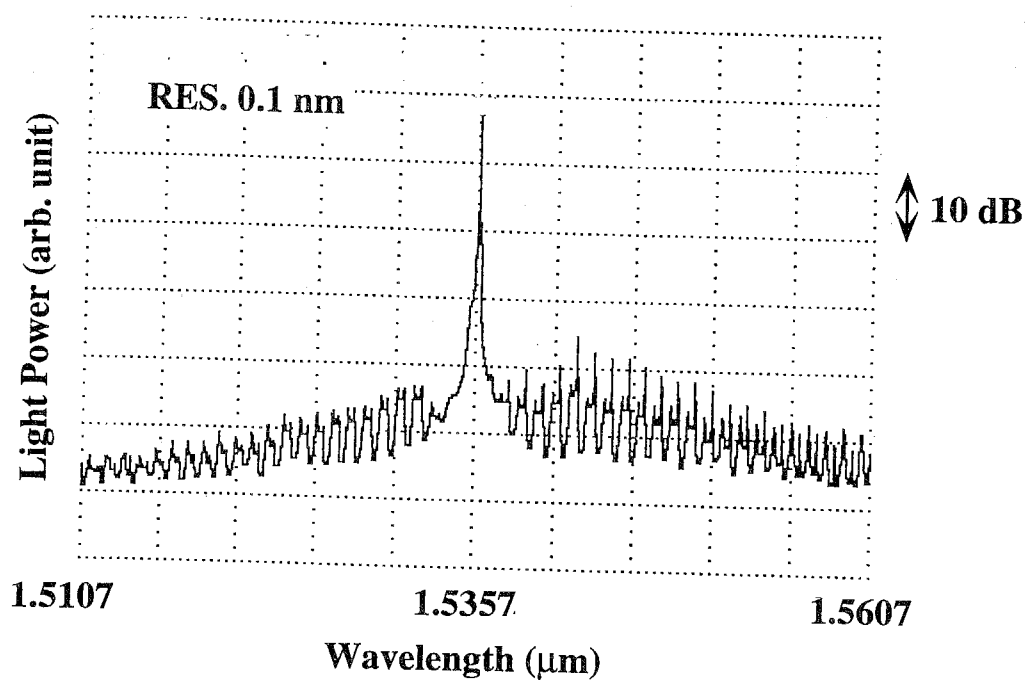
**Fig. 6-5**

Experimental setup for set and reset operations of a side-light-injection MQW bistable laser.
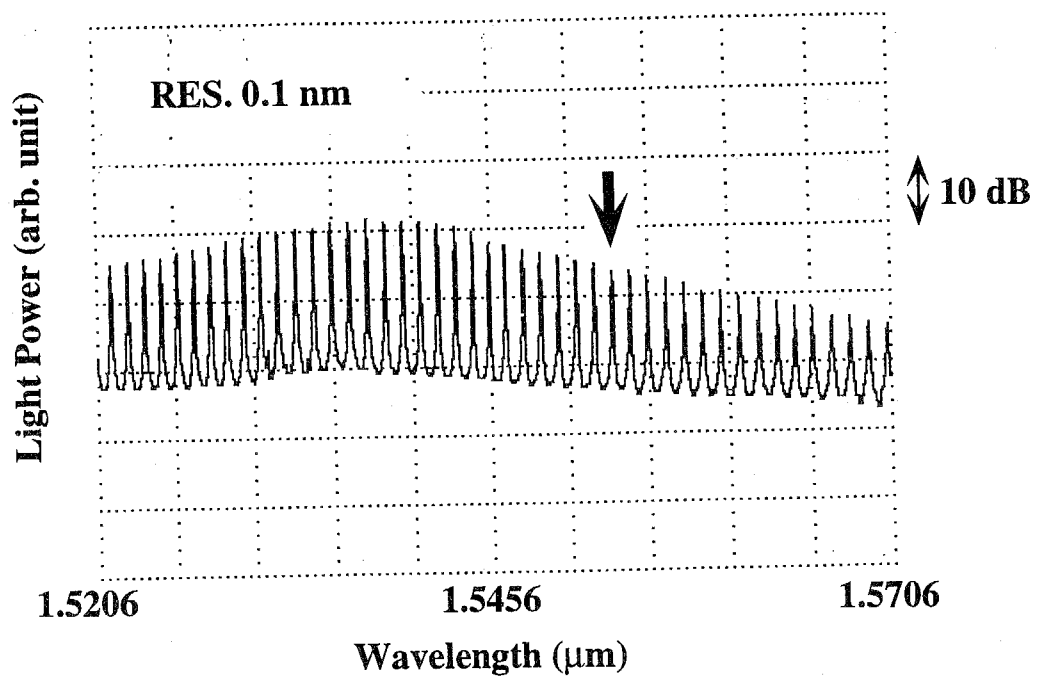
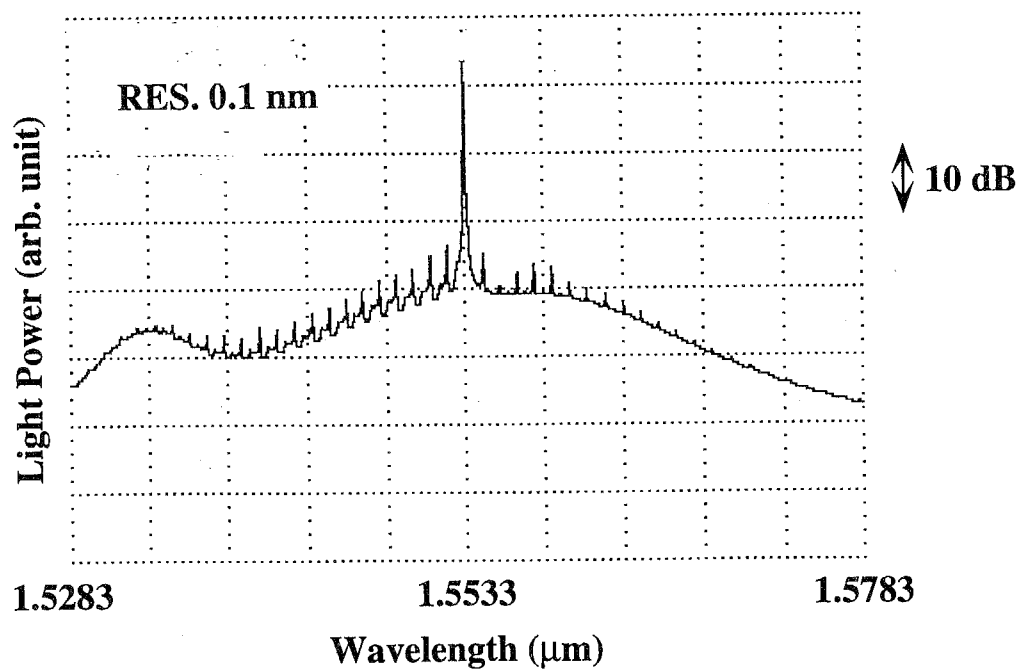(i) Waveguide for set operation



(ii) DFB laser for set operation

Fig.6-6(a)

Optical spectra of light emitted from (i) waveguide region and (ii) DFB laser for set operation.

(i) Waveguide for reset operation



(ii) DFB laser for reset operation

Fig.6-6(b)

Optical spectra of light emitted from (i) waveguide region and (ii) DFB laser for reset operation.

coated, so the input light was affected by the Fabry-Perot resonance of the waveguide regions especially for reset operation.

The set operation is performed when the main laser was in the spontaneous emission state and input light was injected into the saturable absorption region biased at +0.29 V. The input/output light characteristics for set operation is shown in Fig. 6-7(a). The gain current of the main laser was set 0.2 mA below the turn-on threshold current. Threshold input light power of 24 μW was obtained. On the other hand, the reset operation was obtained when the main laser was lasing and the input light was injected into the gain quenching region biased at +1.00 V (Fig. 6-7(b)). The threshold input light power was 1.25 mW. A lower threshold power of 570 μW was also obtained with a smaller wavelength offset (the deviation of lasing wavelength from input light wavelength was 3 nm) [4]. In this case, the gain current of the main laser was biased 0.1 mA above the electrical turn-off current. The on/off ratio was 10:1, which is much higher than the ratios reported in References 5 and 6. I have demonstrated the turn-on and turn-off characteristics by injecting light with memory operation in a side-light-injection-type bistable laser for the first time [4]. The lasing and nonlasing spectra of the bistable laser region are shown in Fig. 6-8. The input light was not detected within the detection limit and the superior isolation ratio was confirmed.

In these experiments, the input light wavelength for set and reset operations were selected intentionally to be different. But the set and reset operations with the same input light wavelength was also obtained [4]. The input light is not affected by the Fabry-Perot resonance modes of the bistable laser, so the range of both set and reset operations with the same input light wavelength can be wider than in-line light-injection-type bistable lasers.
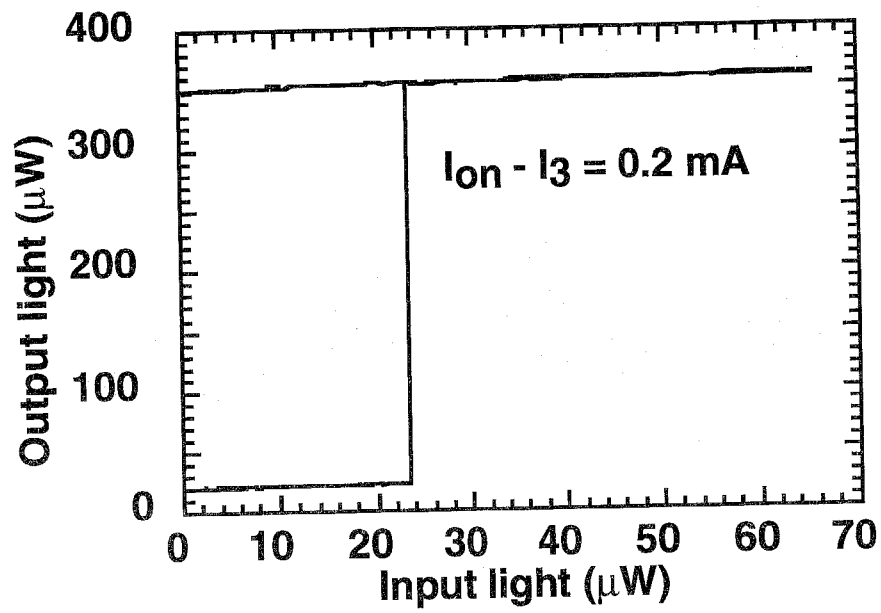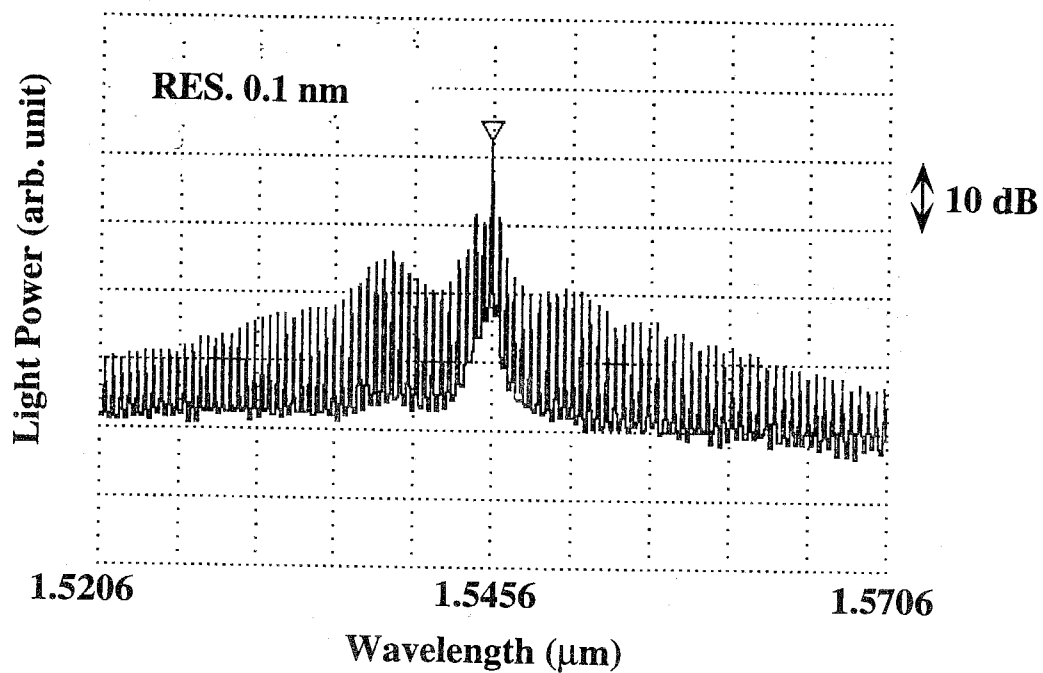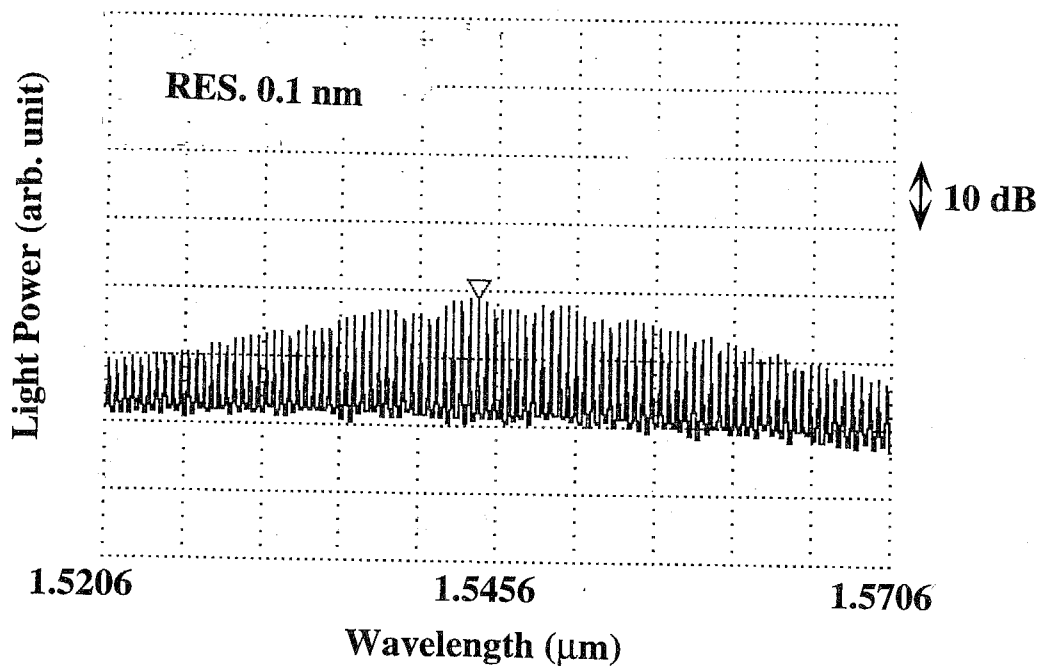
(a) Set operation
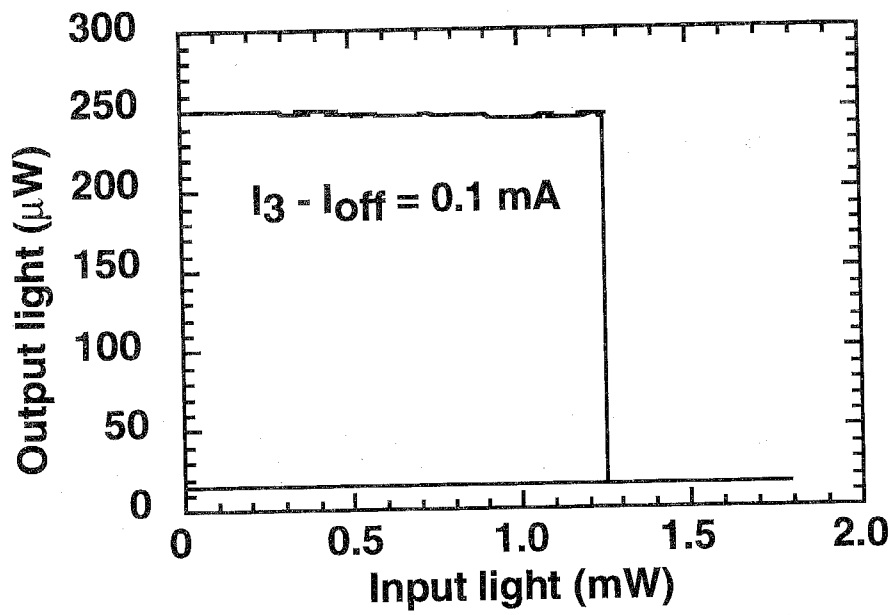


(b) Reset operation

Fig. 6-7

Static input / output light characteristics of (a) set and (b) reset operations.

**Fig.6-8**

Optical spectra of light emitted from bistable laser region.
(a) Lasing state and (b) spontaneous emission state.

## 6.3 Dynamic Characteristics

### 6.3.1 Switching Operation

Figure 6-9 illustrates the set and reset operations of the side-light-injection MQW bistable laser [7], [8], which uses only injected light to perform these operations. Dynamic memory operation with set and reset by input light has been achieved. The bias current of the main laser of the side-light-injection MQW bistable laser was set 0.6 mA above the electrical turn-off current. Lower switching power for reset operation can be obtained when the bias current is set near turn-off threshold current, but this causes the recovery time after the first peak to be slow and sometimes diminishes the lasing. The width of both the set and reset lights is 5 ns. The spikes seen at the onset of the output light are not the amplified input signal but are the lasing light from the main bistable laser itself. The change of carrier density in the laser cavity is attributed to these spikes.

### 6.3.2 Turn-on Time

The dependence of the turn-on time on input light peak power is shown in Fig. 6-10. In Figs. 6-10, the estimated input light power did not include coupling loss due to wavelength difference between the resonance mode in the waveguide region and the input light. This situation is valid when the wavelength sensitivity in the waveguide region is low because the peak to valley ratio of the Fabry-Perot mode is small due to the large absorption in the saturable absorption region. The calculation curves as shown in Fig. 5-7(a) are shown in the same figures. Comparing the experimental and calculation results, it is found that the differential gain in the bistable laser region was 1.0 to $2.0 \times 10^{-16}$ cm$^2$. The turn-on time decreased as the input light power increased, which is the same relationship seen for the two-segmented MQW bistable laser [2]. The turn-on time was about 200 ps when the input light peak power was 1 mW.
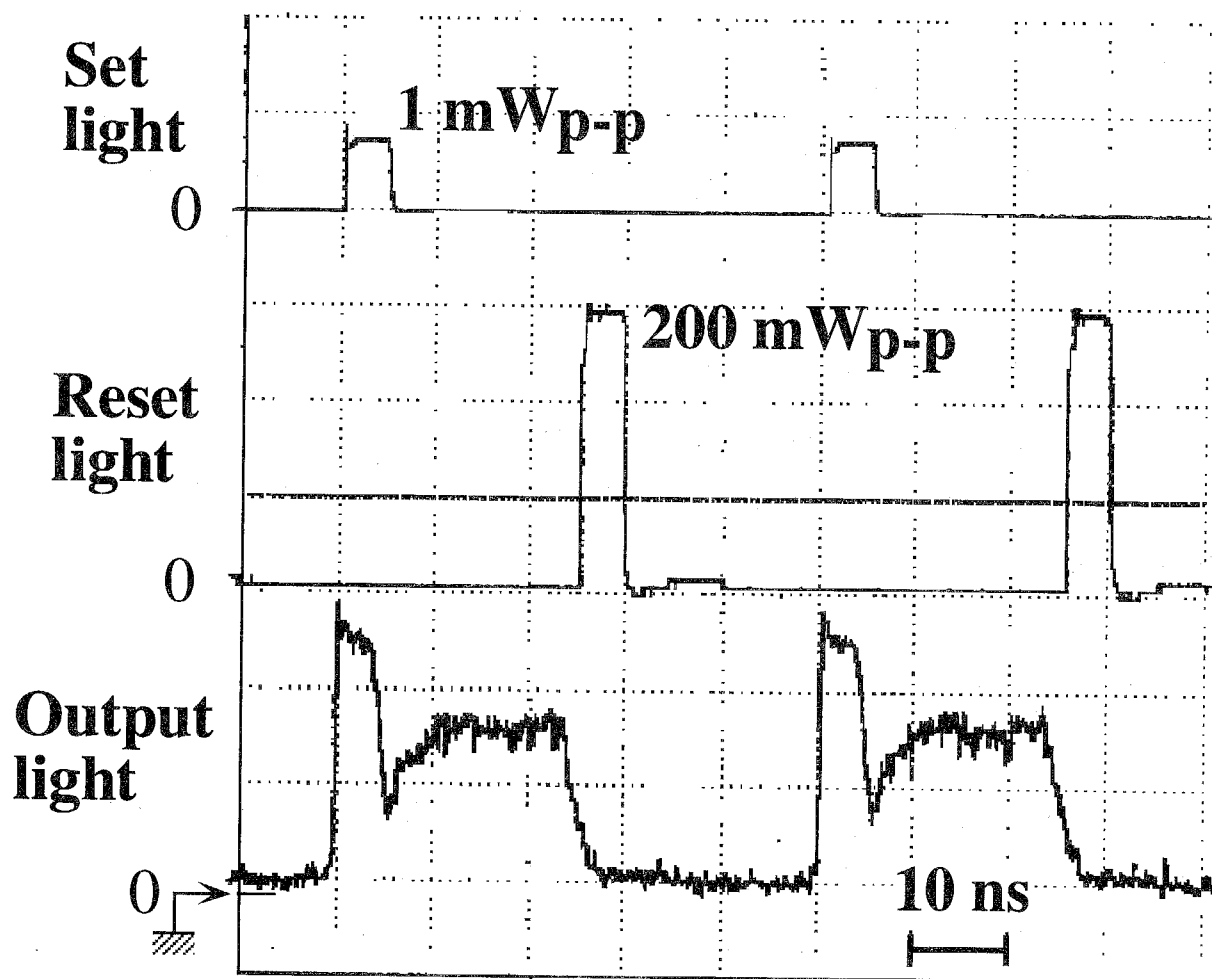
**Fig. 6-9**

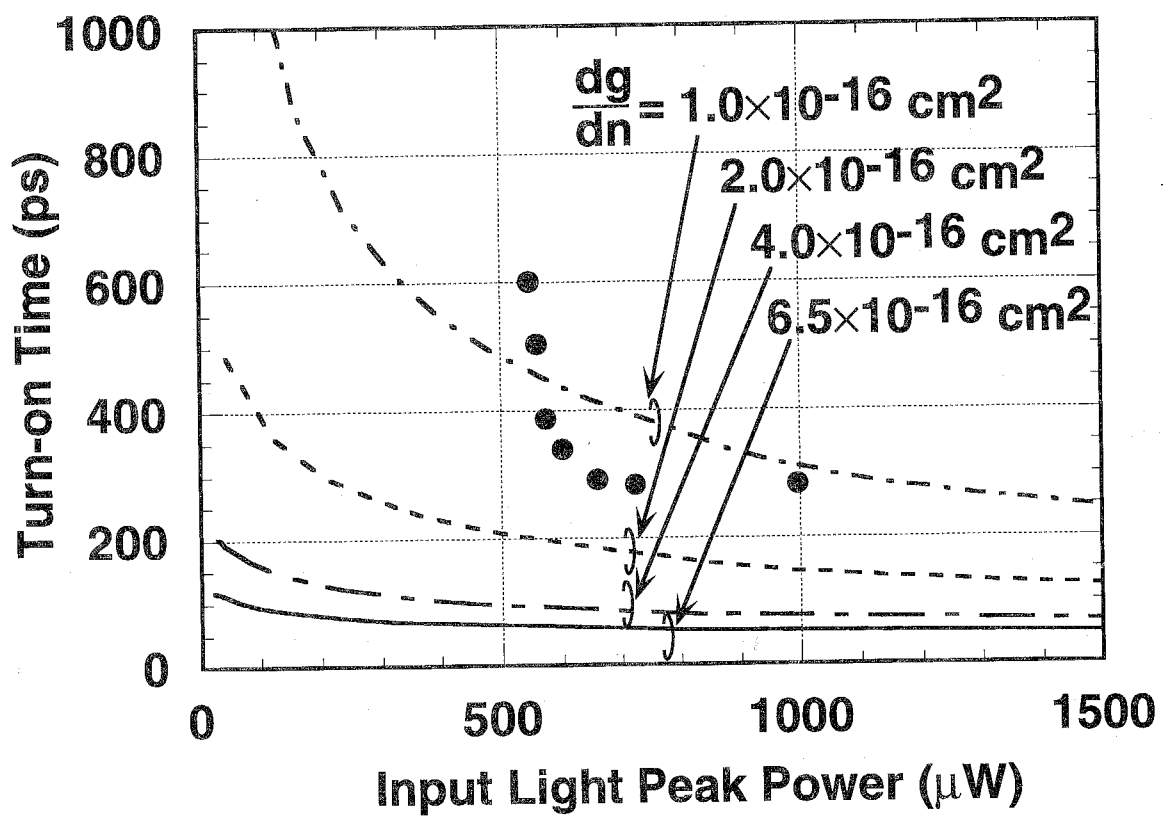**Set and reset operations of a side-light-injection MQW bistable laser.**

**Fig. 6-10**

Turn-on time dependence on input light peak power. Dots represents
experimental results, and lines represent calculation results.

Defining the switching energy as a product of turn-on time and the input light peak power, it is 200 fJ. The turn-on time is slower than that obtained in the two-segmented MQW bistable laser with the same active region material, i.e., 6 periods of InGaAs/InAlAs. The reasons for this slower turn-on time are the following:

(1) The intrinsically higher switching power, which is indicated by comparing Figs. 4-15 and Fig. 6-7(a). This is caused by the smaller intersections of the saturable absorption region, which are limited by the ridge width.

(2) The insufficient input light power. This is due to the smaller Fabry-Perot resonance gain between the forward and the backward waveguide regions, which is in turn caused by the lower current-injection level.

The turn-on time can therefore be reduced by introducing a large-gain material and enhancing the gain in the waveguide region.

### 6.3.3 Turn-off Time

The turn-off time decreased gradually as the input light power increased, as shown in Fig. 6-11, reaching less than 2 ns when the input light peak power was 200 mW. This power corresponds to the average power of 20 mW at a 10% duty cycle. The product of turn-off time and input light peak power, i.e., switching energy, is 400 pJ. The turn-off time is limited mainly by the input light power because the threshold switching power is rather high. The reasons for the nanosecond-order turn-off time, longer than that expected from the theoretical predictions in Fig. 5-9, are probably the insufficient input light due to high threshold input light power and small differential gain coefficient caused by high threshold current.

The calculated turn-off time (the same as Fig.5-9) assuming the optical coupling loss of -8 dB is shown in the figures. The coupling loss of -8 dB was derived so that the differential gain in this case coincides with that mentioned in the previous section (1.0 to $2.0 \times 10^{-16}$ cm$^2$). The reason for the coupling loss is considered to be due to the wavelength deviation of the input light from the lasing mode and the resultant
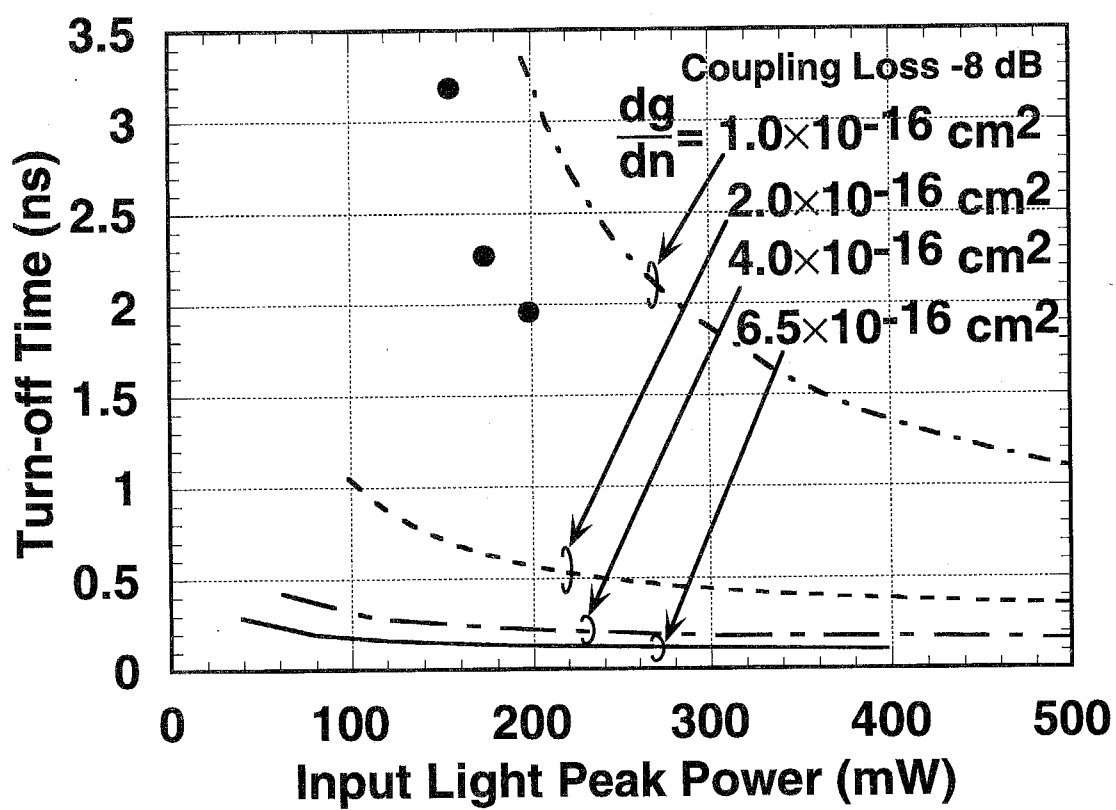
Fig. 6-11

Turn-off time dependence on input light peak power. Dots represent
the experimental results and lines represent calculated results.

insufficient gain in the waveguide region. The net gain in the Fabry-Perot-type waveguide for reset operation can be derived from the peak to valley ratio of the Fabry-Perot resonance in Fig. 6-6(b)(i) [9], and it was 30.6 cm$^{-1}$. When the input light wavelength is the same as lasing wavelength, the Fabry-Perot gain of 13 dB can be obtained. However, the input light power was very large enough to cause gain saturation in the waveguide, which compensated the Fabry-Perot gain. And also, it is considered that the coupling loss of -8 dB can be caused by 1.5-Å wavelength deviation between the input light and the Fabry-Perot mode of the waveguide (using eqn.(3.6) to (3.9)). In order to avoid the wavelength sensitivity, it is suitable to use the waveguide as a traveling wave amplifier by forming antireflection coating [10][11].

As mentioned in Section 5.4, the turn-off time can be reduced by using large-gain materials such as InGaAs/InAlAs MQW structures with a large number of quantum wells. Enhancing the gain in the waveguide region is one way to decrease the turn-off threshold input light power, which results in the relative increment of the input light power and high-speed reset operation. As noted in Section 6.3.2, the methods for reducing the turn-on and turn-off time are almost the same.

## 6.4 Comparison between In-line and Side-light-injection MQW bistable laser Performance

The performance of in-line and side-light-injection MQW bistable lasers are listed in Table 6-1. Because of their structure differences, the switching power of the side-light-injection-type is greater than that of in-line-type. In the in-line-type, the interaction length of the saturable absorber with input light can be change by changing the length of the absorption region. And also, the amplification of input light by Fabry-Perot resonance affects the reduction of threshold input light power. In side-light-injection-type, on the other hand, the interaction length along the light propagation is restricted by the ridge width of bistable laser section as mentioned in Section 6.3.2. Larger threshold input light power causes the switching time to be slower for both set

**Table 6-1**

Performance of in-line and side-light-injection type MQW bistable lasers.

| | In-line type | Side-light-injection type |
|---|---|---|
| Saturable absorber size | 10 $\mu$m | Absorber 6 $\mu$m<br>Quenching 6 $\mu$m |
| Hysteresis control | 0~30 mA<br>($V_c$=+0.6 V~-0.6 V) | 0~30 mA<br>(V=+1.0 V~-0.6 V) |
| Switching power | turn-on < 10 $\mu$W<br>or < 10 fJ<br>turn-off < 10 pJ | turn-on 20 $\mu$W<br>or 200 fJ<br>turn-off 400 pJ |
| Switching speed | turn-on <100 ps<br>turn-off <100 ps | turn-on 200 ps<br>turn-off 2 ns |
| Wavelength sensitivity | 50 nm<br>Fabry-Perot resonance | Fabry-Perot resonance |

and reset operations. A switching time less than a nanosecond, however, is possible. And larger switching power can be solved by the improvement of the gain in the waveguide region as mentioned in previous section.

The other method for low threshold switching power and fast switching time for both set and reset operations is to widen the saturable absorption region and the gain quenching region. In Chapter 5 and this chapter, uniform-width ridge structure was assumed. So the length of the saturable absorption region and the gain quenching region along the bistable laser cavity is restricted by the ridge width of the waveguide region because too much wide ridge structure degrades the coupling efficiency between the fiber and the waveguide. Tapered-shape waveguide [11], however, can overcome this problem and is expected to enhance the efficiency of both absorption saturation and gain quenching. For this structure, the length of the saturable absorption and the gain quenching region must be optimized for maintaining low threshold current and the controllability of hysteresis characteristics.

In terms of the wavelength sensitivity, both structures showed wide sensitivity. In in-line light-injection scheme, wavelength sensitivity is intrinsically modulated due to Fabry-Perot resonance mode, whereas it is potentially flat in side-light-injection scheme. But in this experiment, Fabry-Perot resonance affected the switching power and speed because of no antireflection coatings. The formation of antireflection coatings is expected to be effective for lowering the wavelength sensitivity. Actually, a flat wavelength sensitivity over about 100 nm was obtained in the side-light-injection scheme [10],[11].

As well as the in-line light-injection MQW bistable laser, the polarization sensitivity of the switching power is thought to be inevitable. But fortunately, the waveguides for input light can be formed independent of the bistable laser region, for example, by using regrowth. So introducing tensile strained quantum well structure is considered to reduce polarization dependence [12][13], maintaining the TE mode selectivity in the bistable laser.

Considering the superior potentiality such as wavelength independence and polarization independence as well as the all-optical set and reset operations, the side-light-injection MQW bistable laser can be applied to the multi-channel wavelength division multiplexed (WDM) system. The bit rate is less than that for in-line-type, but around 1 Gbit/s or higher is possible by improving the waveguide gain and introducing the MQW structure with large differential gain.

## 6.5 Summary

In conclusion, we have demonstrated that set and reset operations can be achieved by using only injection light in a side-light-injection MQW bistable laser. These operations are achieved by saturable absorption and by gain quenching. Voltages applied to electrically separated intersections of the main laser and the waveguide regions flexibly control whether their intersection works as a saturable absorption region or a gain quenching region. Subnanosecond turn-on time and several-nanosecond turn-off time were obtained, and both time are reduced by high-power input light. Optimizing the MQW structure, widening the saturable absorption and gain quenching region as well as improving gain in the waveguide region are important for achieving a subnanosecond switching time. Reducing the threshold switching power enables cascade combinations and thus the construction of all-optical signal processing systems.

# References

[1] Y. Kawamura, A. Wakatsuki, Y. Noguchi and H. Iwamura, "InGaAs/InGaAlAs MQW lasers with InGaAsP guiding layers grown by gas source molecular beam epitaxy", IEEE Photon. Technol. Lett., vol.3, pp.960-962, 1991.

[2] H. Uenohara, H. Iwamura and M. Naganuma, "Switching characteristics of InGaAs/InP multiquantum well voltage-controlled bistable laser diodes", Jpn. J. Appl. Phys., vol.29, pp.L2442-L2444, 1990.

[3] K. Wakita, Y. Kawamura, Y. Yoshikuni, H. Asahi and S. Uehara, "Anisotropic electroabsorption and optical modulation in InGaAs/InAlAs multiple quantum well structures", IEEE J. Quantum Electron., vol.22, pp.1831-1836, 1986.

[4] H. Uenohara, Y. Kawamura, H. Iwamura, K. Nonaka, H. Tsuda and T. Kurokawa, "Side-light-injection MQW bistable laser using saturable absorption and gain quenching", Electron. Lett., vol.28, pp.1973-1974, 1992.

[5] W. J. Grande and C. L. Tang, "Semiconductor laser logic gate suitable for monolithic integration", Appl. Phys. Lett., vol.51, pp.1780-1782, 1987.

[6] S. Wakabayashi, T. Tsuruta, K. Idota, Y. Takeuchi, M. Ohshima and Y. Toyoda, "Side-diode-injection laser for optical logic", Proc. Int. Topical Meeting on Photonic Switching, Kobe, 1990, pp. 122-124.

[7] H. Uenohara, Y. Kawamura, H. Iwamura, K. Nonaka, H. Tsuda and T. Kurokawa, "Set and reset operation dependence on input light intensity of a side-light-injection MQW bistable laser", Electron. Lett., vol.29, pp.1609-1610, 1993.

[8] H. Uenohara, Y. Kawamura, H. Iwamura, K. Nonaka, H. Tsuda and T. Kurokawa, "Operation characteristics of a side-light-injection multiple-quantum-well bistable laser for all-optical switching", Jpn. J. Appl. Phys., vol.33, Part I, pp.815-821, 1994.

[9] B.W. Hakki and T.L. Paoli, "Gain spectra in GaAs double-heterostructure injection lasers", J. Appl. Phys., vol. 46, pp.1299-1306, 1975.

[10] K. Nonaka, H. Tsuda, H. Uenohara, H. Iwamura and T. Kurokawa, "Optical nonlinear characteristics of a side-injection light-controlled laser diode with a

multiple-quantum-well saturable absorption region", IEEE Photon. Technol. Lett., vol.5, pp.139-141, 1993.

[11] H. Tsuda, K. Nonaka, K. Hirabayashi, H. Uenohara, H. Iwamura and T. Kurokawa, "Wide range wavelength conversion experiments using a side-injection light-controlled bistable laser diodes", Appl. Phys. Lett., vol.63, pp.3116-3118, 1993.

[12] P.J.A. Thijs, L.F. Tiemeijer, P.I. Kuindersma, J.J.M. Binsma and T. van dongen, "High performance 1.5 μm wavelength InGaAs-InGaAsP strained quantum well lasers and amplifiers", IEEE J. Quantum Electron., vol.27, pp.1426-1439, 1991.

[13] K. Magari, M. Okamoto, H. Yasaka, K. Sato, Y. Noguchi and O. Mikami, "Polarization insensitive traveling wave type amplifier using strained multiple quantum well structure", IEEE Photon. Tech. Lett., vol.2, pp.556-558, 1990.

# Chapter 7 Ultimate Response of Multiple Quantum Well Bistable Lasers

This chapter evaluates the ultimate response of MQW bistable laser by analyzing their performance. To do this in detail, the transient response of the saturable absorber under applied electric field was measured by using pump-probe measurement. The dependence of the carrier escape time for InGaAs/In(Ga)AlAs MQWs on barrier thickness and barrier height have been studied. Absorption saturation due to phase space filling caused by photogenerated carriers and following electric-field screening dominates the transient electroabsorption signals. The carrier escape time was estimated by fitting the experimental results to calculations and was found to be strongly affected by the barrier thickness. Escape time for MQW region of less than 5 ps occur under high electric fields, and the escape time for the optical confinement layer is about one order of magnitude longer.

Introducing these experimentally derived carrier escape time into the rate equations given in Chapter 3 shows that the turn-off time limit under a high applied voltage should be less than 10 ps. A MQW structure with a larger differential gain can provide faster turn-on and turn-off time. Under the optimized driving conditions with minimum turn-on and turn-off time, the repetition rate in the memory operation is limited by the relaxation oscillation and can be higher than 5 to 10 GHz.

## 7.1 Principle of Transient Response of Saturable Absorber

Chapter 3 analyzed the dynamic characteristics of the two-segmented MQW bistable laser and evaluated the dependence of the turn-on and turn-off time on input signal power and MQW structures. In these calculations, however, the carrier escape time for the saturable absorption region was given as a parameter independent of the applied voltage height. They thus did not adequately take into account the dependence of carrier escape time on applied voltage. To investigate the switching speed limit, it is

important to examine the time response of the saturable absorber, especially under applied electric fields.

The structure dependence of carrier escape time and its numerical analysis including two processes, i.e., excitonic saturation caused by phase space filling and field screening effect, have recently been reported for the AlGaAs/GaAs system [1],[2]. For long-wavelength systems, on the other hand, there were few reports [3] and the influence of the MQW structure on carrier sweep-out has not been reported.

J. A. Cavaillès et al. derived the carrier escape time for the MQW structure by using the electroabsorption model [2]. The principle of this model is shown in Fig.7-1. Now assuming the input light wavelength is the same as the heavy-hole exciton peak wavelength at flat band condition, the applied reverse bias voltage causes large absorption due to the red-shift of the absorption edge. This is the so-called quantum confined Stark effect (QCSE). Just after the pump light is injected into the MQW structure, electrons are excited from the valence band to the conduction band. These photogenerated carriers in the MQW region cause phase space filling. So the absorption due to two-dimensional excitons saturates, and this results in the transmission increment. Then the excited carriers move from the MQW region toward the electrodes because the external electric field is applied between the p and n electrodes. Electrons or holes moving in the optical confinement layers cancel the external electric field, i.e., the field screening occurs. Then the absorption spectrum shifts toward shorter wavelengths. Therefore when the input light wavelength is shorter than the exciton peak wavelength, a situation typical of a bistable laser with reverse bias voltage, the absorption is enhanced following the initial transmission increment. The pump-probe signal can be written as follows:

$$\frac{\Delta T}{T}(t) = C_{\text{fil}} \times \exp(-\frac{t}{\tau_{\text{fil}}}) + C_{\text{fld}} \times \Delta F_{\text{QW}}(t) \tag{7.1}$$

where $\Delta T/T(t)$ is the relative change in the probe transition, $C_{\text{fil}}$ and $C_{\text{fld}}$ are the amplitudes of the phase space filling and field screening contributions, and $\Delta F_{\text{QW}}(t)$ is
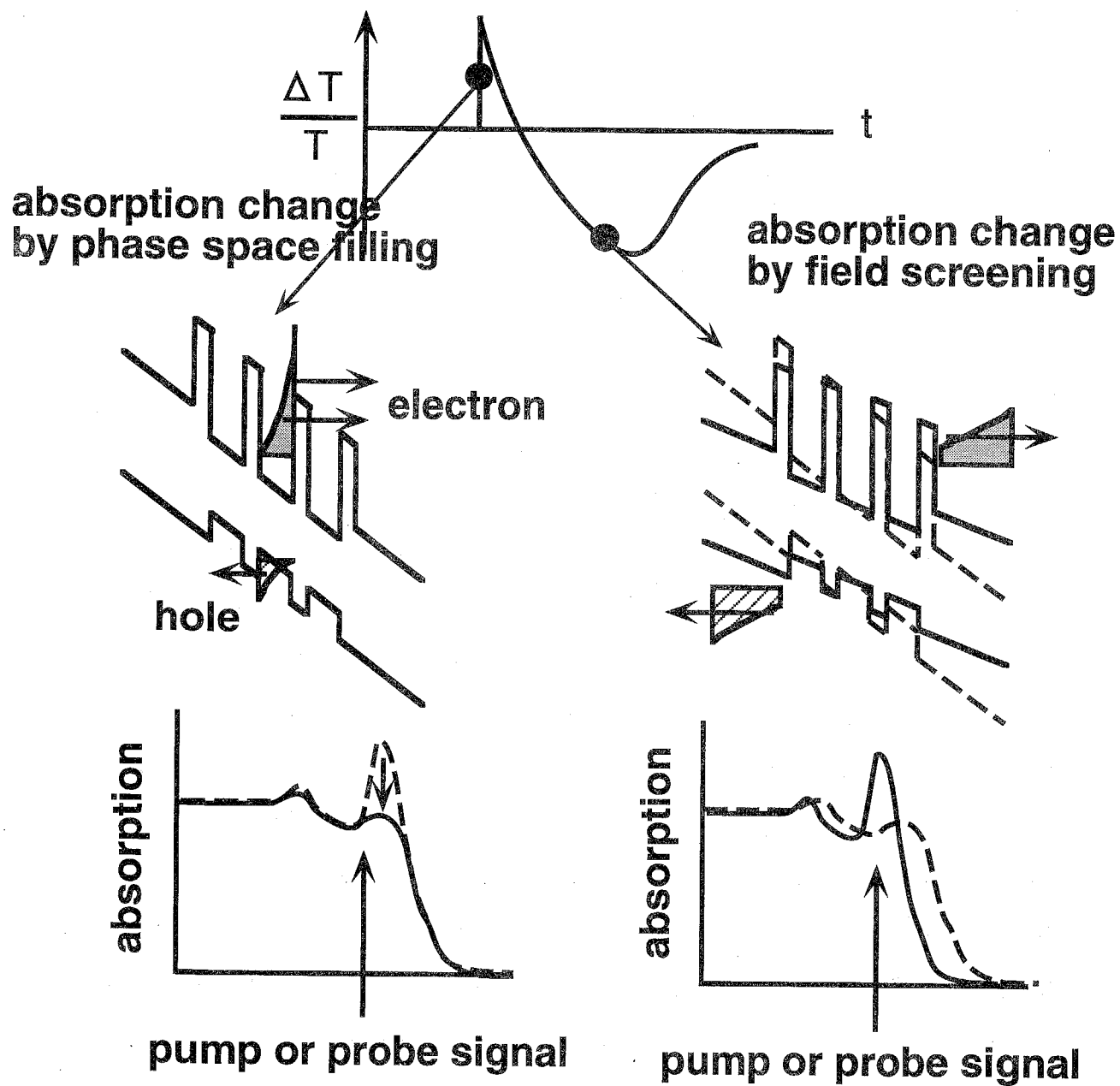
**Fig. 7-1**

Principle of the time response of the MQW saturable absorber.

the electric-field variation in the quantum well region. The term $\Delta F_{QW}(t)$ is given by solving Poisson's equation for the carrier density of the MQW region and is represented in the following equation:

$$\frac{\Delta F_{QW}}{F_0} = \frac{1}{2}\{(\exp(-\frac{t}{\tau_{fld}})-1)\times(1+\frac{2v\tau_{fld}}{D})+\frac{2vt}{D}\}$$
$$\text{if } t < \frac{d_n}{v} \qquad\qquad (7.2)$$
$$= \frac{1}{2}[\exp(-\frac{t}{\tau_{fld}})\times\{1-\frac{2v\tau_{fld}}{D}(\exp(\frac{d_n}{v\tau_{fld}})-1)\}+\frac{d_n-d_p}{D}]$$
$$\text{if } t \geq \frac{d_n}{v}$$

where $F_0$ is the initial field resulting from the photogenerated carriers in the MQW structure, $v$ is the saturated drift velocity, $D$ is the width of the intrinsic region, and $d_n$ and $d_p$ are the widths of the n-side and p-side optical confinement layers. By fitting eqns. (7.1) and (7.2) to the experimental data, the carrier escape time for the MQW, $\tau_{fil}$, and that for the optical confinement layer, $\tau_{fld}$, can be inferred.

## 7.2 Pump-probe Measurement

A pump-probe measurement was performed using a 1.535-μm DFB laser. The lasing wavelength was almost adjusted to nearly the heavy-hole exciton peak wavelength of all of the samples under the flat-band condition. This is almost the same situation as that of voltage-controlled MQW bistable lasers. The gain-switched light pulses from the DFB laser were compressed by a normal dispersion fiber, followed by amplification by erbium-doped fiber amplifiers (EDFA) and soliton-effect compression by anomalous dispersion fibers [4], [5]. The resultant pulse width was 540 fs with a 100 MHz repetition rate. The pump and probe light pulse were separated by a 90:10 fiber coupler, and light was coupled into and collected from the sample by microscope objectives. An InGaAs p-i-n detector was used to measure differential transmitted light power with a lock-in technique. The average optical powers coupled into the sample were about 800 μW for the pump and 50 μW for the probe.

An InGaAs/In(Ga)AlAs MQW structure, which was the same as that used for the MQW bistable laser [6], was grown by gas source molecular beam epitaxy on an $n^+$-InP substrate [7]. The layer structure is shown in Fig. 7-2. The structure consisted of a Si-doped InP cladding layer, a 900-Å-thick undoped InGaAsP ($\lambda_g = 1.2$ μm) lower optical confinement layer, an undoped MQW structure, a 900-Å-thick undoped InGaAsP ($\lambda_g = 1.2$ μm) upper optical confinement layer, a Be-doped InP cladding layer, and a Be-doped InGaAs contact layer. The structure for an MQW bistable laser was used because the operating speed limit of the device itself was of interest. The upper and lower optical confinement layer were undoped to reduce the free carrier loss and the threshold current. In five of the samples, the barrier thickness ($L_B$) and barrier height ($\Delta E_c$) were varied to enable investigation of the structure dependence (Table 7-1). The value of the barrier height $\Delta E_c$ of the InGaAs/In$_{0.52}$Al$_{0.48}$As is from Reference 8 while the other values were decided by interpolating from the Al composition. A 350-μm-diameter circular mesa was formed by wet chemical etching, on which a ring electrode with inner and outer diameters of 200 and 300 μm was patterned. The InGaAs contact layer inside the ring electrode was removed to avoid absorption of the input light for vertical light injection.

Figure 7-3 shows the measured change of the transmitted light power of a sample #1 ($L_B = 30$ Å, $\Delta E_c = 0.5$ eV, $N_w = 10$). A reverse bias voltage of -10 V to -1 V was applied to the sample. Just after the pump light pulse, the photogenerated carriers generated in the wells caused phase-space filling and the transmission increased. The applied electric field swept-out the photogenerated carriers from the wells and, as a result, changed the pump-probe signal. Under low bias voltage (> -5 V), the recovery time decreased as the reverse bias voltage increased. In this case, the recovery time is defined as the interval between the time when the input light is injected and that when the transmission goes back to initial level. This seems to be due to the carrier extraction effect from the MQW, which effect is caused by the applied electric field. Under high bias voltage (< -5 V), the pump-probe signals showed a slow transmission increase under some bias conditions and a fast transmission decrease
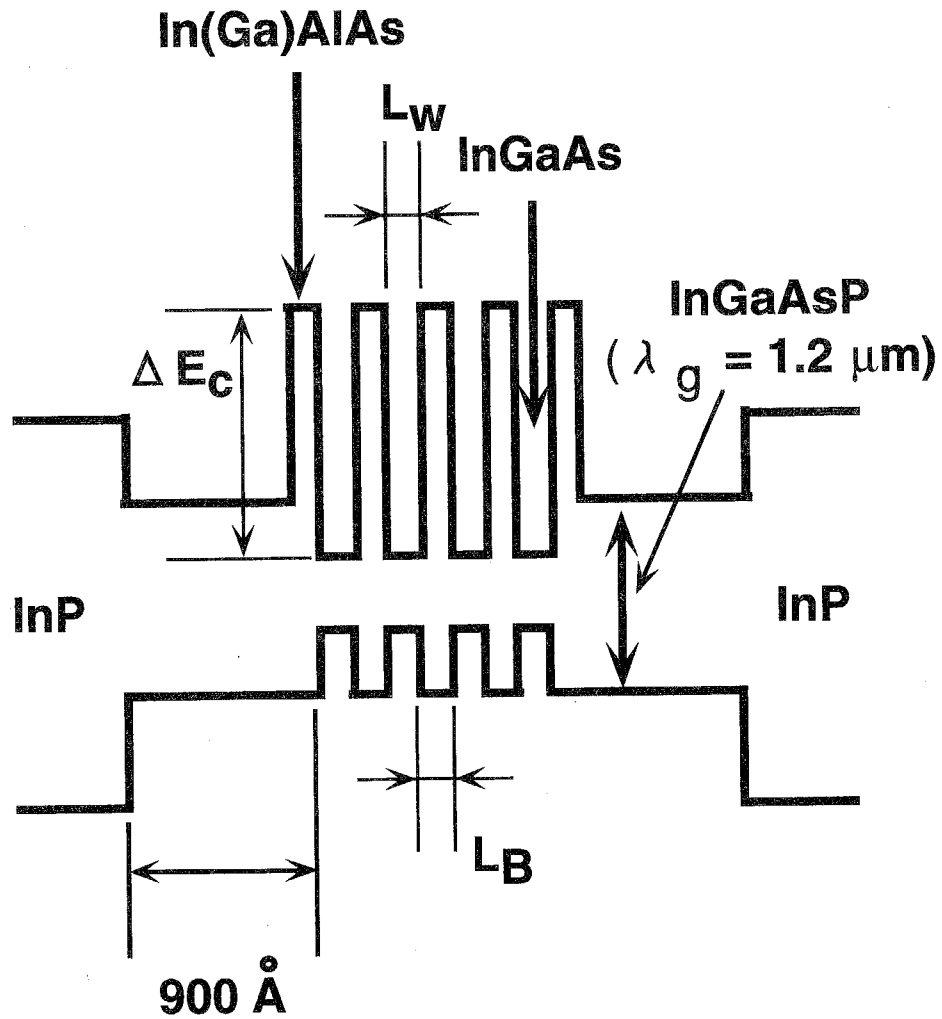
**Fig. 7-2**

The energy band diagram of the InGaAs/In(Ga)AlAs MQW structure. $L_B$ represents the In(Ga)AlAs barrier thickness and $\Delta E_c$ the conduction band discontinuity.
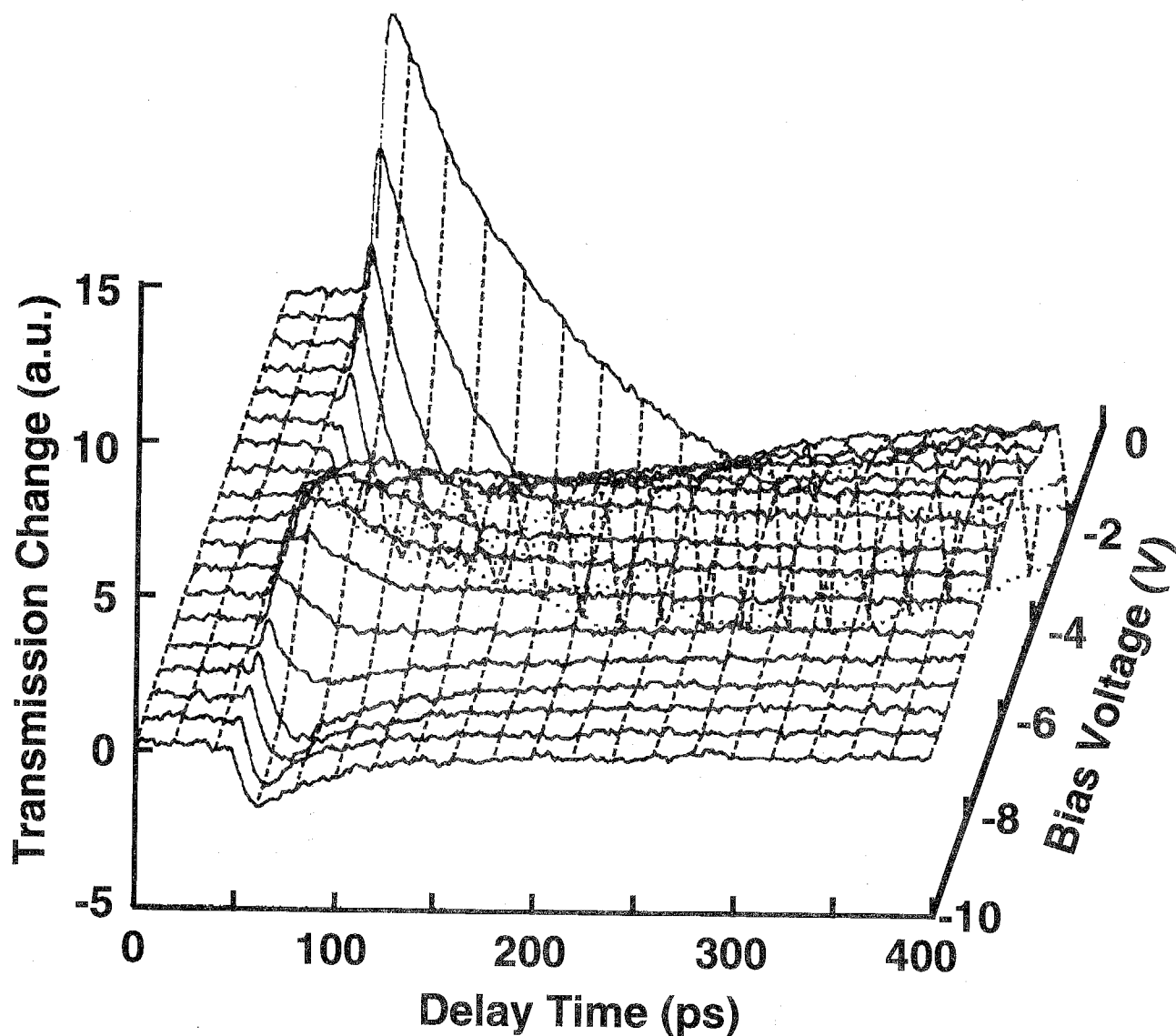
Fig. 7-3

Pump-probe signal as a function of the bias voltage. The measured structure is an InGaAs/InAlAs ($\Delta E_c = 0.5$ eV) MQW with barrier thickness $L_B = 30$ Å and the well number $N_W = 10$.

under other condition, according to the change of the absorption spectrum. This is because the QCSE under a high applied electric field causes the heavy-hole exciton to significantly deviate from the pump and probe wavelength. Figure 7-4 shows the barrier thickness dependence of the pump-probe signal at almost the same applied electric field. The dramatic change despite the slight difference in the barrier thicknesses implies the important role of the tunneling effect in the InGaAs/In(Ga)AlAs MQW structure.

## 7.3 Estimation of Carrier Escape Time

Although the absorption recovery time can be reduced by using a thin-barrier structure, the following absorption enhancement takes a rather long time and affects the repetition rate when the MQW structure is used as a saturable absorber. The measured pump-probe signals were fitted to calculations results by using eqns. (7.1) and (7.2), and the carrier escape time was estimated.. The fitted curves are shown by the dotted curves in Fig. 7-4. The agreement is good in all cases. Figures 7-5 (a) and (b) show the carrier escape time derived for the barrier thickness and barrier height dependence of the MQW structures listed in Table 7-1. The applied electric fields were calculated by dividing the applied voltage by the thickness of the MQW structure, while considering the built-in voltage. The red-shift of the exciton peak wavelength from photocurrent measurement indicates that the external electric field was actually applied to the MQW region. Solid symbols represent the carrier escape time for the MQW and open symbols represent that for the optical confinement layer. From these two figures, we can see that

(1) The carrier escape time decrease as the reverse bias voltages increases because of the carrier extraction effect caused by the applied electric field.

(2) On comparing #1, #2 and #3 in Table I, the dependence of carrier escape time from the MQW on the barrier thickness is very large, as seen in Fig. 7-4. This large dependence is caused by the tunneling probability of the MQW barrier. The carrier
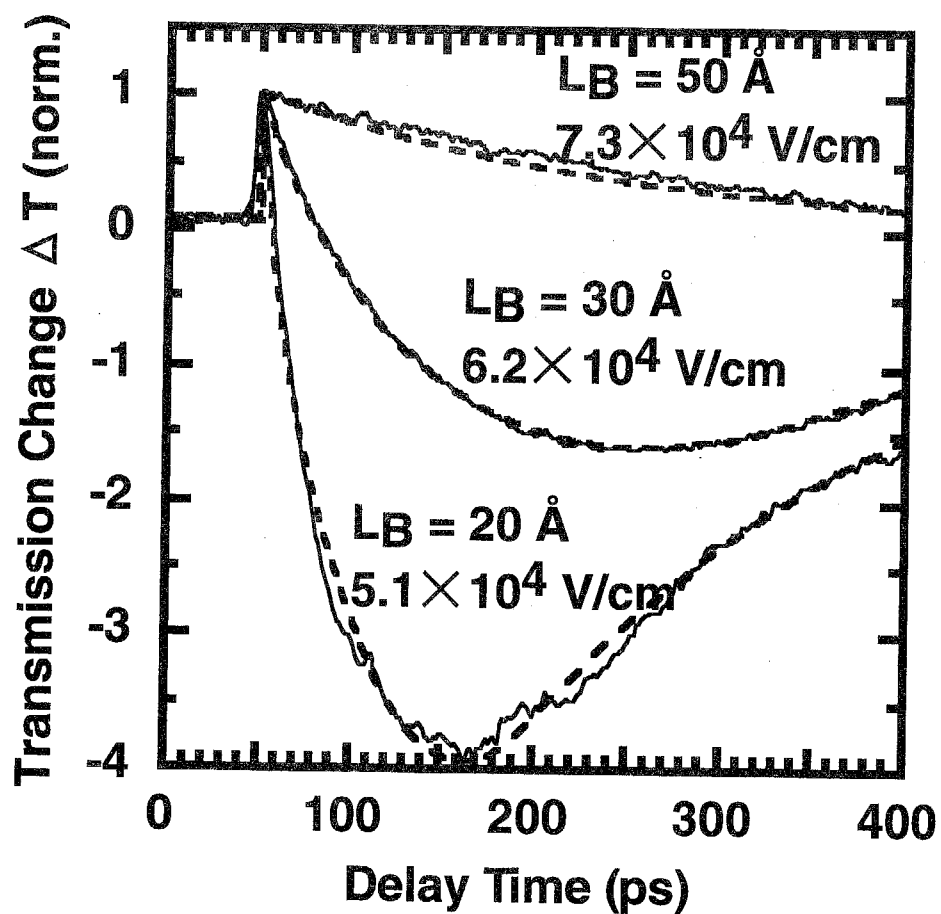
**Fig. 7-4**

Pump-probe signal dependence on the barrier thickness ($L_B$ = 20, 30, 50 Å). The solid lines show the measured results and the dotted lines show the fitted results.
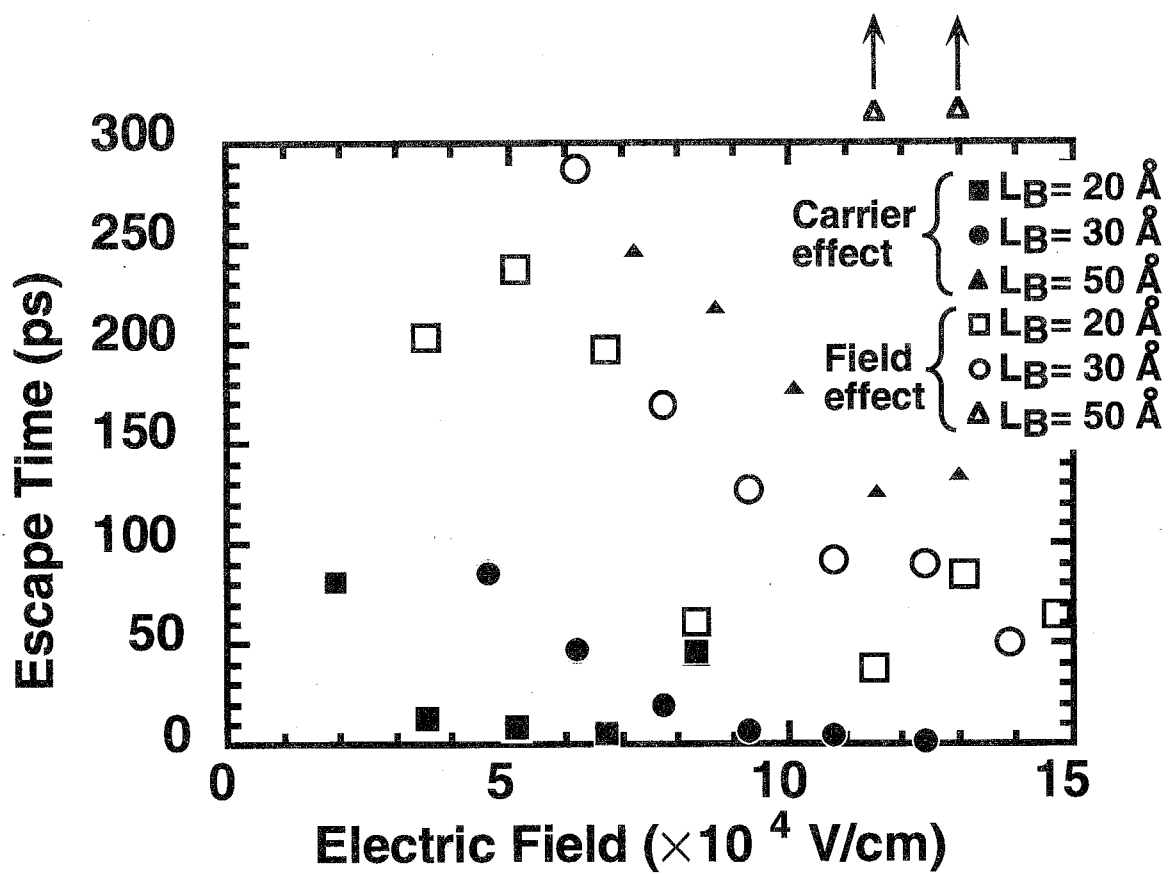
**Fig. 7-5 (a)**

Carrier escape time versus applied electric field for barrier thickness dependence.
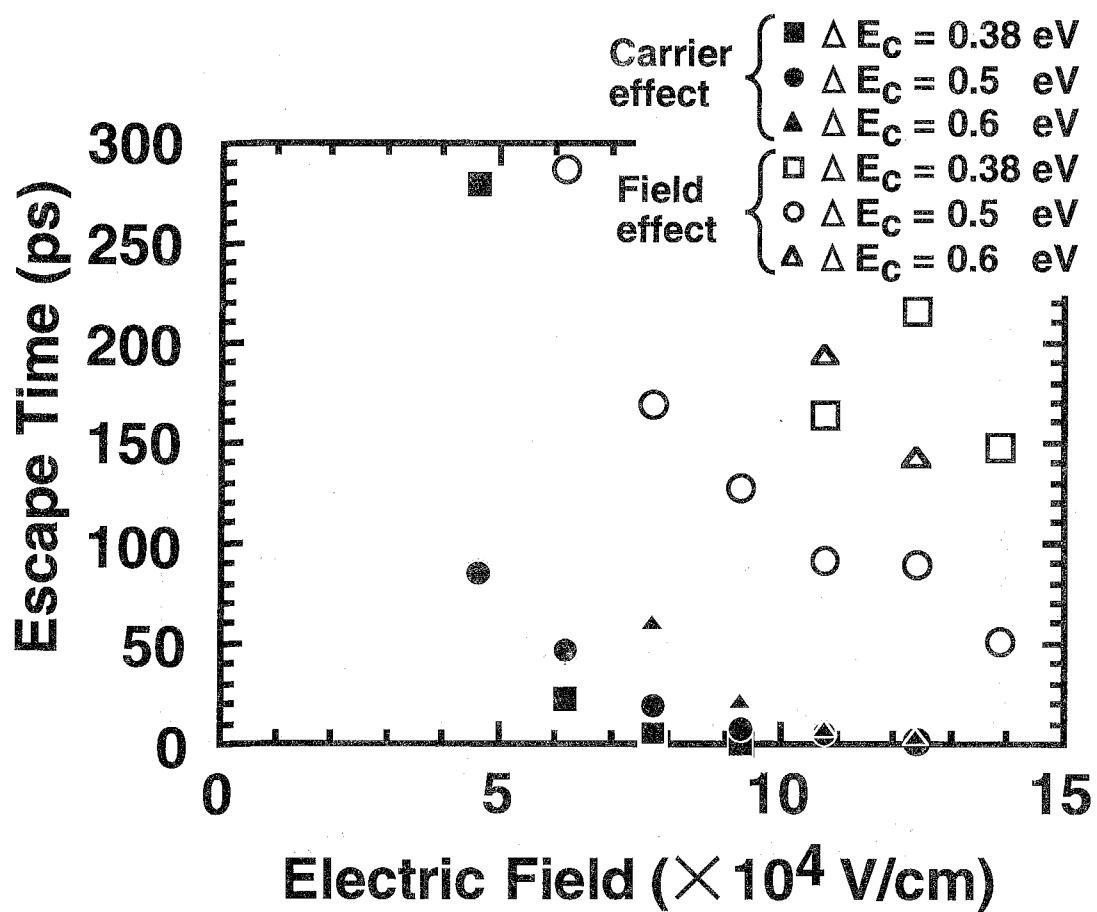
**Fig. 7-5 (b)**

Carrier escape time versus applied electric field for barrier height dependence.

## Table 7-1
### Parameters for the measured structures.

| No. | Barrier thickness $L_B$ (Å) | Barrier height $\triangle E_c$ (eV) | Well number $N_W$ | Well thickness $L_W$ (Å) |
|---|---|---|---|---|
| 1 | 30 | 0.5 | 10 | 90 |
| 2 | 20 | 0.5 | 10 | 90 |
| 3 | 50 | 0.5 | 10 | 90 |
| 4 | 30 | 0.38 | 10 | 90 |
| 5 | 30 | 0.6 | 10 | 90 |

escape time contributed by the phase space filling is as short as the GaAs/AlGaAs system [1], [2]. This result differs from that of Gupta et al. [3] because the tunneling through the thin barrier affects the carrier escape time in our experiment.

(3) On comparing structures #1, #4, and #5 in Table 7-1, the dependence of carrier escape time on barrier height can be seen. The barrier height dependence is probably due to the enhancement of tunneling probability and the increase of the thermionic emission rate. This dependence, however, is smaller than the barrier thickness dependence because the conduction band discontinuity is much higher than that of GaAs systems and the number of carriers contributing to the phenomenon mentioned above is small.

(4) The carrier escape time for the optical confinement layer is almost an order of magnitude larger than that for the MQW region. The latter is reduced to less than 5 ps, while the former is about 50 ps in less than $1.5 \times 10^5$ V/cm range.

Faster carrier escape from the optical confinement layer can be obtained by shifting the heavy-hole exciton to shorter wavelengths, and an escape time less than 50 ps could be obtained.

It is concluded that a thin barrier and a lower barrier height achieve fast carrier escape, but a barrier thickness of 20-30 Å and a barrier height of 0.38-0.50 eV are suitable for large nonlinearity. And the total carrier escape time is limited by the escape time for the optical confinement layer.

## 7.4 Estimation of Ultimate Switching Speed

### 7.4.1 Turn-off time Estimation

In Section **3.3.2**, the switching speed limit was estimated by solving rate equations. The results for the turn-on time are valid, but those for the turn-off time need further consideration because the dependence of the carrier escape time on applied electric field was not taken into consideration. Now that the actual carrier escape time

for the saturable absorption region has been evaluated, the switching speed that is actually feasible can be estimated by using these results of carrier escape time.

The rate equations used are based on eqns. (3.1) to (3.6). The situation that the bistable laser is a single mode laser and the input light wavelength is equal to the lasing wavelength is assumed because the low switching power and the resultant fast switching speed are expected. The main difference between the calculations in section **3.3.2** and those in this section is that the carrier escape time here is a function of the applied electric field. In Section **3.3.2**, the carrier escape time and the applied voltage height were given independently even though they are actually dependent each other. The carrier escape time used in the calculations here are based on Figs. 7-5(a) and (b) or on the well number dependence shown in Fig. 7-6. The measured MQW structures consisted of InGaAs(90Å)/InAlAs(30Å). The numbers of wells were 6 and 10. The carrier escape time for the MQW layer and the optical confinement layer were almost the same regardless of the different number of wells because of fast tunneling and thermionic emission rate from MQW and because of the same thicknesses of the optical confinement layers.

The calculated turn-off time is shown in Fig.7-7 as a function of applied voltage height. The MQW structure assumed is 6 periods of InGaAs(90Å)/InAlAs(30Å) so as to be the same as that for carrier escape time measurement. In the calculation, the bias voltage to the saturable absorption region was set so that the hysteresis width was 10 mA. The bias current offset from turn-on threshold current was varied from 1 to 9 mA as a parameter. The shape of the reset voltage was assumed to be complete square, i.e., the transition time of the reset voltage pulse was very small (0 ps). The turn-off time decreases with increasing applied voltage height because of the faster carrier escape and the large absorption change. This time is shorter when the bias current approaches turn-off threshold current because the absorption recovery is easily achieved. The effect of absorption saturation was also estimated by the hysteresis width dependence, and that is shown in Fig. 7-8. In calculating the curves in this figure, the bias voltage to the saturable absorption region
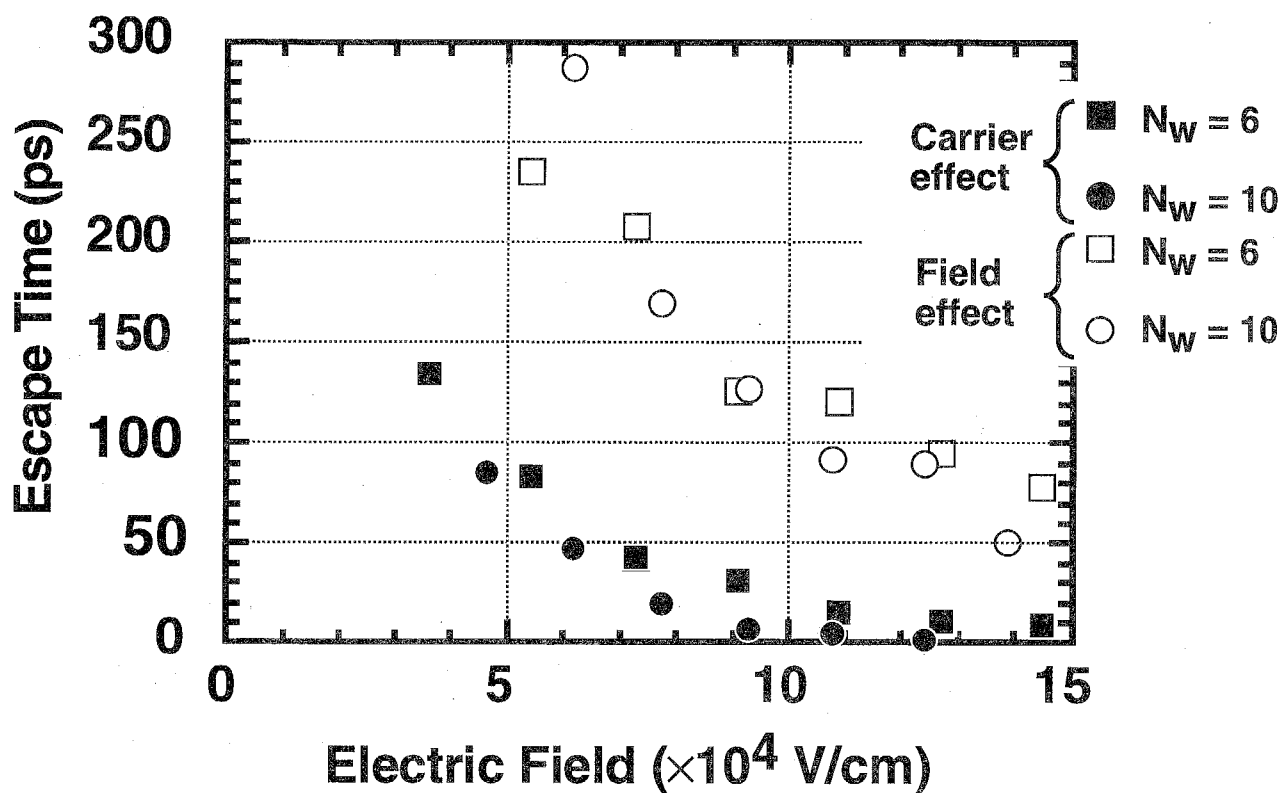
**Fig. 7-6**

Carrier escape time dependence on applied electric field. The MQW structure consist of InGaAs(90Å)/InAlAs(30Å). The numbers of wells are 6 and 10.
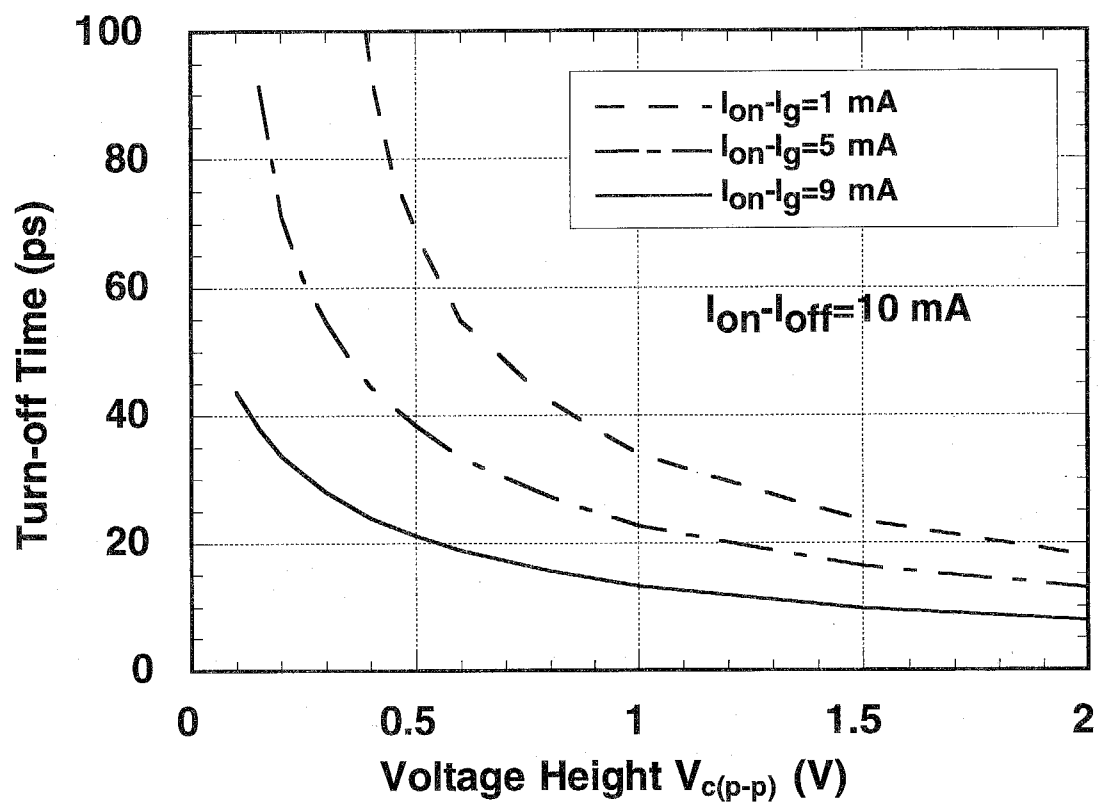
**Fig.7-7**

Calculated turn-off time versus applied voltage height. The hysteresis width is fixed at 10 mA and the difference between bias current and the turn-on current is varied. 6 periods of InGaAs/InAlAs MQW is assumed.
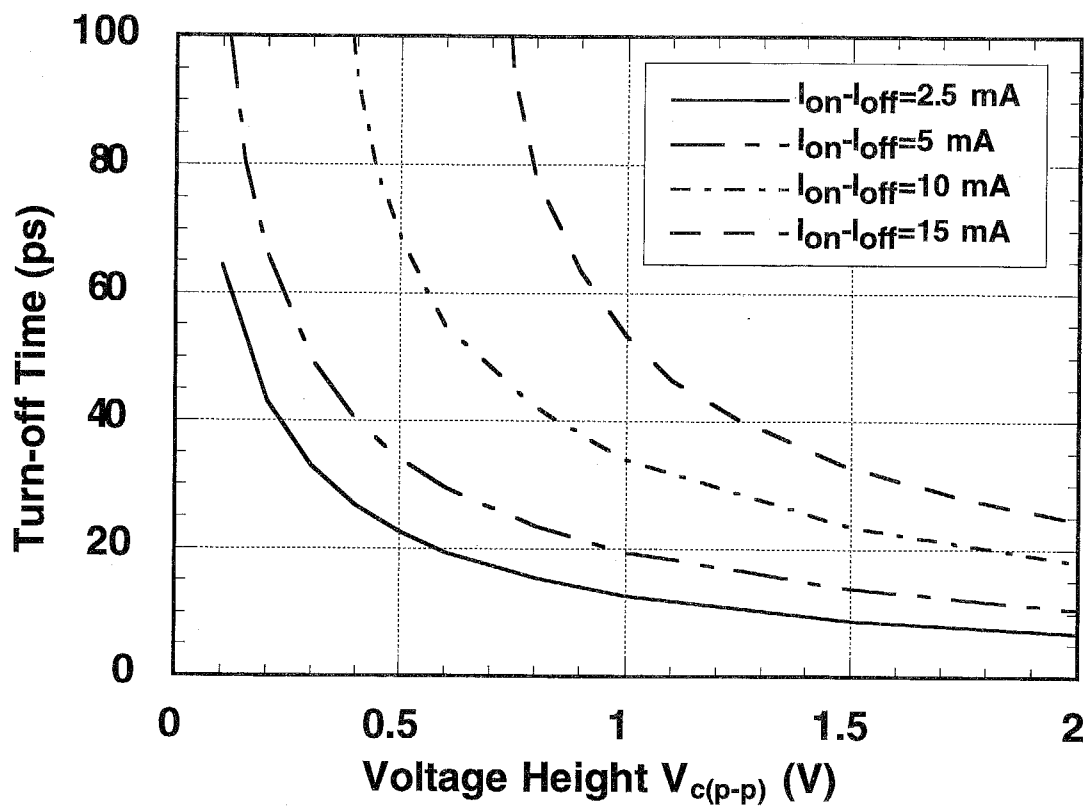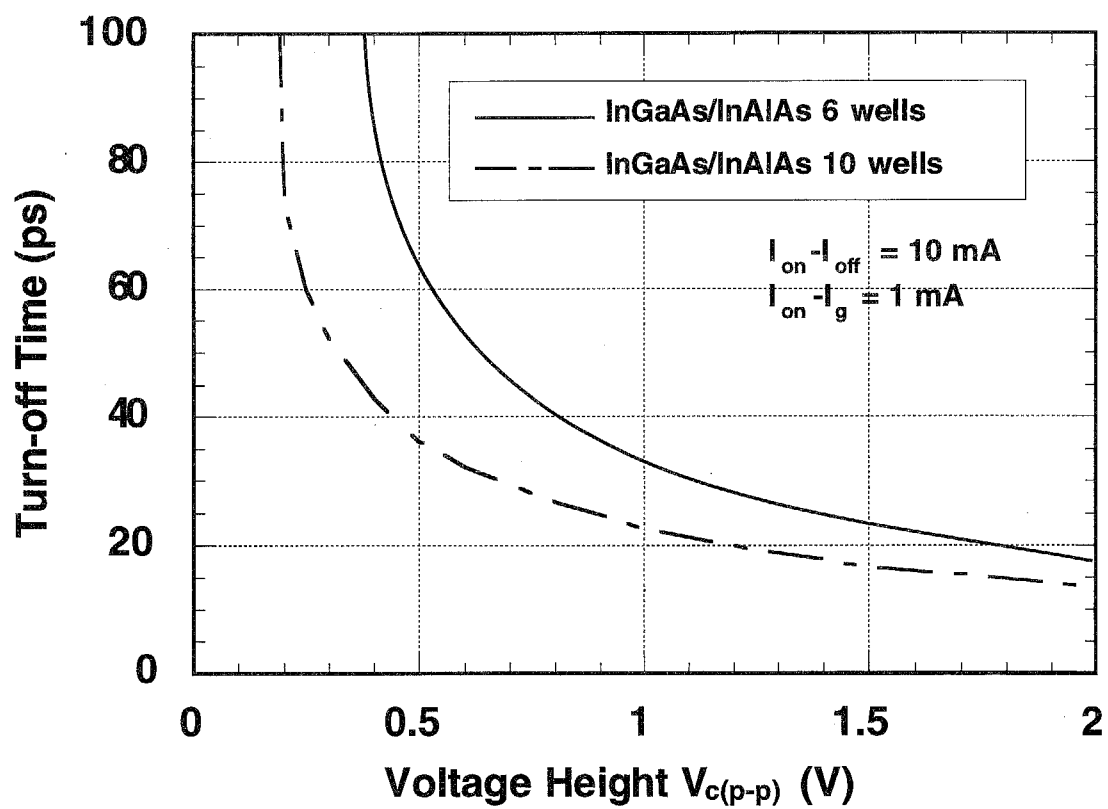
**Fig. 7-8**

Calculated turn-off time versus applied voltage height. The hysteresis width
is varied from 2.5 mA to 15 mA. The difference between bias current and
the turn-on current is fixed at 1 mA. 6 periods of InGaAs/InAlAs MQW is
assumed.

**Fig. 7-9**

Calculated dependence of turn-off time on MQW structures. MQWs consist of InGaAs/InAlAs.

was set so that the hysteresis width was 2.5, 5, 10, and 15 mA. The difference of the bias current from turn-on current was fixed to be 1 mA. As shown in the figure, the turn-off time can be reduced by narrowing the hysteresis width. In both Fig. 7-7 and Fig. 7-8, the turn-off time can be reduced to be less than 10 ps. Figure 7-9 illustrates the turn-off time dependence on the differential gain in the gain region. The hysteresis width and the offset of the bias current from the turn-on current were fixed to be 10 mA and 1 mA, respectively. The parameters for InGaAs/InAlAs with 6 and 10 wells listed in Table 3-1 were used in the calculations. The larger differential gain improves the carrier to photon interaction rates, so the turn-off time is shorter with larger differential gain. This is the same result shown in Section **3.3.2**.

## 7.4.2 Repetition Time Estimation

Now let me consider the total operation speed in view of both turn-on time and turn-off time. Figure 7-10 shows these time as a function of bias current when the hysteresis width was fixed to 10 mA. The input light intensity and the applied voltage height were varied as parameters in Fig. 7-10(a) and (b), respectively. Comparing Figs. 7-10(a) and (b), we can see that the sum of the turn-on and turn-off time is almost constant at all bias currents between the hysteresis when the input light intensity is high (50 kW/cm$^2$) and the applied voltage height is large (2 V peak to peak). They are less than 40 ps. For practical use, it is favorable that the turn-on time and turn-off time does not change very much with fluctuations of the input light intensity or applied voltage height. Thus the bias current near turn-on threshold current (for example, 1 mA offset) is suitable for actual switching operations. The turn-on and turn-off time varies when the hysteresis width changes and this is illustrated in Figs. 7-11(a) and (b). The sum of the turn-on and turn-off time, however, is almost the same as that shown in Fig. 7-10, and that is less than 40 ps at an input light intensity of 50 kW/cm$^2$ and an applied voltage height of 2 V, within the hysteresis width of 2.5 to 15 mA. The hysteresis
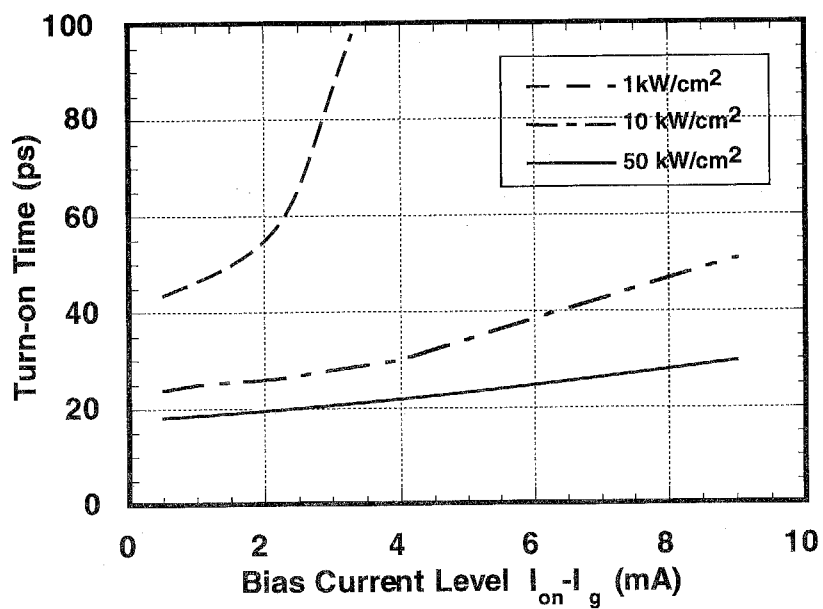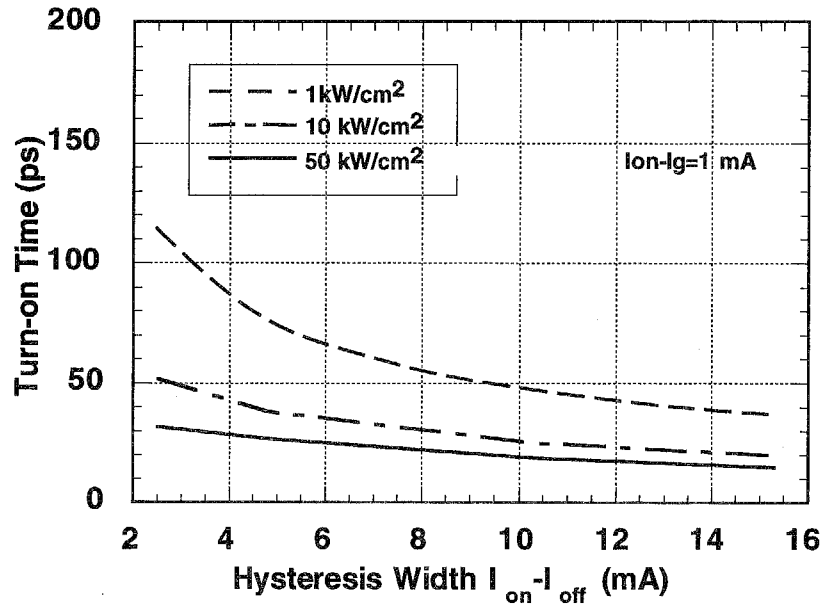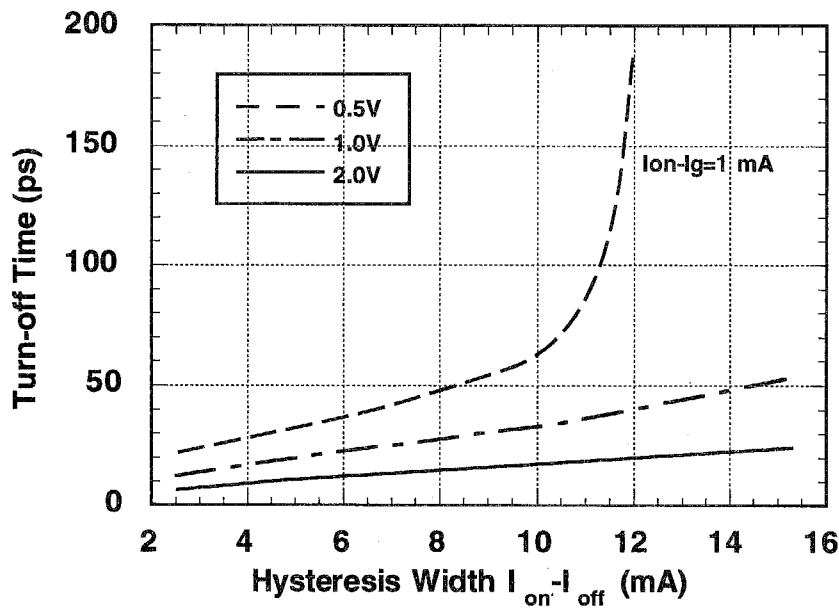
(a) Turn-on time
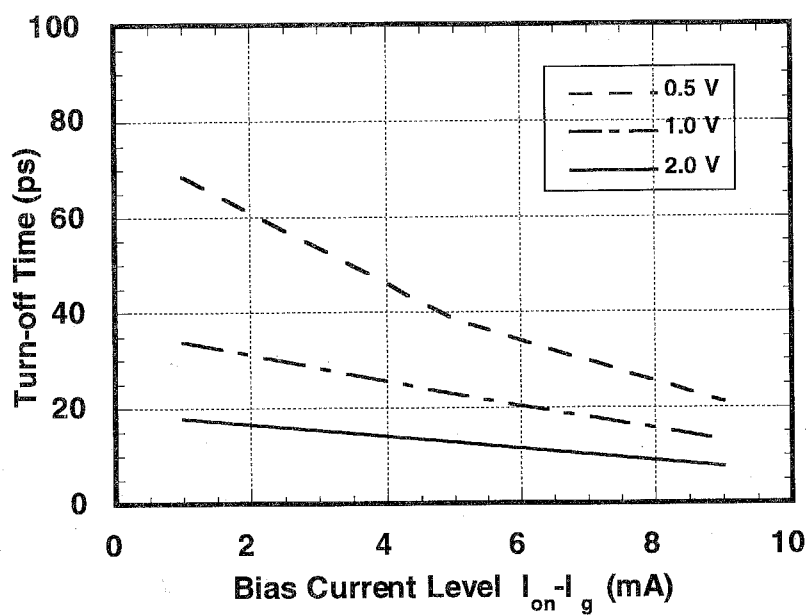


(b) Turn-off time

**Fig. 7-10**

(a) Turn-on and (b) turn-off time as a function of bias current level. 6 periods of InGaAs/InAlAs MQW is assumed.

(a) Turn-on time



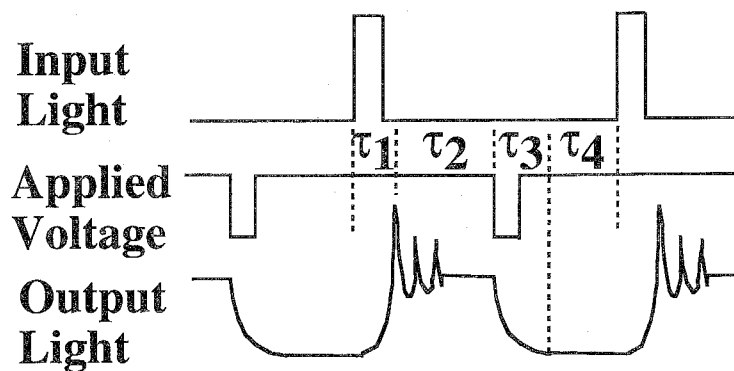(b) Turn-off time

**Fig. 7-11**

(a) Turn-on and (b) turn-off time as a function of hysteresis width.
6 periods of InGaAs/InAlAs MQW is assumed.

width of more than 2.5 mA and less than 10 mA is preferable in view of the constant total switching time when the input signal fluctuates.

From Figs. 7-9, 7-10, and 7-11, we can conclude that the optimized structure is a material with a large differential gain and that the optimized driving condition is a hysteresis width less than 10 mA and a bias current offset from the turn-on current of about 1 mA. Because of the degradation of turn-off time due to parasitic CR constant response, hysteresis width around 5 mA may be better. Besides the input light and reset voltage fluctuations, the change of threshold current or lasing wavelength due to the laser temperature fluctuation must be considered. The laser temperature is stabilized within 0.1 degrees by Peltier control. The threshold current change is proportional to $\exp(\Delta T/T_0)$ where $\Delta T$ is the temperature change and $T_0$ is characteristic temperature. Assuming $T_0$ is 50 K, which is typical value in the long-wavelength laser diode, and the threshold current is 50 mA, the resultant threshold change is 0.1 mA. It is found that the driving conditions mentioned above is sufficient for obtaining stable fast switching operations. On the other hand, the lasing wavelength change caused by thermal change of refractive index is 0.1 Å assuming the thermal change of lasing wavelength is 1 Å/K. The Fabry-Perot gain for input light reduces to 94 % due to this wavelength change when the net gain of 33.4 cm$^{-1}$ (mentioned in Section **4.3.2**) and eqns.(3.6) to (3.9) are used. This is also within the tolerance of the stable operation. The sum of the turn-on and turn-off time (total switching time) is then less than 40 ps. When the switching energy is defined as the product of the input power and the switching time, it is several femtojoules in set operation and less than a picojoules in reset operation.

Next, I will describe the repetition time limit of the voltage-controlled MQW bistable laser. The time response of the bistable laser is illustrated in Fig.7-12. The repetition time is the sum of the (i) turn-on time $\tau_1$, (ii) the duration of lasing state (which is called "on time $\tau_2$" in the following), (iii) turn-off time $\tau_3$, and (iv) the duration of nonlasing state (which is called "off time $\tau_4$" in the following). It is easily predicted that the last term depends on the input light intensity because the carrier density in the saturable absorption region is lower than that under steady state just after

Repetition time = $\tau_1$ : turn-on time +

$\tau_2$ : on time +

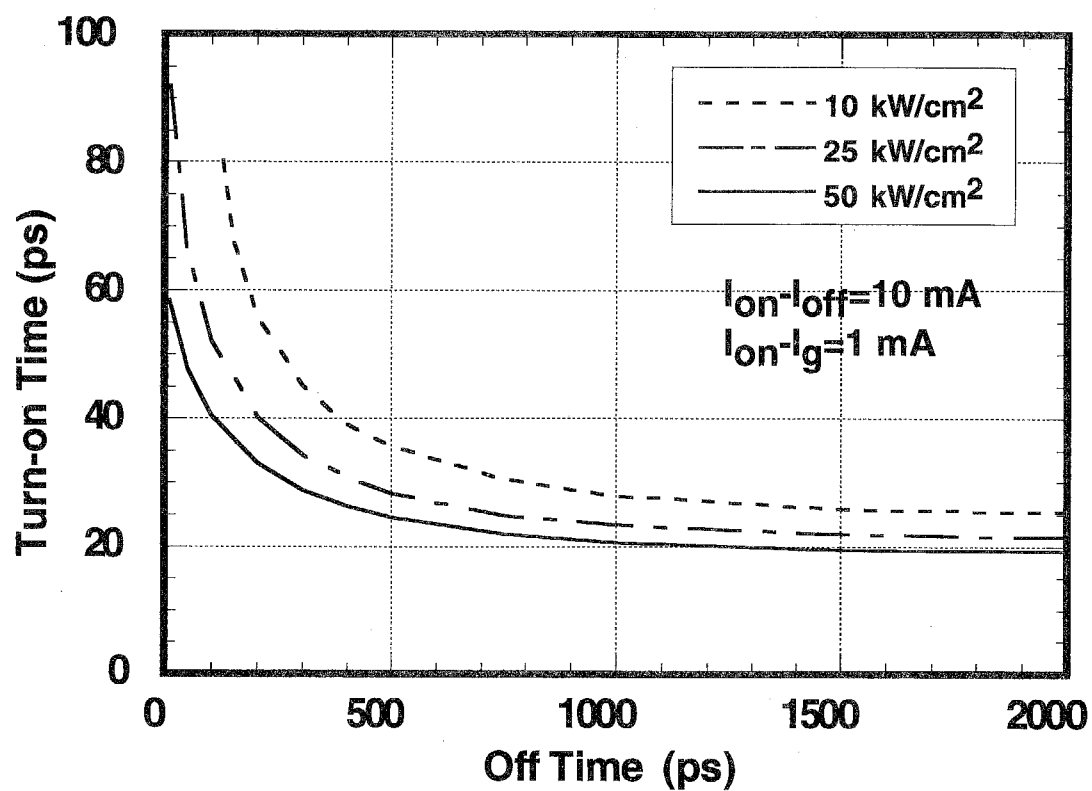$\tau_3$ : turn-off time +

$\tau_4$ : off time

Fig. 7-12

Schematic of the time response of the bistable laser.

the applied voltage returns from the reset voltage to the bias state due to ultrafast-rate carrier extraction by applied reverse bias voltage. This phenomenon is reflected in the increased turn-on time. The calculated turn-on time after the reset operation is shown in Fig. 7-13. In this calculation, the bias voltage was set so that the hysteresis width was 10 mA and the bias current offset from the turn-on current was 1 mA. The interval between the trailing edge of the reset voltage and the following injected light pulse (off time) was varied. The widths of the injected light pulse and the reset voltage pulse were set to 25 ps in estimating the highest possible switching speed. As can be seen in the figure, the turn-on time is almost constant for longer time intervals longer than 1000 ps (1 ns). It increases suddenly, however, when the time interval approaches zero. High-power input light can reduce the turn-on time because the large injected photon density compensates the shortage of carriers in the saturable absorption region and is easily saturates the absorption. The dependence of the turn-on time change on differential gain is shown in Fig. 7-14. The differential gain is larger in InGaAs/InAlAs than in InGaAs/InGaAsP or in materials with a larger number of quantum wells. The fluctuation of the carrier density is suppressed and also the excitation rate is faster in the materials with larger differential gain, resulting in the small increase of the turn-on time. Figure 7-15 illustrates the turn-on time change when the time interval is fixed at 10 ps. A larger input light pulse and the use of a material with a large differential gain can reduce the change of turn-on time. In the InGaAs/InAlAs MQW structure, the turn-on time is less than 25 ps when the input light intensity is greater than 100 kW/cm$^2$.

The third term (iii) can be controlled flexibly but it must be larger than the first peak of the relaxation oscillation. Now, we define the interval between the bistable laser turns-on and the application of the reset voltage as the half period of the relaxation oscillation. The relaxation oscillation frequency $f_r$ is usually given by [9]

$$f_r = \frac{1}{2\pi}\sqrt{\frac{2v_g}{hv} \bullet \frac{\xi_{MQW}}{wN_wL_w} \bullet \frac{\alpha_m + 2\alpha_{th}}{2\alpha_{th}L} \bullet (\frac{dg}{dn})(1 - \varepsilon S)P_{out}} \qquad (7.3)$$

**Fig.7-13**

The dependence of turn-on time on the off time. Input light intensity is varied as a parameter. 6 periods of InGaAs/InAlAs MQW is assumed.
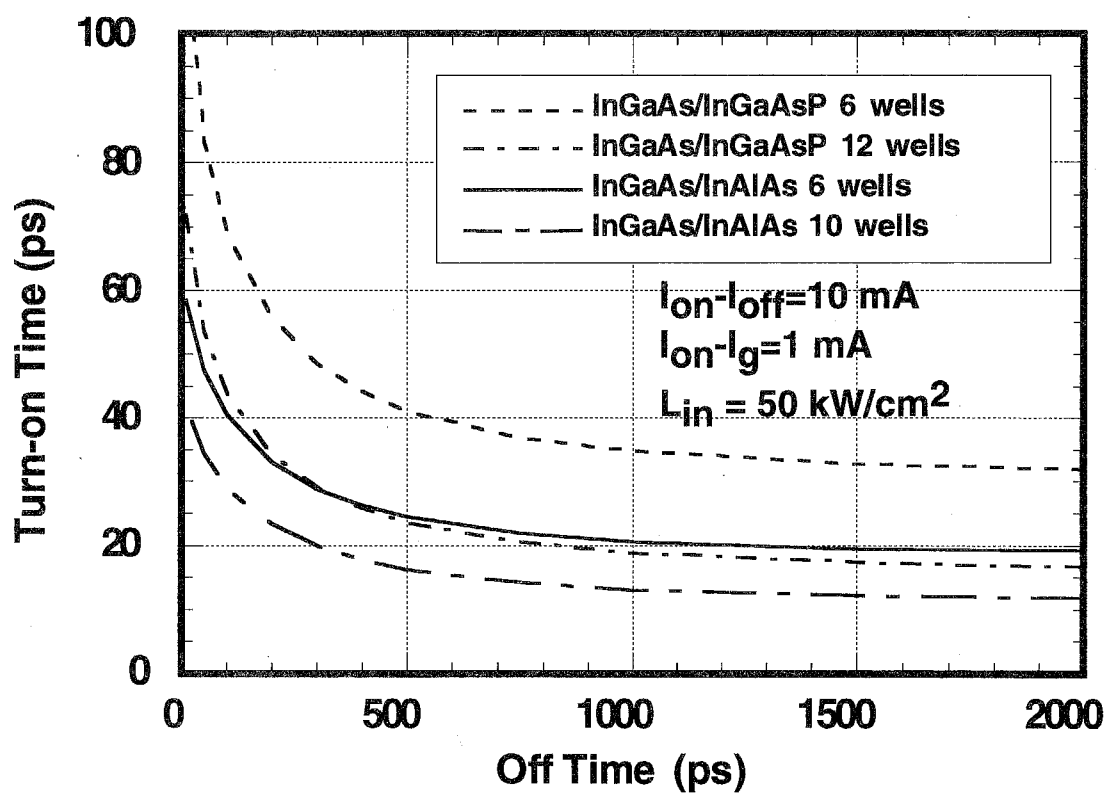
**Fig. 7-14**

The dependence of turn-on time as a function of the off time. Four kinds of MQW structure are used for calculations.
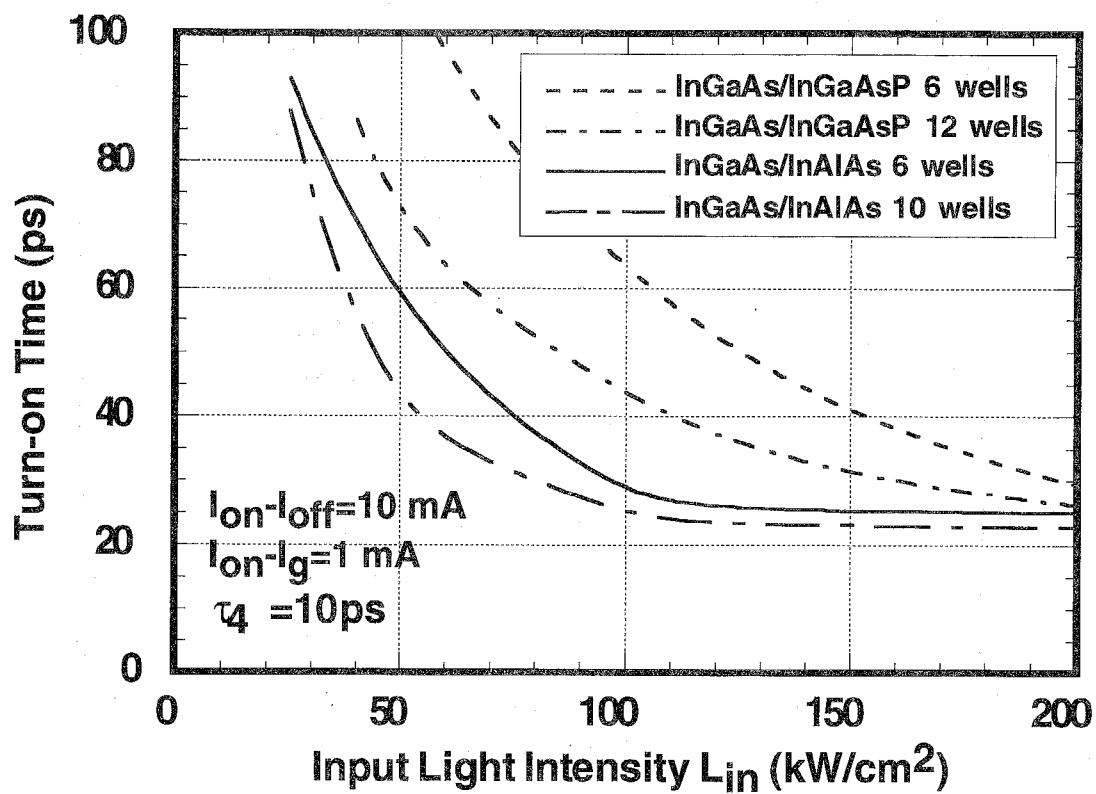
**Fig. 7-15**

Calculated turn-on time as a function of input light intensity.
The off time is fixed at 10 ps.

where dg/dn is the differential gain coefficient, $P_{out}$ is measured output power, $v_g$ is group velocity, hv is photon energy, $\xi_{MQW}$ is the optical confinement factor, w is ridge width, $N_w$ is well number, $L_w$ is well thickness, $\alpha_m$ is mirror loss, $\alpha_{th}$ is threshold gain, L is cavity length, and S is photon density in the cavity . But in the case of light injection operation, it differs from that given by eqn. (7.3) because the injected photons causes the photon density to differ from the steady state. The relaxation oscillation under light injection was therefore estimated by using the rate equations (3.1)-(3.6). The relaxation oscillation frequency obtained for 10-well InGaAs/InAlAs was 5.1 GHz, which corresponds to an interval time of 98 ps. The resultant repetition time is summarized in Fig.7-16. It is 158 ps (the turn-on time is 25 ps, the on time is 98 ps, the width of the reset voltage is 25 ps which is longer than the turn-off time, and the off time is 10 ps). It is thus found that the relaxation oscillation frequency is the factor limiting the repetition rate. Now assuming that the relaxation oscillation frequency is 15 GHz (the fastest -3 dB bandwidth in the 1.55 μm range is 18 GHz [10]), the interval between the first light peak and the reset voltage can be reduced to 33 ps, the repetition rate over 10 GHz is achieved.

Increasing the relaxation oscillation frequency should thus result in higher repetition rates. The differential gain can be increased by using structures with more quantum wells, with a higher conduction band offset, or with strained-layer superlattice. And photon density $P_0$ can be increased and photon lifetime $\tau_p$ decreased by lowering the bias voltage because the absorption increases in the saturable absorption region.

And the transient response of reset operation in an actual device is degraded by the parasitic capacitance as described in Chapter 4. In the proposed device, the polyimide reduces the capacitance of the saturable absorption region. For further improvement, Fe-doped InP buried heterostructure would be better because of its more pronounced electron trap effect. In addition to this, the laser module including microstrip line and contact region between a laser, a strip line and a coaxial connector must be sophisticated.

## Repetition time

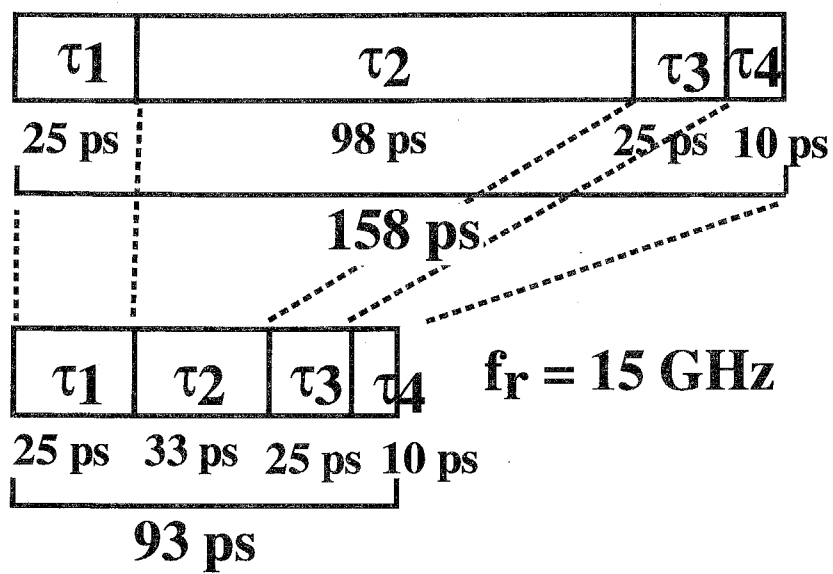**InGaAs/InAlAs 10 wells**

$$f_r = 5.1 \text{ GHz}$$



| τ1 | τ2 | τ3 | τ4 |
|---|---|---|---|
| 25 ps | 98 ps | 25 ps | 10 ps |

**158 ps**

| τ1 | τ2 | τ3 | τ4 |
|---|---|---|---|
| 25 ps | 33 ps | 25 ps | 10 ps |

$$f_r = 15 \text{ GHz}$$

**93 ps**

**Fig. 7-16**

**Repetition time estimation.**

When the ideal structure and laser module can be fabricated, the repetition rate over 10 GHz is expected as mentioned above. The objective device is an in-line light-injection-type, so the system with single wavelength use is suitable. The device can be applied to the time division multiplexed system with few channel and ultrafast bit-rate, or with many channel and 500 Mbit/s to 1 Gbit/s bit-rate.


## 7.5 Summary


I have investigated the switching speed limit of the MQW bistable laser, including the carrier escape time dependence on the applied electric field strength. I evaluated the carrier escape time by performing pump-probe measurements for InGaAs/In(Ga)AlAs MQW structures and deriving the structure dependence of the carrier escape time, that is, its dependence on barrier thickness, barrier height, the number of wells. The escape time for the MQW region is very dependent on the barrier thickness but not on the barrier height, or the well number.

Evaluation of the switching speed of the MQW bistable laser revealed that a turn-off time of less than 10 ps can be attained by optimizing the MQW structure and the driving conditions. Estimating the turn-on time, the turn-off time, the duration of lasing state (on time), and the duration of nonlasing state (off time), reveals that repetition rate higher than 10 GHz can be expected. To obtain a repetition rate of 5 to 10 GHz, the MQW structure with large number of quantum wells, high conduction band offset, or strained-layer superlattice are suitable because they have a large differential gain.

## References

[1] A. M. Fox, D. A. B. Miller, G. Livescu, J. E. Cunningham, and W. Y. Jan, "Quantum well carrier sweep out : Relation to electroabsorption and exciton saturation", IEEE J. Quantum Electron., vol.27, pp. 2281-2295, 1991.

[2] J. A. Cavaillès, D. A. B. Miller, J. E. Cunningham, P. L. K. Wa, and A. Miller, "Simultaneous measurements of electron and hole sweep-out from quantum wells and modeling of photoinduced field screening dynamics", IEEE J. Quantum Electron., vol.28, pp.2486-2497, 1992.

[3] S. Gupta, L. Davis and P.K. Bhattacharya, "Optical time-of-flight measurement of carrier transport in GaAs/AlxGa1-xAs and $In_{0.53}Ga_{0.47}As/In_{0.52}Al_{0.48}As$ multiquantum wells", Appl. Phys. Lett., vol. 60, pp. 1456-1458, 1992.

[4] R. Takahashi, T. Kagawa, Y. Kawamura and H. Iwamura, "Ultrafast optical nonlinearity in low-temperature grown InGaAs/InAlAs superlattices on InP and its applications to MSM-PDs in the 1.55 $\mu$m wavelength region", 20th International Symposium on GaAs and Related Compounds, LN-3, Freiburg, Germany, 1993.

[5] H. Uenohara, R. Takahashi, Y. Kawamura, and H. Iwamura, "Carrier escape time dependence on multiple quantum well structure in InGaAs/In(Ga)AlAs systems", Appl. Phys. Lett., vol.64, no.23, pp.3130-3132, 1994.

[6] H. Uenohara, Y. Kawamura, H. Iwamura, K. Nonaka, H. Tsuda and T. Kurokawa, "Operation characteristics of a side-light-injection multiple-quantum-well bistable laser for all-optical switching", Jpn. J. Appl. Phys., vol.33, Part I, pp.815-821, 1994.

[7] Y. Kawamura, A. Wakatsuki, Y. Noguchi and H. Iwamura, "InGaAs/InGaAlAs MQW lasers with InGaAsP guiding layers grown by gas source molecular beam epitaxy", IEEE Photon. Technol. Lett. vol.3, pp.960-962, 1991.

[8] R. People, K. W. Wecht, K. Alavi and A. Y. Cho, "Measurement of the conduction-band discontinuity of molecular beam epitaxial grown $In_{0.52}Al_{0.48}As/In_{0.53}Ga_{0.47}As$, $N$-$n$ heterojunction by $C$-$V$ profiling", Appl. Phys. Lett., vol.43, pp.118-120, 1983.

[9]  K. Uomi, T. Tsuchiya, H. Nakano, M. Aoki, M. Suzuki and N. Chinone, "High-speed and ultralow-chirp 1.55 µm multiquantum well λ/4-shifted DFB lasers", IEEE J. Quantum Electron., vol.27, pp.1705-1713, 1991.

[10] K. Uomi, H. Nakano and N. Chinone, "Intrinsic modulation bandwidth in ultra-high-speed 1.3 and 1.55 µm GaInAsP DFB lasers", Electron. Lett., vol.25, pp.1689-1690, 1989.

# Chapter 8 Conclusion

The applicability of voltage-controlled multiple quantum well (MQW) bistable laser to all-optical signal processing was pursued analytically and experimentally. And the feasibility of the side-light-injection-type MQW bistable laser was examined for the purpose of all-optical set and reset operations. The results obtained by this work are summarized as follows:

## (1) Analysis of in-line light-injection multiple quantum well bistable laser characteristics

The static and dynamic characteristics of two-segmented MQW bistable laser with an in-line light-injection scheme have been examined analytically by changing the differential gain coefficient, i.e., MQW materials, the voltage applied to the saturable absorption region, the bias current, and the input light power. It is shown that the shorter saturable absorption region of less than 10 μm is superior in view of small threshold current and easy controllability of hysteresis width. The differential gain coefficient was found to affect both turn-on and turn-off time. The turn-on time was also found to decrease when the bias current approaches the turn-on threshold current and the input light power increases, and the turn-off time decreased with decreasing the carrier lifetime. These results indicate that the high-speed set and reset operations of about 10 ps can be obtained by using a material with a large gain, by injecting high-power input light, and by applying a large voltage height to the saturable absorption region.

## (2) Performance of in-line light-injection multiple quantum well bistable lasers

The two-segmented MQW bistable lasers were fabricated and their performance were examined. The controllability of the hysteresis characteristics by applied voltage to

the saturable absorption region was confirmed. This characteristics was also obtained reproducibly. The results predict that InGaAs/InAlAs MQW has superior characteristic such that the bias voltage is lower at the emergence of hysteresis and the fast switching time is expected.

The switching operation by input light indicated that the MQW bistable laser had a wide wavelength sensitivity and a potential for switching in less than 100 ps. From the reset operation by changing applied voltage to the saturable absorption region, it is observed that the turn-off time decreased when the voltage height increased and a switching time could be shorter than 100 ps.

It is shown that the in-line light-injection MQW bistable laser could perform fast switching operation with the repetition rate over several Gbit/s.

## (3) Analysis of side-light-injection multiple quantum well bistable lasers

The side-light-injection-type bistable laser was proposed as a bistable laser for the all-optical functional device. The possibility of the set operation using absorption saturation and the reset operation using gain quenching in one device was demonstrated analytically. The driving conditions for set and reset operations possible was investigated. The improvement of switching power and speed by introducing the MQW structure with large differential gain, or by enhancing the waveguide gain was predicted. It was also shown that the turn-on and turn-off time of less than a nanosecond could be obtained.

## (4) Performance of side-light-injection multiple quantum well bistable lasers

The side-light-injection-type MQW bistable laser has been fabricated and its static and dynamic characteristics have been investigated. With this device, as with the two segmented MQW bistable laser, the hysteresis width and threshold current could be

controlled by adjusting the voltages applied to the saturable absorption region and the gain quenching region. With regard to the static input light characteristics, a set operation of several tens of microwatts and a reset operation of about one milliwatt were obtained in one device and under the same bias conditions for the first time. And also, stable set and reset operations were observed.

Experimental evaluation of dynamic set and reset operations in one device showed that the turn-on time decreased with increasing input light power and a turn-on time of about 200 ps could be obtained, and that the turn-off time of 2 ns was achieved with high input light power. These results indicate the possibility of constructing Gbit/s repetition rate all-optical signal processing systems.

### (5) Ultimate response of multiple quantum well bistable laser

The maximum switching speed possible with a voltage-controlled MQW bistable laser was investigated analytically by taking into account the carrier escape time for the MQW structure. The carrier escape time estimation was done by using pump-probe technique to measure the transient response of the absorption saturation of MQW structures. Carrier escape time was evaluated by fitting the measured curve to the theoretical curve and was used in predicting that very high-speed switching operations could be performed when a large reverse bias voltage pulse was applied for the reset operation. It is found that the carrier escape time for the optical confinement layer could be reduced to less than 50 ps.

By introducing the dependence of carrier escape time on the applied electric field, it was revealed that the switching speed of a MQW bistable laser (the sum of turn-on and turn-off time) could be reduced to less than 40 ps. And also it is shown that the repetition rate was limited by the relaxation oscillation frequency and could be improved by optimizing the MQW structure; for example, by using a material with a large differential gain. These results indicate the applicability of ultrafast repetition rate of 5 to 10 GHz.

The vast potential of the MQW bistable laser and the possibility of developing it for use in all-optical functional devices have thus been demonstrated both theoretically and experimentally. The MQW bistable laser can widely contribute not only to high-speed demultiplexing in transmission systems or data storage in the optical signal processing systems, but also to the development of all-optical functional devices in the near future.

# Acknowledgments

# List of Publications and Conferences

## A. Papers

1. H. Uenohara, H. Iwamura and M. Naganuma, "Switching characteristics of InGaAs/InP multiquantum well voltage-controlled bistable laser diodes", Jpn. J. Appl. Phys., Vol.29, No. 12, pp.L2442-L2444, 1990.

2. H. Uenohara, Y. Kawamura, H. Iwamura, K. Nonaka, H. Tsuda and T. Kurokawa, "Side-light-injection MQW bistable laser using saturable absorption and gain quenching", Electron. Lett., Vol. 28, No. 21, pp.1973-1975, 1992.

3. H. Uenohara, Y. Kawamura, H. Iwamura, H. Tsuda and T. Kurokawa, "Set and reset operation dependence on input light intensity of a side-light-injection MQW bistable laser", Electron. Lett., Vol. 29, No. 18, pp.1609-1611, 1993.

4. H. Uenohara, Y. Kawamura, H. Iwamura, K. Nonaka and T. Kurokawa, "Operation characteristics of a side-light-injection multiple-quantum well bistable laser for all-optical switching", Jpn. J. Appl. Phys., Vol.33, No. 1B, pp.815-821, 1994.

5. H. Uenohara, R. Takahashi, Y. Kawamura and H. Iwamura, "Carrier escape time dependence on multiple quantum well structure in InGaAs/In(Ga)AlAs systems", Appl. Phys. Lett., Vol.64, No.23, pp.3130-3132, 1994.

6. H. Uenohara, Y. Kawamura and H. Iwamura, "Long wavelength multiple quantum well voltage-controlled bistable laser diodes", submitted to IEEE J. Quantum Electron.

## B. International Conferences

1. H. Uenohara, H. Iwamura and M. Naganuma, "Switching characteristics of InGaAs/InP MQW voltage-controlled bistable laser diodes", the 22nd Conference on Solid State Devices and Materials, D-4-4, Sendai, Japan, August, 1990.

2. H. Uenohara, Y. Kawamura, H. Iwamura, K. Nonaka, H. Tsuda and T. Kurokawa, "All optical switching ON/OFF characteristics of a side-light-injection MQW bistable laser", IEEE Lasers and Electro-Optics Society 1992 Annual Meeting, EOS/OTA3.4, Boston, U.S.A., November, 1992.

3. H. Uenohara, Y. Kawamura, H. Iwamura, K. Nonaka, H. Tsuda and T. Kurokawa, "Dynamic set and reset operations of a side-light-injection MQW bistable laser", the 1993 International Conference on Solid State Devices and Materials, D-7-2, Chiba, Japan, 1993.

4. H. Uenohara, R. Takahashi, Y. Kawamura and H. Iwamura, "Theoretical investigation of ultimate response of multiple quantum well voltage-controlled bistable laser diodes", submitted to IOOC'95.

## C. Technical Group Meetings and Symposium

1. H. Uenohara, H. Iwamura and M. Naganuma, "Operation characteristics of InGaAs/InP MQW bistable laser diodes", Integrated Opto-electronics Meeting, IOE90-15, 1990.

2. H. Uenohara and H. Iwamura, "Estimation for low switching power and high-speed of a side-lighti njection bistable laser diode", to be presented in Opto-electronics Meeting, 1995.

## D. Domestic Meetings

1. H. Uenohara, H. Iwamura and M. Naganuma, "The characteristics of InGaAs/InP MQW bistable laser", 37th Spring Meeting of Japan Society of Applied Physics, 29a-SA-16, Saitama, March 1990.

2. H. Uenohara, H. Iwamura and M. Naganuma, "The turn-off characteristics of voltage-controlled MQW bistable laser diodes", 51th Autumn Meeting of Japan Society of Applied Physics, 27a-R-3, Iwate, September 1990.

3. H. Uenohara, H. Tsuda, H. Iwamura and T. Kurokawa, "Switching operation of MQW bistable laser diodes", 52th Autumn Meeting of Japan Society of Applied Physics, 11a-ZM-6, Okayama, October 1991.

4. H. Uenohara, Y. Kawamura and H. Iwamura, "InGaAs/InAlAs MQW bistable laser diodes", 39th Spring Meeting of Japan Society of Applied Physics, 29a-SF-19, Chiba, March 1992.

5. H. Uenohara, Y. Kawamura and H. Iwamura, "Side-light-injection MQW bistable laser diodes", 53th Autumn Meeting of Japan Society of Applied Physics, 16p-V-16, Osaka, September 1992.

6. H. Uenohara, R. Takahashi, Y. Kawamura and H. Iwamura, "Dependence of recovery time of saturable absorption on InGaAs/In(Ga)AlAs MQW structure", 54th Autumn Meeting of Japan Society of Applied Physics, 29a-ZX-8, Hokkaido, September 1993.

7. H. Uenohara, R. Takahashi, Y. Kawamura and H. Iwamura, "Theoretical estimation of dynamic response of InGaAs/InGaAsP MQW voltage-controlled bistable lasers", to be presented in 1995 IEICE general conference.

## E. Patents

1. H. Uenohara, H. Iwamura and M. Naganuma, "Semiconductor bistable laser", 3-240285.

2. H. Uenohara, H. Iwamura and M. Naganuma, "Semiconductor bistable laser", 4-218990.

3. H. Uenohara, H. Iwamura, H. Tsuda and T. Kurokawa, "Semiconductor bistable laser", 5-13867.